Nicolaus Copernicus University in Toruń
Faculty of Physics, Astronomy and Informatics
Department of Atomic, Molecular and Optical Physics

COLLISION-INDUCED LINE-SHAPE EFFECTS IN MOLECULAR SPECTRA

NIODEM STOLARCZYK

Dissertation submitted in partial fulfillment
of the requirements for the degree of
DOCTOR OF PHYSICS

Thesis supervised by dr hab. Piotr Wcisło, prof. NCU
Department of Atomic, Molecular and Optical Physics
Institute of Physics, Nicolaus Copernicus University in Toruń

Toruń 2024

ACKNOWLEDGMENTS

I wish to thank my mentor and supervisor, Piotr Wcisło, for support, guidance and availability, both on professional and personal grounds.

I would like to thank Iouli E. Gordon for his kind hospitality during my two internships at Harvard-Smithsonian Center for Astrophysics. These two stays were crucial for the research relevant to this dissertation.

I would like to express my gratitude to all collaborators directly involved in the research articles constituting this dissertation and anyone who has supported my research and education. In particular, I would like to mention Roman Ciuryło, Daniel Lisak, Franck Thibault, Grzegorz Kowzan, Hubert Cybulski, Szymon Wójtewicz, Michał Słowiński, Hubert Jóźwiak, Maciej Gancewski, Kamil Stankiewicz, and Mikołaj Zaborowski.

The research presented within this dissertation was supported and partially financed by the National Science Centre (project no 2019/35/B/ST2/01118). The project was co financed by the Polish National Agency for Academic Exchange under the PHC Polonium program (Grant No. dec. PPN/X/PS/318/2018). The research is a part of the program of the National Laboratory FAMO in Toruń, Poland.

Calculations have been partially carried out using resources provided by the Wroclaw Centre for Networking and Supercomputing (http://wcss.pl), Grant No. 546. We gratefully acknowledge Polands high-performance computing infrastructure PLGrid (HPC Centers: ACK Cyfronet AGH, PCSS, CI TASK) for providing computer facilities and support within computational Grants No. PLG/2022/015576, PLG/2023/016409, PLG/2023/016279.

CONTENTS

STRESZCZENIE

Niniejsza rozprawa przedstawia badania z dziedziny teoretycznej spektroskopii molekularnej, których celem jest symulowanie zderzeniowo indukowanych kształtow profili linii spektralnych wyprowadzonych z zasad pierwszych. Kluczowym elementem tej pracy jest opracowanie i udoskonalenie metodologii symulacji profili linii widmowych przy użyciu parametrów uzyskanych z obliczeń rozpraszania kwantowego *ab initio*, oraz przetestowane jej na kilku rzeczywistych układach, takich jak H_2-He, HD-He, D_2-H_2 H_2-Ar i CO-Ar.

Nasza metodologia pozwala na symulowanie kształtów linii w pełni z zasad pierwszych, umożliwiając bezpośrednie porównanie wyników teoretycznych i doświadczalnych. Dzięki temu możlwa jest precyzyjna weryfikacja poprawności naszych obliczeń w oparciu o najdokładniejsze dane eksperymentalne. Niniejsza rozprawa doktorska obejmuje serię testów eksperymentalnych, potwierdzających dokładność symulowanych profili kształtu linii widmowych w kilku zderzeniowych układach molekularnych, w zakresie ciśnienia obejmującym sześć rzędów wielkości. Dzięki naszym obliczeniom rozpraszania kwantowego i dokładnemu modelowaniu kształtu linii spektralnej, odtwarzamy widma eksperymentalne z dokładnością na poziomie poniżej procenta.

Wykorzystując naszą metodologię, stworzyliśmy pierwsze bazy danych parametrów kształtów linii widmowych opatre w pełni na obliczeniach *ab initio*. Nasze zestawy danych pozwalają na symulowanie kształtów linii poza modelem Voigta, uwzględniających zależność rozszerzenia i przesunięcia od prędkości molekuły, oraz efekt Dickego. Niniejsza rozprawa prezentuje kompletne zestawy danych przejść rowibracyjnych molekuł H_2 i HD, zaburzonych helem, oraz najważniejszych linii molekuły HD zaburzonej H_2.

W nineijszej rozprawie zawarto również nowe metody opisu kształtu linii widmowych w reżimie zdominowanym przez zderzenia zmieniajce prędkość. Symulacje linii w tych warunkach, przy użyciu dotychczasowych metod, wymagały wydajnej infrastruktury obliczeniowej. W tej pracy pokazujemy, że kształt linii w tych warunkach można opisać za pomocą profilu Lorentza oraz podajemy analityczne wyrażenia umożliwiające obliczenie efektywnych szerokości i przesunięcia linii.

ABSTRACT

This dissertation presents a study of theoretical molecular spectroscopy, aiming to provide highly-accurate spectral line profiles derived from first principles. Central to this work is the development and refinement of a methodology for simulating spectral line profiles using parameters obtained from *ab initio* quantum scattering calculations, and testing it for several molecular systems, including H_2-He, HD-He D_2-H_2 H_2-Ar and CO-Ar.

Our methodology bridges theoretical calculations with experimental results by allowing one to compare simulated and measured lines, thereby validating its accuracy against highly-accurate experimental spectra. This dissertation features a series of experimental tests, proving the accuracy of the simulated spectral line-shape profiles with several molecular collisional systems, at pressures spanning six orders of magnitude. With our quantum-scattering calculations and careful modelling of the spectral line shape, we reproduce these high-accuracy experimental spectra at sub-percent level of agreement.

In addition to validating the methodology against experimental data, this dissertation contributes to the field by generating expansive datasets of spectral line-shape parameters. We apply our methodology to create the first datasets of spectral line-shape parameters based entirely on the *ab initio* calculations. Our datasets allow one to simulate the shapes of the spectral lines beyond the Voigt model, taking into account the speed dependence of the broadening and shift, as well as the Dicke effect. This dissertation presents complete sets of rovibrational transitions of the helium-perturbed H_2 and HD molecules, as well as the most important lines of the HD-H_2 system.

The dissertation presents a novel approach of description the spectral lines in the regime of frequent velocity-changing collisions. Using the previous methods to simulate the spectral lines under these conditions requires carrying out exhaustive numerical simulations. This dissertation shows, that the line profiles in these conditions can be described by a simple Lorentz profile. We provide analytical expressions for effective width and shift of this profile.

PUBLICATIONS CONSTITUTING THE DISSERTATION

A High-precision cavity-enhanced spectroscopy for studying the H_2–Ar collisions and interactions

N. Stolarczyk, G. Kowzan, F. Thibault, H. Cybulski, M. Słowiński, Y. Tan, J. Wang, A.-W. Liu, S.-M. Hu, P. Wcisło

The Journal of Chemical Physics 158, 094303 (2023)

DOI: 10.1063/5.0139229

B CO-Ar collisions: *ab initio* model matches experimental spectra at a sub percent level over a wide pressure range

E. A. Serov, **N. Stolarczyk**, D. S. Makarov, I. N. Vilkov, G. Yu. Golubatnikov, A. A. Balashov, M. A. Koshelev, P. Wcisło, F. Thibault, M. Yu. Tretyakov

Journal of Quantitative Spectroscopy and Radiative Transfer 272, 107807 (2021)

DOI: 10.1016/j.jqsrt.2021.107807

C The first comprehensive dataset of beyond-Voigt line-shape parameters from *ab initio* quantum scattering calculations for the HITRAN database: He-perturbed H_2 case study

P. Wcisło, F. Thibault, **N. Stolarczyk**, H. Jóźwiak, M. Słowiński, M. Gancewski, K. Stankiewicz, M. Konefał, S. Kassi, A. Campargue, Y. Tan, J. Wang, K. Patkowski, R. Ciuryło, D. Lisak, R. Kochanov, L. S. Rothman, I. E. Gordon

Journal of Quantitative Spectroscopy and Radiative Transfer 260, 107477 (2021)

DOI: 10.1016/j.jqsrt.2020.107477

D Accurate calculations of beyond-Voigt line-shape parameters from first principles for the He-perturbed HD rovibrational lines: A comprehensive dataset in the HITRAN DPL format

K. Stankiewicz, **N. Stolarczyk**, H. Jóźwiak, F. Thibault, P. Wcisło

Journal of Quantitative Spectroscopy and Radiative Transfer 276, 107911 (2021)

DOI: 10.1016/j.jqsrt.2021.107911

E Accurate reference spectra of HD in an H_2–He bath for planetary applications

H. Jóźwiak, **N. Stolarczyk**, K. Stankiewicz, M. Zaborowski, D. Lisak, S. Wójtewicz, P. Jankowski, K. Patkowski, K. Szalewicz, F. Thibault, I.E. Gordon, P. Wcisło

Astronomy & Astrophysics in press (2024)

DOI: 10.1051/0004-6361/202449889

F Collisional line-shape effects in accurate He-perturbed H_2 spectra

M. Słowiński, H. Jóźwiak, M. Gancewski, K. Stankiewicz, **N. Stolarczyk**, Y. Tan, J. Wang, A.-W. Liu, S.-M. Hu, S. Kassi, A. Campargue, K. Patkowski, P. S. Żuchowski, R. Ciuryło, F. Thibault, P. Wcisło

Journal of Quantitative Spectroscopy and Radiative Transfer 277, 107951 (2022)

DOI: 10.1016/j.jqsrt.2021.107951

G Inhomogeneous broadening, narrowing and shift of molecular lines under frequent velocity-changing collisions

N. Stolarczyk, P. Wcisło, R. Ciuryło

Journal of Quantitative Spectroscopy and Radiative Transfer 287, 108246 (2022)

DOI: 10.1016/j.jqsrt.2022.108246

H Spectral line shape in the limit of frequent velocity-changing collisions

N. Stolarczyk, P. Wcisło, R. Ciuryło

Physical Review A 108, 032810 (2023)

DOI: 10.1103/PhysRevA.108.032810

INTRODUCTION

The main goal of this dissertation is to provide high-accuracy theoretical molecular spectra, arising from the first principles. Within this dissertation we worked on development and refinement of the methodology of simulating the spectral line profiles from the spectral line-shape parameters obtained through the *ab initio* quantum scattering calculations. While the quantum-scattering calculations are a part of the methodology pipeline, this dissertation focuses on calculations of the spectral line-shape parameters and modelling of the line profile. The methodology allows one to connect the theoretical calculations with the experimental results, through the comparison of the simulated and measured lines. We tested and validated the methodology against the highly-accurate experimental spectra. With the *ab initio* calculations, we provided the datasets of the spectral line-shape parameters for the HITRAN database, as well as prepared application-oriented dataset for astrophysical research. Finally, we addressed the computational challenges of simulating the spectral lines in the regime of frequent velocity-changing collisions and developed new, simple and efficient approach to describe the shape of the spectral line in these conditions.

The foundation of describing the shapes of isolated molecular transitions was established by Woldemar Voigt in 1912 [1]. Even though eleven decades have passed, the Voigt profile is still sufficiently accurate to model the majority of the spectral lines for laboratory and observational applications. The Voigt profile is also a reference point, and its extensions give rise to the sophisticated and extremely accurate spectral line-shape profiles. Within this dissertation we calculate the Voigt profile parameters, the collisional broadening and shift. We also consider the speed dependences of the broadening and shift parameters [2, 3]. Finally, we take into account the Dicke effect, which is described by the complex Dicke parameter [4]. These six parameters, together with the intensity and position, encompass all the necessary information to model the shape of the spectral line within the Hartman-Tran model [5–9] and its extensions [10–12].

The pioneering articles of Michael Baranger from 1958 [13–15], extended by Ugo Fano [16], and Abraham Ben-Rueven [17, 18], ultimately concluded by Siegfried Hess [19], constitute a framework connecting the phenomenological molecular spectroscopy with the collisional transport theory. Our methodology relies on the use of the generalized Hess method [19–21] to calculate the spectral line-shape parameters and application of the suitable line-shape profile to simulate the shapes of the molecular optical resonances.

This dissertation is devoted to testing, applying and extending the methodology of simulating the spectral lines from first principles. Articles **A**, **B**, **C**, **E** and **F** focus on validation of our theoretical spectral lines by comparison with highly-accurate experimental spectra. Articles **C** and **D** aim to provide two complete, comprehensive datasets, allowing one to simulate the spectral lines of the two isotopologues of molecular hydrogen with minimal effort, still maintaining high accuracy. The data can be accessed through the supplementary material to our work, or through the HITRAN database. A dataset of the most important HD lines perturbed by He and H_2 is also featured in article **E**. The data in articles **C**, **D** and **E** are reported in the double-power-law (DPL) temperature-dependence format, which allows one to simulate the spectral lines at temperatures between 20 and 1000 K. Articles **E**, **F**, **G** and **H** are devoted to the part of the methodology concerning the shapes of the optical lines. In article **E**, we discuss the applicability of our methodology to astrophysical research and highlight the advantages of our approach over traditionally-used tools. In article **F**, we introduce analytical tools to quantize the uncertainties of our methodology on the final line-shape profile, which will support the future conclusions of the fundamental research, drawn through the comparison of the experimental profiles with the simulated ones. Finally, in Articles **G** and **H**, we derive new approach of modelling the spectral lines in the regime of the frequent velocity-changing collisions, thus extending the applicability of our methodology to this range at significantly lower computational cost.

In article **A** we put our methodology to a test against the experimental spectra. We compare the results of the most accurate *ab initio* quantum scattering calculations with the state-of-the-art experimental spectra of the S(1) 3-0 line of H_2 perturbed by Ar. This molecular system offers unique conditions to validate our *ab initio* methodology due to the high mass ratio between the collisional partners, as well as pronounced speed dependence of collisional broadening and shift [22, 23]. We test the accuracy of several approaches to generate the synthetic spectra by adopting a sequence of corrections to the theoretical model. In the most accurate version, our *ab initio* profile reproduces the experimental measurements with 1.58% agreement. We find that the calculated and measured pressure shift differ by 20%. Careful analysis of both the experimental and theoretical uncertainties leds to the conclusion that the shift parameter is extremely sensitive to the inaccuracies of the potential energy surface (PES).

Article **B** constitutes another test of our methodology. Not only do we calculate the collisional line-shape parameters based on two independent potential energy surfaces, but also we verify their accuracy on theoretical data measured with three different spectrometers: the Video spectrometer, operating at pressures from 10 to 500 mTorr, the Radioacoustic detection spectrometer, operating at pressures between 0.1 and 2 Torr, and the Resonator spectrometer, allowing us to perform measurements at range from 772 to 1525 Torr. This research shows that our *ab initio* spectral line-shape methodology reproduces the experimental measurements with accuracy below one percent, at pressure range spanning six orders of magnitude.

While the works **A** and **B** focus on single transitions, the articles **C** and **D** demonstrate the capabilities of our *ab initio* methodology of calculating the spectral line-shape parameters on a broad array of molecular lines. We perform our collision-induced line-shape calculations to prepare two datasets containing 3480 lines of He-perturbed H_2 (article **A**), and 11575 lines of He-perturbed HD (article **B**). Both datasets are provided in the double-power-law (DPL) temperature dependence format [24, 25]. These datasets allow one to model the entire rovibrational spectrum of H_2 and HD with high accuracy (below 1% for the tested lines), at temperature range between 20 and 1000 K. Both datasets have been made available in the HITRAN database.

In article **E** we focus on providing the first accurate data for the molecule-molecule collisional system. We calculate highly-accurate line-shape parameters of the three H_2-perturbed HD lines essential from the perspective of planetary research. We analyze the accuracy of the spectral line-shape models at thermodynamical conditions known to be present in the atmospheres of the Solar Systems giant planets. We find that, under these conditions, a key role is played by the speed dependence of collisional broadening and shift, as well as the Dicke effect. Therefore, applying the traditional Voigt profile might alter the effective height and width of the spectral line by as much as a factor of two. We also report significant difference between H_2- and He-perturbed spectra of HD, indicating the importance of using different data, depending on the composition of the planetary atmospheres in the astrophysical analyses. The article is supplemented with the accurate dataset of thee HD lines perturbed by H_2 and He, which should increase the accuracy of the future astrophysical research.

In article **F**, we perform highly-accurate test of our *ab initio* methodology against experimental data of the S(1) 3-0 and Q(1) 2-0 lines of H_2 perturbed by He. We use the experimental data to verify that each of the six independent collisional line-shape effects (pressure broadening and shift, their speed dependences, and the real and imaginary part of the complex Dicke effect) contributes to improving the accuracy of the spectral line-shape modelling. From the perspective of this dissertation, the most important result of article **F** is the development of analytical tools allowing one to assess the uncertainties of the final spectral line profiles, based on the uncertainties of the parameters in use.

Applying our spectral line-shape methodology in the regime of frequent velocity-changing collisions is a computational challenge [10, 11, 26]. Modelling the spectral lines with high accuracy requires extremely efficient computational infrastructure and can be too time-consuming to be performed in real time. In articles **G** and **H**, we explore the behaviour of the spectral lines in the regime of the frequent velocity-changing collisions. We demonstrate that the sophisticated line profiles (i.e., Hartman-Tran profile, or quadratic speed-dependent hard collision profile [7–9], and the billard ball profile [10, 11]) take the form equivalent with a simple Lorentz profile. We derive analytical formulas to calculate the broadening and shift of this effective Lorentz profile. Our approximations offer important insights in the line-shape theory: the speed-dependence of collisional width gives rise to effective narrowing of the line, while the presence of the speed-dependence of the collisional shift broadens the profile. We also quantify the nontrivial influence of the thermal average of the product of speed dependence of the broadening and shift on the effective line shift parameter.

AUTHOR CONTRIBUTION STATEMENT

Article A

In Article **A**, I was responsible for the comparison of theoretical and experimental data. I processed the raw experimental data and calculated the values of the spectral line-shape parameters from the generalized spectroscopic cross sections. I simulated the synthetic shapes of the spectral line in several configurations of physical assumptions and based on different models. Once the discrepancy between theoretical and experimental line shape arose, I investigated its source, by estimating the inaccuracies and propagation of the errors on various stages of the methodology on the final line shape.

My work is described in Secs. III.B (part), III.C, IV, V, VI and the Appendix.

I wrote and edited the majority of the manuscript, including the preparation of the corresponding figures and tables. I was responsible for coordination of the project and drawing the conclusions of this research.

Article B

In Article **B**, I was responsible for the comparison of theoretical and experimental data. I calculated the values of the spectral line-shape parameters from the generalized spectroscopic cross sections, including their speed dependences and temperature dependences. I simulated the synthetic shapes of the spectral line, applying the model suitable for each of the three measurement apparatuses. I applied a series of the line-shape models to probe the occurrence of different physical phenomena under varying conditions. The tests performed by me delivered the proof of validity of our *ab initio* methodology of simulating the spectral line shapes in very wide pressure range.

My work is described in Secs. 3.4, 3.5, 3.6, 4, 5 as well as the two Appendices, A and B.

I wrote and edited approximately half of the manuscript, including the preparation of the corresponding figures and tables. I was responsible for drawing the conclusions of this research.

Article C

In article **C**, I calculated the spectral line shape parameters, including their speed dependences, from the generalized spectroscopic cross sections. I performed interpolation and extrapolation of the subset of the *ab initio* data to populate the entire dataset of the parameters for 3480 lines. I refined and optimized the DPL fitting procedure. For each of the lines, I provided the DPL temperature dependences and prepared the input files consistent with the HITRAN database format.

My work is described in Secs. 2 (part), 3.2, 3.3, 3.4, and 4.

I wrote the part of the manuscript concerning my results, including the preparation of the corresponding figures and tables.

Article D

In article **D**, I calculated the spectral line shape parameters, including their speed dependences, from the generalized spectroscopic cross sections. I performed interpolation and extrapolation of the subset of the *ab initio* data to populate the entire dataset of the parameters for 11575 lines. For each of the lines, I provided the DPL temperature dependences and prepared the input files consistent with the HITRAN database format.

My work is described in Secs. 2.1 and 3.2.

I wrote the part of the manuscript concerning my results, including the preparation of the corresponding figures.

Article E

In Article **E**, I calculated the spectral line shape parameters, including their speed dependences, from the generalized spectroscopic cross sections. I provided the DPL temperature dependences and prepared the input files consistent with the HITRAN database format. I prepared the thermodynamical conditions overview of the Solar System giant planets and simulated the shapes of the spectral lines in the respective regimes. I estimated the error introduced by using the simple Voigt profile at these regimes. Using the pre-existing experimental apparatus, I performed measurements of the H_2-perturbed D_2 lines and compared these with the *ab initio* data to validate our methodology. Finally, I provided a comparison of our *ab initio* results with the other available experimental data.

My work is described in Secs. 2 (part), 3, 4 (part), and the Appendices D and E.

I wrote the part of the manuscript concerning my results, including the preparation of the corresponding figures and tables. I was partially responsible for drawing the conclusions of this research.

Article F

In article **F**, my contribution was the analysis of the propagation of the uncertainties of the line-shape parameters to the final uncertainty of the spectral line shape. I assessed the uncertainty of the theoretical spectral line profile (in terms of residuals and relative root mean square error, rRMSE) for the analyzed transition. I developed analytical tools to estimate the propagation of the uncertainty on the broadening and shift parameters on the final spectral lines.

My work is described in Secs. 4.3 and the Appendix A.

I wrote the part of the manuscript concerning my results, including the preparation of the corresponding figures.

Article G

In article **G**, I worked with the theoretical derivation of the model of the spectral line in the regime of the frequent velocity-changing collisions. I conduced the mathematical reasoning, validated the results numerically, as well as by comparison with the existing data.

The role of the co-authors was mostly supporting, mentoring and consulting the results. Almost entire manuscript concerns my work.

I wrote almost the entire manuscript, including the preparation of the corresponding figures and tables. The co-authors have written the Appendix B.

Article H

In article **H**, I worked with extending the theoretical model developed in article **G** to include the mass ratio of the collisional partners. I conduced the mathematical reasoning, validated the results numerically, using the data from the *ab initio* calculations.

The role of the co-authors was mostly supporting, mentoring and consulting the results. Almost entire manuscript concerns my work.

I had the primary role in writing the manuscript, including the preparation of the corresponding figures and tables. The co-authors have written both the Appendices A and B.

BIBLIOGRAPHY

[1] W. Voigt. Über das Gesetz der Intensitätsverteilurg innerhalb der Linien eines Gasspektrnms. *Sitzber. K.B. Akad. Wiss. München, Math-Phys. Klasse*, pages 603–620, 1912.

[2] R. Ciuryło, R. Jaworski, J. Jurkowski, A. S. Pine, and J. Szudy. Spectral line shapes modeled by a quadratic speed-dependent Galatry profile. *Phys. Rev. A*, 63:032507, 2001. `doi:10.1103/PhysRevA.63.032507`.

[3] R Ciuryło. Shapes of pressure- and doppler-broadened spectral lines in the core and near wings. *Phys Rev A*, 58(2):1029–1039, 1998. `doi:10.1103/PhysRevA.58.1029`.

[4] RH Dicke. The effect of collisions upon the doppler width of spectral lines. *Phys Rev*, 89(2):472–473, 1953. `doi:10.1103/PhysRev.89.472`.

[5] D. Bohm and E. P. Gross. Theory of plasma oscillations. A. Origin of medium-like behavior. *Phys. Rev.*, 75:1851–1864, Jun 1949. `doi:10.1103/PhysRev.75.1851`.

[6] M Nelkin and A Ghatak. Simple binary collision model for Van Hove's $G_s(r,t)$. *Phys Rev*, 135(1A):A4–A9, 1964. `doi:10.1103/PhysRev.135.A4`.

[7] H Tran, N H Ngo, and J-M Hartmann. Efficient computation of some speed-dependent isolated line profiles. *J. Quant. Spectrosc. Radiat. Transfer*, 129:199–203, 2013. `doi:10.1016/j.jqsrt.2013.06.015`.

[8] H Tran, N H Ngo, and J-M Hartmann. Erratum to "efficient computation of some speed-dependent isolated line profiles" [J. Quant. Spectrosc. Radiat. Transfer 2013; 129: 199–203]. *J. Quant. Spectrosc. Radiat. Transfer*, 134:104, 2014. `doi:10.1016/j.jqsrt.2013.10.015`.

[9] Jonathan Tennyson, Peter F. Bernath, Alain Campargue, Attila G. Császár, Ludovic Daumont, Robert R. Gamache, Joseph T. Hodges, Daniel Lisak, Olga V. Naumenko, Laurence S. Rothman, Ha Tran, Nikolai F. Zobov, Jeanna Buldyreva, Chris D. Boone, Maria Domenica De Vizia,

Livio Gianfrani, Jean-Michel Hartmann, Robert McPheat, Damien Weidmann, Jonathan Murray, Ngoc Hoa Ngo, and Oleg L. Polyansky. Recommended isolated-line profile for representing high-resolution spectroscopic transitions (IUPAC technical report). *Pure Appl. Chem.*, 86:1931–1943, 2014. `doi:10.1515/pac-2014-0208`.

[10] Michael J. Lindenfeld. Self–structure factor of hard-sphere gases for arbitrary ratio of bath to test particle masses. *J. Chem. Phys.*, 73:5817–5829, 1980. `doi:10.1063/1.440066`.

[11] P. F. Liao, J. E. Bjorkholm, and P. R. Berman. Effects of velocity-changing collisions on two-photon and stepwise-absorption spectroscopic line shapes. *Phys. Rev. A*, 21:1927–1938, Jun 1980. `doi:10.1103/PhysRevA.21.1927`.

[12] Robert Blackmore, Sheldon Green, and Louis Monchick. Dicke narrowing of the polarized Stokes–Raman Q branch of the v=0$\rightarrow$1 transition of D_2 in He. *J. Chem. Phys.*, 91(7):3846–3853, 1989. `doi:10.1063/1.457640`.

[13] Michel Baranger. Simplified quantum-mechanical theory of pressure broadening. *Phys. Rev.*, 111:481–493, Jul 1958. `doi:10.1103/PhysRev.111.481`.

[14] Michel Baranger. Problem of overlapping lines in the theory of pressure broadening. *Phys. Rev.*, 111:494–504, Jul 1958. `doi:10.1103/PhysRev.111.494`.

[15] Michel Baranger. General impact theory of pressure broadening. *Phys. Rev.*, 112:855–865, Nov 1958. `doi:10.1103/PhysRev.112.855`.

[16] U. Fano. Pressure broadening as a prototype of relaxation. *Phys. Rev.*, 131:259–268, Jul 1963. `doi:10.1103/PhysRev.131.259`.

[17] A. Ben-Reuven. Symmetry considerations in pressure-broadening theory. *Phys. Rev.*, 141:34, 1966. `doi:10.1103/PhysRev.141.34`.

[18] A. Ben-Reuven. Impact broadening of microwave spectra. *Phys. Rev.*, 145:7, 1966. `doi:10.1103/PhysRev.145.7`.

[19] S Hess. Kinetic theory of spectral line shapes. The transition between doppler broadening and collisional broadening. *Physica*, 61(1):80–94, 1972. `doi:10.1016/0031-8914(72)90035-3`.

[20] GC Corey and FR McCourt. Dicke narrowing and collisional broadening of spectral lines in dilute molecular gases. *J Chem Phys*, 81(5):2318–2329, 1984. `doi:10.1063/1.447930`.

[21] L Monchick and LW Hunter. Diatomic–diatomic molecular collision integrals for pressure broadening and Dicke narrowing: A generalization of Hess's theory. *J Chem Phys*, 85(2):713–718, 1986. `doi:10.1063/1.451277`.

[22] P. Wcisło, H. Tran, S. Kassi, A. Campargue, F. Thibault, and R. Ciuryło. Velocity-changing collisions in pure H_2 and H_2-Ar mixture. *J Chem Phys*, 141(7):074301, aug 2014. `doi:10.1063/1.4892414`.

[23] P Wcisło, F Thibault, H Cybulski, and R Ciuryło. Strong competition between velocity-changing and phase- or state-changing collisions in h_2 spectra perturbed by Ar. *Phys Rev A*, 91:052505, 2015. `doi:10.1103/PhysRevA.91.052505`.

[24] RR Gamache and B Vispoel. On the temperature dependence of half-widths and line shifts for molecular transitions in the microwave and infrared regions. *J Quant Spectrosc Radiat Transf*, 217:440–452, 2018. `doi:10.1016/j.jqsrt.2018.05.019`.

[25] N Stolarczyk, F Thibault, H Cybulski, H Jóźwiak, G Kowzan, B Vispoel, IE Gordon, LS Rothman, RR Gamache, and P Wcisło. Evaluation of different parameterizations of temperature dependences of the line-shape parameters based on ab initio calculations: Case study for the HITRAN database. *J Quant Spectrosc Radiat Transf*, 240:106676, 2020. `doi:10.1016/j.jqsrt.2019.106676`.

[26] P Wcisło, A Cygan, D Lisak, and R Ciuryło. Iterative approach to line-shape calculations based on the transport-relaxation equation. *Phys Rev A*, 88(1):012517, 2013. `doi:10.1103/physreva.88.012517`.

The Journal of Chemical Physics
ARTICLE
scitation.org/journal/jcp

High-precision cavity-enhanced spectroscopy for studying the H_2–Ar collisions and interactions

Cite as: J. Chem. Phys. **158**, 094303 (2023); doi: 10.1063/5.0139229
Submitted: 19 December 2022 • Accepted: 13 February 2023 •

N. Stolarczyk,[1,2,a)] G. Kowzan,[1] F. Thibault,[3] H. Cybulski,[4] M. Słowiński,[1] Y. Tan,[2] J. Wang,[2] A.-W. Liu,[2] S.-M. Hu,[2] and P. Wcisło[1,b)]

AFFILIATIONS

[1] Faculty of Physics, Institute of Physics, Astronomy and Informatics, Nicolaus Copernicus University in ToruńGrudziądzka 587-100Toruń, Poland
[2] Hefei National Laboratory for Physical Sciences at Microscale, iChem Center, University of Science and Technology of China, Hefei 230026, China
[3] Univ Rennes, CNRS, IPR (Institut de Physique de Rennes)-UMR 6251, F-35000 Rennes, France
[4] Faculty of Physics, Kazimierz Wielki University, al. Powstańców Wielkopolskich 2, 85-090 Bydgoszcz, Poland

[a)] Author to whom correspondence should be addressed: NikodemStolarczyk319@gmail.com
[b)] Electronic mail: piotr.wcislo@umk.pl

ABSTRACT

Information about molecular collisions is encoded in the shapes of collision-perturbed molecular resonances. This connection between molecular interactions and line shapes is most clearly seen in simple systems, such as the molecular hydrogen perturbed by a noble gas atom. We study the H_2–Ar system by means of highly accurate absorption spectroscopy and *ab initio* calculations. On the one hand, we use the cavity-ring-down-spectroscopy technique to record the shapes of the S(1) 3-0 line of molecular hydrogen perturbed by argon. On the other hand, we simulate the shapes of this line using *ab initio* quantum-scattering calculations performed on our accurate H_2–Ar potential energy surface (PES). In order to validate the PES and the methodology of quantum-scattering calculations separately from the model of velocity-changing collisions, we measured the spectra in experimental conditions in which the influence of the latter is relatively minor. In these conditions, our theoretical collision-perturbed line shapes reproduce the raw experimental spectra at the percent level. However, the collisional shift, δ_0, differs from the experimental value by 20%. Compared to other line-shape parameters, collisional shift displays much higher sensitivity to various technical aspects of the computational methodology. We identify the contributors to this large error and find the inaccuracies of the PES to be the dominant factor. With regard to the quantum scattering methodology, we demonstrate that treating the centrifugal distortion in a simple, approximate manner is sufficient to obtain the percent-level accuracy of collisional spectra.

I. INTRODUCTION

Molecular hydrogen is a benchmark system for studying non-classical effects due to its large molecular rotational constant. Collisions involving H_2 display many atypical features, since H_2 does not provide any inelastic scattering channels at temperatures up to several hundred K.[1] Due to this, collision-induced spectroscopic effects in the molecular hydrogen spectrum are dominated by velocity-changing collisions.[2] Thus, the rovibrational lines of H_2 are strongly affected by the Dicke narrowing.[3,4] Moreover, the speed dependence of collisional broadening and shift[5,6] as well as their interplay with the velocity-changing collisions[4] are unusual in the spectral lines of molecular hydrogen.

Due to its simplicity, the H_2 molecule is accessible for the calculations from first principles, which makes it a perfect system to study the entire methodology of *ab initio* line-shape calculations, from intermolecular potential-energy surfaces (PES) to the quantum scattering calculations, velocity-changing collisions models, and spectral line-shape profiles.[1,7–12]

Experimental measurements of the H_2–H_2 interaction, as well as interactions with noble gas atoms, have been performed for decades.[13–17] Recently, Perreault *et al.* measured rotationally inelastic scattering of HD with molecular deuterium[18] and with helium atoms[19] in supersonic beams at 1 K. Subsequent quantum scattering calculations[20] found very good agreement with the measurements.

In this paper, we report an analysis of a more complex system, i.e., H_2 perturbed by argon. The interaction with a 20-times-heavier perturber hampers the modeling of the velocity-changing collisions. Indeed, this problem has already been addressed in Refs. 4 and 9 and required a separate treatment of speed and velocity-changing collisions. Here, we adjust the experimental conditions in order to diminish the importance of the velocity-changing collision model and focus on the still-unresolved problem of the difference between the theoretical and experimental line shift.[4]

This work analyzes the S(1) 3-0 transition in molecular hydrogen perturbed by argon. We perform highly accurate cavity ring-down spectroscopy (CRDS) measurements to collect the collision-induced spectral line shapes. Simultaneously, we perform fully *ab initio* quantum scattering calculations on our accurate H_2–Ar PES to simulate the theoretical line profiles.

We consider several different approaches to describing the theoretical spectral line-shape profiles, gradually adding subsequent corrections to the model. Starting from the base case, we refine our methodology by including the effects of centrifugal distortion in a simplified manner (simple CD), a more complete treatment of centrifugal distortion (full CD), and the effects of vibrational coupling (VC). Neglecting these effects in our calculations results in the 6% error of the pressure broadening and shift parameters, γ_0 and δ_0. (Note that error in other line-shape parameters has a much smaller impact on the resulting spectra.[10] Although for molecular hydrogen the effect of the Dicke parameter is non-negligible, its value is insensitive to CD and VC corrections.) Both the full CD treatment and inclusion of the VC significantly increase the complexity of the calculations. Additionally, for VC, the computational cost is significantly increased relative to simpler cases. We find that just the inclusion of the simplified CD already accounts for the majority of the corrections and reduces the error in the line–shapes parameters from 6% to below 1%. This finding would result in a significant reduction of the numerical cost of future *ab initio* line-shape calculations. One should, however, perform additional tests prior to generalizing this observation to other transitions and molecular collisional systems.

While we achieve agreement at a level of 1.6% between theory and measurement in terms of the shape of the line, the experimental and theoretical values of the shift parameter, δ_0, differ by 20%. We consider various factors both on the theoretical and experimental side to explain this discrepancy. We find that the δ_0 parameter is exceptionally sensitive to various computational aspects of our *ab initio* methodology and that the major contribution to this difference originates from inaccuracies of the PES.

II. CAVITY-ENHANCED MEASUREMENTS

We perform the cavity ring-down spectroscopy (CRDS) measurements of the S(1) 3-0 line of H_2 perturbed by Ar using the experimental setup presented in Fig. 1. We use a 1-m long optical cavity with a finesse equal to 63 000. The reflectivity of the cavity mirrors is 99.995%, and one of the two mirrors is attached to a piezoelectric servomechanism in order to match the cavity modes with the probe laser frequency. We use a Ti:sapphire laser source (Coherent 899-21) pumped by a 532-nm solid laser (Verdi-18). A beam from the probe laser after the acousto-optic modulator (AOM2) and the electro-optic modulator (EOM) is locked to a temperature-stabilized (ΔT ≈ 10 mK at 302 K) ultralow expansion (ULE) etalon with the Pound–Drever–Hall method.[21] In this way, the probe laser frequency could be tuned with sub-MHz resolution. The absolute frequency is calibrated by a wavemeter with an accuracy better than 10 MHz. The cavity ring-down spectra are recorded in step-scan mode. A single step usually consists of 100 ring-down events initiated by chopping the laser beam with the AOM1. We apply a least squares fitting procedure to fit the exponential curve to the ring-down signal to retrieve the absorption coefficient at a given point. See Refs. 22 and 23 for the detailed description of each subsystem of the setup.

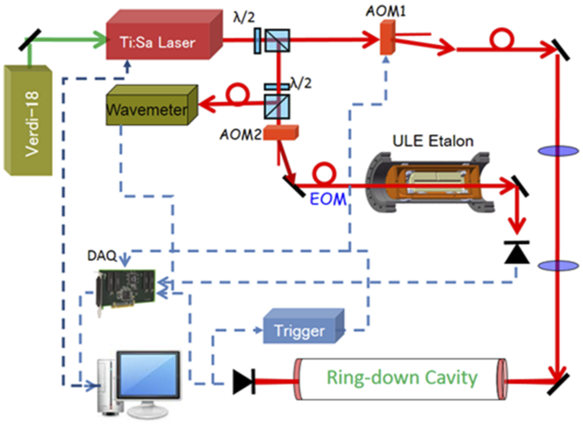

FIG. 1. Cavity ring-down spectrometer in Hefei laboratory. AOM and EOM are the acousto- and electro-optic modulators, respectively, and Verdi-18 is the laser source used for Ti:Sapphire laser pumping. The frequency of the laser is stabilized to the ultra-low-expansion (ULE) etalon, allowing us to reach the stability of 10 MHz.

The spectra are collected at room temperature for different proportions of the H_2 to Ar partial pressures, i.e., 1:1, 1:2, 1:4, and 1:7, with the H_2 pressure being kept 12.4 kPa. The accuracy of the pressure gauge is 1%.

III. *AB INITIO* LINE-SHAPE CALCULATIONS

This section discusses the theoretical analysis of the shape of the isolated S(1) 3-0 rovibrational spectral line of H_2 perturbed by Ar. We perform fully *ab initio* calculations within the framework of the generalized Hess method (GHM).[24–26] In the following subsections, we provide details of the potential energy surface (PES), quantum scattering calculations, generalized spectroscopic cross sections, as well as calculations of the line-shape parameters and line-shape model.

A. Potential energy surface

We use our H_2–Ar potential energy surface (PES)[4] calculated by means of the spin-restricted coupled-cluster with single, double, and perturbative triple excitations [CCSD(T)] method employing the large aug-cc-pCVQZ basis set.[27–30] This basis was further extended with a set of $3s3p2d2f1g1h$ midbond functions,[31,32] denoted as 332 211, with exponents of 0.90, 0.30, and 0.10 for s and

p, 0.60 and 0.20 for d and f, and 0.30 for g and h functions that were placed in the middle of the van der Waals bond.

The interaction energies corrected for the basis set superposition error using the counterpoise (CP) method[33] were evaluated using the MOLPRO program 2010.1[34] and 2012.1[35] versions. In the calculations, all electrons were correlated.

To accurately reproduce features of the H_2–Ar PES, the calculations of intermolecular interaction energy were performed for 2960 geometries of the system. The intermolecular distance R was varied in a range from 1.70 to 20.00 Å (37 points in total) covering some part of the repulsive wall (up to about 20 000 cm^{-1}), the entire van der Waals well and long-range (interaction energy slightly above -5×10^{-3} cm^{-1}) regions. The values of the θ angle were chosen to correspond to the abscissas of nine-point Lobatto–Gauss quadrature. Because of the symmetry of the system, the calculations were done only for five different angles. The H–H bond length r_{HH} was stretched from 0.30 to 1.8 Å in steps of 0.10 Å.

Our PES is expanded in the basis of even Legendre polynomials up to the 8th order. To include the effects of centrifugal distortion (CD) and vibrational coupling (VC), the matrix elements for the collisional coupling between the rovibrational wavefunctions of H_2, $\langle v'j'|V_l(R,r_{\text{HH}})|v''j''\rangle$, were calculated for $v', v'' = 0, \ldots, 5$ and $j', j'' = 1, 3, \ldots, 15$, where v and j stand for the vibrational and rotational quantum numbers, while $'$ and $''$ mark the final and initial states, respectively.

Finally, we have repeated the PES calculations, taking into account relativistic effects. To do so, the CCSD(T) calculations were performed using the second-order Douglas–Kroll–Hess (DKH) Hamiltonian[36–38] with the aug-cc-pCVQZ-DK basis set.[39] The basis set was also enhanced with the 332 211 midbond functions placed in the middle of the van der Waals bond. The calculations were done for all the 2960 geometries of the system. In Sec. IV, we compare the results obtained with these two versions of PES.

B. Generalized spectroscopic cross sections and spectral line-shape parameters

The scattering problem was solved at different levels of approximation to estimate the influence of CD and VC. In all the cases, S-matrices were obtained by solving the close coupling equations numerically[40,41] with the log-derivative propagator[42,43] using the MOLSCAT code.[44] The equations were propagated starting at either the separation distance, R set to 1.01 or 1.7 Å, but we found the differences between these two cases to be negligible. The maximum propagation distance was set to at least 20 Å. To determine whether it needs to be increased, we calculated the position of the furthest classical turning point in the centrifugal potential, R_{cent}. If $2.5R_{\text{cent}}$ was larger than 20 Å, the maximum propagation distance was set to $2.5R_{\text{cent}}$. We verified that increasing the distance beyond that point (e.g., to $4.0R_{\text{cent}}$) resulted in negligible differences. We obtained the values of $\langle v'j'|V_l(R,r_{\text{HH}})|v''j''\rangle$ for $R > 20$ Å in two ways. For $v' = v''$, $l = 0$, the matrix elements were extrapolated with a simple phenomenological dependence, a/R^n, fitted in the 15 Å $< R <$ 20 Å region. In the remaining cases, the values of the matrix elements for distances approaching $R = 20$ Å were already negligible; therefore, they were set to zero for R's beyond that point. The S-matrices were calculated at kinetic energies up to 2300 cm^{-1} at 286 points.

In the base case, in which the CD was not accounted for, the scattering equations were propagated for collisional matrix elements with $j' = j'' = 0$. Subsequently, CD was partially included by using the collisional matrix elements with $j' = j'' = 1$ in the ground vibrational state and with $j' = j'' = 3$ in the excited vibrational state. Finally, CD was fully accounted for by using the collisional matrix elements with j' and j'' matching the actual rovibrational levels included in the basis used to perform the calculations. In all the preceding cases, the scattering problem was solved separately in the ground vibrational manifold ($v' = v'' = 0$) for the initial radiative state $(v, j) = (0, 1)$ and in the excited vibrational manifold ($v' = v'' = 3$) for the final radiative state $(v, j) = (3, 3)$. The full CD calculations were subsequently expanded to include collisional coupling between different vibrational levels (VC). This was done by performing a separate set of calculations for the (0, 1) state and the (3, 3) state. The basis for scattering calculations in the former state included all open channels in the $v = 0, 1, 2$ vibrational manifolds and one closed channel in the $v = 0$ manifold. Similarly, the basis for the (3, 3) state scattering calculations included all open channels in the $v = 1, 2, 3$ vibrational manifolds and one closed channel in the $v = 3$ manifold. The $v = 0$ state was not included because the matrix elements for the collisional coupling to that state from the $v = 3$ state were negligible.

Figure 2 shows the generalized spectroscopic cross sections, which are calculated directly from the S-matrices.[25,45] The depicted cross sections were calculated with relativistic corrections of the PES including relativistic corrections, full CD, and VC (the cross sections are appended in the supplementary material). Unless stated otherwise, all the calculations within this work were performed with these cross sections.

We use these cross sections (σ_0^q denotes the broadening and shift cross section, and σ_1^q denotes the Dicke cross section) to calculate the line-shape parameters: the speed-dependent pressure broadening, $\gamma(v)$, and shift, $\delta(v)$, as well as the complex Dicke parameter, $\widetilde{\nu}_{\text{opt}}$,

$$\gamma(v) + i\delta(v) = \frac{1}{k_B T}\frac{v_{\text{pm}}^2}{\pi^{3/2} c v} e^{-\frac{v^2}{v_{\text{pm}}^2}} \int_0^\infty \sigma_0^q(v_i, j_i, v_f, j_f; E_{\text{kin}} = x k_B T) x^2 e^{-x^2} \times \sinh\left(\frac{2vx}{v_{\text{pm}}}\right) \mathrm{d}x, \tag{1}$$

$$\widetilde{\nu}_{\text{opt}} = \frac{1}{2\pi c}\frac{1}{k_B T}\langle v_r\rangle M_2 \int_0^\infty \mathrm{d}x x e^{-x}\left(\frac{2}{3} x \sigma_1^q(v_i, j_i, v_f, j_f; E_{\text{kin}} = x k_B T) - \sigma_0^q(v_i, j_i, v_f, j_f; E_{\text{kin}} = x k_B T)\right), \tag{2}$$

where c is the speed of light in vacuum, v is the active molecule speed, v_{pm} is the most probable perturber speed, $\langle v_r\rangle$ is the mean relative speed of the colliding partners, k_B is the Boltzmann constant, T is the temperature, and $M_2 = \frac{m_p}{m+m_p}$, with m and m_p being the masses of the active and perturbing molecules, respectively.

Figure 3 presents the speed dependences of the pressure broadening and shift obtained from the quantum-scattering calculations. The solid black curves present the *ab initio* speed-dependent pressure broadening and shift for the S(1) 3-0 transition in H_2 perturbed by Ar. The dashed lines mark the pressure broadening

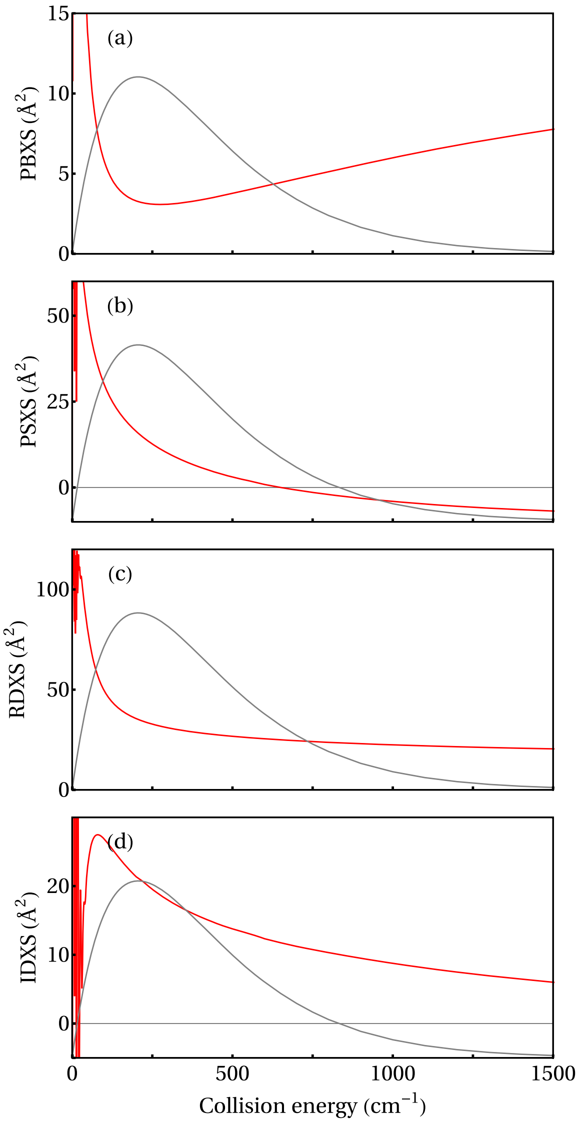

FIG. 2. Generalized spectroscopic cross sections for the S(1) 3-0 transition in H_2 perturbed by Ar are shown with red curves. (a) Pressure broadening cross section, PBXS. (b) Pressure shift cross section, PSXS. (c) Real part of the Dicke cross section, RDXS. (d) Imaginary part of the Dicke cross section, IDXS. The depicted cross sections are the results of the fully *ab intio* quantum scattering calculations with the relativistic PES, and the full CD and VC effects taken into account [the row (e) in Table I]. To quantify the statistical contributions of different collision energies, we present the Maxwell-Boltzmann distribution of the relative absorber–perturber speed at T = 296.65 K (gray thin curves). We include the cross sections in numerical form in the supplementary material.

and shift parameters averaged over the Maxwell–Boltzmann speed distribution, i.e.,

$$\gamma_0 + i\delta_0 = \frac{1}{2\pi c}\frac{1}{k_B T}\langle v_r\rangle \int dx\; x e^{-x}\sigma_0^q(v_i, j_i, v_f, j_f; E_{kin} = x k_B T). \tag{3}$$

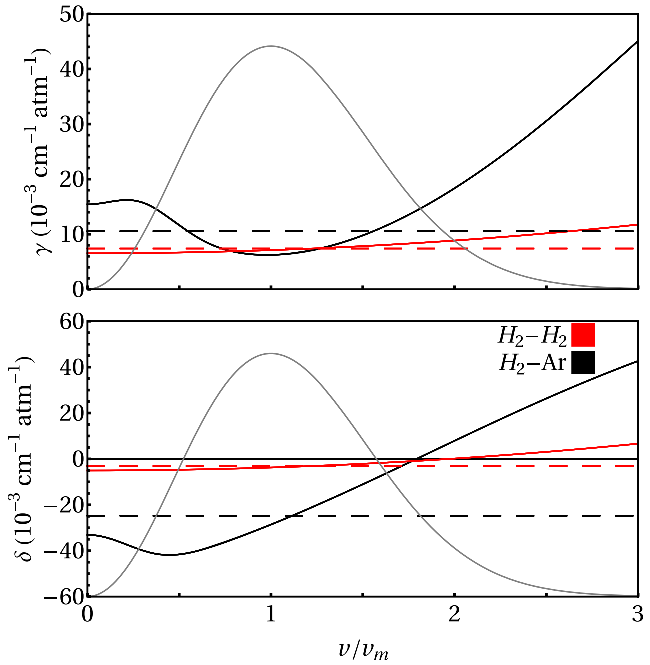

FIG. 3. Speed dependences of γ and δ for the S(1) 3-0 line in H_2 perturbed by Ar (black solid curves). We evaluate the exact speed dependence based on our fully *ab initio* quantum scattering calculations [the row (e) in Table I]. For comparison, we plot the speed dependence of γ and δ for the self-perturbed H_2 (continuous red curves), based on Table 2(f) of Ref. 13. Dashed lines mark the speed-averaged values (i.e., γ_0 and δ_0, respectively) with the same color notation. With gray curves, we mark the Maxwell–Boltzmann distribution of molecule speed. The data are presented for T = 296.65 K.

To describe the H_2–H_2 collisions, we make use of the line-shape parameters derived experimentally in Ref. 13 [see Table 2(f) therein]. The parameters were reported within the quadratic approximation, i.e.,

$$\gamma(v) + i\delta(v) \approx \gamma_0 + i\delta_0 + (\gamma_2 + i\delta_2)\left(\frac{v^2}{v_m^2} - \frac{3}{2}\right), \tag{4}$$

where[5,11]

$$\gamma_2 + i\delta_2 = \frac{v_m}{2}\frac{d}{dx}(\gamma(v) + i\delta(v))\Big|_{v=v_m}, \tag{5}$$

with v_m being the most probable absorber speed. The red curves in Fig. 3 present the speed-dependent pressure broadening and shift for the self-perturbed H_2 S(1) 3-0 line, with the corresponding dashed lines marking γ_0 and δ_0 for this system.

It is seen from Fig. 3 that the H_2–Ar system displays a much stronger speed-dependence than H_2–H_2. Even though the speed-averaged broadening parameters are similar, their speed dependences vary significantly. The speed-dependent shift parameter is roughly ten times greater in the H_2–Ar system than in H_2–H_2.

Despite using the fully *ab initio* speed dependence of γ and δ for the H_2–Ar system, we also calculate the parameters of the quadratic approximation (γ_2 and δ_2) to quantitatively express the magnitudes of the speed dependences. The quadratic parameters are determined by the slope of the speed-dependent parameters at the most probable speed [Eq. (5)]. While the speed dependence of the shift is described well enough by the slope at this single point, this is not the case for the broadening. The speed-dependent broadening has a minimum near $v = v_m$ (see Fig. 3); hence, the γ_2 parameter is close to zero, which does not reflect the actual strong speed dependence of $\gamma(v)$.

In Table I, we report the values of the six collisional line-shape parameters, i.e., the pressure broadening and shift, γ_0 and δ_0, their speed dependences, γ_2 and δ_2, and the real and imaginary parts of the Dicke parameter, $\widetilde{\nu}^r_{\mathrm{opt}}$ and $\widetilde{\nu}^i_{\mathrm{opt}}$. Rows (a)–(e) present the H_2–Ar parameters obtained with our fully *ab initio* calculations described in this section. Each subsequent row includes additional effects taken into account, i.e., the simplified and full CD [(b) and (c)], relativistic PES corrections (rel) (d), and VC (e). Row (f) presents the same parameters as row (e); however, δ_0 was adjusted to the experimental data [see Sec. IV B]. The last row presents the H_2–H_2 parameters taken from Ref. 13.

Relativistic corrections to the PES as well as the CD and VC effects have a small impact on the line-shape parameters (see Table I). CD influences the line-shape parameters at the 2%–6% level, except for $\widetilde{\nu}^r_{\mathrm{opt}}$, which is hardly influenced at all. Interestingly, the simplified form of CD is a good approximation to the full CD; the larger influence on γ_2 (3% change) is due to the atypical behavior of $\gamma(v)$; see the discussion regarding Fig. 3. The relativistic correction to the PES has a small impact (below 2%) on the values of the line-shape parameters [again, γ_2 does not well reflect $\gamma(v)$ due to its atypical speed dependence (see Fig. 3) and the large relative change in γ_2 has a small influence on the line shape]. Similarly, VC has a very small (sub-percent) impact on the line-shape parameters. An important conclusion from the discussion on the theoretical results from Table I, from the perspective of quantum scattering calculations, is that it suffices to include only the simple CD (which does not add any numerical cost) to reduce the systematic theoretical error in the line-shape parameters from 6% to below 1% (here, we focus on γ_0 and δ_0 as they have the largest influence on the line shape; in the case of H_2 $\widetilde{\nu}^r_{\mathrm{opt}}$ has also a large influence on the line shape, but $\widetilde{\nu}^r_{\mathrm{opt}}$ is almost completely insensitive to the CD and VC corrections). This conclusion is crucial from the perspective of the optimization of the computational methodology since the inclusion of the VC increases the calculation time by a factor of ~50.

C. Line-shape model

Our *ab initio* calculations allow us to simulate a complete line profile from first principles, with no collisional parameters fitted to the experiment. We fix all the Ar-induced collisional line-shape parameters at the values obtained from our quantum-scattering calculations; see row (e) in Table I.

To simulate the theoretical profiles, we make use of the billiard ball profile.[46,47] Within this model, the description of velocity-changing collisions is based on a hard-sphere approximation of the interaction potential. The billiard ball profile is superior to the commonly used hard- and soft-collision profiles as it allows one to take into account the mass ratio, α, between the collisional partners,[10] which is especially important for the considered H_2–Ar system with $\alpha \approx 20$. In the case of such a large mass ratio, the relaxation of the velocity vector is described by two different rates.[9] The decays of its magnitude and direction are independent and require using two different time constants.[9] The hard- and soft-collision models fail in this case as they are both described by a single-parameter decay. We use the fully *ab initio* speed dependences of γ and δ [see Eq. (1)] for the Ar-perturbation contribution, while for the self-perturbation contribution we use the quadratic approximations taken from Ref. 13 [see Eq. (4)]. These two contributions are proportional to the partial pressures of the two gases.

Since our experimental setup is not equipped with the absolute frequency reference, we fit the central frequency (the same value for all four pressures). We also fit the baseline, slope, and area of each of the four lines (separate values for each pressure). Since the lowest pressure of the experiment is below the applicability range of the direct diagonalization approach to the billiard ball profile calculations,[11] we implemented the iterative approach[48] for the lowest pressure.

IV. EXPERIMENTAL VALIDATION OF THE THEORETICAL RESULTS

Figure 4 shows a direct comparison of our experimental and theoretical results. The top panel in the figure contains the measured points (black dots) and the theoretical spectral lines (red curves) calculated with the parameters from the row (e) in Table I. Panels (a)–(g) in Fig. 4 present the absolute residuals between the calculated

TABLE I. Spectral line-shape parameters for the S(1) 3-0 line in H_2 (all the line-shape values are expressed in the units of 10^{-3} cm^{-1} atm^{-1}). The fully *ab initio* speed dependence of γ and δ for the H_2–Ar system was employed. We also list the γ_2 and δ_2, defined by Eq. (5), to quantitatively express the magnitude of speed dependence. The Doppler width at $T = 296.5$ K is $\omega_D = 64.0 \times 10^{-3}$ cm^{-1}. Each row presents the parameters calculated with different effects taken into account: simple CD, full CD, relativistic effects in PES (rel), and VC. Letters (a)–(f) correspond to the annotations in Fig. 4.

		γ_0	δ_0	γ_2	δ_2	$\widetilde{\nu}^r_{\mathrm{opt}}$	$\widetilde{\nu}^i_{\mathrm{opt}}$
(a)	Without CD, rel, VC	10.5	−24.7	0.415	17.6	72.8	−15.6
(b)	Simple CD	11.2	−25.8	0.405	18.2	72.3	−16.2
(c)	Full CD	11.2	−25.9	0.390	18.2	72.3	−16.1
(d)	Full CD + rel	11.2	−26.5	0.259	18.1	72.3	−15.8
(e)	Full CD + rel + VC	11.3	−26.4	0.347	17.8	72.1	−16.1
(f)	H_2–Ar adjusted δ_0	11.3	−33.0	0.347	17.8	72.1	−16.1
	H_2–H_2, experimental[13]	7.2	−3.4	0.7	1.7	41.3	0.0

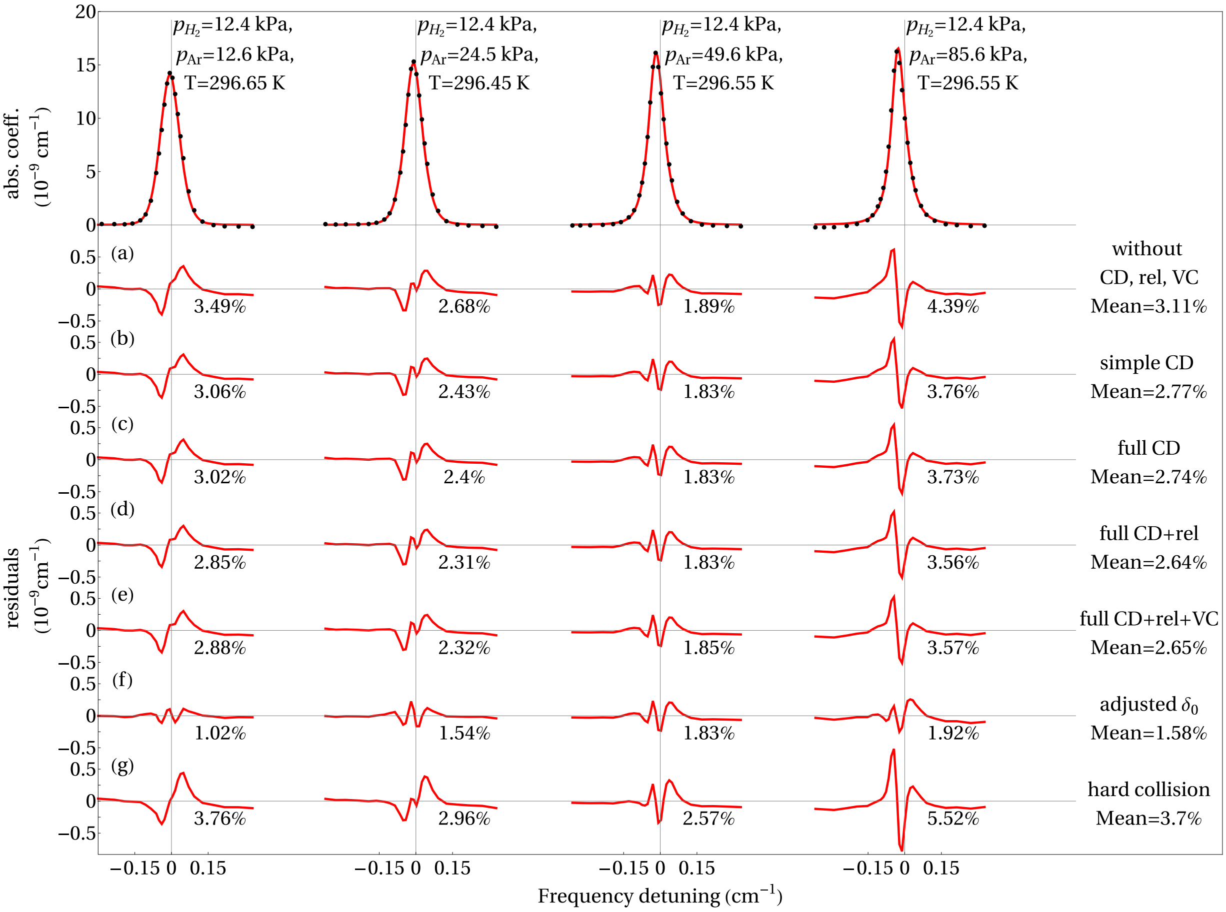

FIG. 4. The spectral line shapes of the S(1) 3-0 transition in H_2 perturbed by Ar. The top panel shows a direct comparison between the experimental (black dots) and fully *ab initio* (red curves) spectra. Panels (a)–(g) show the absolute residuals accompanied by the relative root-mean-square errors (rRMSE) calculated within ±FWHM of the line. The rightmost column contains the mean rRMSE of all pressures for a given model. Panels (a)–(f) correspond to the (a)–(f) rows of Table I, and the spectra were calculated with the respective parameters. Panel (a) shows the residuals from the fully *ab initio* model without CD, VC, and relativistic PES corrections (rel). Subsequently, we include simple (b) and full (c) CD, vibrational coupling **VC** (d), and relativistic corrections to PES (e). In panel (f), we adjust the pressure shift parameter, δ_0, with a multi-spectrum fitting procedure. Panel (g) shows exactly the same comparison as panel (e), but the billiard-ball velocity-changing collision model is replaced with the hard-collision model.

and measured profiles, as well as the relative root-mean-square error (rRMSE), calculated within ±full width at half maximum (FWHM) from the line center.

A. Experimental validation of the fully *ab initio* model

Panels (a)–(e) in Fig. 4 show the residuals of the fully *ab initio* profile described in Sec. III. The theoretical line-shape model entirely originates from the first principles, and no line-shape parameter was adjusted in this comparison.

We present several different approaches to describe the theoretical spectral line shape profiles, gradually adding subsequent corrections to the model. At each level of theory improvement, we obtain slightly different values of the spectral line-shape parameters (see Table I). While the parameters are modified by up to several percent, the corresponding differences in the line shapes (reflected by the rRMSE values) are well below a percent. The reason is twofold. On the one hand, the differences in the line-shape parameters are partially compensated by fitting the area and line position. On the other hand, the way the changes in line-shape parameters propagate on the spectra is not straightforward, this topic is covered in Appendix A of Ref. 10.

Similarly to the discussion on the line-shape parameters (see Sec. III B and Table I), the most significant improvement to the resulting line shapes is caused by taking into account the simple CD. Relativistic corrections to the PES, as well as including the full CD (in addition to the simple CD) and VC effects, have almost no effect on the rRMSE. Again, the important conclusion is that reaching the sub-percent accuracy does not require taking into account the very computationally expensive full CD and VC. Our most advanced fully *ab initio* model is in 2.65% agreement with experimental data; see panel (e) in Fig. 4.

B. *Ab initio* model with adjusted shift

The asymmetric shapes of the residuals in Figs. 4(a)–4(e) indicate that the mismatch between the experimental and theoretical spectra is mainly caused by the incorrect value of the calculated pressure shift parameter, δ_0. Indeed, adjusting δ_0 in a multispectrum fitting procedure decreases the mean rRMSE to 1.58% and results in much smaller residuals; see panel (f) in Fig. 4. The experimental δ_0 parameter is 20% larger than the calculated value (see Table I). We analyze this discrepancy in Sec. V. The conclusion is that our fully *ab initio* calculations result in a 20% discrepancy in the δ_0 parameter compared to experimental spectra, but the collision-perturbed shapes of the experimental line are reconstructed at the 1%-level.

C. The role of the velocity-changing collision model

In this section, we benefit from having accurate experimental spectra and *ab inito* line-shape parameters to test the role of a velocity-changing collision model. In our ultimate *ab initio* simulation [Fig. 4(e)], we use an advanced, realistic line-shape model, i.e., the billiard ball profile.[46,47] In this section, we substitute the billiard-ball model with a simpler and widely used hard-collision[49] profile that is much less computationally expensive [see Fig. 4(g); in panel (g), we use exactly the same values of the line-shape parameters and the full speed dependences as in (e) and only change the velocity-changing collisions model]. It is clearly seen that this modification deteriorates the agreement with the experimental spectra, as quantified by the rRMSE increase from 2.65% to 3.7%.

It should be noted that in this work the theory–experiment comparison is done in the pressure range, in which the sensitivity to the velocity-changing collisions model is relatively small. At higher pressures, above the Dicke minimum, the velocity-changing collision model has a much larger influence. We discuss this issue in Appendix; see also Fig. 5 and Ref. 4.

V. ANALYSIS OF THE DISCREPANCY IN PRESSURE SHIFT PARAMETER

We showed in Sec. IV B that, although our theoretical *ab initio* line-shape model accurately reproduces the shape of the experimental spectra, the calculated collision-induced line shift, δ_0, deviates from the experimental one by 20%. This section aims at providing an explanation for this discrepancy. In Sec. V A, we estimate the uncertainty of the experimental δ_0, which is dominated by uncertainties of the *ab initio* line-shape model used in spectrum fits. In Sec. V B, we estimate the uncertainty of the calculated δ_0.

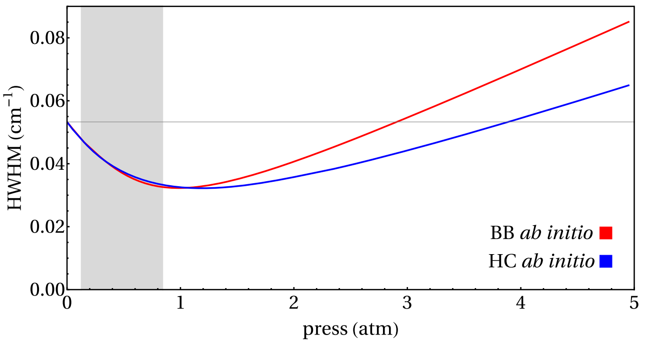

FIG. 5. Pressure dependence of the half width at half maximum (HWHM) of a spectral line. We consider two velocity-changing collision models: the *ab initio* billiard-ball model (BB *ab initio*) and the *ab initio* hard-collision model (HC *ab initio*). The gray zone marks the partial pressure range of Ar covered in our experiments. It is seen that in the range considered by us, the HWHM of the two line-shape models is almost the same.

A. Uncertainty of the experimental δ_0

The measurement uncertainties that can affect the fitted δ_0, such as the inaccuracies of the frequency measurement or statistical uncertainties, are negligible in our case. The dominant contribution to the experimental uncertainty of δ_0 comes from the uncertainty of the fitted line-shape model. By distorting the line-shape model within the estimated confidence range, we estimate the corresponding uncertainty of δ_0.

To determine the experimental value of the δ_0 parameter, we simulate the fully *ab initio* billiard ball profile and fit δ_0; see row (f) in Table I and panel (f) of Fig. 4. To determine the uncertainty of the fitted δ_0, we repeated the fit with the line-shape parameters distorted within their estimated confidence range. We include the influence of the three line-shape effects: the model of velocity-changing collisions, the narrowing and asymmetries related to the Dicke effect described by the complex Dicke parameter, $\widetilde{\nu}_{\mathrm{opt}}$, and the speed dependence of the pressure shift, δ_2 (the role of the speed dependence of the pressure broadening, γ_2, is negligible).

To estimate the uncertainties originating from the velocity-changing collision model, we substitute the kinetic-based billiard ball model with the phenomenological hard-collision model. Then, we generate an *ab initio* profile with this simplified model and repeat the fit of δ_0. We obtain a 6% smaller value of the adjusted δ_0 in this way. The estimation of this uncertainty is conservative since the difference between the hard-collision and billiard-ball collision kernels is much smaller than the difference between the billiard-ball collision kernel and the actual one; see panels (c) and (d) in Fig. 2 in Ref. 9.

In the line-shape model, the operator of the velocity-changing collisions is scaled by the Dicke parameter. To estimate the uncertainty originating from the Dicke parameter uncertainty, we repeat the δ_0 fit with modified (within their uncertainty range) real and imaginary parts of the Dicke parameter. We obtained a 3% change in δ_0.

Similarly, to estimate the uncertainty originating from the uncertainty of the speed dependence of the pressure shift, δ_2, we repeat the fit with its value altered (within its uncertainty range), obtaining a 1% change in the fitted δ_0.

A minor role is played by the uncertainties of the measurement devices. The inaccuracy of the pressure gauge of 1% adds 1% uncertainty to the δ_0 parameter since δ_0 is obtained by dividing the actual shift by pressure. Additionally, the stability of the laser is 10 MHz $\approx 0.33\,356 \times 10^{-3}$ cm^{-1}. The accuracy of the pressure shift parameter is directly connected to the frequency read; thus, the maximum inaccuracy of δ_0 due to laser instability is 1%.

Table II presents the full uncertainty budget. The top panel summarizes the uncertainty of the experimental δ_0. The uncertainty originating from the velocity-changing collisions model is dominant (6%), and the total combined uncertainty is 12%.

TABLE II. The budget of the experimental and theoretical uncertainties of the δ_0 parameter.

Uncertainty contribution	$u(\delta_0)$
Uncertainty of the experimental δ_0	
Velocity-changing collisions model	6%
$\widetilde{\nu}_{\text{opt}}$ uncertainty	3%
δ_2 uncertainty	1%
Pressure measurement uncertainty	1%
Laser maximum instability	1%
Combined experimental uncertainty	12%
$\delta_0 = (-33.0 \pm 4.0) \times 10^{-3}$ cm^{-1} atm^{-1}	
Uncertainty of the theoretical δ_0	
PES inaccuracy	21%
CC calculation convergence	1%
Combined theoretical uncertainty	22%
$\delta_0 = (-26.4 \pm 5.6) \times 10^{-3}$ cm^{-1} atm^{-1}	

B. Uncertainty of the theoretical δ_0

Theoretical values of the line-shape parameters are obtained by performing quantum scattering calculations on our PES, as we described in Sec. III. The corresponding uncertainties of the quantum scattering calculations and the PES propagate to the uncertainty of the calculated δ_0.

To estimate the uncertainties originating from the close-coupling quantum scattering calculations, we repeat the calculations varying the numerical steps and other convergence parameters. The uncertainty of δ_0 estimated this way turns out to be smaller than 1%.

To estimate the uncertainty of δ_0 originating from the PES uncertainty, in the first step, we estimate the maximum inaccuracy of the PES. The inaccuracy of the PES can be estimated by the relative difference between the non-relativistic PES value and its best extrapolation to the complete basis set. The highest discrepancy turns out to be at the bottom of the PES well, where the difference between the PES (-54.39 cm^{-1}) and the extrapolated value is -0.72 cm^{-1}, which is 1.3%. We treat this value as the maximum inaccuracy of the PES. In the second step, we modify the PES by scaling the isotropic part of the potential in the upper rovibrational state by 1.3%. We find that such distortion of the PES results in a 21% change of the theoretical δ_0; therefore, we treat this value as our estimate of the uncertainty due to the PES inaccuracy (see Table II).

C. Combined uncertainties

The uncertainty budget of both theoretical and experimental values of the δ_0 parameter is summarized in Table II. Considering the uncertainties, we obtained the experimental $\delta_0 = (-33.0 \pm 4.0) \times 10^{-3}$ cm^{-1} atm^{-1} and the theoretical $\delta_0 = (-26.4 \pm 5.6) \times 10^{-3}$ cm^{-1} atm^{-1}. The dominant contribution to the uncertainty budget results from the inaccuracies of the PES.

VI. SUMMARY

In this work, we focused on the S(1) 3-0 transition in molecular hydrogen perturbed by argon. We collected the experimental collision-induced spectral line shapes with the highly accurate cavity ring-down spectrometer of the Hefei laboratory. We also simulated the theoretical line profiles based on the fully *ab initio* quantum scattering calculations on our accurate H_2–Ar PES.

We verified the accuracy of several different approaches to model the theoretical line shapes, gradually adding subsequent corrections to our methodology. We considered the following effects: simplified centrifugal distortion (CD), full CD, and vibrational coupling (VC). We have found that neglecting these effects in our calculations resulted in a 6% error in the pressure broadening and shift parameters. Our numerical calculation revealed that the inclusion of the full CD and VC increased the calculation time by a factor of ~50. We have shown that the simplified CD already accounts for the majority of the corrections and allows us to achieve a sub-percent error of the line-shape parameters.

While the theoretical and experimental spectra agreed within 1.58%, the measured and calculated shift parameters, δ_0, differed by 20%. We analyzed this discrepancy, from both the theoretical and experimental perspective, to find that the δ_0 parameter is exceptionally sensitive to some computational aspects of our *ab initio* methodology; we found that the major contribution to this discrepancy originated from the inaccuracies of the PES.

SUPPLEMENTARY MATERIAL

The supplementary material includes the generalized spectroscopic cross sections of the S(0) 3-0 transition of H_2 perturbed by argon, which was used in our analysis.

ACKNOWLEDGMENTS

N.S. was supported by the Polish National Science Center (Project No. 2019/35/N/ST2/04145). P.W. and M.S. were supported by the Polish National Science Center (Project No. 2019/35/B/ST2/01118). G.K. was supported by the National Science Center, Poland Scholarship (Grant No. 2017/24/T/ST2/00242). Y.T. and S.M.H. acknowledge the support from the Chinese Academy of Sciences (Grant No. XDC07010000). The research is a part of the program of the National Laboratory FAMO in Toruń, Poland. The project is co-financed by the Polish National Agency for Academic Exchange under the PHC Polonium French-Polish program (dec. PPN/X/PS/318/2018). Calculations have been partially carried out using resources provided by the Wroclaw Center for Networking and Super-computing (http://wcss.pl) (Grant Nos. 294 and 546). We gratefully acknowledge Poland's high-performance computing infrastructure PLGrid (HPC Centers: ACK Cyfronet AGH, PCSS, CI TASK) for providing computer facilities and support within computational grant (No. PLG/2022/015576).

AUTHOR DECLARATIONS

Conflict of Interest

The authors have no conflicts to disclose.

Author Contributions

N. Stolarczyk: Conceptualization (equal); Data curation (equal); Formal analysis (lead); Funding acquisition (equal); Investigation (lead); Methodology (lead); Software (equal); Supervision (supporting); Visualization (lead); Writing – original draft (lead); Writing – review & editing (equal). **G. Kowzan**: Data curation (equal); Formal analysis (supporting); Funding acquisition (supporting); Investigation (supporting); Methodology (supporting); Software (supporting); Validation (equal); Visualization (supporting); Writing – original draft (supporting); Writing – review & editing (equal). **F. Thibault**: Conceptualization (equal); Formal analysis (supporting); Investigation (supporting); Software (supporting); Supervision (supporting); Validation (equal); Writing – review & editing (supporting). **H. Cybulski**: Data curation (equal); Investigation (supporting); Methodology (supporting); Software (supporting); Validation (equal); Writing – review & editing (supporting). **M. Słowiński**: Software (supporting). **Y. Tan**: Data curation (equal); Formal analysis (equal); Investigation (equal); Methodology (equal); Resources (equal). **J. Wang**: Data curation (equal); Formal analysis (equal); Investigation (equal); Methodology (equal); Resources (equal). **A.-W. Liu**: Data curation (equal); Formal analysis (equal); Investigation (equal); Methodology (equal); Resources (equal). **S.-M. Hu**: Data curation (equal); Formal analysis (equal); Investigation (equal); Methodology (equal); Project administration (supporting); Supervision (supporting). **P. Wcisło** Conceptualization (equal); Formal analysis (supporting); Funding acquisition (supporting); Investigation (supporting); Supervision (equal); Writing – original draft (supporting); Writing – review & editing (supporting).

DATA AVAILABILITY

The data that support the findings of this study are available within the article and its supplementary material.

APPENDIX: THE ROLE OF THE VELOCITY-CHANGING COLLISIONS

The line width of the H_2 molecule interacting with a heavier perturber strongly depends on the velocity-changing collision model,[4,8,50–53] see Fig. 5. To accurately reproduce the shape of a line, the velocity-changing model needs to include the absorber-to-perturber mass ratio.

A proper modeling of the velocity-changing collisions is of critical importance above the Dicke minimum [around 1.2 atm in the case of the S(1) 3-0 line considered in this paper, see Fig. 5]. In this regime, the direction of the velocity vector of an active molecule (here H_2) thermalizes much faster than its magnitude (speed).[4,9] Hence, above the Dicke minimum, the Doppler broadening is eliminated and the main role is played by the speed-dependent effects, in particular, the inhomogeneous broadening due to the speed-dependence of collisional shift.[2]

Table 1 of Ref. 9 shows that the thermalization rate of speed strongly depends on the absorber-to-perturber mass ratio. In the case of velocity thermalization, this dependence is much weaker. Therefore, to model the velocity-changing collisions properly, one needs to take into account two different time constants, describing the speed and velocity decays independently, and including the dependence on the mass ratio.

The present paper, however, does not aim at studying the velocity-changing collisions (which was thoroughly covered in Refs. 9 and 4). Within this research, we focus on explaining the difference between experimental and theoretical δ_0. Hence, our goal is to reduce any additional uncertainties and inaccuracies coming from the velocity-changing collision model. Therefore we study the regime below the Dicke minimum, see the grayed area in Fig. 5, where the impact of the velocity-changing collision model is the least pronounced. The half-width at half maximum (HWHM) of the billiard-ball profile (that takes into account the mass ratio and the two different relaxation rates) and hard-collision profile is almost equal at the considered pressure range. The divergence of the two curves becomes clearly visible at higher pressures, above the Dicke minimum. Figure 4 reveals relatively small inaccuracy arising from a simplification of the velocity-changing model [compare the performance of the fully *ab initio* billiard-ball profile[46,47] (e) and the hard-collision profile[49] (g)].

REFERENCES

[1] F. Thibault, P. Wcisło, and R. Ciuryło, "A test of H_2-He potential energy surfaces," Eur. Phys. J. D **70**, 236 (2014).

[2] N. Stolarczyk, P. Wcisło, and R. Ciuryło, "Inhomogeneous broadening, narrowing and shift of molecular lines under frequent velocity-changing collisions," J. Quant. Spectrosc. Radiat. Transfer **287**, 108246 (2022).

[3] V. G. Cooper, A. D. May, E. H. Hara, and H. F. P. Knapp, "Dicke narrowing and collisional broadening of the $S_0(0)$ and $S_0(1)$ Raman line of H_2," Can. J. Phys. **46**, 2019–2023 (1968).

[4] P. Wcisło, F. Thibault, H. Cybulski, and R. Ciuryło, "Strong competition between velocity-changing and phase- or state-changing collisions in H_2 spectra perturbed by Ar," Phys. Rev. A **91**, 052505 (2015).

[5] P. Wcisło, F. Thibault, N. Stolarczyk, H. Jóźwiak, M. Słowiński, M. Gancewski, K. Stankiewicz, M. Konefał, S. Kassi, A. Campargue, Y. Tan, J. Wang, K. Patkowski, R. Ciuryło, D. Lisak, R. Kochanov, L. Rothman, and I. Gordon, "The first comprehensive dataset of beyond-Voigt line-shape parameters from *ab initio* quantum scattering calculations for the HITRAN database: He-perturbed H_2 case study," J. Quant. Spectrosc. Radiat. Transfer **260**, 107477 (2021).

[6] N. Stolarczyk, F. Thibault, H. Cybulski, H. Jóźwiak, G. Kowzan, B. Vispoel, I. E. Gordon, L. S. Rothman, R. R. Gamache, and P. Wcisło, "Evaluation of different parameterizations of temperature dependences of the line-shape parameters based on *ab initio* calculations: Case study for the HITRAN database," J. Quant. Spectrosc. Radiat. Transfer **240**, 106676 (2020).

[7] F. Chaussard, X. Michaut, R. Saint-Loup, H. Berger, P. Joubert, B. Lance, J. Bonamy, and D. Robert, "Collisional effects on spectral line shape from the Doppler to the collisional regime: A rigorous test of a unified model," J. Chem. Phys. **112**, 158–166 (2000).

[8] H. Tran, F. Thibault, and J.-M. Hartmann, "Collision-induced velocity changes from molecular dynamic simulations in H_2–Ar: A test of the Keilson–Storer model and of line-broadening/shifting calculations for the Q(1) Raman line," J. Quant. Spectrosc. Radiat. Transfer **112**, 1035–1042 (2011).

[9] P. Wcisło, H. Tran, S. Kassi, A. Campargue, F. Thibault, and R. Ciuryło, "Velocity-changing collisions in pure H_2 and H_2–Ar mixture," J. Chem. Phys. **141**, 074301 (2014).

[10] M. Słowiński, H. Jóźwiak, M. Gancewski, K. Stankiewicz, N. Stolarczyk, Y. Tan, J. Wang, A.-W. Liu, S.-M. Hu, S. Kassi, A. Campargue, K. Patkowski, P. S. Żuchowski, R. Ciuryło, F. Thibault, and P. Wcisło, "Collisional line-shape effects in accurate He-perturbed H_2 spectra," J. Quant. Spectrosc. Radiat. Transfer **277**, 107951 (2022).

[11] P. Wcisło, F. Thibault, M. Zaborowski, S. Wójtewicz, A. Cygan, G. Kowzan, P. Masłowski, J. Komasa, M. Puchalski, K. Pachucki, R. Ciuryło, and D. Lisak, "Accurate deuterium spectroscopy for fundamental studies," J. Quant. Spectrosc. Radiat. Transfer **213**, 41 (2018).

[12] M. Słowiński, F. Thibault, Y. Tan, J. Wang, A.-W. Liu, S.-M. Hu, S. Kassi, A. Campargue, M. Konefał, H. Jóźwiak, K. Patkowski, P. Żuchowski, R. Ciuryło, D. Lisak, and P. Wcisło, "H_2-He collisions: *Ab initio* theory meets cavity-enhanced spectra," Phys. Rev. A **101**, 052705 (2020).

[13] P. Wcisło, I. E. Gordon, H. Tran, Y. Tan, S. M. Hu, A. Campargue, S. Kassi, D. Romanini, C. Hill, R. V. Kochanov, and L. S. Rothman, "The implementation of non-Voigt line profiles in the HITRAN database: H_2 case study," J. Quant. Spectrosc. Radiat. Transfer **177**, 75–91 (2016).

[14] W. K. Bischel and M. J. Dyer, "Temperature dependence of the Raman linewidth and line shift for the Q(1) and Q(0) transitions in normal and para-H_2," Phys. Rev. A **33**, 3113–3123 (1986).

[15] L. A. Rahn and G. J. Rosasco, "Measurement of the density shift of the H_2 Q(0–5) transitions from 295 to 1000 K," Phys. Rev. A **41**, 3698–3706 (1990).

[16] L. A. Rahn, R. L. Farrow, and G. J. Rosasco, "Measurement of the self-broadening of the H_2 Q(0–5) Raman transitions from 295 to 1000 K," Phys. Rev. A **43**, 6075–6088 (1991).

[17] W. E. Perreault, H. Zhou, N. Mukherjee, and R. N. Zare, "Resonant cold scattering of highly vibrationally excited D_2 with Ne," J. Chem. Phys. **157**, 144301 (2022).

[18] W. E. Perreault, N. Mukherjee, and R. N. Zare, "Quantum control of molecular collisions at 1 kelvin," Science **358**, 356–359 (2017).

[19] W. E. Perreault, N. Mukherjee, and R. N. Zare, "HD (v = 1, j = 2, m) orientation controls HD–He rotationally inelastic scattering near 1 K," J. Chem. Phys. **150**, 174301 (2019).

[20] M. Morita and N. Balakrishnan, "Stereodynamics of rotationally inelastic scattering in cold He + HD collisions," J. Chem. Phys. **153**, 091101 (2020).

[21] R. W. P. Drever, J. L. Hall, F. V. Kowalski, J. Hough, G. M. Ford, A. J. Munley, and H. Ward, "Laser phase and frequency stabilization using an optical resonator," Appl. Phys. B **31**, 97–105 (1983).

[22] C.-F. Cheng, Y. R. Sun, H. Pan, J. Wang, A.-W. Liu, A. Campargue, and S.-M. Hu, "Electric-quadrupole transition of H_2 determined to 10^{-9} precision," Phys. Rev. A **85**, 024501 (2012).

[23] C.-F. Cheng, Y. R. Sun, H. Pan, Y. Lu, X.-F. Li, J. Wang, A.-W. Liu, and S.-M. Hu, "Cavity ring-down spectroscopy of Doppler-broadened absorption line with sub-MHz absolute frequency accuracy," Opt. Express **20**, 9956–9961 (2012).

[24] S. Hess, "Kinetic theory of spectral line shapes. The transition between Doppler broadening and collisional broadening," Physica **61**, 80–94 (1972).

[25] L. Monchick and L. W. Hunter, "Diatomic-diatomic molecular collision integrals for pressure broadening and Dicke narrowing: A generalization of Hess's theory," J. Chem. Phys. **85**, 713 (1986).

[26] G. C. Corey and F. R. McCourt, "Dicke narrowing and collisional broadening of spectral lines in dilute molecular gases," J. Chem. Phys. **81**, 2318–2329 (1984).

[27] T. H. Dunning, Jr., "Gaussian basis sets for use in correlated molecular calculations. I. The atoms boron through neon and hydrogen," J. Chem. Phys. **90**, 1007 (1989).

[28] R. A. Kendall, T. H. Dunning, Jr., and R. J. Harrison, "Electron affinities of the first-row atoms revisited. systematic basis sets and wave functions," J. Chem. Phys. **96**, 6796 (1992).

[29] D. E. Woon and T. H. Dunning, Jr., "Gaussian basis sets for use in correlated molecular calculations. III. The atoms aluminum through argon," J. Chem. Phys. **98**, 1358 (1993).

[30] K. A. Peterson and T. H. Dunning, Jr., "Accurate correlation consistent basis sets for molecular core-valence correlation effects: The second row atoms Al-Ar, and the first row atoms B-Ne revisited," J. Chem. Phys. **117**, 10548 (2002).

[31] F. M. Tao and Y. K. Pan, "Moller–Plesset perturbation investigation of the He_2 potential and the role of midbond basis functions," J. Chem. Phys. **97**, 4989 (1992).

[32] F.-M. Tao and Y.-K. Pan, "Ab initio potential energy curves and binding energies of Ar_2 and Mg_2," Mol. Phys. **81**, 507 (1994).

[33] S. F. Boys and F. Bernardi, "The calculation of small molecular interactions by the differences of separate total energies. some procedures with reduced errors," Mol. Phys. **19**, 553 (1970).

[34] H.-J. Werner, P. J. Knowles, G. Knizia, F. R. Manby, M. Schütz *et al.*, MOLPRO, version 2010.1, a package of *ab initio* programs, 2010, see http://www.molpro.net.

[35] H.-J. Werner, P. J. Knowles, G. Knizia, F. R. Manby, M. Schütz *et al.*, MOLPRO, version 2012.1, a package of *ab initio* programs, 2012, see http://www.molpro.net.

[36] A. Wolf, M. Reiher, and B. A. Hess, "The generalized Douglas-Kroll transformation," J. Chem. Phys. **117**, 9215 (2002).

[37] M. Reiher and A. Wolf, "Exact decoupling of the Dirac Hamiltonian. I. General theory," J. Chem. Phys. **121**, 2037 (2004).

[38] M. Reiher and A. Wolf, "Exact decoupling of the Dirac Hamiltonian. II. The generalized Douglas-Kroll-Hess transformation up to arbitrary order," J. Chem. Phys. **121**, 10945 (2004).

[39] W. A. de Jong, R. J. Harrison, and D. A. Dixon, "Parallel Douglas-Kroll energy and gradients in NWChem: Estimating scalar relativistic effects using Douglas-Kroll contracted basis sets," J. Chem. Phys. **114**, 48 (2001).

[40] A. M. Arthurs and A. Dalgarno, "The theory of scattering by a rigid rotator," Proc. Math. Phys. Eng. Sci. **256**, 540–551 (1960).

[41] M. S. Child, *Molecular Collision Theory* (Academic Press, 1974).

[42] D. E. Manolopoulos, "An improved log derivative method for inelastic scattering," J. Chem. Phys. **85**, 6425–6429 (1986).

[43] M. H. Alexander and D. E. Manolopoulos, "A stable linear reference potential algorithm for solution of the quantum close-coupled equations in molecular scattering theory," J. Chem. Phys. **86**, 2044–2050 (1987).

[44] J. M. Hutson and C. R. Le Sueur, "MOLSCAT: A program for non-reactive quantum scattering calculations on atomic and molecular collisions," Comput. Phys. Commun. **241**, 9–18 (2019).

[45] J. Schaefer and L. Monchick, "Line broadening of HD immersed in He and H_2 gas," Astron. Astrophys. **859**, 265 (1992).

[46] D. A. Shapiro, R. Ciuryło, J. R. Drummond, and A. D. May, "Solving the line-shape problem with speed-dependent broadening and shifting and with Dicke narrowing. I. Formalism," Phys. Rev. A **65**, 012501 (2002).

[47] R. Ciuryło, D. A. Shapiro, J. R. Drummond, and A. D. May, "Solving the line-shape problem with speed-dependent broadening and shifting and with Dicke narrowing. II. Application," Phys. Rev. A **65**, 012502 (2002).

[48] P. Wcisło, A. Cygan, D. Lisak, and R. Ciuryło, "Iterative approach to line-shape calculations based on the transport-relaxation equation," Phys. Rev. A **88**, 12517 (2013).

[49] D. Bohm and E. P. Gross, "Theory of plasma oscillations. A. Origin of medium-like behavior," Phys. Rev. **75**, 1851–1864 (1949).

[50] S. Green, "Raman Q-branch line shapes as a test of the H_2–Ar intermolecular potential," J. Chem. Phys. **93**, 1496–1501 (1990).

[51] S. Green, D. W. Schwenke, and W. M. Huo, "Raman Q-branch line shapes as a test of a H_2–Ar intermolecular potential," J. Chem. Phys. **101**, 15–19 (1994).

[52] L. Waldron and W.-K. Liu, "Hydrogen-rare gas interactions and Raman line shapes," J. Chin. Chem. Soc. **48**, 439–448 (2001).

[53] L. Waldron, W.-K. Liu, and R. J. Le Roy, "Collisional broadening and shifting of Raman lines, and the potential energy surface for H_2–Ar," J. Mol. Struct.: THEOCHEM **591**, 245–253 (2002).

Journal of Quantitative Spectroscopy & Radiative Transfer 272 (2021) 107807

Contents lists available at ScienceDirect

Journal of Quantitative Spectroscopy & Radiative Transfer

journal homepage: www.elsevier.com/locate/jqsrt

CO-Ar collisions: *ab initio* model matches experimental spectra at a sub percent level over a wide pressure range

E.A. Serov[a,*], N. Stolarczyk[c], D.S. Makarov[a], I.N. Vilkov[a], G. Yu. Golubiatnikov[a], A.A. Balashov[a], M.A. Koshelev[a], P. Wcisło[c], F. Thibault[b], M. Yu. Tretyakov[a]

[a] *Institute of Applied Physics, Russian Academy of Sciences, 46 Ulyanov str., Nizhny Novgorod, 603950, Russia*
[b] *Univ Rennes, CNRS, Institut de Physique de Rennes, UMR 6251, Rennes F-35000, France*
[c] *Institute of Physics, Faculty of Physics, Astronomy and Informatics, Nicolaus Copernicus University in Torun, Grudziadzka 5, 87–100 Torun, Poland*

ARTICLE INFO

Article history:
Received 7 April 2021
Revised 4 June 2021
Accepted 14 June 2021
Available online 20 June 2021

Keywords:
Quantum scattering calculations
Line-shape parameters
Millimeter-wavelength range
BWO-based spectroscopy
Carbon monoxide
Wide pressure range

ABSTRACT

We use three independent spectroscopic techniques, operating in the millimeter-wavelength range, to study molecule-atom collisions, and validate our quantum-scattering calculations on two recent potential energy surfaces. We study the first pure rotational transition in a CO molecule perturbed by Ar. This molecular system is a good prototype of atmospherically relevant cases. It is, on the one hand, affordable for calculation of the line shape parameters by modern *ab initio* methods, and on the other hand, is very convenient for experimental studies because of its regular, well spaced rotational spectrum having a moderate intensity. We show that the simulated collision-perturbed spectra, which are based on our fully *ab initio* calculations, agree with the experimental line profiles at sub-percent level over a wide range (more than four orders of magnitude) of pressures. We demonstrate that the agreement between theory and experiment can be further improved if the model accounts for the collisional transfer of an optical coherence between different rotational transitions (the line-mixing effect). We show that the two surfaces tested in this work lead to a very similar agreement with the experiment. Capability of calculating line shape parameters in a broad range of temperatures is demonstrated.

1. Introduction

One of the major goals of molecular spectroscopy is the development of a model of radiation propagation, applicable to the widest possible range of spectral and thermodynamic conditions. Spectroscopic information accumulated and regularly updated in devoted databases and development of more and more sophisticated theoretical methods allow modeling of the observed spectra with a permanently increasing accuracy. In spectral intervals of single lines the experimental data can be reproduced with relative deviation down to 0.1 % or even better. However, such a good agreement is achieved, as a rule, by adjusting the number of line-shape parameters or, in other words, by fitting a theoretical model to experimental spectra. Moreover, the observed spectra can be distorted by various apparatus effects, which are modeled by introducing empirical functions having additional adjustable parameters. As a result, the parameters of the model retrieved from one experiment may not provide an agreement with another experimental data at the same level of accuracy. Such disagreements, however, are very small in comparison with cases where the line shape parameters are obtained by one or another interpolation and/or extrapolation method. Modern spectroscopic applications, such as, for example, remote sensing of planetary atmospheres, require parameters for billions of molecular lines at very different thermodynamic conditions, which is impossible to obtain from experiment. That is why simplified semi-empirical methods are widely used for calculating the line-shape parameters. Development of semi-empirical methods is complicated by difficulties in accurate representation of molecular collisions, which is known to be the crucial issue determining the shape of the observed molecular spectra [1,2]. Modeling of a collision requires knowledge of the full-dimensional intermolecular interaction potential. The *ab initio* methods of calculating the potential energy points for a multiplicity of mutual geometries of colliding molecules and further representation of the numerically obtained potential energy surface (PES) in functional form are known. A fairly good surface can now be produced in a reasonable time for relatively large molecular systems. However each particular case is still considered as a distinguished result. Moreover, even if the potential is known, accurate calculation of the molecular collision dynamics is a challenge for modern physics because any two colliding molecules are, in fact,

---

[*] Corresponding author.
E-mail address: serov@ipfran.ru (E.A. Serov).

https://doi.org/10.1016/j.jqsrt.2021.107807

one multi-particle quantum system with many internal degrees of freedom.

We believe that one of the most promising approaches in resolving the problem of molecular collision characterization is the following. It is based on highly accurate interaction potential calculated *ab initio* by modern quantum chemical methods. The potential is used for determining the generalized spectroscopic cross sections on the basis of *ab initio* quantum scattering calculations [3–6]. At the next step, the numerical parameters quantifying various aspects of molecular collisions are derived from the cross sections. The retrieved parameters are verified by using them in the best available statistical model of the collision-perturbed shape of molecular lines [1,2,7–10], which is directly compared with high quality experimental data.

The success of this approach was recently demonstrated by the example of the simplest cases corresponding to collisions of H_2 with He [11–13], HD with He [14] and D_2 with D_2 [10]. To advance further in this direction, the approach was recently used for the study of collisions between the CO molecule and Ar based on the shapes of two and five rovibrational transitions in the P branch of the fundamental and second-overtone bands, respectively [15,16]. The unprecedented subpercent level of consistency between theory and experiment achieved in these studies evidences that *ab initio* calculations can provide reliable data for spectroscopic databases widely used by various applications. Note that CO lines are used in remote sensing as a fire smoke tracer and Ar is the third most abundant molecule in dry atmosphere.

In this work, we extend the previous studies on CO-Ar collisions [15,16] by exploring a different spectral regime in which other collisional effects can be observed. We study the collisional perturbation of the shape of the lowest rotational transition $j = 1 \leftarrow 0$ (R(0) line) in a CO molecule (colliding with Ar) in its ground vibrational state located in the 3-mm wavelength range. Such a choice allows us to exclude the influence of vibrational excitation and neglect centrifugal distortion thus focusing on the analysis of pure collisional effects including the line mixing, which did not manifest itself in the previous studies [15,16]. Another advantage of the selected spectral range is an easily achievable pressure range where the molecular dipole oscillation dephasing (relatively optical probe-radiation) due to the Doppler effect is negligible compared to the collisional dephasing (pure collisional regime). This allows one to disregard the Dicke narrowing and the correlations between velocity changing and dephasing collisions, which mask the manifestation of other collisional effects in the infrared range. We show that the simulated collision-perturbed spectra agree with the experimental line profiles at a sub-percent level over a wide range of pressures.

The regular well-spaced pure rotational spectrum of the CO molecule is very well studied both experimentally and theoretically. Line positions are known with sub-kHz accuracy from Lamb-dip measurements [17]. Pressure broadening, shifting and wind effect (speed dependence of collisional relaxation) of the spectrum were extensively studied [18–23]. The collisional coupling effect of CO lines perturbed by either Ar or He was explored only for the fundamental rovibrational band [24–27], the first [24,28] and the second [29] overtone band. To the best of our knowledge, the collisional effects manifesting themselves in the shape of pure rotational lines of the CO spectrum were never studied at elevated (near atmospheric) pressures.

For this study, we employ three different, by principle of operation, spectrometers with complementary abilities covering a pressure range from about 10 microbars up to 2 bars. This gives us a unique opportunity to release the quite common problem of systematic instrumental error if only one experimental setup is used. The broad pressure range allows continuous tracing of molecular line shape variation in the collisional regime under conditions changing from highly rarefied to dense gas.

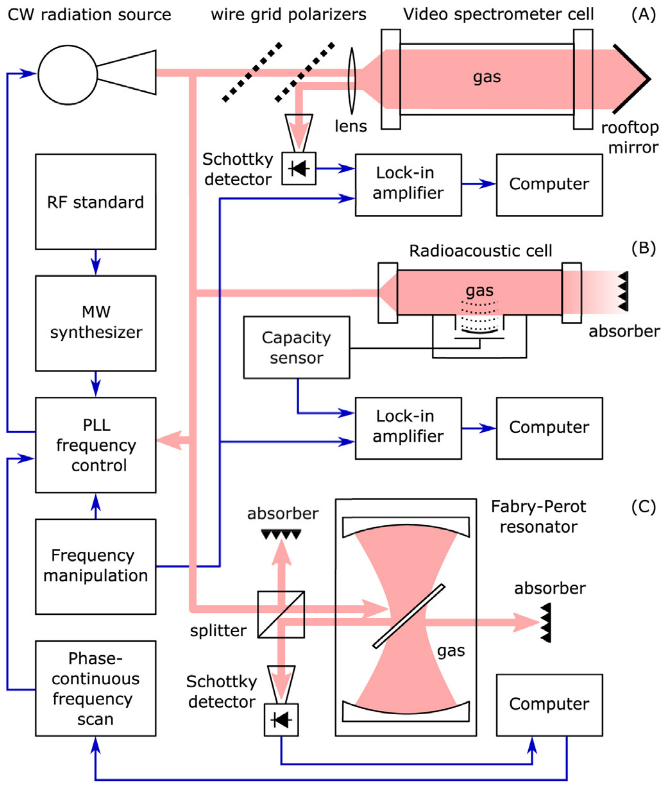

Fig. 1. Block diagram of the spectrometers used for measurements at various pressures. Section (A) shows the video spectrometer, section (B), the spectrometer with radioacoustic detection (RAD), and section (C), the resonator spectrometer.

The paper is organized as follows. Section 2 provides a brief description of the experimental setup and spectra acquisition. Section III presents details of the *ab initio* quantum-scattering calculations and line shape modeling. Comparison of theoretically calculated and experimental profiles is given and discussed in Section 4. The conclusions are summarized in Section 5. As a complementary work, Appendix A discusses the complex Dicke parameters and Appendix B provides the pressure broadening, pressure shift, complex Dicke parameters, and line mixing parameters for the R(0) line of CO in Ar over a wide range of temperatures.

2. Experiment

The unified diagram of our three spectrometers is presented in Fig. 1. All three setups utilize the continuous-wave, highly stable coherent radiation from a backward-wave oscillator (BWO) with the phase-locked loop (PLL) synchronization of the source frequency against the harmonic of the reference microwave synthesizer (HP8340B in the video spectrometer and Anritsu MG3692C in the radio-acoustic and the resonator spectrometers) synchronized with radio-frequency rubidium standard (GPS-12RG). The radiation power is about 10 mW. The radiation bandwidth is much less than 1 kHz, which allows neglecting the spectral resolution of the instrument in the absorption data analysis. More details on the radiation source and its precision digital frequency control can be found in [30] and references therein.

We used high-purity gases with natural isotopic composition from local suppliers. The declared gas purity was 99.995% for CO and 99.998% for Ar. Gas temperature in all experiments was maintained near room conditions and continuously monitored by several platinum sensors with 0.2 K uncertainty. Gas pressure was measured by membrane sensors (MKS Baratron-626B, Inficon CDG0250 and Pfeiffer CCR-362) of the corresponding pressure range with declared accuracy of 0.2–0.25 % of reading.

Particular features of our spectrometers and experimental details are given in the next three subsections.

2.1. Video spectrometer

The direct absorption video spectrometer [31,32] was used for recording spectra at gas pressures of 10–500 mTorr (Fig. 1A). A beam of the linear-polarized millimeter-wave radiation formed by a horn antenna and a 20-cm focal length lens is directed to a stainless steel tube (2 m long and 11 cm in diameter) with high-density polyethylene windows serving as a gas cell. The radiation beam after the first pass of the cell is reflected back by the rooftop mirror (rotating radiation polarization by 90 degrees) and after the second pass is directed to the detector by a wire grid polarizer. A Schottky diode is used as a detector. The linear dependence of the detector output voltage *versus* radiation power was tested and calibrated. The radiation power was reduced to ~1 mW by the second wire grid polarizer in order to minimize the molecular transition saturation and the corresponding distortion of the absorption profile at low gas pressures. The gas absorption coefficient is determined using the well known equation derived from the Beer-Lambert-Bouguer law:

$$\alpha(\nu) = -\frac{1}{L_c} ln\left(\frac{P(\nu)}{P_0(\nu)}\right), \tag{1}$$

where P and P_0 denote the radiation power at frequency ν detected with and without absorbing gas, respectively ($P_0(\nu)$ is the baseline), and L_c is the absorption path length. The power recordings can be obtained by scanning the radiation source frequency through the desired range using radiation amplitude modulation (AM) and synchronous detection of the signal at the modulation frequency. The AM technique allows direct retrieval of the absorption profile by Eq. (1), but requires that the spectrometer baseline does not change during the measurement cycle. Providing the requested stability is not an easy task with the more than 4-m long radiation path. Even a small temperature-related variation of the radiation interference pattern or mean power may significantly distort the absorption profile. To reduce the baseline impact on the absorption shape, radiation frequency modulation (FM) is employed instead of AM. We use frequency manipulation or modulation by square wave form with preset deviation and synchronous detection at modulation frequency. This is achieved by using an arbitrary function generator (HMF2550) as the reference for the PLL system of the BWO. The recorded profile in this case is a difference of two true absorption profiles shifted up and down from the original one by the deviation frequency (finite difference derivative of the original profile). The smaller the frequency deviation, the less the baseline impact on the observed profile. The deviation values used in this study are less than 1 kHz. Even though for the final comparison with calculated absorption we selected the recordings for which the experimental perturbation of the baseline was the smallest.

2.2. Radioacoustic detection spectrometer

A spectrometer with radioacoustic detection of absorption (RAD) [33–36] was used for line profile studies in the pressure range 0.1–2 Torr (Fig. 1B). Radiation from the source is directed to the cell (copper tube with a diameter of 2 cm and a length of 10 cm) by a horn antenna. When molecules in the cell absorb radiation, their collisional relaxation leads to an increase in the temperature and pressure of the gas. If the amplitude of CW radiation is modulated by a periodic signal, the absorption causes respective pressure oscillations, *i.e.*, generates an acoustic wave, which is detected by a sensitive microphone and transformed into an electric signal by the resonance capacity sensor circuit. This signal is acquired using a lock-in amplifier referenced by the modulation frequency.

The acoustic signal S is directly proportional to the radiation power P_{abs} absorbed by the gas:

$$S \propto P_{abs} = P_0(\nu) - P(\nu) = P_0(\nu)(1 - e^{-\alpha(\nu)L_c}) \tag{2}$$

In this case, $P_0(\nu)$ and $P(\nu)$ denote the radiation power at the input and output of a gas cell, respectively. Under conditions of a low optical depth ($\alpha L_c \ll 1$, which is well satisfied for the CO line under study) and assuming that α does not depend on power, the output signal is directly proportional to the studied gas absorption coefficient and to the radiation power fed to the cell, $S \propto P_0\alpha(\nu)L_c$.

According to the principle of operation, the signal should appear only within the absorption lines and be absent outside the lines. However, a small baseline is present in this spectrometer due to the following technical reason: the absorption of radiation in the elements of the gas cell (mainly in the windows) leads to their heating and related secondary (nonradiative) heating of the gas, producing an additional acoustic signal.

Frequency manipulation with preset deviation (approximately equal to the half width at half maximum of the line under study) is employed, which leads to the reduction of the baseline effect and recording of absorption in the shape of a finite difference derivative of the original profile, as was described above in the video spectrometer subsection. Relatively small size of the cell and related radiation paths allow for good thermal and mechanical insulation, providing very stable experimental conditions. Experimental spectra are obtained by averaging of multiple recordings, which allows to reduce the instrumental noise. Back and forth frequency scanning around line center is used to minimize the effect of the instrumental time constant on the line center position.

2.3. Resonator spectrometer

The most wide-band recordings of the studied line in the CO–Ar mixture were obtained with a resonator spectrometer [37] (Fig. 1C). Two types of BWO were used as a sources, namely, OB-76 (frequency range 105–148 GHz) and OB-86 (frequency range 105–198 GHz). The absorption coefficient is retrieved from the change in the Fabry-Perot resonator Q-factor when it is filled with the studied gas. A high quality (Q-factor~ 10^6) resonator is placed inside the vacuum chamber equipped with the active temperature control system. The input and output windows of the chamber are produced from irradiated bulk polytetrafluoroethylene (PTFE) that has improved mechanical properties in comparison with the standard PTFE. The surfaces of the windows are corrugated using a special profile, which, in a manner similar to infrared and optical antireflective coatings, provides a low reflectivity of the windows in a wide frequency range [38].

The total pressure of the gas mixture ranged from 772 to 1525 Torr, while the relative fraction of CO varied from 3 to 14 %. The experimental conditions are listed in the Table 1. The CO and Ar densities were calculated from partial pressures using the virial equation of state and the data on the second virial coefficient [39,40]. The contribution of the third and subsequent terms of the virial equation expansion can be neglected under experimental conditions. Maximal relative difference between the calculated density and the corresponding ideal gas density was about 0.1%.

The baseline of the spectrometer, corresponding to the intrinsic resonator losses, was recorded when the chamber was filled with argon. The pressure of argon was chosen to provide the resonator optical length similar to that of the resonator filled with a mixture

Table 1
Resonator spectrometer experimental conditions.

#	T_{gas}, K	p_{CO}, Torr	p_{Ar}, Torr	n_{CO}, amg	n_{Ar}, amg	freq. range, GHz	exp. error, 10^{-8} cm^{-1}
1	297.4	24.91	747.4	0.03012	0.9038	105–148	0.5
2	296.6	49.82	747.9	0.06041	0.9069	105–148	0.7
3	296.8	74.74	747.5	0.09057	0.9058	105–148	1.6
4	296.4	124.6	747.9	0.1512	0.9075	105–198	1.6
5	297.5	124.6	995.2	0.1507	1.2034	105–198	2.5
6	296.9	125.3	1120	0.1518	1.3573	105–148	2.2
7	296.7	124.6	1245	0.1511	1.5107	105–148	2.3
8	297.7	124.6	1399	0.1506	1.6896	105–198	4.0

of CO and Ar with selected mixing ratio. The baseline was determined at the frequencies of sequential TEM$_{00q}$ eigenmodes of the resonator by measuring their widths in the frequency domain. The interval between adjacent frequencies is 294 MHz. After the baseline recording, the chamber was evacuated and then filled with the desired amount of CO and then Ar. The gas mixing inside the chamber was accelerated by a fan. Reaching of equilibrium density was controlled by the time dependence of the width of the resonance mode located near the CO line center (~115 GHz). As a rule, stable conditions were obtained in about one hour after the gas inlet when the resonance curve width reached a constant value within the statistical uncertainty.

The gas absorption coefficient was calculated from the formula

$$\alpha = \frac{4\pi}{c}(\Delta f_{gas} - \Delta f_{bln}), \tag{3}$$

where Δf_{gas} and Δf_{bln} are the resonance curve half widths at half maximum (HWHM), measured when the resonator is filled with studied mixture and non-absorbing gas, respectively.

The statistical uncertainty of the curve HWHM after averaging over 100 back and forth scans is about 8 Hz, which corresponds to the uncertainty of the absorption coefficient $5 \cdot 10^{-9}$ cm^{-1}. Additional uncertainty in the measured absorption is caused by parasitic reflections of radiation in the quasioptical-waveguide system, which is used for resonator excitation and registration of the resonance response. The reflection patterns are not exactly identical when the baseline and the studied gas spectrum are recorded. Hence, the obtained spectrum includes some systematic modulation of the resonance curve width, which depends on the distance between the quasioptical-waveguide system and the resonator. The effect is more pronounced the wider are the resonances. To reduce this effect, we averaged several spectra obtained for different positions of the quasioptical-waveguide system, as was described in detail in [37].

Thereby we obtain several individual spectra and the averaged spectrum for the desired conditions. An example of experimental spectrum (# 1, Table 1) obtained by averaging 4 individual recordings and 50×multiplied differences between the averaged spectrum and individual recordings are shown in Fig. 2. The scattering of individual spectra is somewhat larger than the aforementioned statistical uncertainty and amounts from $1.2 \cdot 10^{-8}$ cm^{-1} at line wings to $1.8 \cdot 10^{-8}$ cm^{-1} near the line centre. However, the real uncertainty of the averaged spectrum is sufficiently lower due to reducing the systematic effect of parasitic reflection of radiation by averaging of the recordings obtained at different phases of these reflections. The uncertainty can be estimated from the residual after fitting the proper model profile to the averaged spectrum. Before fitting the model to the R(0) line, the absorption of other CO lines contributing to the experimental spectrum was calculated and subtracted from experimental spectra (see Section 4 for details). If we take the van Vleck-Weisskopf model updated by inclusion of the line mixing and speed dependence of collisional relaxation (as is discussed in detail in Section 3) with the additional smooth pedestal corresponding to the CO-Ar continuum and fit it to the averaged experimental spectrum (Fig. 2), then the standard deviation of residual is $5 \cdot 10^{-9}$ cm^{-1}. Estimated uncertainties of all experimental recordings are given in Table 1.

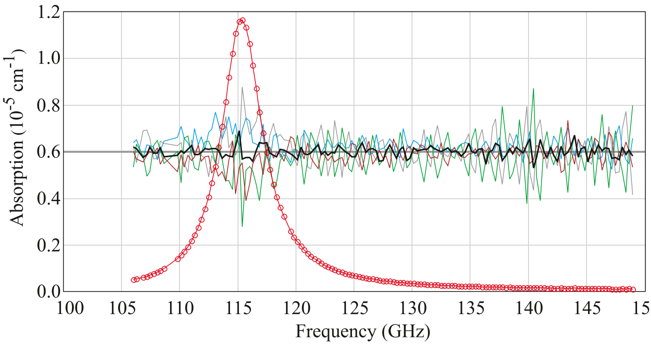

Fig. 2. Averaged experimental spectrum of a CO-Ar mixture at room temperature for p_{CO} = 24.91 Torr and p_{Ar} = 747.4 Torr (red line). Blue, green, brown and gray lines are the 50×multiplied differences between single records obtained at different distances between the quasioptical system and the resonator, and the averaged spectrum. Thick black line is the 50×(Exp− Fit.) residual for the model given by Eq. (26). All residuals are shifted up by $0.6 \cdot 10^{-5}$ cm^{-1} for clarity. (For interpretation of the references to colour in this figure legend, the reader is referred to the web version of this article.)

3. *Ab initio* quantum-scattering calculations and perturbation of the shape of molecular resonance

3.1. Quantum scattering calculation

Quantum dynamical calculations were performed on either the potential energy surface (PES) of Sumiyoshi and Endo [41] already used by some of us in [15,16,42] or a more recent one of Cybulski [16]. These two three-dimensional PESs, $V(r, R, \theta)$, where r is the CO intramolecular distance, R the distance between the CO centre of mass and the Ar atom, and θ the angle between $\vec{r}$ and $\vec{R}$, were first expanded in the basis of Legendre polynomials up to the 10th order:

$$V(r, R, \theta) = \sum_{L} V_L(r, R) P_L(\cos\theta). \tag{4}$$

Then the radial coupling terms, $V_L(r, R)$, were averaged over the CO rovibrational wave functions $\chi_{\mathrm{v},j}(r)$ in order to provide the rovibrational potential coefficients:

$$V_{L,\mathrm{v}j,\mathrm{v}'j'}(R) = \int_0^\infty \chi_{\mathrm{v}'j'}(r) V_L(r, R) \chi_{\mathrm{v}j}(r) dr, \tag{5}$$

where the subscripts v and j designate vibrational and rotational quantum numbers and vj, v$'j'$ are the states coupled by the PES. The $\chi_{\mathrm{v}j}(r)$ functions were determined by using the DVR-FBR method (discrete variable representation — finite basis representation) on the CO potential of Murrell and Sorbie [43] updated by Huxley and Murrell [44]. We have checked that the centrifugal distortion has no effect, as well as vibrational coupling terms, thus we denote these terms $V_L(R)$ for $V_{L,00,00}(R)$. Scattering matrix elements relevant for the calculations of generalized spectroscopic collisional cross sections were obtained from close-coupling calculations using the non-reactive MOLSCAT code [45], or its parallelized version [46], for kinetic energies[1] between 0.1 to 2000 cm^{-1}. Other technical details regarding the use of MOLSCAT code for the system under study can be found in [15,16,42,47–52].

---

[1] All the energies are expressed in cm^{-1}, thus E stands for E/hc with h, the Planck constant, and c, the speed of light, in cm/s.

3.2. Generalized cross sections

Following the generalized Hess method (GHM) [53,54], the spectroscopic collisional cross sections are expressed as

$$\sigma_\lambda^q(j_i'j_f',j_ij_f;E_{kin}) = \frac{\pi}{k^2}(-1)^{(j_i+j_i')}\left(\frac{[j_i']}{[j_i]}\right)^{1/2}$$
$$\times \sum_{J_i,J_f,\ell,\ell',\bar{\ell},\bar{\ell}'} [J_i][J_f]\left([\ell][\ell'][\bar{\ell}][\bar{\ell}']\right)^{1/2}(i)^{-\ell+\ell'+\bar{\ell}-\bar{\ell}'}$$
$$\times \begin{pmatrix} \ell & \bar{\ell} & \lambda \\ 0 & 0 & 0 \end{pmatrix}\begin{pmatrix} \ell' & \bar{\ell}' & \lambda \\ 0 & 0 & 0 \end{pmatrix}\begin{bmatrix} j_i & j_i' & \bar{\ell} & \bar{\ell}' \\ j_f & \ell & j_f' & \ell' \\ q & J_f & J_i & \lambda \end{bmatrix}$$
$$\times [\delta_{j_ij_i'}\delta_{j_fj_f'}\delta_{\ell\ell'}\delta_{\bar{\ell}\bar{\ell}'} -$$
$$\langle j_i\ell\left|S^{J_i}(E_{kin}+E_i)\right|j_i'\ell'\rangle\langle j_f\bar{\ell}\left|S^{J_f}(E_{kin}+E_f)\right|j_f'\bar{\ell}'\rangle^*]. \quad (6)$$

In Eq. (6), the vibrational quantum number have been omitted since we consider only the ground vibrational state. Primes indicate post-collisional values. In Liouville space such a cross section describes the coupling of a line $|if\rangle\rangle$ (for short) with a line $|i'f'\rangle\rangle$. The various ℓ and $\bar{\ell}$ relate to the end-over-end rotational energy of the interacting pair. The close coupling (CC) S-matrix elements are expressed in the total angular momentum representation, $\vec{J}$, which is conserved during a collision (*e.g.*, $\vec{J_i} = \vec{j_i} + \vec{\ell}$). They are evaluated for different total energies equal to the relative kinetic energy of the colliding pair plus the rotational energy. k is the modulus of the wave vector associated with that collisional energy, $E_{kin} = (\hbar k)^2/2\mu$, with μ being the reduced mass of the CO-Ar system. q stands for the tensor order of the radiation-matter interaction ($q = 0$, 1 and 2 correspond to isotropic Raman Q lines, electric dipole transitions, and anisotropic Raman or quadrupolar transitions, respectively). In addition, [X] stands for 2X+1, (: : :) refers to the 3-j symbol and $\begin{bmatrix} : & : & : \\ : & : & : \end{bmatrix}$, to the 12-j symbol of the second kind [55]. Finally, λ is the rank of the velocity tensor.

It has been recognized [5,53,54,56,57] that for $\lambda = 0$, such a GHM cross section reduces to the standard spectroscopic cross section [58,59] as derived from the impact approximation and leading to the so-called relaxation matrix in the line space [60]. Therefore, the real and imaginary parts of these diagonal cross sections provide the collisional half-widths and shifts, while off-diagonal terms provide the usual line coupling terms.

Since the considered line lies in the millimeter-wave range we have to take into account both the couplings with the neighboring R lines and their "mirror" lines located at negative frequencies. The latter correspond to the "anti-resonant" contribution of the familiar VVW profile. A R(j) line involves a Δj=+1 optical transition while its mirror component involves a Δj = -1 transition [58], thus, we will denote it P(j+1). For later use we also remind the reader of the following relation :

$$\sigma_0^1(j_f'j_i',j_fj_i;E_{kin}) = \left(\frac{[j_i][j_f']}{[j_i'][j_f]}\right)^{1/2}\sigma_0^{1*}(j_i'j_f',j_ij_f;E_{kin}) \quad (7)$$

that can be derived from Eq. (6) and the unitarity of the S-matrix. This relation, valid for pure rotational lines, implies [58] in particular that the collisional width of a R(j) line equals the width of the P(j+1) line, and that the shifts of these lines are just the opposite.

The second kind of generalized Hess cross sections, tied to λ = 1, has recently been discussed in the literature [6,11,14,61]. Since the orientation and magnitude of the velocity may change in the course of a dephasing collision, this cross section is associated with the diffusion of the polarization of the spectral transition. Therefore, there is a first correlation between the velocity changing and dephasing collisions. This correlation appears naturally in Hess [3] theory.

3.3. Off-diagonal relaxation matrix elements

The standard off-diagonal cross sections merit to be separately discussed, since we used different methods in order to determine them. Since we are only interested in the R(0) line at low or moderate pressures, it is fortunately not useful to calculate a full relaxation matrix [60]. Due to their high computational cost, we have only calculated the CC σ_0^1(R($j = 0-5$);R(0);E_{kin}) and σ_0^1(P($j = 1-4$);R(0);E_{kin}) cross sections for kinetic energies between 0.1 and 2000 cm^{-1}. To complete (for $j \geq 5$) these sets of non-diagonal cross sections we made use of the energy corrected sudden approximation (ECSA) (for a review see Ref. [62]).

The ECSA exploits an inelastic cross section out of j = 0 (or of cross sections from $j' \neq 0$ to j = 0 using the micro-reversibility). This allows one to express all non-diagonal generalized cross sections in terms of such standard state-to-state cross sections, $\sigma(L \equiv j \to 0)$, where it is customary [62] to replace j by L, via

$$\sigma_0^q(j_i'j_f',j_ij_f;E_{kin}) = -\left(\frac{[j_i']}{[j_i]}\right)^{1/2}$$
$$\sum_L [L]F^q(j_i'j_f',j_ij_f;L)\frac{\sqrt{\Omega_{j_i}\Omega_{j_f}}}{\Omega_L}\sigma(L\to 0;E_{kin}) \quad (8)$$

Here, the Percival-Seaton spectroscopic coefficients are given by

$$F^q(j_i'j_f',j_ij_f;L) = (-1)^q\left([j_i][j_i'][j_f][j_f']\right)^{1/2}$$
$$\times \begin{pmatrix} j_i & L & j_i' \\ 0 & 0 & 0 \end{pmatrix}\begin{pmatrix} j_f & L & j_f' \\ 0 & 0 & 0 \end{pmatrix}$$
$$\times \begin{Bmatrix} j_i & j_f & q \\ j_f' & j_i' & L \end{Bmatrix}, \quad (9)$$

where {:::} denotes a 6j symbol. In fact, since $j_i = 0$ by virtue of the triangular rule, implied by the first 3-j symbol, there is only one L value for the R(0) line, with $L = j_i'$ that contributes to the summation.

The Ω's adiabaticity factors, figuring in Eq. (8), were first introduced by DePristo et al. [63] to correct for the sudden approximation. Based on our previous studies on CO$_2$ – Ar [64] and CO – Ar [26], we have preferred to use the form of these factors proposed by Bonamy et al. [65]:

$$\Omega_j = \left[1 + \frac{1}{12}\left(\omega_{j,j-1}\tau_c\right)^2\right]^{-1}, \quad (10)$$

where τ_c is the effective duration of a collision and $\omega_{j,j-1}$ is the angular frequency spacing between adjacent levels. The relaxation matrix elements (in cm^{-1}) are deduced from a Maxwell-Boltzmann thermal average of these cross sections,

$$\langle\langle l'|W|l\rangle\rangle = \frac{n_{Ar}\bar{v}_r}{2\pi c}\langle\sigma_0^1(l',l;E_{kin})\rangle \quad (11)$$

where $|l\rangle\rangle$ and $|l'\rangle\rangle$ stand for the $|if\rangle\rangle$ and $\left|i'f'\right\rangle\rangle$ lines, respectively, $\bar{v}_r$ is the mean relative speed at a given temperature T, n_{Ar} is the number density of the bath composed of argon, and

$$\left\langle\sigma_0^1(l',l;E_{kin})\right\rangle = \frac{1}{(k_BT)^2}\int_0^\infty E_{kin}e^{-E_{kin}/k_BT}\ \sigma_0^1(l',l;E_{kin})\ dE_{kin}. \quad (12)$$

Finally, the relaxation matrix elements that obey the detailed balance principle, $W_{l'l}\cdot\rho_l = W_{ll'}\cdot\rho_{l'}$, where the ρ's are the thermal equilibrium populations of the initial level of the optical transition, are given by

$$W_{l'l} = -\frac{n_{Ar}}{2\pi c}\frac{\rho_{i_>}}{\rho_{j_i}}[i_<]\left([j_i][j_i']\right)^{-1/2}\left(\Omega_{i_>}\Omega_{f_>}\right)^{1/2} \times \sum_{L\neq 0}[L]F^1(j_i'j_f', j_ij_f; L)\frac{1}{\Omega_L}\mathcal{R}(L\rightarrow 0; T) \tag{13}$$

with $\mathcal{R}(L\rightarrow 0; T)$, the rate constant associated with the downward cross sections $\sigma(L\rightarrow 0)$. In the line shape literature, this rate is often expressed in terms of the so-called ”basic rates” : $\mathcal{R}(L\rightarrow 0; T) \equiv \bar{v}_r Q_L'(T)$, where $Q_L'(T)$ is actually the thermally averaged cross section:

$$Q_L'(T) = \frac{1}{(k_BT)^2}\int_0^\infty E_{kin}\, e^{-E_{kin}/k_BT}\ \sigma(L\rightarrow 0; E_{kin})\ dE_{kin}. \tag{14}$$

In Eq. (13), $i_>$ ($i_<$) and $f_>$ stand for the maximum (resp. minimum) value of (j_i, j_i') and (j_f, j_f'). Thus, to generate the necessary off-diagonal relaxation matrix elements we only need to have at our disposal the downward rates to $j = 0$ or equivalently the basic rates $Q_L'(T)$. Thanks to our scattering calculations over a large grid of kinetic energies, we have in fact $\sigma(L\rightarrow 0; E_{kin})$, and thus the rate constants $\mathcal{R}(L\rightarrow 0; T)$ up to $L = 20$.

In addition, in Ref. [26], the basic rates were modeled using a hybrid exponential-power (EP) law [66]:

$$Q_L'(T) \ = \ \frac{A(T)}{[L(L+1)]^\alpha}\ e^{-\beta\frac{E_L}{k_BT}}. \tag{15}$$

The adjustable parameters, A, α, and β, are given in Table V of Ref. [26]. From this table the effective duration τ_c, at room temperature T, of a collision can also be easily deduced.

To conclude this section, we have therefore three sets of relaxation matrix elements: a limited set obtained from our *ab initio* CC calculations and including the couplings of the R(0) line with its 5 neighbouring R lines and the couplings with the P(1) to P(4) lines located at negative frequencies, a second set coming from our mixed CC/ECSA calculations, and a third one derived from the fitted basic rates of Ref. [26].

3.4. Line-shape parameters

It is well known [62] that the real and (minus) imaginary parts of the diagonal relaxation matrix elements are the standard collisional Lorentzian halfwidth and shift parameters of a line:

$$\Gamma_{0,l} = Re(W_{ll}), \tag{16}$$

$$\Delta_{0,l} = -Im(W_{ll}). \tag{17}$$

In the first order with respect to pressure, to the Lorentzian line profile a dispersive contribution that comes from the line mixing must be added. This dispersive component is characterized by the Rosenkranz [67,68] line mixing parameter

$$Y_l = 2\sum_{l'\neq l}\frac{d_{l'}}{d_l}\frac{W_{l'l}}{\nu_l - \nu_{l'}}, \tag{18}$$

where d_l is the reduced dipole matrix element for the line $|l\rangle\rangle$,

$$d_l = (-1)^{j_f}\left[j_f\right]^{1/2}\begin{pmatrix} j_f & j_i & 1 \\ 0 & 0 & 0\end{pmatrix}, \tag{19}$$

and ν_l denotes its position in the spectrum in cm^{-1}. As for rovibrational spectra having regular R and P branches we can split Eq. (18) into two contributions:

$$Y_l = 2\sum_{l'_+\neq l}\frac{d_{l'_+}}{d_l}\frac{W_{l'_+l}}{\nu_l - \nu_{l'_+}} + 2\sum_{l'_-}\frac{d_{l'_-}}{d_l}\frac{W_{l'_-l}}{\nu_l - \nu_{l'_-}}, \tag{20}$$

the first contribution being associated with the intra-branch couplings, *i.e.*, R lines located at positive frequencies, and the second one with the inter-branch couplings, *i.e.*, P lines at negative frequencies.

Since $\Gamma_{0,l}$, $\Delta_{0,l}$, and Y_l are proportional to the number density of the bath gas, these parameters, normalized by the bath gas pressure, are widely used as spectroscopic coefficients:

$$\Gamma_{0,l} = p\gamma_{0,l} \tag{21}$$

$$\Delta_{0,l} = p\delta_{0,l} \tag{22}$$

$$Y_l = py_l. \tag{23}$$

Note that $Y_l = \left(Y_l^{\mathrm{r}} + iY_l^{\mathrm{i}}\right)$ is a complex line-mixing parameter. In the following discussion we limit our focus to the parameters concerning the R(0) line; therefore, we omit the line-count subscript l for simplicity.

The speed dependence of the line-shape [1,2] parameters also affects the line profile. Due to our quantum dynamical calculations for various energies we are in a position to provide the absolute active molecule speed dependence of the above parameters,

$$\Gamma(v) + i\Delta(v) = \frac{n}{2\pi c}\frac{2}{\sqrt{\pi}v\overline{v}_p}\int_0^\infty dv_r v_r^2 e^{-\frac{v^2+v_r^2}{\overline{v}_p^2}}\ \sinh\left(\frac{2vv_r}{\overline{v}_p^2}\right)\sigma_0^q(v_r), \tag{24}$$

where n is the number density of the bath molecules, v, v_r and $\overline{v}_p$ are the speed of the active molecule, relative absorber-to-perturber speed and most probable perturber speed. Note that Eq. (24) deals with the diagonal cross section of the line under consideration. The same equation can be utilized to determine the speed dependence of the off-diagonal relaxation matrix elements and, thus, to derive the speed dependence of the line mixing parameter. The latter was evaluated and found to be negligible under our experimental conditions in accordance with conclusions of work Ref. [69]. The use of the speed dependent parameter $Y(v)$ instead of the speed averaged value Y in calculations of the line shape (Eq. (26)) leads to variations at the level of about 2 × 10^{-11} cm^{-1}, which is 160 times lower than the resonator spectrometer sensitivity. So in what follows we report only the speed averaged value of the line mixing.

3.5. The results of the quantum scattering calculations

Fig. 3 presents kinetic energy dependent pressure broadening and shift cross sections (top panels), as well as the off-diagonal cross sections (middle panels) for $\sigma_0^1(R(j=1-5); R(0); E_{kin})$ cross sections. Similar calculations (not shown) were performed for $\sigma_0^1(P(j=1-4); R(0); E_{kin})$ cross sections (as well as for the diagonal elements of the P(1) line located at negative frequency). The pressure-normalized, speed-dependent collisional half-width and shift of the R(0) line at 297.5 K are plotted in the bottom panels of Fig. 3. The thermally averaged relaxation matrix elements at 297.5 K related to the R(0)-R($j' \neq 0$) off diagonal cross sections are shown in Fig. 4 where they are compared with our mixed CC/ECSA values and the fitted ECS values [26].

Having at our disposal various sets of relaxation matrix elements we are in position to determine the line mixing parameter of the R(0) line at 297.5 K. In the following, for short, we call Y_{++} and Y_{+-} the contributions of the intra- and inter-branch couplings (Eq. (20)). Using the CC relaxation matrix elements between the R(0)-R(j=1-5) lines, we found the value Y_{++}= 6.87 × 10^{-3} atm^{-1} while the R(0)-P(j=1-4) relaxation matrix elements lead to Y_{+-}= -1.83 × 10^{-3} atm^{-1}. Thus, our CC initial value for the line mixing parameter is $y = 5.04$ × 10^{-3} atm^{-1}. In the second step, in order to include more terms in the summation (Eq. (20)) leading to this parameter, we have included higher off-diagonal ECSA relaxation matrix elements derived from our present set of CC rate constant $\mathcal{R}(L\rightarrow 0; T)$ up to $L = 20$, thus including line mixing terms up to

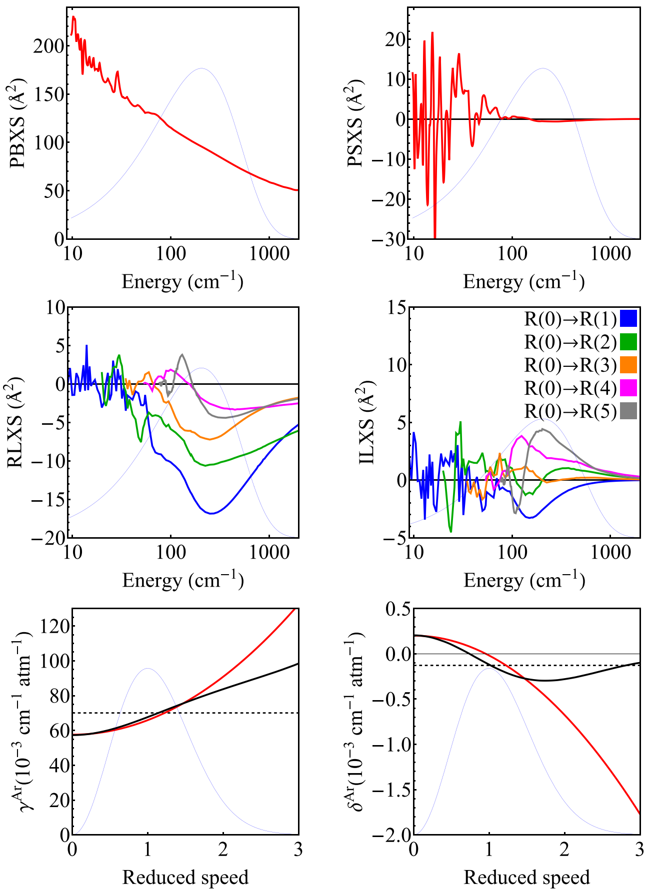

Fig. 3. *Ab initio* calculation results for the CO-Ar collisional system: top and middle panels: Pressure broadening and pressure shift cross sections (PBXS and PSXS), real and imaginary parts of the line mixing cross sections (RLXS and ILXS). Thin blue lines mark the Maxwell-Boltzmann distribution of the kinetic energy of perturber (Ar) molecules. Bottom panels: reduced speed (v/v_m) dependence of pressure broadening ($\gamma^{Ar} = \Gamma^{Ar}/p^{Ar}$) and shifting ($\delta^{Ar} = \Delta^{Ar}/p^{Ar}$) coefficients. Black curves are the *ab initio* data and red curves stand for the quadratic approximation. Dashed horizontal lines mark the speed-averaged values with respect to the Maxwell-Boltzmann speed distribution (thin blue lines). The results presented in this figure were calculated with Cybulski's PES [16]. (For interpretation of the references to colour in this figure legend, the reader is referred to the web version of this article.)

the R(20) and P(20) lines. This leads to a final value of 4.71× 10^{-3} atm^{-1}. Note that using the fitted rates [26] instead of the present rates leads to a close value of 4.82 × 10^{-3} atm^{-1}. This is not surprising because, at room temperature, taking into account the line mixing with the nine neighbouring lines (P(4) to R(5)) provides the main contribution to this parameter and the above values converge to better than 2 %, retaining the intra- and inter-branch coupling terms up to $j = 10$. In addition, one can see in Fig. 4 that the present ECSA set and the previous fitted one are indeed very close for L greater than about 8. Anyway, it is difficult to claim that our final value of the line mixing parameter is accurate to better than 7%. Indeed, the use of our present CC rates in conjunction with the ECSA, leads to the value of 4.7 × 10^{-3} atm^{-1}. This remarkable agreement with our final value is accidental because the separate contributions from the intra- and inter "branch are in fact quite different (Y_{++}=8.81 and $Y_{+-} = -4.11$, in 10^{-3} atm^{-1}). Nevertheless, our prediction of the line mixing parameter is also comparable to experimental or more or less accurately calculated values for the R(0) line of CO in various baths [24,27,28,70].

Finally, the relaxation matrix has complex-valued elements. Thus, we should be theoretically able to provide the imaginary part of the line mixing coefficient of the R(0) line. Indeed, our *ab initio* CC $W(R(j{=}1\text{-}5;R(0))$ have an imaginary part (right middle panel of Fig. 3) as well as the $W(P(j{=}1\text{-}4;R(0))$ leading to the total value 0.01 × 10^{-3} atm^{-1} for the imaginary part of this coefficient. Due to the largely predominance of the couplings with the first 9 neighbouring lines this certainly gives a correct order of magnitude of this part. Of course, since $Q_L^{'}(T)$ are real, it is not possible to extrapolate using the ECSA. The absolute value of this imaginary part is much lower than the real part and has thus been neglected in the line shape analysis.

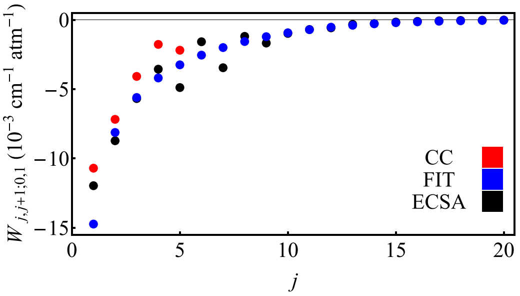

Fig. 4. Real part of relaxation matrix elements normalized by bath gas pressure coupling the line R(0) to the R(1) to R(20) lines calculated at 297.5 K. Full CC: red symbols; ECSA from our CC downward rates $\mathcal{R}(j \to 0; T)$: black symbols; fitted values [26]: blue symbols. Note that the blue and black dots overlay for $j \geq 10$. (For interpretation of the references to colour in this figure legend, the reader is referred to the web version of this article.)

Table 2
Ab initio spectral line-shape parameters for the CO-Ar collisional system calculated with the PES of Cybulski [16] and Sumiyoshi [41]. The calculations were performed for T = 297.5 K and the broadening and shifting coefficients are expressed in units of 10^{-3}cm^{-1}atm^{-1}, while the units of the line mixing are 10^{-3}atm^{-1}. The last column presents relative differences between the coefficients originating from the different PESs.

coefficients	Cybulski PES	Sumiyoshi PES	difference (%)
γ_0^{Ar}	69.7	70.9	1.7
δ_0^{Ar}	-0.13	-0.15	13
γ_2^{Ar}	8.2	8.7	5.7
δ_2^{Ar}	-0.22	-0.19	16
y^r	5.04	-	-
y^i	0.01	-	-

As a last remark, we point out that the present calculation of the line mixing parameter was done with Cybulski's PES [16]. Comparing the state-to-state cross sections out of $j = 0$ ($\sigma(j = 0 \to j'; E_{kin})$), the spectroscopic cross sections and the thermally averaged values obtained with the two used PESs [16,41], we have no doubt that Sumiyoshi *et al.* PES will lead to a very similar value of the line mixing parameter.

The thermally averaged, at 297.5 K and pressure-normalized line-shape parameters derived from the present *ab initio* calculations are gathered in Table 2. Appendix B provides their temperature dependence.

3.6. The model of a collision-perturbed shape of molecular resonance

The center frequency, ν_0, of the R(0) line of CO in the ground vibrational state equals 3.845033413(16) cm^{-1} [17]. The contribution of the Doppler broadening effect is quantified by its HWHM [71],

$$\Gamma_D = \nu_D\sqrt{\ln(2)} = \frac{\nu_0}{c}\sqrt{\frac{2k_BT}{m}\ln(2)}, \tag{25}$$

where $\nu_D = \nu_0\frac{v_m}{c}$ is the most probable Doppler shift, k$_B$, T and m are Boltzmann constant, temperature, and mass of the active molecule, respectively. In the case of the R(0) 0-0 line studied in

Table 3
Comparison of the speed-averaged CO-Ar collisional pressure broadening parameter values in different pressure ranges. The Doppler HWHM Γ_D value is $4.49 \times 10^{-6}\mathrm{cm}^{-1}$ at 296 K.

device	pressure range	Γ_0^{Ar} range [cm^{-1}]
resonator	772–1525 Torr	(7.08- 14.0)×10^{-2}
RAD	634–2049 mTorr	(5.79 - 18.7)×10^{-5}
VID	93.4–221.8 mTorr	(8.55 - 20.3)×10^{-6}

this paper, $\Gamma_D = \ 4.49 \times 10^{-6}$ cm^{-1} at 296 K. On the other hand, the collisional broadening parameter, Γ_0 scales linearly with pressure p.

Within this study we performed measurements in a wide pressure range, which affected the ratio between Γ_D and Γ_0. Table 3 presents the values of Γ_0 parameters in each of our three pressure ranges. While in the high-pressure regime Γ_0 dominates over Γ_D by at least two orders of magnitude, the parameters become commensurable in the intermediate- and low-pressure regimes. The Γ_0/Γ_D ratio determines the choice of a proper spectral line shape profile that we use to compare theoretical calculations with experimental data from each of the three spectrometers.

3.6.1. High-pressure collisional regime

This section describes the line-shape model used to simulate the theoretical spectra that we compare with the resonator spectrometer data. The contribution of the Doppler broadening effect is negligible compared to the collisional broadening, see Table 3. We can also disregard the influence of the velocity-changing collisions. To justify this we compared the speed-dependent Hard Collision profile [1] and the speed-dependent Lorentz profile. In our high pressure range, the two models differ on the level of 0.06%, which is much smaller than the other systematic uncertainties, in particular the one related to the choice of PES. Since we analyze the line in the microwave spectral range at high pressure, we have to take into account the influence of the radiation-term-related scaling factor proportional to ν^2/ν_0^2, as well as the slope coming from the negative-frequency peak (ignoring these two effects would make the residuals four times higher). A line-shape model which includes these two effects is called the van Vleck-Weisskopf (VVW) profile [72]. A modified version of the original VVW profile, including the line mixing and speed dependence of collisional broadening and shift can be expressed as [67,73]

$$I(\nu) = 4\pi^{-\frac{3}{2}} Re\Bigg(\left(\frac{\nu}{\nu_0}\right)^2 \int_0^\infty e^{-x^2} x^2 \left(\frac{1+iY_+}{\Gamma(v)+i(\nu-\nu_0-\Delta(v))} + \frac{1+iY_-}{\Gamma(v)+i(\nu+\nu_0+\Delta(v))}\right)dx\Bigg). \tag{26}$$

Here, $\Gamma(v)$ and $\Delta(v)$ denote the speed-dependent pressure broadening and shift parameters, As discussed below Eq. (7) the positive- and negative-frequency resonances have the same width and opposite shift; intuitively their line mixing parameters are equal in magnitude but have an opposite sign. This couple of lines behaves as an object and its image in a mirror (see Ref.[74] and references therein). The later property can be demonstrated for any couple of pure rotational lines starting from Eq. (20) using the symmetry of the cross section (Eq. (7)) and the reduced dipole moments (Eq. (19)). At a more detailed level, one can show, using the notations introduced in Section 3.5, that $Y_{++} = -Y_{--}$ and $Y_{+-} = -Y_{-+}$, thus $Y_+ = -Y_-$.

The integral is performed over the Maxwell-Boltzmann speed distribution; $x = \frac{v}{v_m}$, where v and v_m are the active molecule speed and its most probable speed. To model the speed dependence of the pressure broadening and shift parameters, we used the quadratic approximation defined as [42]

$$\Gamma(v) = \Gamma_0 + \Gamma_2\left(x^2 - \frac{3}{2}\right), \tag{27a}$$

$$\Delta(v) = \Delta_0 + \Delta_2\left(x^2 - \frac{3}{2}\right), \tag{27b}$$

The two bottom panels Fig. 3 present the fully *ab initio* speed dependent pressure broadening and shift (continuous black lines) and their quadratic approximations (continuous red lines) for the CO-Ar system. Thin blue lines denote the Maxwell-Boltzmann distribution of the active molecule velocity. γ_0^{Ar} and δ_0^{Ar}, marked with dashed horizontal lines, are the speed-averaged pressure-independent spectral line-shape parameters, obtained from averaging the collisional cross sections [6]. γ_2^{Ar} and δ_2^{Ar}, which quantify the speed dependence, are calculated using the condition that the quadratic function has the same slope as the *ab initio* speed dependence at the most probable speed of the active molecule [42]. These four line-shape coefficients are reported in Table II. The line-shape parameters are the sums of the fully *ab initio* CO – Ar collisional coefficients and of the CO – CO coefficients weighed by partial pressures (see the convention defined in Eqs. (21) and (22)). The speed dependent CO – CO coefficients for the line broadening and shifting were taken from the previous experiments [23]. The line mixing effect was never studied in the pure rotational band of CO, so we utilized the same value of Y for modeling both CO – Ar and CO – CO collisions. This can be justified by the following reasoning. The value is in a reasonable agreement with data from Ref. [75] (which is for the 2-0 band). The divergence between Y parameters for the 2-0 and 0-0 bands should not be large because of the weak dependence of the collisional cross-section within small vibrational excitations. Potential impact of inaccuracy of the used value is expected to be negligible because of (i) weakness of the effect at present experimental conditions, (ii) relatively small amount of CO in the sample and (iii) insignificant difference in y coefficients for pure- and foreign-pressure broadening lines [75]. To verify this statement we doubled the related value of y in the model. The modification led to an increase of the observed minus calculated spectrum rRMSE by 0.03%.

The same approach was used for the spectra modeling at intermediate and low pressures discussed below.

3.6.2. Intermediate- and low-pressure collisional regime

This section describes the spectral line-shape model that we used to validate our *ab initio* theoretical calculations on the data from radioacoustic detection and video spectrometers. Since their principle of operation relied on the frequency modulation technique, with precisely known deviation, the experimental profiles have a dispersive shape,

$$I(\nu) = I_{\mathrm{VP}}(\nu + \delta\nu) - I_{\mathrm{VP}}(\nu - \delta\nu), \tag{28}$$

where $\delta\nu$ is the frequency deviation value. As the pressure gets lower, the line is significantly narrower and the factor $\left(\frac{\nu}{\nu_0}\right)^2 \approx 1$. Similarly, the influence of the negative peak present in the VVW model can be neglected. In the intermediate- and low- pressure regimes the collisional broadening no longer dominates over the Doppler broadening and both effects are taken into account within the framework of the speed-dependent Voigt profile (with inclusion of the line mixing) [10,76],

$$I_{\mathrm{VP}}(\nu) = \frac{2}{\nu_D}\pi^{-\frac{3}{2}} Re\Bigg(\int_0^\infty e^{x^2}\frac{x}{i} \ln\left(\frac{\Gamma_{\Omega_R}(v) - i(\nu-\nu_0-\Delta(v)) + i\nu_D x}{\Gamma_{\Omega_R}(v) - i(\nu-\nu_0-\Delta(v)) - i\nu_D x}\right)dx\Bigg). \tag{29}$$

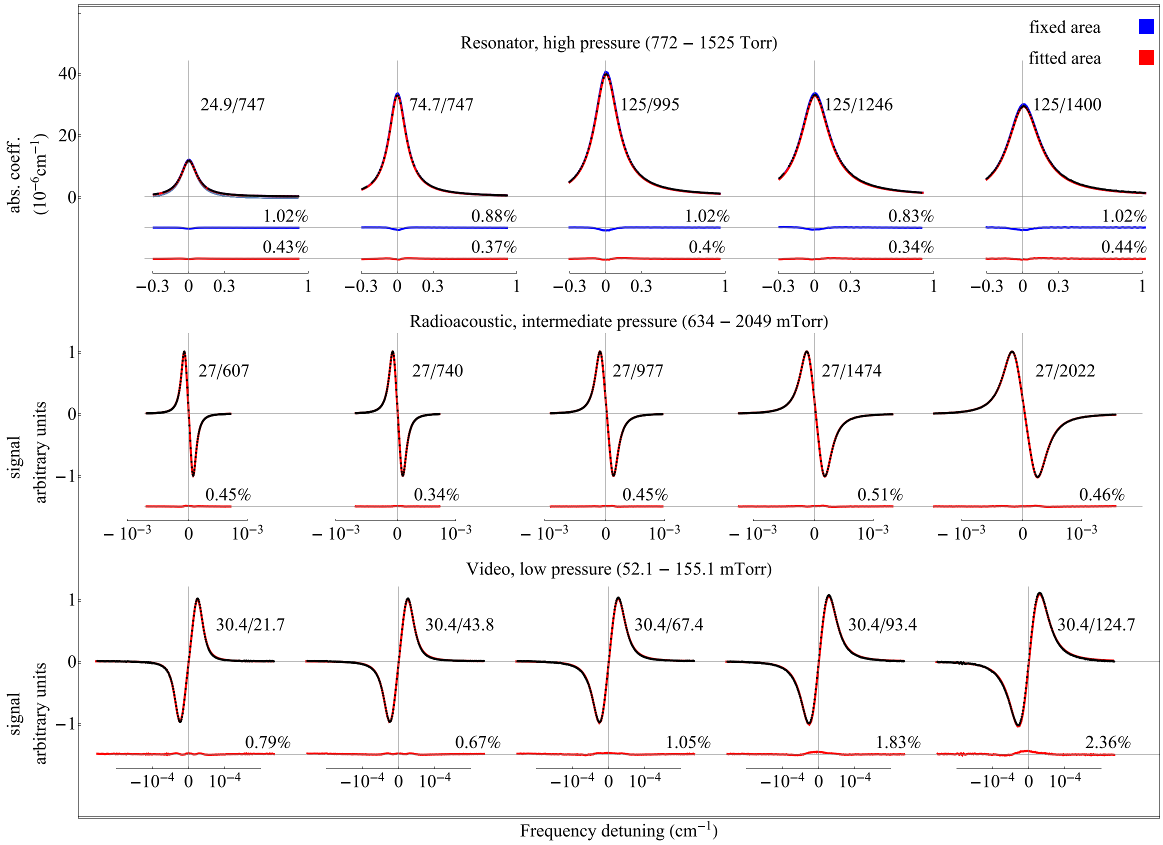

Fig. 5. Direct validation of the *ab initio* quantum-scattering calculations (performed on the PES of Cybulski [16]) on accurate experimental spectra of the R(0) line in CO perturbed by collisions with Ar atoms. The three panels from the bottom to the top show the results obtained with the three spectrometers in a very wide range of pressures from 52 mTorr to 1525 Torr (exact values of the CO and Ar pressures are given above each profile; the first/second value corresponds to the CO/Ar pressure). All the three spectrometers measure the absorption coefficient $\alpha(\nu)$, which is directly seen in the case of a resonator spectrometer (top panel). In the cases of radioacoustic and video detection spectrometers (middle and bottom panels), the line profiles have dispersive shapes due to the frequency demodulation techniques relevant for these spectrometers, see Section 2. The black dots are the experimental spectra and the red lines are the *ab initio* profiles. In the case of a resonator spectrometer (the top panel), the absolute vertical scale is accessible and the synthetic *ab initio* profiles can be generated based on the line intensity taken from the best literature value [78,79], see the blue lines (for the red lines, the line intensity was fitted). The differences between the experimental and *ab initio* profiles are shown below each graph with respective color notation. To quantify how well the theory agrees with experiments, we report for each profile the relative (with respect to the profile peak value) root mean square errors (rRMSE) of the experiment-theory differences calculated within the ±FWHM range around the line center, see the numbers (in percent) above the residuals. The spectra were acquired at $T \approx 297$ K (resonator spectrometer), $T \approx 299.35$ K (radioacoustic detection spectrometer), and $T \approx 298.15$ K (video spectrometer). (For interpretation of the references to colour in this figure legend, the reader is referred to the web version of this article.)

The effective broadening parameter

$$\Gamma_{\Omega_R}(\nu) = \sqrt{(\Gamma(\nu))^2 + \Omega_R^2} \tag{30}$$

includes the Rabi frequency Ω_R characterizing transition saturation by a radiation power. It can be determined as a product of the amplitude of the electric field of the radiation and matrix element of the transition dipole moment [77]. Under conditions of our study with radioacoustic spectrometer, Ω_R was estimated for the R(0) line as 0.11–0.13 MHz, which is comparable to the Doppler half-width. For video spectrometer recordings, the Rabi frequency was about an order of magnitude lower. While the role of the Doppler effect is pronounced only in the lowest pressure range, one could expect the Dicke narrowing effect to play a role. To estimate its influence, we compared the simplest Dicke-narrowed speed-dependent Hard Collision profile [1] with the speed-dependent Voigt profile. In the considered pressure regime, the two models differ on the level of 0.05% (the relative root-mean-square error calculated within ± FWHM of the line profile, rRMSE=0.05%), which is much smaller than the systematic uncertainty related to the choice of PES, and hence we neglect the Dicke narrowing.

4. Direct comparison of the *ab initio* synthetic profiles with the measured spectra

Having performed both the *ab initio* calculations and accurate line-shape measurements, we compare our synthetic line-shape profiles with the experimental results in Fig. 5. In each of the 15 spectra presented in Fig. 5 the line-shape parameters are fixed to our *ab initio* values (obtained from Cybulski's PES [16]). The top panel presents five absorption profiles measured with the resonator spectrometer in our highest pressure range (772–1525 Torr). We compared the experimental data with the *ab initio* calculations by adjusting only the baseline and slope (*i.e.*, constant and linear with the frequency terms added to the line shape model) to compensate for the possible effect of unaccounted far line wings together with an absorption by molecular pairs (bimolecular absorption) and fixing the intensity parameter to the best literature value [78,79], see the blue curves in Fig. 5. We also performed an alternative analysis, adjusting the intensity parameter individually for each line to focus only on the collisional line-shape effects and exclude intensity uncertainty, see the red residuals on the top panel of Fig. 5.

Similarly, to compare the *ab initio* data with experimental results collected with the radioacoustic detection and video spectrometers, we performed a multi-spectrum fitting procedure, ad-

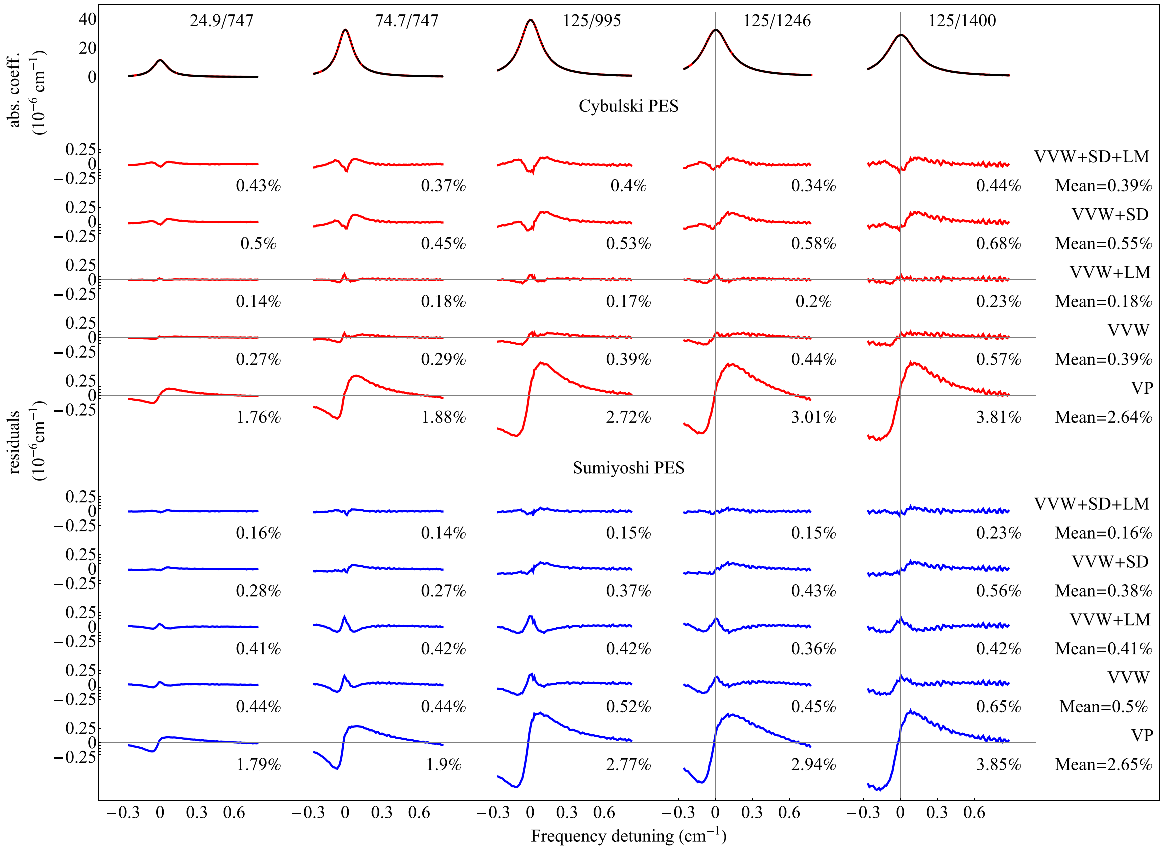

Fig. 6. Comparison of the absolute differences between theoretical and experimental spectra (red lines and black dots on the top panel) collected with a resonator spectrometer for different line-shape models and PESs. The ten lower panels present how taking into account different collisional effects influences the agreement with experimental data. The results displayed with red lines are the absolute residuals calculated using the Cybulski's PES [16], while the blue lines correspond to the results obtained with the Sumiyoshi's PES [41]. The absolute differences between the *ab initio* synthetic data and the experimental spectra are accompanied by relative root mean square errors (rRMSE) of the experiment-theory differences calculated within the ±FWHM range around the line center, see the numbers (in percent) above the residuals. In the right part of the figure we list the abbreviations we used for the profiles (VP=Voigt Profile, VVW=van Vleck-Weisskopf Profile, LM=line mixing, and SD=speed dependence of the collisional broadening and shift), as well as the mean rRMSE resulting from the use of the given model. Since we did not calculate the *Y* parameter for Sumiyoshi's PES, the contribution of LM in each case is based on Cybulski's PES. (For interpretation of the references to colour in this figure legend, the reader is referred to the web version of this article.)

justing Ω_R (which depends on apparatus settings). These techniques do not give direct access to the absolute line intensities; therefore we adjusted the intensity of each line separately. To account for the apparatus effect relevant for the radioacoustic and video spectrometers, we fitted a frequency-proportional scaling factor, as well as the baseline and slope. Five lines measured with a radioacoustic spectrometer in the intermediate-pressure range (634-2049 mTorr) are displayed on the middle panel of Fig. 5 together with the corresponding theoretical data. Similarly, five spectra collected with a video spectrometer in the low-pressure regime (52.1–155.1 mTorr), accompanied by their theoretical counterparts are located on the bottom panel of Fig. 5.

The absorption corresponding to other lines of CO spectrum is small, but not negligible in the frequency range under study. This additional absorption was modeled as follows and subtracted from experimental spectra before their comparison with *ab initio* profiles. The van Vleck-Wesskopf line shape function was used with an additional term taking into account the line mixing effect in the first order of pressure (so-called Rosenkranz profile [67]). The far wings of the profile were truncated at 25 cm^{-1} detuning from its maximum as suggested in [80]. The line-by-line sum of such profiles was calculated for all (excluding the studied one) rotational lines of CO isotopologues in the ground and vibrational states with integrated intensities larger than 10^{-28} cm/molec following the HITRAN2016 line list and using line intensities and self-broadening coefficients from this database [81]. Ar-broadening coefficients were adopted from [47], assuming the same rotational dependence and independence on vibrational state. The rotational dependence of the line mixing parameters was evaluated on the basis of our ECSA off-diagonal relaxation elements. Then the line mixing coefficients for all rotational lines (excluding the R(0) line) were calculated by scaling this dependence using the R(0) line coefficient value calculated in this work and reported in Table 2.

Below each of the 15 spectra displayed in Fig. 5, we present absolute residuals, *i.e.*, differences between theoretical and experimental data. As was mentioned in the previous paragraph, two sets of residuals are displayed on the top panel, corresponding to the analysis with fitted (red curves) and fixed (blue curves) line intensity. Each residual is accompanied by the value of the relative root mean square error (rRMSE, expressed in %) to quantify the agreement between theoretical and experimental data.

In the case of the resonator spectrometer data, we obtained percent-level rRMSE when the area was fixed to the database value, while adjusting it brought residuals below 0.5 % for each of the five lines. In the case of the radioacoustic spectrometer data, the agreement between theoretical and experimental lines expressed in terms of rRMSE was at a level of 0.5 %. The situation was much different in the case of the video spectrometer data. Indeed, the studied pressure range included a region where the effect of baseline fluctuations is not negligible. Among 106 scans, we selected a series of five, sharing the same Rabi frequency, whose baseline fluctuations were the smallest. The remaining baseline deformation, due to the apparatus, was reduced by subtracting a third-order polynomial from the raw data. Ultimately, we achieved a rRMSE within 0.7- 2.3 %, which was dominated by the apparatus effect, and not by the *ab initio* calculations.

In the next step of our analysis, we examined how neglecting different line-shape effects can affect the agreement between theoretical and experimental data for the case of a resonator spectrometer. Fig. 6 presents a direct comparison of ten different approaches to model the line shape profile. In this case, the line intensity was a fitting parameter. Similarly to the convention applied in Fig. 5, each residual curve is followed by the numerical value of rRMSE. Additionally, the performance of each model is summarized in the right part of the picture by the mean rRMSE. The figure shows two sets of data, either obtained by using Cybulski's PES [16] (red residuals), or by using Sumiyoshi's PES [41] (blue residuals). For comparison, we begin with the simple Voigt profile (VP), which is conventional for the IR and visible spectral ranges, where the condition $\nu_0 \gg$ HWHM is strictly fulfilled. A significant improvement is observed after employing the van Vleck-Weisskopf profile (VVW) confirming its superiority for broad lines in the microwave range [82]. A 1.7 % difference between two PESs in Γ_0 (see Table II) becomes notable at this step. Taking into account the line mixing (LM) effect leads to an even better agreement between theory and experiment for both PESs (recall that the LM parameter is determined from scattering calculations performed on Cybulskis PES.) At this step we see that something is still missing. W-shape residuals that are characteristic for the SD effect manifestation are seen for both PESs. Now, if we disregard the LM, but just take into account the SD effect, the residuals show the asymmetric skew typical for the LM effect, which is more prominent for Sumiyoshi's PES. This step improves the agreement as compared to a simple VVW analysis in the case of Sumiyoshi's PES, but worsens the agreement for Cybulski's PES. Note that the theoretical SD of the width and shift (the latter plays an insignificant role in our case) are very similar for both PESs and the 1.7 % difference in widths become crucial. Clearly, the role of the LM is preponderate over the SD broadening at the highest pressures. The final SDVVWLM profile accounting for both effects shows the best agreement with the experimental data for Sumiyoshi's PES, while this is not the case for Cybulski's PES. On the one hand, this result seemingly demonstrates the advantage of the Sumiyoshi PES and could be tentatively explained as a slight underestimation of the line width using Cybulski's PES, thus compensating the line narrowing due to the SD effect. On the other hand, we should admit that there are other influencing issues leading either to the theoretical underestimation of the width or to the additional line broadening due to some experimental artifact, which may compensate for the inaccuracy of Sumiyoshis PES and thus hide the advantage of the Cybulskis PES. Therefore, we avoid any judgment on which of the two PESs is more accurate and conclude that the influence of SD effect is of the same order as influence of PESs (around 0.2 %), which is similar to overall accuracy we reach in our ultimate comparison.

5. Discussion and conclusions

The results gathered in Figs. 5 and 6 show that our theoretical *ab initio* calculations predict the collision-perturbed shapes of the spectral lines to the sub-percent level. The most broadband spectra were collected with a resonator spectrometer. These spectra are the most advantageous for our goal because of (i) the absolute vertical scale in units of absorption coefficient, which allows to fix the line intensity, (ii) the clear manifestation of the line mixing effect, and (iii) the smallest impact from the apparatus contributions. These spectra are in 0.15-0.38% agreement with the *ab initio* calculations, depending on the chosen PES. We also achieved a 0.4% level of accuracy for spectra recorded with radioacoustic spectrometer in the intermediate-pressure range. The residuals in the low-pressure regime are dominated by the apparatus effect and do not allow us to state the agreement at the same level of accuracy. However, the experimental data still reveal good agreement with theoretical profiles, implying that our *ab initio* calculations are valid in a wide pressure range, spanning 50 mTorr to 1500 Torr.

The very good agreement between theoretical and experimental data obtained at room temperature allows us to assert that the same level of accuracy of our *ab initio* calculations can be expected within a quite broad range of temperatures. This follows from the fact that the calculations are performed on a grid of kinetic energies covering a range between 0.1 and 2000 cm^{-1}, corresponding to about 1.5 - 2800 K in terms of thermal energy k_BT. To demonstrate such a capability we provide in Appendix B the results of calculation of line shape parameters calculation for a number of temperatures within this range. This additional data may be helpful for future experimental or theoretical works, as well as for population of spectroscopic databases.

Thus, using the example of the R(0) line of the ground vibrational state of CO molecules colliding with Ar, we have demonstrated that the state-of-the-art *ab initio* calculations are able to reproduce the observed shape of atmospherically relevant molecules at a sub percent level of uncertainty, which is quite sufficient for most present day applications.

Declaration of Competing Interest

The authors declare that they have no known competing financial interests or personal relationships that could have appeared to influence the work reported in this paper.

CRediT authorship contribution statement

E.A. Serov: Investigation, Formal analysis. **N. Stolarczyk:** Formal analysis, Writing - review & editing. **D.S. Makarov:** Formal analysis, Data curation. **I.N. Vilkov:** Investigation. **G.Yu. Golubiatnikov:** Investigation, Methodology. **A.A. Balashov:** Investigation. **M.A. Koshelev:** Investigation, Methodology. **P. Wcisło:** Methodology, Writing - original draft. **F. Thibault:** Investigation, Writing - original draft. **M.Yu. Tretyakov:** Conceptualization, Supervision.

Acknowledgments

Experiment was supported in parts by the Russian State project (0030-2021-0016) and Russian Science Foundation (17-19-01602). Financial support from RFBR project No. 18-55-16006 is acknowledged. P.W. was supported by National Science Centre, Poland, Project No. 2018/31/B/ST2/00720. N.S. was supported by National Science Centre, Poland, Project No. 2019/35/B/ST2/01118. The project was co-financed by the Polish National Agency for Academic Exchange under the PHC Polonium program (dec. PPN/X/PS/318/2018).

Appendix A. The complex Dicke parameter

Other effects due to collisions affect the line shape. Hess [3], a long time ago, approximated the collision operator by two relaxation frequencies, $\tilde{\omega}_A$ and $\tilde{\omega}_R$ (the generalized Hess parameters). By doing so, he solved a semi-classical kinetic equation which takes into account the internal motion and the drift term due to the translational motion leading to the Dicke narrowing. This theory was later on completed [53,54] essentially by making a link with the formalism in Liouville space and the scattering matrix leading to a close coupling expression of the generalized Hess spectroscopic cross sections (Eq. (6)). Following the generalized Hess notations, the complex pressure broadening and shift coefficient is denoted as

$$\tilde{\omega}_A = \Gamma - i\Delta = n_b\, \tilde{\omega}_0^{00}(q). \tag{A.1}$$

The quantity $\tilde{\omega}_R$ takes into account the correlation between the translational and internal motions and is expressed in terms of two, mass weighted collision integrals,

$$\tilde{\omega}_R = n_b \frac{m_a}{m_a+m_b}\tilde{\omega}_0^{00}(q) \; + \; \frac{2}{3} n_b \frac{m_b}{m_a+m_b}\tilde{\omega}_1^{11}(q). \tag{A.2}$$

These collision integrals are in turn derived from the GHM cross sections,

$$\tilde{\omega}_\lambda^{s,s'}(q) = \bar{v}_r \int dx x^{(s+s'+2)/2} e^{-x} \sigma_\lambda^q (E_{kin} = x k_B T). \tag{A.3}$$

Making the link between Hess profile [3] and various profiles that take into account the Dicke narrowing [1,2], some of us recognized [6] that the frequency of the velocity changing collisions is indeed

$$\tilde{\nu}_{opt} \equiv \tilde{\omega}_R - \tilde{\omega}_A. \tag{A.4}$$

In the following, we call $\tilde{\nu}_{opt}$ the complex Dicke parameter [14,15]. Note that this parameter contributes both to the broadening and shift of a line because it is complex valued.

Appendix B. Temperature dependence of the line shape parameters

This Appendix describes the temperature dependence of the spectral line-shape parameters of the R(0) line of CO in Ar. For simplicity, we omit the Ar superscript within this section, as the CO-CO parameters are excluded from this discussion. We performed fully *ab initio* line-shape calculations to obtain the set of spectroscopic coefficients γ_0, δ_0, γ_2, δ_2, $\tilde{\nu}^{\mathrm{r}}_{\mathrm{opt}}$, $\tilde{\nu}^{\mathrm{i}}_{\mathrm{opt}}$, and y^{r} at temperatures between 100 and 700 K. Table B.4 provides the pressure broadening and shift coefficients, as well as the complex Dicke parameter and the real part of the line mixing coefficient for selected temperatures between 10 and 700 K. Between 77 and 300 K we estimate an error of the order of 0.5% for these data. Below 25 K the error maybe of the order of a few percents due to the resonances that may appear in the kinetic energy dependent cross sections. At 700 K we may have an error of this order, too, due to the methods of quadrature used and extrapolation above E_{kin} = 2000 cm^{-1} (see Eq. (A.3)).

Table B.4
Line shape parameters for the pure rotational R(0) line of CO in argon and for selected temperatures: pressure broadening coefficients (γ_0), pressure shift coefficients (δ_0), real and imaginary parts of the complex Dicke parameter ($\tilde{\nu}_{opt}$), and the real part of the line mixing coefficient (y). The units are 10^{-3} cm^{-1} atm^{-1} (except y, which is in 10^{-3} atm^{-1}). The first entries are obtained with Cybulski's PES [16] and the second ones with Sumiyoshi's PES [41].

T(K)	γ_0	δ_0	$\tilde{\nu}^{\mathrm{r}}_{\mathrm{opt}}$	$\tilde{\nu}^{\mathrm{i}}_{\mathrm{opt}}$	y^{r}
10	975.25	0.08	123.58	14.73	-1.32
	1016.00	2.58	121.22	-2.62	
25	467.45	4.92	58.93	4.38	1.73
	476.48	3.90	57.90	1.12	
50	274.20	2.98	34.05	0.68	4.66
	276.75	2.10	35.16	-0.05	
77	197.60	1.54	24.20	-0.14	5.83
	199.37	1.13	25.21	-0.35	
100	162.00	0.88	19.58	-0.26	6.18
	163.67	0.65	20.40	-0.35	
150	118.80	0.23	13.90	-0.21	6.11
	120.40	0.14	14.45	-0.23	
195	96.98	0.01	11.05	-0.14	5.72
	98.50	-0.04	11.45	-0.15	
240	82.50	-0.08	9.20	-0.09	5.26
	83.93	-0.11	9.52	-0.09	
273	74.60	-0.11	8.22	-0.06	4.94
	75.94	-0.14	8.50	-0.07	
297	69.80	-0.12	7.63	-0.05	4.71
	71.10	-0.14	7.88	-0.05	
400	55.21	-0.13	5.92	-0.01	3.90
	56.35	-0.14	6.05	-0.01	
500	46.30	-0.11	4.87	0.00	3.30
	47.25	-0.12	4.90	0.00	
600	40.05	-0.09	4.05	0.00	2.85
	40.85	-0.10	3.98	0.00	
700	35.35	-0.07	3.27	0.00	2.49
	36.00	-0.08	3.15	0.00	

The double-power-law (DPL) temperature dependence of the spectral line-shape parameters adopted in the HITRAN database [13,42] is defined by the following equation:

$$X(T) = \sum_{i=1}^{2} \mathrm{Coeff}_i \left(\frac{T_{ref}}{T} \right)^{\mathrm{Exp}_i}, \tag{B.1}$$

where X stands for any particular line-shape parameter, T_{ref} is 296 K, and Coeff$_i$ and Exp$_i$ are the numerical coefficients. The DPL representation of the temperature dependence of the real part

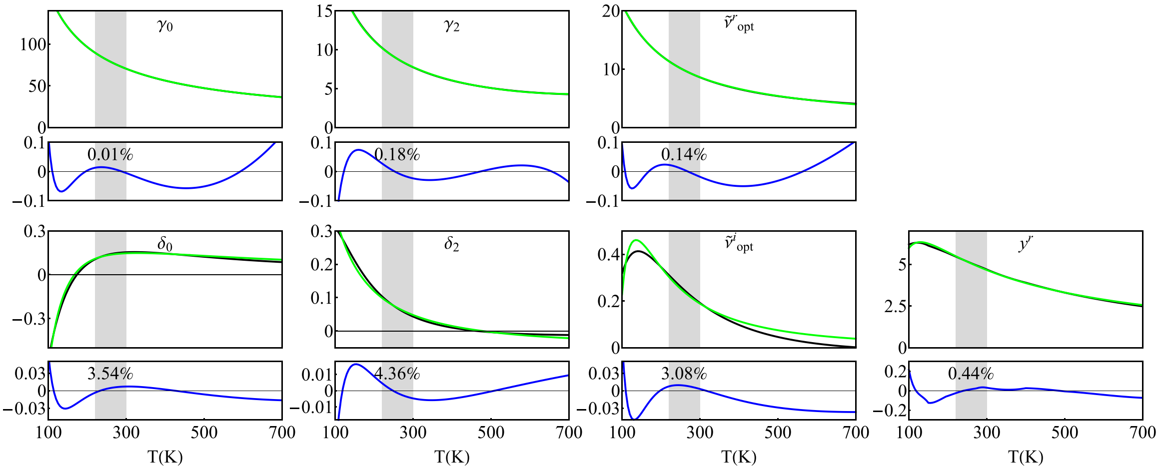

Fig. B.7. Temperature dependences of the spectral line-shape parameters of the R(0) line of CO in Ar. For simplicity, we omit the Ar superscripts in this figure. Each of the seven main plots presents the *ab initio* (black curves) and their double-power-law (DPL) representations [42] (green curves). The units of the vertical axes of the plots are 10^{-3}cm^{-1}atm^{-1}, except for the y^r coefficient having the unit of 10^{-3}atm^{-1}. Below each graph we show residuals, as well as the relative root-mean-square value of the residuals in the prioritized temperature range (the area between 220 and 300K marked with gray background), normalized by the mean value of the corresponding line-shape coefficient in this range. (For interpretation of the references to colour in this figure legend, the reader is referred to the web version of this article.)

Table B.5
The parameters of the DPL representation of the CO-Ar R(0) line-shape parameters. The units of coefficients 1 and 2 are $10^{-3}\text{cm}^{-1}\text{atm}^{-1}$ (except for $\bar{y}$ and $\bar{y'}$ in units of 10^{-3}atm^{-1}) and exponents 1 and 2 are dimensionless. All the DPL coefficients are defined by Eq. (B.1), following the original formulation from Ref. [42].

parameter	Coeff_1	Coeff_2	Exp_1	Exp_2
γ_0(T)	-1.0319	72.2319	1.8536	0.7946
δ_0(T)	100.34175	-100.48787	1.47913	1.47659
γ_2(T)	0.0147	7.8418	-4.4324	0.8909‘
δ_2(T)	-4.048	4.098	0.696	0.721
$\widetilde{\nu}^{\mathrm{r}}_{opt}$(T)	-0.1	8.816	3.13	0.926
$\widetilde{\nu}^{\mathrm{i}}_{opt}$(T)	-19.892	20.085	2.5151	2.5069
y^{r}(T)	-651.20	655.89	1.1897	1.1854

of the line-mixing parameter, Y^{r} has not yet been considered in the HITRAN database. Nonetheless, we applied the DPL function Eq. (B.1) to the Y parameter similarly to the other line-shape parameters.

Fig. B.7 presents a comparison of our *ab initio* data with their DPL representations. While adjusting the DPL function to the *ab initio* data, we performed a weighted fitting procedure, prioritizing the temperature range corresponding to the terrestrial atmosphere (between 220 and 300 K, marked with gray areas in Fig. B.7; we used $\times 10$ weights in this range). Below each of the seven graphs, we plot absolute residuals and give the relative root mean square error (rRMSE) in the prioritized temperature range, normalized by the mean value of the considered line-shape parameter in the prioritized range. While the accuracy achieved for the γ_0, γ_2 and $\widetilde{\nu}^r_{\text{opt}}$ is on the per mile level or better (0.01% for γ_0), the values of rRMSE values for δ_0, δ_2, and $\widetilde{\nu}^i_{\text{opt}}$ are relatively high due to the low value of the normalization factor in the denominator. Table B.5 contains the set of coefficients required to reconstruct the DPL parameterization of our R(0) line defined by Eq. (B.1).

References

[1] Hartmann J-M, Boulet C, Robert D. Collisional effects on molecular spectra. Amsterdam: Elsevier; 2008.

[2] Hartmann J-M, Tran H, Armante R, Boulet C, Campargue A, Forget F, Gianfrani L, Gordon I, Guerlet S, Gustafsson M, Hodges JT, Kassi S, Lisak D, Thibault F, Toon GC. Recent advances in collisional effects on spectra of molecular gases and their practical consequences. J Quant Spectrosc Radiat Transfer 2018;213:178–227.

[3] Hess S. Kinetic theory of spectral line shapes. the transition between Doppler broadening and collisional broadening. Physica 1972;61:80–94.

[4] Schaefer J, Köhler W. Quantum calculations of rotational and NMR relaxation, depolarized Rayleigh and rotational Raman line shapes for H2(HD)–He mixtures. Physica A 1985;129:469.

[5] Demeio L, Green S, Monchick L. Effects of velocity changing collisions on line shapes of HF in Ar. J Chem Phys 1995;102:9160–6. doi:10.1063/1.468864.

[6] Thibault F, Patkowski K, Żuchowski PS, Jóźwiak H, Ciuryło R, Wcisło P. Rovibrational line-shape parameters for H2 in He and new H2-He potential energy surface. J Quant Spectrosc Radiat Transfer 2017;202:308.

[7] Blackmore R. A modified Boltzmann kinetic equation for line shape functions. J Chem Phys 1987;87:791.

[8] Ciuryło R, Shapiro DA, Drummond JR, May A. Solving the line-shape problem with speed-dependent broadening and shifting and with Dicke narrowing. II. application. Phys Rev A 2002;65:012502.

[9] May A, Liu W-K, McCourt F, Ciuryło R, Stoker JS-F, Shapiro D, Wehr R. The impact theory of spectral line shapes: a paradigm shift. Can J Phys 2013;91:879.

[10] Wcisło P, Thibault F, Zaborowski M, Wójtewicz S, Cygan A, Kowzan G, Masłowski P, Komasa J, Puchalski M, Pachucki K, Ciuryło R, Lisak D. Accurate deuterium spectroscopy for fundamental studies. J Quant Spectrosc Radiat Transfer 2018;213:41.

[11] Jóźwiak H, Thibault F, Stolarczyk N, Wcisło P. Ab initio line-shape calculations for the S and O branches of H_2 perturbed by He. J Quant Spectrosc Radiat Transfer 2018;219:313–22. doi:10.1016/j.jqsrt.2018.08.023.

[12] Słowiski M, Thibault F, Tan Y, Wang J, Liu A-W, Hu S-M, Kassi S, Campargue A, Konefał M, Jówiak H, Patkowski K, Żuchowski P, Ciuryło R, Lisak D, Wcisło P. H_2–He collisions: *Ab initio* theory meets cavity-enhanced spectra. Phys Rev A 2020;101:052705.

[13] Wcisło P, Thibault F, Stolarczyk N, Jóźwiak H, Słowinski M, Gancewski M, Stankiewicz K, Konefał M, Kassi S, Campargue A, Tan Y, Wang J, Patkowski K, Ciuryło R, Lisak D, Kochanov R, Rothman LS, Gordon IE. The first comprehensive dataset of beyond-Voigt line-shape parameters from *ab initio* quantum scattering calculations for the HITRAN database: He-perturbed H_2 case study. J Quant Spectrosc Radiat Transfer 2021;260:107477.

[14] Thibault F, Martnez RZ, Bermejo D, Wcisło P. Line-shape parameters for the first rotational lines of HD in He. Mol Astrophys 2020;19:100063. doi:10.1016/j.molap.2020.100063.

[15] Kowzan G, Wcisło P, Słowiski M, Masłowski P, Viel A, Thibault F. Fully quantum calculations of the line-shape parameters for the Hartmann-Tran profile: A CO-Ar case study. J Quant Spectrosc Radiat Transfer 2020;243:106803. doi:10.1016/j.jqsrt.2019.106803.

[16] Kowzan G, Cybulski H, Wcisło P, Słowiński M, Viel A, Masłowski P, Thibault F. Subpercent agreement between ab initio and experimental collision-induced line shapes of carbon monoxide perturbed by argon. Phys Rev A 2020;102:012821. doi:10.1103/PhysRevA.102.012821.

[17] Winnewisser G, Belov SP, Klaus T, Schieder R. Sub-Doppler measurements on the rotational transitions of carbon monoxide. J Mol Spectrosc 1997;184:468–72.

[18] Read WG, K W Hillig I, Cohen EA, Pickett HM. The measurement of absolute absorption of millimeter radiation in gases: the absorption of CO and O2. IEEE Trans Antennas Propag 1988;36:1136–43.

[19] Mader H, Guarnieri A, Doose J, Nissen N, Markov VN, Shtanyuk AM, Andrianov AF, Shanin VN, Krupnov AF. Comparative studies of $J-J=1-0$ CO line parameters in frequency and time domains. J Mol Spectrosc 1996;180:183–7.

[20] Markov VN, Mader H. Pressure self-shift of the $J=1-0$ line of carbon monoxide. J Mol Spectrosc 2001;205:350–2. doi:10.1006/jmsp.2000.8277.

[21] Yamada K, Abe H. The line broadening and shift effects on the CO $J=5-4$ transition at 576 GHz induced by collisions with rare gases. J Mol Spectrosc 2003;217:87–92.

[22] Colmont J-M, Nguyen L, Rohart F, Wlodarczak G. Lineshape analysis of the $J=3-2$ and $J=5-4$ rotational transitions of room temperature CO broadened by N_2, O_2, CO_2 and noble gases. J Mol Spectrosc 2007;246:86–97.

[23] Seleznev AF, Fedoseev GV, Koshelev MA, Tretyakov MY. Shape of collision-broadened lines of carbon monoxide. J Quant Spectrosc Radiat Transfer 2015;161:171–9.

[24] Thibault F, Boissoles J, Le Doucen R, Farrenq R, MorillonChapey M, Boulet C. Line-by-line measurements of interference parameters for the 0-1 and 0-2 bands of CO in He, and comparison with coupledstates calculations. J Chem Phys 1992;97(7):4623–32. doi:10.1063/1.463865.

[25] Boissoles J, Thibault F, Domenech JL, Bermejo D, Boulet C, Hartmann JM. Temperature dependence of line mixing effects in the stimulated Raman Q-branch of CO in He: a further test of close coupling calculations. J Chem Phys 2001;115(16):7420–8. doi:10.1063/1.1394752.

[26] Martínez RZ, Domenech JL, Bermejo D, Thibault F, Bouanich J-P, Boulet C. Close coupling calculations for rotational relaxation of CO in argon: Accuracy of energy corrected sudden scaling procedures and comparison with experimental data. J Chem Phys 2003;119(20):10563–74. doi:10.1063/1.1620506.

[27] Predoi-Cross A, Esteki K, Rozario H, Naseri H, Latif S, Thibault F, Malathy Devi V, Smith M, Mantz A. Theoretical and revisited experimentally retrieved He-broadened line parameters of carbon monoxide in the fundamental band. J Quant Spectrosc Radiat Transfer 2016;184:322–40. doi:10.1016/j.jqsrt.2016.08.007.

[28] Predoi-Cross A, Bouanich JP, Benner DC, May AD, Drummond JR. Broadening, shifting, and line asymmetries in the $2\leftarrow0$ band of CO and CO–N_2 : Experimental results and theoretical calculations. J Chem Phys 2000;113(1):158–68. doi:10.1063/1.481783.

[29] Bendana FA, Lee DD, Wei C, Pineda DI, Spearrin RM. Line mixing and broadening in the $\nu(1-3)$ first overtone bandhead of carbon monoxide at high temperatures and high pressures. J Quant Spectrosc Radiat Transfer 2019;239:106636. doi:10.1016/j.jqsrt.2019.106636.

[30] Krupnov AF, Tretyakov MY, Belov SP, Golubiatnikov GY, Parshin VV, Koshelev MA, Makarov DS, Serov EA. Accurate broadband rotational BWO-based spectroscopy. J Mol Spectrosc 2012;280:110–18. doi:10.1016/j.jms.2012.06.010.

[31] Golubiatnikov GY, Belov SP, Leonov II, Andriyanov AF, Zinchenko II, Lapinov AV, Markov VN, Shkaev AP, Guarnieri A. Precision sub-Doppler millimeter and submillimeter Lamb-dip spectrometer. Radiophys Quantum El 2014;56:599–609.

[32] Golubiatnikov GY, Belov SP, Lapinov AV. The features of the frequency-modulation method when studying the shapes of the spectral lines of nonlinear absorption. Radiophys Quantum El 2017;59:715–26. doi:10.1007/s11141-017-9740-z.

[33] Krupnov AF. Academic Press, L; 1979. p. 217–56.

[34] Tretyakov MY, Koshelev MA, Makarov DS, Tonkov MV. Precise measurements of collision parameters of spectral lines with a spectrometer with radioacoustic detection of absorption in the millimeter and submillimeter ranges. Instrum Exp Tech 2008;51(1):78–88.

[35] Koshelev MA, Tsvetkov AI, Morozkin MV, Glyavin MY, Tretyakov MY. Molecular gas spectroscopy using radioacoustic detection and high-power coherent subterahertz radiation sources. J Mol Spectrosc 2017;331:9–16. doi:10.1016/j.jms.2016.10.014.

[36] Golubiatnikov GY, Koshelev MA, Tsvetkov AI, Fokin AP, Glyavin MY, Tretyakov MY. Sub-terahertz high-sensitivity high-resolution molecular spectroscopy with a gyrotron. IEEE Trans Terahertz Sci Technol 2020;10(5):502–12. doi:10.1109/TTHZ.2020.2984459.

[37] Koshelev MA, Leonov II, Serov EA, Chernova AI, Balashov AA, Bubnov GM, et al. New frontiers in modern resonator spectroscopy. IEEE Trans Terahertz Sci Technol 2018;8:773–83.

[38] Vlasov SN, Koposova EV, Kornishin SY, Parshin VV, Perminov DA, Serov EA. Wideband windows for vacuum devices of millimeter and submillimeter wavelength ranges. Radiophys Quantum El 2020;63:106–13.

[39] Dymond JH, Marsh KN, Wilhoit RC, Wong KC. Virial coefficients of pure gases and mixtures subvolume A: virial coefficients of pure gases. Berlin, Heidelberg, New York: Springer-Verlag; 2002.

[40] Dymond JH, Marsh KN, Wilhoit RC. Virial coefficients of pure gases and mixtures subvolume B: virial coefficients of mixtures. Berlin, Heidelberg, New York: Springer-Verlag; 2003.

[41] Sumiyoshi Y, Endo Y. Three-dimensional potential energy surface of Ar — CO. J Chem Phys 2015;142:024314. doi:10.1063/1.4905268.

[42] Stolarczyk N, Thibault F, Cybulski H, Jóźwiak H, Kowzan G, Vispoel B, et al. Evaluation of different parameterizations of temperature dependences of the line-shape parameters based on ab initio calculations: case study for the HITRAN database. J Quant Spectrosc Radiat Transfer 2020;240:106676. doi:10.1016/j.jqsrt.2019.106676.

[43] Murrell JN, Sorbie KS. New analytic form for the potential energy curves of stable diatomic states. J Chem Soc, Faraday Trans 2 1974;70:1552–6. doi:10.1039/F29747001552.

[44] Huxley P, Murrell JN. Ground-state diatomic potentials. J Chem Soc, Faraday Trans 2 1983;79:323–8. doi:10.1039/F29837900323.

[45] Hutson J.M., Green S.. MOLSCAT version14, Collaborative Computational Project 6 of the UK Science and Engineering Research Council, Daresbury Laboratory, UK1995;.

[46] McBane G.C.. PMP Molscat, a parallel version of Molscat version 14, available at Grand Valley State University2005;http://faculty.gvsu.edu/mcbaneg/pmpmolscat.

[47] Luo C, Wehr R, Drummond JR, May AD, Thibault F, Boissoles J, Launay JM, Boulet C, Bouanich J-P, Hartmann J-M. Shifting and broadening in the fundamental band of CO highly diluted in He and Ar: A comparison with theory. J Chem Phys 2001;115(5):2198–206. doi:10.1063/1.1383049.

[48] Thibault F, Martínez RZ, Domenech JL, Bermejo D, Bouanich J-P. Raman and infrared linewidths of CO in Ar. J Chem Phys 2002;117(6):2523–31. doi:10.1063/1.1494975.

[49] Wehr R, Vitcu A, Ciuryło R, Thibault F, Drummond JR, May AD. Spectral line shape of the $P(2)$ transition in CO-Ar: uncorrelated ab initio calculation. Phys Rev A 2002;66:062502. doi:10.1103/PhysRevA.66.062502.

[50] Mantz AW, Thibault F, Cacheiro JL, Fernandez B, Pedersen TB, Koch H, Valentin A, Claveau C, Henry A, Hurtmans D. Argon broadening of the ^{13}CO R(0) and R(7) transitions in the fundamental band at temperatures between 80 and 297 K: comparison between experiment and theory. J Mol Spectrosc 2003;222(2):131–41. doi:10.1016/S0022-2852(03)00200-5.

[51] Wehr R, Ciuryło R, Vitcu A, Thibault F, Drummond JR, May AD. Dicke-narrowed spectral line shapes of CO in Ar: Experimental results and a revised interpretation. J Mol Spectrosc 2006;235(1):54–68. doi:10.1016/j.jms.2005.10.009.

[52] Wehr R, Vitcu A, Thibault F, Drummond JR, May AD. Collisional line shifting and broadening in the fundamental P-branch of CO in Ar between 214 and 324 K. J Mol Spectrosc 2006;235(1):69–76. doi:10.1016/j.jms.2005.10.004.

[53] Corey GC, McCourt FR. Dicke narrowing and collisional broadening of spectral lines in dilute molecular gases. J Chem Phys 1984;81:2318–29. doi:10.1063/1.447930.

[54] Monchick L, Hunter LW. Diatomic-diatomic molecular collision integrals for pressure broadening and Dicke narrowing: a generalization of Hess's theory. J Chem Phys 1986;85:713–18. doi:10.1063/1.451277.

[55] Yutsis AP, Levinson I, Vanagas VV. Mathematical apparatus of the theory of angular momentum. Jerusalem: Israel Program for Scientific Translations; 1962. doi:101007/978-3-662-10403-3.

[56] Schaefer J, Monchick L. Line shape cross sections of HD immersed in He and H_2 gas. I. Pressure broadening cross sections. J Chem Phys 1987;87:171–81. doi:10.1063/1.453612.

[57] Schaefer J, Monchick L. Line broadening of HD immersed in He and H_2 gas. A&A 1992;265:859–68.

[58] Ben-Reuven A. Impact broadening of microwave spectra. Phys Rev 1966;145:7–22. doi:10.1103/PhysRev.145.7.

[59] Shafer R, Gordon RG. Quantum scattering theory of rotational relaxation and spectral line shapes in H_2 - He gas mixtures. J Chem Phys 1973;58:5422–43. doi:10.1063/1.1679162.

[60] Fano U. Pressure broadening as a prototype of relaxation. Phys Rev 1963;131:259–68. doi:10.1103/PhysRev.131.259.

[61] Martínez RZ, Bermejo D, Thibault F, Wcisło P. Testing the ab initio quantum-scattering calculations for the D_2-He benchmark system with stimulated Raman spectroscopy. J Raman Spectrosc 2018;49(8):1339–49. doi:10.1002/jrs.5391.

[62] Lévy A, Lacome N, Chackerian C. Collisional line mixing. In: Rao KN, Weber A, editors. Spectroscopy of the Earth's Atmosphere and Interstellar Medium. Academic Press; 1992. p. 261–337. ISBN 978-0-12-580645-9. doi:10.1016/B978-0-12-580645-9.50008-3.

[63] DePristo AE, Augustin SD, Ramaswamy R, Rabitz H. Quantum number and energy scaling for nonreactive collisions. J Chem Phys 1979;71(2):850–65. doi:10.1063/1.438376.

[64] Thibault F, Boissoles J, Boulet C, Ozanne L, Bouanich JP, Roche CF, Hutson JM. Energy corrected sudden calculations of linewidths and line shapes based on coupled states cross sections: the test case of CO_2-argon. J Chem Phys 1998;109(15):6338–45. doi:10.1063/1.477187.

[65] Bonamy L, Thuet JM, Bonamy J, Robert D. Local scaling analysis of state-to-state rotational energy-transfer rates in N_2 from direct measurements. J Chem Phys 1991;95(5):3361–70. doi:10.1063/1.460841.

[66] Millot G. Rotationally inelastic rates over a wide temperature range based on an energy corrected sudden exponential power theoretical analysis of Raman line broadening coefficients and Q branch collapse. J Chem Phys 1990;93(11):8001–10. doi:10.1063/1.459329.

[67] Rosenkranz PW. Shape of the 5 mm oxygen band in the atmosphere. IEEE Trans Antennas Propag 1975;23(4):498–506. doi:10.1109/TAP.1975.1141119.

[68] Smith EW. Absorption and dispersion in the O_2 microwave spectrum at atmospheric pressures. J Chem Phys 1981;74(12):6658–73. doi:10.1063/1.441112.

[69] Boulet C, Hartmann J-M. Toward measurements of the speed-dependence of line-mixing. J Quant Spectrosc Radiat Transfer 2021;262:107510. doi:10.1016/j.jqsrt.2021.107510.

[70] Esteki K, Predoi-Cross A, Povey C, Ivanov S, Ghoufi A, Thibault F, Smith MAH. Room temperature self- and H_2-broadened line parameters of carbon monoxide in the first overtone band: theoretical and revised experimental results. J Quant Spectrosc Radiat Transfer 2017;203:309–24. doi:10.1016/j.jqsrt.2017.04.008.

[71] Ciuryło R. Shapes of pressure- and Doppler-broadened spectral lines in the core and near wings. Phys Rev A 1998;58:1029–39. doi:10.1103/PhysRevA.58.1029.

[72] Vleck JHV, Weisskopf VF. On the shape of collision-broadened lines. Rev Mod Phys 1945;17:227–36. doi:10.1103/RevModPhys.17.227.

[73] Makarov DS, Vilkov IN, Koshelev MA, Aderkina AA, Tretyakov MY. Collisional coupling of the molecular oxygen $^{16}O_2$ fine-structure lines under low pressures. Radiophys Quantum El 2018;60(10):808–23. doi:10.1007/s11141-018-9849-8.

[74] Rosenkranz P. Interference coefficients for overlapping oxygen lines in air. J Quant Spectrosc Radiat Transfer 1988;39(4):287–97. doi:10.1016/0022-4073(88)90004-0.

[75] Malathy DV, Benner DC, Smith MH, Mantz AW, Sung K, Brown LR. Spectral line parameters including temperature dependences of self- and air-broadening in the 2←0 band of CO at 2.3 µm. J Quant Spectrosc Radiat Transfer 2012;113:1013–33.

[76] Voigt W. Aber das Gesetz der Intensittsverteilurg innerhalb der Linien eines Gasspektrnms. Sitzber KB Akad Wiss Mnchen, Math-Phys Klasse 1912:603–20.

[77] Demtröder W. Laser spectroscopy: basic concepts and instrumentation. 35th. New York, NY, USA: Springer; 2008.

[78] Coxon JA, Hajigeorgiou PG. Direct potential fit analysis of the $X^1\Sigma^+$ ground state of CO. J Chem Phys 2004;121(7):2992–3008. doi:10.1063/1.1768167.

[79] Li G, Gordon IE, Rothman LS, Tan Y, Hu S-M, Kassi S, Campargue A, Medvedev ES. Rovibrational line lists for nine isotopologues of the CO molecule in the $X^1\Sigma^+$ ground electronic state. ApJS 2015;216(1):15. doi:10.1088/0067-0049/216/1/15.

[80] Clough SA, Kneizys FX, Davies RW. Line shape and the water vapor continuum. Atmos Res 1989;23:229–41.

[81] Gordon IE, Rothman LS, Hill C, Kochanov RV, Tan Y, Bernath PF, Birk M, Boudon V, Campargue A, Chance KV, Drouin BJ, Flaud J-M, Gamache RR, Hodges JT, Jacquemart D, Perevalov VI, Perrin A, Shine KP, Smith M-AH, Tennyson J, Toon GC, Tran H, Tyuterev VG, Barbe A, Csszr AG, Devi VM, Furtenbacher T, Harrison JJ, Hartmann J-M, Jolly A, Johnson TJ, Karman T, Kleiner I, Kyuberis AA, Loos J, Lyulin OM, Massie ST, Mikhailenko SN, Moazzen-Ahmadi N, Mller HSP, Naumenko OV, Nikitin AV, Polyansky OL, Rey M, Rotger M, Sharpe SW, Sung K, Starikova E, Tashkun SA, Auwera JV, Wagner G, Wilzewski J, Wcisło P, Yu S, Zak EJ. The HITRAN2016 molecular spectroscopic database. J Quant Spectrosc Radiat Transfer 2017;203:3–69. doi:10.1016/j.jqsrt.2017.06.038.

[82] Hill RJ. Water vapor-absorption line shape comparison using the 22-GHz line: the Van Vleck–Weisskopf shape affirmed. Radio Sci 1986;21/3:447–51.

Journal of Quantitative Spectroscopy & Radiative Transfer 260 (2021) 107477

Contents lists available at ScienceDirect

Journal of Quantitative Spectroscopy & Radiative Transfer

journal homepage: www.elsevier.com/locate/jqsrt

The first comprehensive dataset of beyond-Voigt line-shape parameters from *ab initio* quantum scattering calculations for the HITRAN database: He-perturbed H_2 case study

P. Wcisło[a,*], F. Thibault[b], N. Stolarczyk[a], H. Jóźwiak[a], M. Słowiński[a], M. Gancewski[a], K. Stankiewicz[a], M. Konefał[a,c], S. Kassi[c], A. Campargue[c], Y. Tan[d], J. Wang[d], K. Patkowski[e], R. Ciuryło[a], D. Lisak[a], R. Kochanov[f,g], L.S. Rothman[f], I.E. Gordon[f]

[a] *Institute of Physics, Faculty of Physics, Astronomy and Informatics, Nicolaus Copernicus University in Torun, Grudziadzka 5, 87-100 Torun, Poland*
[b] *Univ Rennes, CNRS, IPR (Institut de Physique de Rennes)-UMR 6251, F-35000 Rennes, France*
[c] *University of Grenoble Alpes, CNRS, LIPhy, F-38000 Grenoble, France*
[d] *Hefei National Laboratory for Physical Sciences at Microscale, iChEM, University of Science and Technology of China, Hefei, 230026 China*
[e] *Department of Chemistry and Biochemistry, Auburn University, Auburn, AL 36849, USA*
[f] *Harvard-Smithsonian Center for Astrophysics, Atomic and Molecular Physics Division, Cambridge, MA, USA*
[g] *QUAMER laboratory, Tomsk State University, 36 Lenin Avenue, 634050 Tomsk, Russia*

ARTICLE INFO

Article history:
Received 15 September 2020
Revised 9 December 2020
Accepted 9 December 2020
Available online 11 December 2020

Keywords:
Beyond-Voigt line-shape parameters
HITRAN
H2-He
Ab initio quantum scattering calculations

ABSTRACT

We demonstrate a new method for populating line-by-line spectroscopic databases with beyond-Voigt line-shape parameters, which is based on *ab initio* quantum scattering calculations. We report a comprehensive dataset for the benchmark system of He-perturbed H_2 (we cover all the rovibrational bands that are present in the HITRAN spectroscopic database). We generate the entire dataset of the line-shape parameters (broadening and shift, their speed dependence, and the complex Dicke parameter) from fully *ab initio* quantum-scattering calculations. We extend the previous calculations by taking into account the centrifugal distortion for all the bands and by including the hot bands. The results are projected on a simple structure of the quadratic speed-dependent hard-collision profile. We report a simple and compact formula that allows the speed-dependence parameters to be calculated directly from the generalized spectroscopic cross sections. For each line and each line-shape parameter, we provide a full temperature dependence within the double-power-law (DPL) representation, which makes the dataset compatible with the HITRAN database. The temperature dependences cover the range from 20 to 1000 K, which includes the low temperatures relevant for the studies of the atmospheres of giant planets. The final outcome from our dataset is validated on highly accurate experimental spectra collected with cavity ring-down spectrometers. The methodology can be applied to many other molecular species important for atmospheric and planetary studies.

1. Introduction

The collisional line-shape effects, including the beyond-Voigt effects [1–8], play an important role in atomic and molecular physics [9–13]. On one hand, they give access to studying the molecular interactions [14–16] and dynamics [17], but on the other hand they can affect the accuracy of optical metrology based on molecular spectroscopy [18]. In particular, insufficient modeling of the line-shape effects can limit the accuracy of simulations of atmospheric measurements of the Earth [19] and other planets [20] and even modify the retrieved opacity of exoplanetary atmospheres [21,22]. To address this problem, a new relational structure [23] was introduced into the most widely used line-by-line spectroscopic database, HITRAN [24], allowing the beyond-Voigt line-shape effects to be represented [25]. It is, however, remarkably challenging to populate the entire database (all the molecules and their isotopologues over a great spectral range and thermodynamic conditions) with purely experimental beyond-Voigt line-shape parameters, not only due to a large number of transitions to be measured at different conditions and different spectral ranges, but

---

[*] Corresponding author.
E-mail addresses: piotr.wcislo@fizyka.umk.pl, piotr.wcislo@umk.pl (P. Wcisło).

https://doi.org/10.1016/j.jqsrt.2020.107477

also due to strong numerical correlations between the line-shape parameters.

In this article, we demonstrate a new method for populating line-by-line spectroscopic databases with beyond-Voigt line-shape parameters that is based on *ab initio* quantum scattering calculations. We report a comprehensive dataset for the benchmark system of He-perturbed H_2 lines. We cover all the rovibrational bands (with their branches) that are present in HITRAN. We generate the values of the line-shape parameters (broadening and shift, their speed dependence, and the complex Dicke parameter) from fully *ab initio* quantum-scattering calculations. We extend the calculations of the generalized spectroscopic cross sections reported in Refs. [15,26] by taking into account the centrifugal distortion for all the bands and by including the hot bands. We extrapolate the *ab initio* results to populate very weak lines, i.e., higher overtones, $v' \geq 6$, higher rotational numbers, $J' \geq 8$, and high-v' hot bands, $v' \geq 6$; following the standard HITRAN notation, we denote the final and initial states of a transition with primes and double primes, respectively. The results are projected on a simple structure of the quadratic speed-dependent hard-collision (qSDHC) profile [27–29] that is consistent with the recently recommended HITRAN parametrization [30]. We also report a simple and compact formula that allows the speed-dependence parameters (within the quadratic model) to be calculated directly from the generalized spectroscopic cross sections, which considerably speeds up the calculations and makes them numerically more stable. For each line and each line-shape parameter we provide a full temperature dependence within the double-power-law (DPL) representation, which was recently recommended for the HITRAN database [30]. The results are valid for a wide temperature range from 20 to 1000 K, with the 50–200 K range prioritized (in this range the DPL fits have 10 times larger weights), which is relevant for the studies of the atmospheres of giant planets. The final outcome from our dataset is validated on highly accurate experimental spectra collected with cavity ring-down spectrometers [31] demonstrating sub-percent agreement. Incorporation of beyond-Voigt line-shape parameters reported in this paper together with their DPL temperature dependences into the HITRAN database is possible thanks to the recently developed flexible relational structure of HITRAN [23]. The complex structure of this dataset is easily accessible for non-expert HITRAN users thanks to the HITRAN Application Programming Interface (HAPI) [32] that automatically generates spectra at the desired spectral range and thermodynamic conditions chosen by the user.

The atmospheres of the giant planets in the Solar System are greatly dominated by a mixture of molecular hydrogen and atomic helium. Moreover, atmospheres of some types of super-Earth exoplanets are predicted to be dominated by the H_2-He mixture [21]. The spectroscopic studies of giant planet atmospheres are naturally based on the main isotopologue of molecular hydrogen [33]. However, although the abundance of hydrogen deuteride is 4–5 orders of magnitude smaller, HD is noticeable in the spectroscopic studies of giant planets [20,33] due to the much larger intensity of the dipole transitions compared to the weak quadrupole lines in H_2. In total, four combinations of collision partners should be considered to provide a complete reference data for the planetary studies: self-perturbed H_2, He-perturbed H_2, H_2-perturbed HD and He-perturbed HD. In this article, we consider the simplest benchmark case of He-perturbed H_2.

In Section 2, we discuss the general methodology of generating beyond-Voigt line-shape parameters from *ab initio* calculations. Section 3 illustrates the methodology on the examples of two rovibrational lines in He-perturbed H_2. The full comprehensive dataset for He-perturbed H_2 is discussed in Section 4 and the complete dataset is provided in the supplementary material [34].

2. Methodology of generating datasets of the beyond-Voigt line-shape parameters based on the ab initio calculations

A typical approach to populating the HITRAN database with the beyond-Voigt line-shape parameters [24,32] uses the data that were obtained from fitting the advanced profiles to the high-quality experimental spectra [25,35–39], see the red boxes in the flowchart in Fig. 1. It is a challenging task to populate the entire database with the purely experimental approach due to the large number of transitions required to be accurately measured at different conditions. Another difficulty is related to strong numerical correlations between the line-shape parameters, which often results in large systematic errors in the retrieved line-shape parameters. The numerical correlation can be considerably reduced by implementing the multispectrum fitting approach [40–42] which is, however, very demanding from a technical point of view and is still difficult to automatically apply to large experimental datasets.

In this article, we present a new methodology for populating the spectroscopic databases based on *ab initio* calculations. A key factor that enables development of this approach was a demonstration that the fully *ab initio* quantum-scattering calculations can reproduce the shapes of the high-quality collision-perturbed experimental spectra at the subpercent level [31], including the deep non-Voigt regime (by subpercent agreement we mean that the root-mean-square error of the *ab initio* model relative to profile peak (rRMSE) calculated within ±FWHM is smaller than 1%). The flowchart in Fig. 1 illustrates our methodology (see the yellow boxes). The chain of the *ab initio* calculations starts with the quantum-chemical calculations of the PESs [14,15]. In the second step, the PESs are used to perform the quantum-scattering calculations by solving the close-coupling equations, which provide the scattering S-matrices as a function of relative kinetic energy of the collision, E_{kin}. The S-matrices allow us to calculate the generalized spectroscopic cross-sections, $\sigma_\lambda^q(E_{kin})$, that describe the collision perturbation of the optical coherence associated with the considered molecular transition. This approach also allows for the calculations of off-diagonal generalized spectroscopic cross-sections. Thus, for instance, the well-known case of overlapping lines could be considered. However, in this study we limit the discussion to the case of isolated lines, which is relevant for the molecular system considered here at pressures typical for the atmospheres of gas giants. We consider two types of generalized cross-sections that differ by the rank of the velocity tensor, λ. For the zero rank, $\lambda = 0$, σ_λ^q describes perturbation of internal motion of the

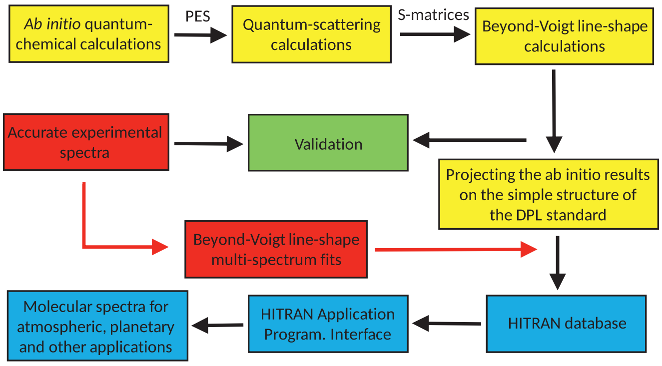

Fig. 1. Diagram illustrating our approach to generating the experimentally validated *ab initio* dataset of the beyond-Voigt line-shape parameters and its incorporation into the HITRAN database. The red arrows show the usual way of populating the database based on experimental spectra analysis only. (For interpretation of the references to color in this figure legend, the reader is referred to the web version of this article.)

molecule, and its real and imaginary parts have spectroscopic interpretation of the pressure broadening and shift cross-sections (PBXS and PSXS, respectively) [43–46]. For $\lambda = 1$, σ^q_λ describes perturbation of translational motion (including the correlations with dephasing and state-changing collisions) and it has spectroscopic interpretation of the complex Dicke cross-section (its real and imaginary parts are denoted as RDXS and IDXS, respectively) [26,47–50]. q is the tensor rank of the spectral transition operator (equal to 1 and 2 for dipole and quadrupole lines, respectively). In principle, σ^q_λ should also be labeled with the quantum numbers specifying the ground and excited levels of the transition (a diagonal cross-section in Liouville space); for the sake of notation clarity we skip them in this article. The two complex cross sections, σ^q_0 and σ^q_1, allow us to calculate the collisional quantities that are needed for modeling the beyond-Voigt shapes of molecular lines, as depicted in the third yellow box in Fig. 1. The basic quantities are the collisional broadening, γ, and shift, δ, of molecular lines expressed as a function of active molecule speed, v, which can be calculated as [3,51]

$$\gamma(v) + i\delta(v) \\ = \frac{1}{2\pi c}\frac{1}{k_BT}\frac{2}{\sqrt{\pi}v\bar{v}_p}\int_0^\infty dv_r v_r^2 e^{-\frac{v^2+v_r^2}{\bar{v}_p^2}} \sinh\left(\frac{2vv_r}{\bar{v}_p^2}\right)\sigma^q_0(v_r), \quad (1)$$

where $\bar{v}_p$ and v_r are the most probable speed of the perturber distribution and relative absorber-perturber speed, respectively. k_B and T are the Boltzmann constant and temperature. Two other line-shape parameters, which quantify the rate of the velocity-changing collisions, are the real, $\tilde{\nu}^{\mathrm{r}}_{\mathrm{opt}}$, and imaginary, $\tilde{\nu}^{\mathrm{i}}_{\mathrm{opt}}$, parts of the complex Dicke parameter, $\tilde{\nu}_{\mathrm{opt}}$, which is calculated as

$$\tilde{\nu}_{\mathrm{opt}} = \tilde{\nu}^{\mathrm{r}}_{\mathrm{opt}} + i\tilde{\nu}^{\mathrm{i}}_{\mathrm{opt}} = \frac{1}{2\pi c}\frac{1}{k_BT}\langle v_r\rangle M_2 \\ \times \int_0^\infty dx\, xe^{-x}\left[\frac{2}{3}x\sigma^q_1(E_{kin} = xk_BT) - \sigma^q_0(E_{kin} = xk_BT)\right], \quad (2)$$

where $M_2 = m_2/(m_1 + m_2)$, and m_1 and m_2 are the masses of the active and perturbing molecules (or atoms), $\langle v_r\rangle = \sqrt{8k_BT/\pi\mu}$ is the average relative speed and μ is the reduced mass of the colliding partners. The variable of integration, x, is a dimensionless kinetic energy of a collision, $x = E_{kin}/(k_BT)$. The quantities expressed by Eqs. (1) and (2) [i.e., $\gamma(v)$, $\delta(v)$, $\tilde{\nu}^{\mathrm{r}}_{\mathrm{opt}}$ and $\tilde{\nu}^{\mathrm{i}}_{\mathrm{opt}}$] carry all the collisional information that comes from our *ab initio* calculations and enters the beyond-Voigt line-shape models. The details of the line-shape calculations based on these quantities can be found in Ref. [6,52,53].

From the perspective of spectroscopy applications and populating the HITRAN database, the full speed dependences, given by Eq. (1), and full *ab initio* line-shape models [53] are far too complex to be stored in the database and are computationally too demanding to be used to analyze large sets of molecular spectra. Therefore, following Ref. [30], we project the full *ab initio* line-shape model on a simple structure of the quadratic speed-dependent hard-collision model (qSDHC) [27–29], in which the speed dependence is approximated with a quadratic function [54]

$$\gamma(v) + i\delta(v) \approx \gamma_0 + i\delta_0 + (\gamma_2 + i\delta_2)\left(v^2/v_m^2 - 3/2\right), \quad (3)$$

where v_m is the most probable absorber speed. The speed-averaged broadening and shift, γ_0 and δ_0, are calculated as real and imaginary parts of a simple average of σ^q_0 over the Maxwellian E_{kin} distribution [3,51]

$$\gamma_0 + i\delta_0 = \frac{1}{2\pi c}\frac{1}{k_BT}\langle v_r\rangle\int_0^\infty dx\, xe^{-x}\sigma^q_0(E_{kin} = xk_BT). \quad (4)$$

Alternatively, γ_0 and δ_0 can be calculated by averaging $\gamma(v)$ and $\delta(v)$ over the Maxwell distribution of active molecule speed, v, yielding exactly the same result as Eq. (4). The two parameters quantifying the speed dependence of the broadening and shift, γ_2 and δ_2, are calculated by demanding that the slope of the quadratic approximation equals the slope of the actual speed dependences at $v = v_m$ [53],

$$\gamma_2 + i\delta_2 = \frac{v_m}{2}\frac{d}{dv}(\gamma(v) + i\delta(v))|_{v=v_m}. \quad (5)$$

Following the generalized Hess method [4,48,50], we directly take the complex Dicke parameter, $\tilde{\nu}_{\mathrm{opt}} = \tilde{\nu}^{\mathrm{r}}_{\mathrm{opt}} + i\tilde{\nu}^{\mathrm{i}}_{\mathrm{opt}}$, as a complex rate of the velocity-changing collisions in the qSDHC model [30]. In the cases of molecules for which the Dicke narrowing is pronounced, we recommend the use of the β correction [25,55] that improves the hard-collision approximation without increasing the cost of the line-shape computations. Note that the β correction is a generic concept valid for any molecular system and does not require any additional parameter to be stored (it depends only on the perturber-to-absorber mass ratio [55]). In total, the most general form of the qSDHC profile requires six line-shape parameters to be stored:

$$\gamma_0, \delta_0, \gamma_2, \delta_2, \tilde{\nu}^{\mathrm{r}}_{\mathrm{opt}}, \tilde{\nu}^{\mathrm{i}}_{\mathrm{opt}}. \quad (6)$$

The recent approach adopted in HITRAN [30] allows the temperature dependences of all the six line-shape parameter to be represented with the double-power-law (DPL):

$$\begin{aligned}
\gamma_0(T) &= g_0(T_{\mathrm{ref}}/T)^n + g_0'(T_{\mathrm{ref}}/T)^{n'},\\
\delta_0(T) &= d_0(T_{\mathrm{ref}}/T)^m + d_0'(T_{\mathrm{ref}}/T)^{m'},\\
\gamma_2(T) &= g_2(T_{\mathrm{ref}}/T)^j + g_2'(T_{\mathrm{ref}}/T)^{j'},\\
\delta_2(T) &= d_2(T_{\mathrm{ref}}/T)^k + d_2'(T_{\mathrm{ref}}/T)^{k'},\\
\tilde{\nu}^{\mathrm{r}}_{\mathrm{opt}}(T) &= r(T_{\mathrm{ref}}/T)^p + r'(T_{\mathrm{ref}}/T)^{p'},\\
\tilde{\nu}^{\mathrm{i}}_{\mathrm{opt}}(T) &= i(T_{\mathrm{ref}}/T)^q + i'(T_{\mathrm{ref}}/T)^{q'},
\end{aligned} \quad (7)$$

where $T_{\mathrm{ref}} = 296$ K. The full parametrization of the collisional line-shape effects requires 24 coefficients per single line, i.e., four coefficients per each of the six line-shape parameters, see Eq. (7). It should be noted that Eq. (7) represent the most general case of the DPL representation adopted in HITRAN [30]. For many molecular systems, not all the collisional effects are important at the considered accuracy level and, for a given experimental temperature range, a simple single-power law suffices. In such cases, one of the two approaches will be adopted in HITRAN. Either a single-power law and a smaller number of line-shape parameters will be stored (e.g., γ_0 and δ_0 for the simple Voigt profile or γ_0, δ_0, γ_2 and δ_2 for the quadratic speed-dependent Voigt profile) or the full DPL parametrization will be adopted but some of the 24 coefficients will be set to zero.

In this article, we show that our approach based on *ab initio* calculations allows us to fully benefit from the DPL parametrization given by Eq. (7). We generated a comprehensive dataset of the beyond-Voigt line-shape parameters for a system for which all the six line-shape parameters are necessary to represent the shapes of molecular lines (i.e., He-perturbed H_2) and we use the DPL parametrization to represent these parameters in a wide temperature range, see Section 3.3 for details.

The HITRAN DPL parametrization, see Eq. (7) and Ref. [30], does not use the exact form of the Hartmann-Tran profile (HT profile) [56] but its modified version, the qSDHC profile. The main difference between these profiles is that for the description of the velocity-changing collisions the HT profile uses the frequency of the velocity-changing collisions, $\tilde{\nu}_{\mathrm{vc}}$, and the correlation parameter, η (first introduced by Rautian and Sobelmann [2]), while the qSDHC profile uses an explicit parametrization with the real, $\tilde{\nu}^{\mathrm{r}}_{\mathrm{opt}}$, and imaginary, $\tilde{\nu}^{\mathrm{i}}_{\mathrm{opt}}$, parts of the complex Dicke parameter. The major advantage of the parametrization used in this work [30] is that it avoids singularities in temperature dependences of the complex Dicke parameter that may appear when the HT parametrization is used [30]. Another advantage of the qSDHC profile is that it does not require to introduce unphysical speed dependence of the complex Dicke parameter, in contrast to the original formulation of the HT profile. For details refer to the Appendices A and B in Ref. [30]; see also Ref. [57].

Hartmann proposed a different approach to populating spectroscopic databases with line-shape parameters based on *ab initio* calculations [58] (see also Section 2 in Ref. [30]). In his approach, the *ab initio* line-shape parameters are used with one of the sophisticated line-shape models to generate reference shapes in a wide range of pressures, and then the reference spectra are fitted with some simpler phenomenological model. In his scheme the fitted line-shape parameters lose their physical meaning but, in principle, the shapes of molecular lines should better agree with experiment. Similar tests were done before, for instance see Ref. [59] (in that work, due to a lack of *ab initio* parameters, a sophisticated line-shape model was used with parameters determined experimentally). Recently, this approach was tested for the requantized Classical Molecular Dynamics Simulations corrected with the use of experimental spectra [60]. However, in the case of the He-perturbed H_2 lines considered here, the difference between the qSDHC profile and the more sophisticated ones are much smaller than the difference with experimental data. Hence that approach [58] would not improve the accuracy of the dataset reported here.

3. Illustration of the methodology for the case of 2-0 Q(1) and 3-0 S(1) lines

In this section, we use an example of two rovibrational lines in He-perturbed H_2 to illustrate the methodology described in Section 2 and shown in Fig. 1. We consider the 2-0 Q(1) and 3-0 S(1) quadrupole lines that were recently accurately measured with the cavity enhanced techniques [31]; in this article we refer to them as reference lines. These measurements were used for accurate validation of the *ab initio* collisional line-shape calculations [31] and more recently these spectra were used for validation of improved quantum-scattering calculations that include centrifugal distortion [61].

3.1. Ab initio *quantum scattering calculations*

The H_2-He PES is three-dimensional, i.e., it depends on the distance between the center of mass of the hydrogen molecule and the helium atom, R, the distance between the two hydrogen atoms, r, and the angle between the intra- and intermolecular axes, θ. The quantum-scattering calculations [15,26] that we used to generate the line-shape parameter dataset are based on the recent state-of-the-art PES that is an extension of the PES published by Bakr, Smith and Patkowski [14] (this PES will be referred to as BSP). The BSP PES was calculated using the coupled-cluster method with single, double and perturbative triple (CCSD(T)) excitations, taking into account also the contributions from the higher coupled-cluster excitations. It was determined for ten intramolecular separations, between 1.1 and 1.75 a_0, which was shown to be insufficient for the detailed studies of processes involving the vibrationally excited H_2 molecule (see Section 2 of Ref. [46] and Appendix C of [15] for details). This issue was addressed in the second version of this PES, BSP2, which extended the range of *ab initio* data points to $r \in [0.65, 3.75]$ a_0. The final version of this PES, BSP3 [15], which was used in this work, has improved asymptotic behavior of the H_2-He interaction energy at large R. The quantum scattering calculations based on the BSP3 PES were recently tested on highly accurate cavity-enhanced measurements of the shapes of He-perturbed H_2 2-0 Q(1) and 3-0 S(1) lines [31] resulting in unprecedented agreement between experimental and theoretical collision-induced line shapes. Furthermore, the BSP3 PES was employed in the studies of purely rotational lines of He-perturbed isotopologues of molecular hydrogen: D_2 [47,62] and HD [63,64].

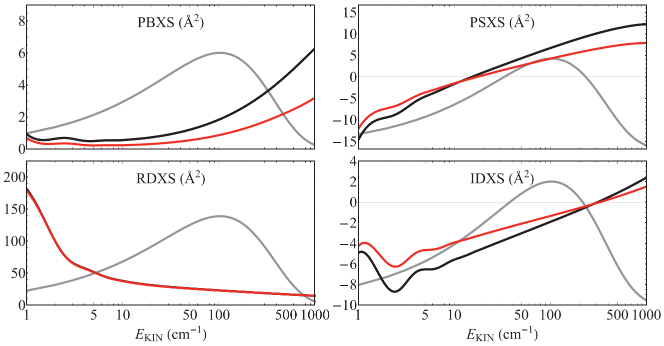

Fig. 2. Examples of the generalized spectroscopic cross sections for the case of 2-0 Q(1) and 3-0 S(1) lines in helium-perturbed H_2, see the red and black lines, respectively. The four panels show the pressure broadening (PBXS), pressure shift (PSXS), and real (RDXS) and imaginary (IDXS) parts of the complex Dicke cross-sections as a function of collision energy. The gray line is the Maxwell-Boltzmann distribution at 296 K in arbitrary units. (For interpretation of the references to color in this figure legend, the reader is referred to the web version of this article.)

For the purpose of dynamical calculations [15,26], the three-dimensional H_2-He PES is projected over Legendre polynomials, P_ξ [15,26,46]:

$$V(R, r, \theta) = \sum_{\xi} v_\xi(R, r) P_\xi(\cos\theta). \tag{8}$$

In the case of homonuclear molecules like H_2, the ξ index takes only even values. Due to the small overall anisotropy of the H_2-He PES, only the first four ξ values are retained throughout the calculations. The $v_\xi(R, r)$ terms are averaged over rovibrational wavefunctions of the unperturbed molecule, $\chi_{v,J}(r)$, leading to the radial coupling terms, $A_{\xi,v,J,v',J'}(R)$, which enter the close-coupled equations. At room temperature the vibrational coupling ($v \neq v'$) can be neglected [15,26]. The influence of the centrifugal distortion (the J dependence of the radial coupling terms) was usually neglected in the scattering calculations for the rovibrational transitions [15,26], as it was suggested that this effect might be masked due to the large contribution from the vibrational dephasing [46]. However, it was shown recently [61,64] that if one aims for sub-percent accuracy of the line-shape parameters, the centrifugal distortion of the potential energy surface must be taken into account. Therefore, the J-dependence of the radial coupling terms $A_{\xi,v,J,v,J'}(R)$ was included in the following analysis.

The scattering calculations were performed using the recently developed BIGOS code [65] for a wide range of relative kinetic energies. The BIGOS code solves the coupled equations in the body-fixed frame of reference using the renormalized Numerov's algorithm [66]. Calculations were carried out for intermolecular distances ranging from 1 to 200 a_0 and three asymptotically closed levels were kept in the basis set. Fig. 2 presents an example of the generalized spectroscopic cross sections for the 2-0 Q(1) and 3-0 S(1) lines.

3.2. *Speed dependence of the broadening and shift, and the quadratic approximation*

The calculations of the γ_0, δ_0, $\tilde{\nu}^{\mathrm{r}}_{\mathrm{opt}}$ and $\tilde{\nu}^{\mathrm{i}}_{\mathrm{opt}}$ parameters are straightforward and require only performing the averaging (with proper weights) of the generalized spectroscopic cross sections over the Maxwell distribution of the relative kinetic energy of a collision, see Eqs. (2) and (4). Calculations of the speed-dependence parameters, γ_2 and δ_2, are, in principle, more complex and require a few additional steps. First, the *ab initio* speed-dependent broadening and shift are calculated from Eq. (1); Fig. 3

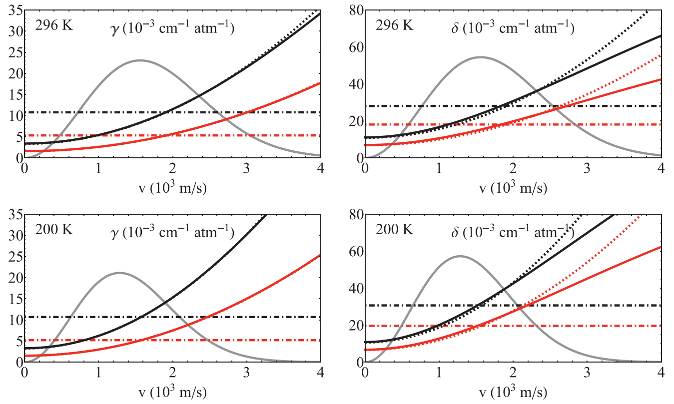

Fig. 3. Examples of the speed dependences of the broadening, γ, and shift, δ, parameters. The red and black lines correspond to the 2-0 Q(1) and 3-0 S(1) lines in helium-perturbed H_2, respectively. The solid lines show the full *ab initio* results and the dotted lines show the quadratic approximations. The dash-dotted lines show the corresponding speed-averaged values. The calculations were done for $T = 296$ K (upper panels) and 200 K (lower panels); the corresponding Maxwell-Boltzmann distributions (in arbitrary units) are plotted as a gray lines. (For interpretation of the references to color in this figure legend, the reader is referred to the web version of this article.)

shows the result for the case of the 2-0 Q(1) and 3-0 S(1) lines. The full speed dependences are approximated with a quadratic function, see Eq. (3). The choice of how the γ_2 and δ_2 parameters are determined is not unique [67,68]. In our methodology we demand that the slopes of the *ab initio* and quadratic speed dependences are equal at the most probable speed, see Eq. (5). This approach is very efficient from a computational perspective. The derivative from Eq. (5) can be done analytically before the integration in Eq. (1) and, hence, the γ_2 and δ_2 parameters can be evaluated directly by averaging the σ_0^q cross section with proper weights

$$\begin{aligned}\gamma_2 + i\delta_2 = {} & \frac{1}{2\pi c}\frac{1}{k_B T}\frac{\overline{v}_p}{\sqrt{\pi}}e^{-y^2} \\ & \times \int_0^\infty \left(2x\cosh(2xy) - \left(\frac{1}{y} + 2y\right)\sinh(2xy)\right) \\ & \times x^2 e^{-x^2}\sigma_0^q(x\overline{v}_p)dx, \qquad (9)\end{aligned}$$

where $x = v_r/\overline{v}_p$ and $y = v_m/\overline{v}_p$, with v_r, v_m and $\overline{v}_p$ being the relative absorber to perturber speed, most probable absorber speed and most probable perturber speed, respectively. Note that $y = \sqrt{\alpha}$, where α is the perturber-to-absorber mass ratio. The quadratic approximations for the 2-0 Q(1) and 3-0 S(1) transitions are shown in Fig. 3 as dotted lines. The results from Fig. 3 were calculated for $T = 296$ K. The accuracy of the quadratic approximation depends on the choice of transition and line-shape parameter. In the cases considered in Fig. 3, the approximation works better for the γ parameter.

3.3. Temperature dependences of the line-shape parameters

The values of the six collisional line-shape parameters, γ_0, δ_0, γ_2, δ_2, $\tilde{\nu}^{\mathrm{r}}_{\mathrm{opt}}$ and $\tilde{\nu}^{\mathrm{i}}_{\mathrm{opt}}$, were calculated in the temperature range from 20 to 1000 K using Eqs. (4), (9) and (2). The examples of these results, for the case of our reference lines, are shown in Fig. 4. To represent these temperature dependences in the HITRAN database, we use the recently recommended DPL approximation [30] for all the six line-shape parameters, see Eq. (7). The DPL fits were done for the $20-1000$ K temperature range enforcing ten times larger fitting weights for the prioritized temperature range from 50 to 200 K (see the gray shadows in Fig. 4), which is relevant for the atmospheres of giant planets. The examples of the DPL fits are shown in Fig. 4 as green lines. The DPL approximation performs best when the temperature dependence is monotonic; when an extremum is clearly seen then the accuracy is worse, see the δ_0 panels in Fig. 4. The amplitude of the residuals for most of the cases is smaller than 1%; their exact values are taken into account in the estimations of the line-shape parameter uncertainties reported in our dataset, see the supplementary materials [34].

Table 1
Examples of the complete records from our DPL line-shape parameter dataset for the cases of the Q(1) 2-0 and S(1) 3-0 lines in H_2 perturbed by He. Coefficients 1 and 2 are in cm^{-1}atm^{-1}. Exponents 1 and 2 are dimensionless. All the DPL coefficients are defined by Eq. (7), following the original formulation from Ref. [30].

	Q(1) 2-0 line			
	Coefficient 1	Coefficient 2	Exponent 1	Exponent 2
$\gamma_0(T)$	$g_0 = 0.29611$	$g'_0 = -0.29076$	$n = -0.30724$	$n' = -0.31188$
$\delta_0(T)$	$d_0 = 1.29146$	$d'_0 = -1.27385$	$m = 0.617$	$m' = 0.622$
$\gamma_2(T)$	$g_2 = 0.114102$	$g'_2 = -0.111618$	$j = 0.2396$	$j' = 0.2453$
$\delta_2(T)$	$d_2 = 0.091305$	$d'_2 = -0.083861$	$k = -0.0013$	$k' = -0.0383$
$\tilde{\nu}^r_{opt}(T)$	$r = 0.04277$	$r' = -0.00417$	$p = 0.6856$	$p' = -0.1236$
$\tilde{\nu}^i_{opt}(T)$	$i = -0.27435$	$i' = 0.26376$	$q = 0.07106$	$q' = 0.05273$
		S(1) 3-0 line		
	Coefficient 1	Coefficient 2	Exponent 1	Exponent 2
$\gamma_0(T)$	$g_0 = 0.012847$	$g'_0 = -0.001465$	$n = -0.11276$	$n' = -0.92775$
$\delta_0(T)$	$d_0 = 1.87405$	$d'_0 = -1.84585$	$m = 0.61066$	$m' = 0.61600$
$\gamma_2(T)$	$g_2 = 0.0493132$	$g'_2 = -0.0440504$	$j = -0.34485$	$j' = -0.38797$
$\delta_2(T)$	$d_2 = 1.5985$	$d'_2 = -1.5867$	$k = -0.01288$	$k' = -0.01602$
$\tilde{\nu}^r_{opt}(T)$	$r = 0.05173$	$r' = -0.01689$	$p = 0.6530$	$p' = 0.2554$
$\tilde{\nu}^i_{opt}(T)$	$i = -0.4136$	$i' = 0.39691$	$q = 0.08613$	$q' = 0.06746$

3.4. Examples of a complete dataset record

In Table 1, we show examples of complete records from our line-shape parameter dataset for the cases of the two reference lines. All the coefficients are defined by Eqs. (7), following the original formulation from Ref. [30]. A set of 24 coefficients per a single molecular transition is required for a full DPL description of the six line-shape parameters. The values of the coefficients gathered in Table 1 are directly taken from the fits shown in Fig. 4. Note that at $T = T_{\mathrm{ref}}$, Eqs. (7) simplify and a given line-shape parameter is simply a sum of the corresponding Coefficient 1 and Coefficient 2; for instance $\gamma_0(T_{\mathrm{ref}}) = g_0 + g'_0$.

3.5. Experimental validation

In this section, we show experimental validation of our line-shape parameter dataset for the cases of the two reference lines. We use the experimental data reported in Ref. [31]. The 2-0 Q(1) line was measured in the Grenoble laboratory at nine pressures from 0.39 to 1.05 atm and at a temperature of 294.2 K. The 3-0 S(1) line was measured in the Hefei laboratory at four pressures from 0.36 to 1.35 atm and at temperature of 296.6 K. The experimental spectra are shown as black dots in Fig. 5. Both experiments are based on high-finesse cavity ring-down spectrometers; the experimental details are given in Ref. [31].

It was demonstrated in Ref. [31] that the synthetic profiles based on the fully *ab initio* calculations agree exceptionally well with the experimental profiles without fitting any of the line-shape parameters. The relative root mean square error (rRMSE) averaged over the pressures calculated within ±FWHM around the line center was 0.33% and 0.99% for the 2-0 Q(1) and 3-0 S(1) lines, respectively [31]. Recently, the agreement with these experimental profiles was confirmed with an improved theoretical approach that includes the centrifugal distortion in the quantum-scattering calculation; rRMSE was 0.38% and 0.86% for the 2-0 Q(1) and 3-0 S(1) lines, respectively [61]. In this section, we show that we can reach an almost equally good agreement if we replace the

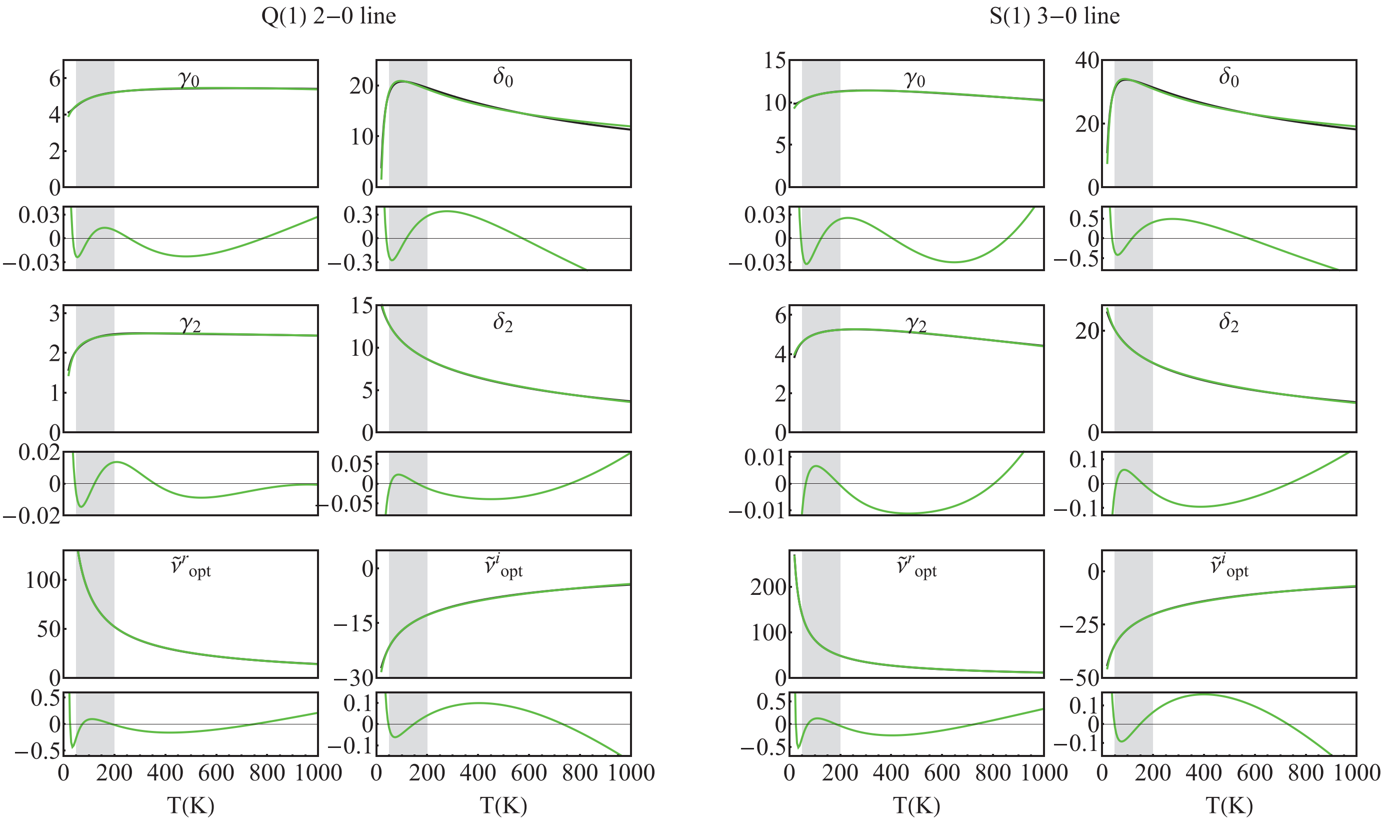

Fig. 4. Examples of the temperature dependences of the six collisional line-shape parameters, γ_0, δ_0, γ_2, δ_2, $\tilde{\nu}^r_{opt}$ and $\tilde{\nu}^i_{opt}$, for the cases of the Q(1) 2-0 and S(1) 3-0 lines in H_2 perturbed by He. The black and green lines are the *ab initio* results and DPL approximations, respectively. The small panels show the residuals from the DPL fits. The vertical axes for all the panels (including residuals) are in 10^{-3}cm^{-1}atm^{-1}. The gray shadows indicate the temperature range prioritized in the DPL fits; this temperature range is relevant for the atmospheres of giant planets. (For interpretation of the references to color in this figure legend, the reader is referred to the web version of this article.)

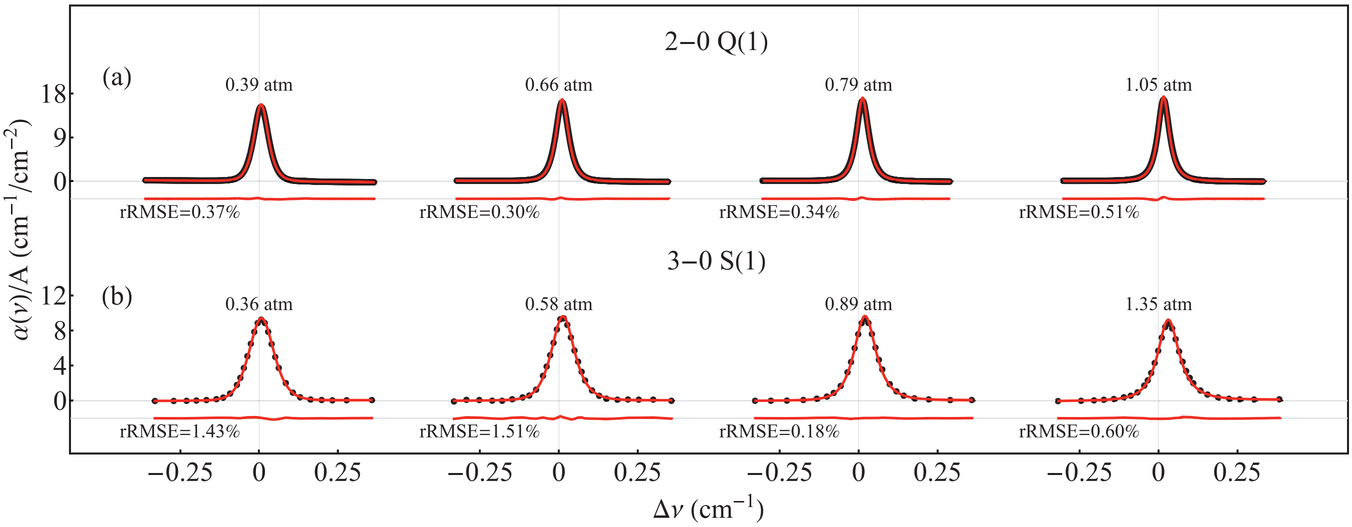

Fig. 5. Comparison of the synthetic spectra of the He-perturbed H_2 lines generated from our DPL HITRAN-format line-shape dataset (red lines) with experimental spectra (black points) collected with cavity ring-down spectrometers. Temperatures for the experimental and synthetic spectra are 294.2 K and 296.6 K for the 2-0 Q(1) and 3-0 S(1) lines, respectively. The red lines below the profiles show the differences between the experimental and synthetic spectra; rRMSE is the corresponding relative root mean square error calculated within ±FWHM around line center (relative means that RMSE is divided by the absorption coefficient at the line peak). (For interpretation of the references to color in this figure legend, the reader is referred to the web version of this article.)

full *ab initio* model with the approximate approach presented in this article, consistent with the HITRAN-format DPL parametrization [30]. The approximation is twofold. First, the full line-shape model [31,53,69] is replaced with a quadratic speed-dependent hard-collision (qSDHC) model. Second, the full *ab initio* temperature dependences are approximated with DPL. The comparison is shown in Fig. 5. The average rRMSE is 0.46% and 0.93% for the 2-0 Q(1) and 3-0 S(1) lines, respectively. It should be emphasized that none of the line-shapes were fitted in this comparison (all of them were taken from our dataset). For this comparison, we only fitted the line area, baseline, background slope and line center (all the pressures were fitted simultaneously and the fitted line center was constrained to be the same for all the pressures). The profiles from Fig. 5 were calculated using the β correction [25,55] to the qSDHC profile, see Section 2 for details. Without the β correction, the average rRMSE considerably deteriorates and equals 1.43% and 1.08% for the 2-0 Q(1) and 3-0 S(1) lines, respectively.

4. Comprehensive dataset of beyond Voigt line-shape parameters for the helium-perturbed H_2 lines

In this section, we discuss the main result of the present paper, i.e., the complete dataset of the beyond-Voigt line-shape parameters for the He-perturbed H_2 rovibrational lines. We provide a full set of the line-shape parameters for all the 3480 H_2 rovibrational electric quadrupole lines present in the HITRAN database [24]. For our basic set of 321 lines (that contains the strongest lines) we directly perform *ab initio* calculations of the generalized spectroscopic cross sections, see Section 3.1. For all the other lines (higher overtones, high-J lines and high-ν' hot bands) we extrapolate the *ab initio* data. The majority of the extrapolated data concerns the hot bands. In this work, we extended the *ab initio* calculations from Refs. [15,26] by taking into account the centrifugal distortion for all the bands and by including the hot bands. We also performed *ab initio* calculations for several dozen other lines with high ν or J numbers, which we use to adjust and validate our extrapolation scheme.

We use our *ab initio* generalized spectroscopic cross sections to calculate the line-shape parameters and their temperature dependences within the HITRAN DPL parametrization [30]. Our *ab initio* calculations of the cross sections were performed for:

- 105 lines from the Q-branches (J'' ranging from 1 to 7; Q(0) is forbidden) from the $\nu' - \nu''$ bands, with $\nu'' = 0,..., 4$ and $\Delta\nu = \nu' - \nu'' = 1,..., 5$,
- 126 lines from the S-branches (J'' ranging from 0 to 5) from the $\nu' - \nu''$ bands, with $\nu'' = 0,..., 5$ and $\Delta\nu = \nu' - \nu'' = 0,..., 5$,
- 90 lines from the O-branches (J'' ranging from 2 to 7) from the $\nu' - \nu''$ bands, with $\nu'' = 0,..., 4$ and $\Delta\nu = \nu' - \nu'' = 1,..., 5$.

For each of these 321 lines, we employ the methodology introduced in Section 2 to populate a complete dataset record defined by Eqs. (7) and illustrated in Table 1.

In Fig. 6, we show an example of the vibrational, ν', and rotational, J'', quantum number dependences of the line-shape parameters generated from our dataset at 150 K and 296 K (the plots do not show the raw *ab initio* data, but the line-shape parameters already reconstructed from our HITRAN-format DPL dataset). We observe a strong dependence of all the six line-shape parameters on the vibrational number ν', and much weaker dependence on the rotational number J'', which is consistent with the phenomenological dataset for self-perturbed H_2 [25]. In Fig. 7, we show the results for different hot bands; the colors indicate the change of the vibrational quantum number $\Delta\nu = \nu' - \nu''$. In contrast to the simplest assumption that for a fixed $\Delta\nu$ the line-shape parameters should hardly depend on ν'' (this was assumed, for instance, in the phenomenological database for the self-perturbed H_2 [25]), we observe a strong dependence on ν'', especially for small $\Delta\nu$ for the γ_0 parameter.

The rovibrational lines in H_2 are exceptionally weak; the strongest line at $T = T_{\mathrm{ref}} = 296$ K is the 1-0 S(1) line with a line intensity of 3.2×10^{-26} cm/molecule. The intensity quickly decreases with J'' and ν'. For instance, the intensity of the 1-0 S(5) line is as small as 2.2×10^{-29} cm/molecule, and the intensity of the 5-0 S(1) line is 0.95×10^{-29} cm/molecule. At lower temperatures that are relevant for giant planet atmospheres, the line intensity decreases with J'' and ν' even faster. For this reason, we limit our full line-shape calculations based on the *ab initio* generalized spectroscopic cross sections to $J' < 8$ and $\nu' < 6$. For the completeness of the dataset, we extrapolate our calculations for higher J'' and ν' lines that are present in HITRAN (in fact, in this procedure we combine extrapolation and interpolation). The extrapolation scheme is as follows. For every branch (O, Q and S), we calculated the values of the line-shape parameters for one high-ν' line per cold/hot band, i.e., we performed additional *ab initio* calculations for the following lines: Q(1) 9-x, S(1) 9-x, O(3) 9-x, with $x = 0,..., 5$. We assumed in our extrapolation that the proportions of the values of the line-shape parameters between the 9-0 and 5-0 bands for other J'' are the same as for the three cases mentioned above (i.e.,

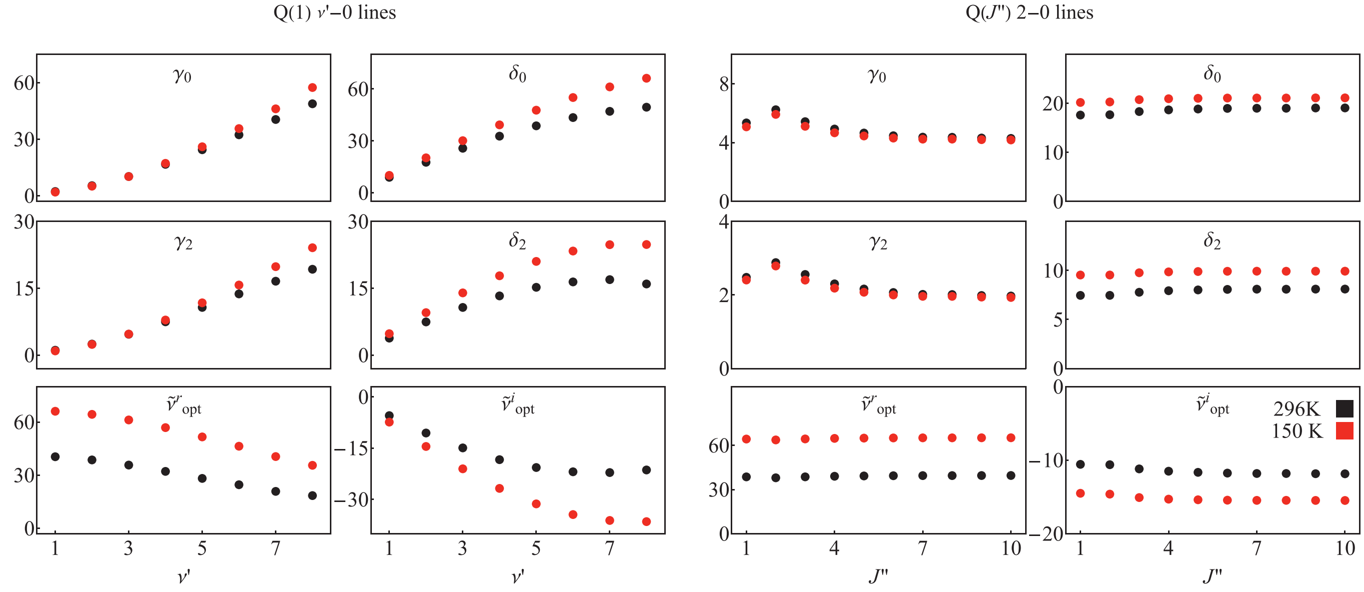

Fig. 6. An excerpt from our dataset illustrating the structure of the dataset and the examples of the vibrational and rotational dependences of all six line-shape parameters. The line-shape parameters are determined for the He-perturbed H_2 rovibrational lines at $T = 150$ and 296 K; refer to red and black colors, respectively. All the parameters are expressed in units of 10^{-3} cm^{-1}atm^{-1}. The values of the line-shape parameters shown in this plot are not directly taken from *ab initio* calculations, but reconstructed from the DPL relations, Eqs. (7), based on the coefficients from our dataset [34]. (For interpretation of the references to color in this figure legend, the reader is referred to the web version of this article.)

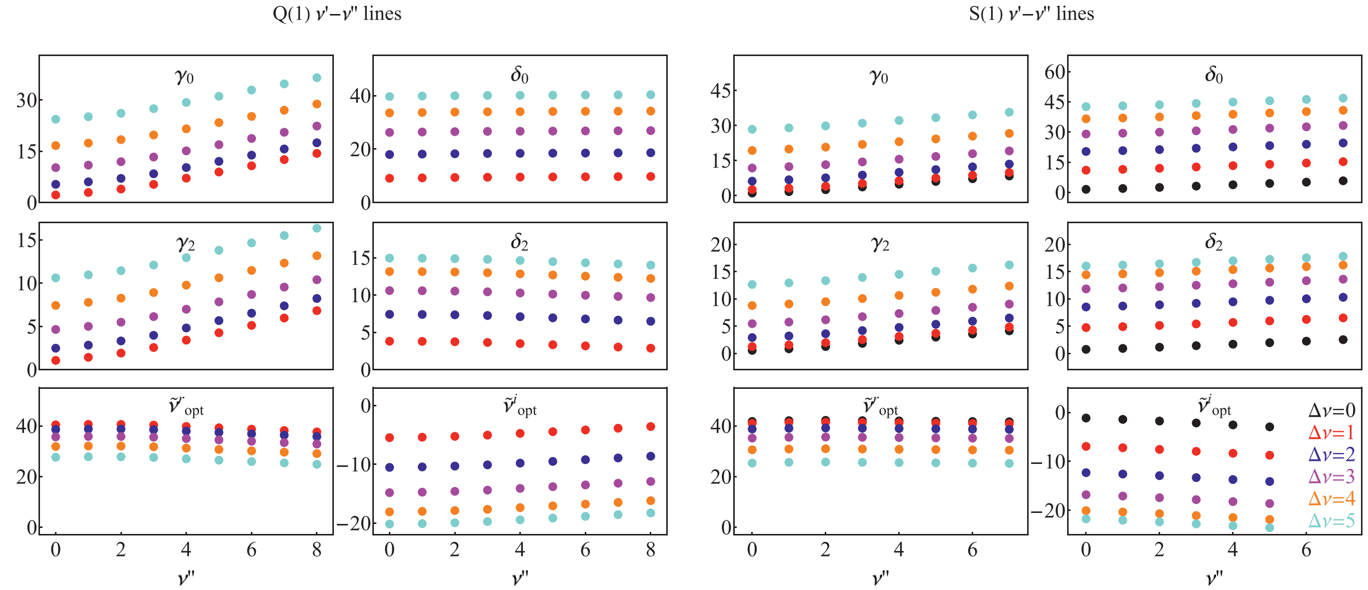

Fig. 7. An excerpt from our dataset illustrating the values of the beyond-Voigt line-shape parameters for different hot bands. The left and right sides of the figure show the results for the Q(1) and S(1) lines, respectively. All the parameters are expressed in units of 10^{-3} cm^{-1}atm^{-1}. The values of the line-shape parameters shown in this plot are not directly taken from *ab initio* calculations, but reconstructed from the DPL relations, Eqs. (7), based on the coefficients from our dataset [34]. The data for $v' = v'' + \Delta v \geq 6$ come from extrapolation.

the same within each branch). In the next step, we interpolated the line-shape parameters for the bands between 5-0 and 9-0 using a quadratic function fitted (separately for every J'') to 4-0, 5-0 and 9-0 data. The same approach was applied to extrapolate the data for hot bands. To populate the dataset for higher J'', we performed fully *ab initio* calculations for the six high-J'' transitions belonging to the 2-0 band: O(10), O(13), Q(8), Q(11), S(8) and S(11) lines. We constrained the same proportions of the line-shape parameters between $J'' = 5, 8$ and 11 (10 and 13 for O branches) for other bands, and we interpolated the values of the line-shape parameters between $J'' = 5$ and 11 (13 for the O bands) with a quadratic function. For $J'' > 11$ ($J'' > 13$ for the O bands) we used linear extrapolation based on the last two J''. This approach (based on the data for the 2-0 band) was used to extrapolate the data for higher J'' for all cold and hot bands. The scheme of data interpolation and extrapolation described above was implemented directly to the raw *ab initio* data before fitting the DPL temperature dependences. The reason for this is that the four DPL coefficients are strongly correlated with each other, and even for neighboring J'' and v' quantum numbers their fitted values can be very different despite similar temperature dependences.

Due to a strong numerical correlation between the DPL coefficients, the uncertainties of the DPL coefficients do not suffice and a full covariance matrix would be needed. For this reason, we do not report an individual uncertainty for every DPL coefficient, but a single uncertainty for the entire DPL function for a given line-shape parameter. The uncertainty consists of two contributions, the first one comes from the DPL approximation, and the second one from *ab initio* calculations. We calculate the DPL contribution as a standard deviation of the difference between the full *ab initio* values of the line-shape parameter and their DPL approximation calculated in the range from 50 to 200 K, see the small panels in Fig. 4. We estimate the uncertainty of our *ab initio* calculations at 1%.

The complete dataset of the line-shape parameters within the DPL representation [30] for the He-perturbed H_2 lines is given in the supplementary materials [34]; the definition of the reported coefficients is given by Eqs. (7). The lines are ordered with increasing transition energy. The above described format of the uncertainties reported in this work does not fit the standard HITRAN uncertainty codes. For this reason, the error codes in HITRAN will be set to *unreported* (code = 0). Nevertheless, all the uncertainties are reported in the supplementary materials [34] in the columns labelled *DPL-err*. In the supplementary materials [34], we also provide the source *ab initio* data that were used to generate the DPL dataset, i.e., the generalized spectroscopic cross sections and line-shape parameters as a function of temperature.

5. Conclusion

We demonstrated a methodology for populating line-by-line spectroscopic databases with beyond-Voigt line-shape parameters that is based on *ab initio* quantum scattering calculations. We provided a comprehensive dataset for the benchmark system of He-perturbed H_2 (we cover all the rovibrational bands that are present in HITRAN). We extended the previous quantum-scattering calculations by taking into account the centrifugal distortion for all the bands and by including the hot bands. The results were projected on a simple structure of the quadratic speed-dependent hard-collision profile. For each line and each line-shape parameter, we provided a full temperature dependence within the double-power-law (DPL) representation. The temperature dependences cover the range from 20 to 1000 K, which also includes the low temperatures relevant for the studies of the atmospheres of giant planets. We demonstrated that the synthetic spectra generated from our dataset agree with highly accurate experimental spectra collected with cavity ring-down spectrometers at a subpercent accuracy level. The methodology can be applied to many other molecular species important for atmospheric and planetary studies.

Declaration of Competing Interest

The authors declare that they have no known competing financial interests or personal relationships that could have appeared to influence the work reported in this paper.

CRediT authorship contribution statement

P. Wcisło: Conceptualization, Methodology, Validation, Writing - original draft, Writing - review & editing. **F. Thibault:** Conceptualization, Methodology, Software, Validation, Writing - original draft, Writing - review & editing. **N. Stolarczyk:** Investigation, Visualization, Methodology, Software, Validation, Data curation, Writing - original draft, Writing - review & editing. **H. Jóźwiak:** Investigation, Methodology, Software, Validation, Data curation, Writing - original draft, Writing - review & editing. **M. Słowiński:** Investigation, Visualization, Methodology, Software, Validation, Data curation, Writing - original draft, Writing - review & editing. **M. Gancewski:** Investigation, Software, Validation, Data curation, Writing - original draft, Writing - review & editing. **K. Stankiewicz:** Investigation, Software, Validation, Data curation, Writing - original draft, Writing - review & editing. **M. Konefał:** Validation. **S. Kassi:** Investigation. **A. Campargue:** Investigation. **Y. Tan:** Investigation. **J. Wang:** Investigation. **K. Patkowski:** Investigation, Software, Validation, Writing - review & editing. **R. Ciuryło:** Conceptualization, Methodology, Writing - review & editing. **D. Lisak:** Conceptualization, Methodology, Writing - review & editing. **R. Kochanov:** Conceptualization, Methodology, Data curation. **L.S. Rothman:** Conceptualization, Methodology, Data curation, Validation, Writing - review & editing. **I.E. Gordon:** Conceptualization, Methodology, Data curation, Validation, Writing - review & editing.

Acknowledgements

P.W. was supported by Polish National Science Centre Project No. 2019/35/B/ST2/01118. N.S. and H.J. were supported by Polish National Science Centre Project No. 2018/31/B/ST2/00720. M.S., M.G. and K.S. were supported by the A next-generation worldwide quantum sensor network with optical atomic clocks project carried out within the TEAM IV Programme of the Foundation for Polish Science cofinanced by the European Union under the European Regional Development Fund. S.K. and A.C. acknowledge funding support from the Agence Nationale de la Recherche (Equipex REFIMEVE+ANR-11-EQPX-0039). M.K. and D.L. were supported by Polish National Science Centre Project No. 2015/18/E/ST2/00585. K.P. was supported by U.S. National Science Foundation CAREER award CHE-1351978. The project was cofinanced by the Polish National Agency for Academic Exchange under the PHC Polonium program (dec. PPN/X/PS/318/2018). The research was part of the program of the National Laboratory FAMO in Toruń, Poland. The HITRAN database is supported by NASA AURA NNX17AI78G and NASA PDART NNX16AG51G grants.

Supplementary material

Supplementary material associated with this article can be found, in the online version, at doi:10.1016/j.jqsrt.2020.107477.

References

[1] Dicke R. The effect of collisions upon the Doppler width of spectral lines. Phys Rev 1953;89:472–3. doi:10.1103/PhysRev.89.472.
[2] Rautian SG, Sobelman II. The effect of collisions on the doppler broadening of spectral lines. Usp Fiz Nauk 1966;90:209. [Sov Phys Usp 1967;9:701]
[3] Berman PR. Speed-dependent collisional width and shift parameters in spectral profiles. J Quant Spectrosc Radiat Transf 1972;12(9):1331–42. doi:10.1016/0022-4073(72)90189-6.
[4] Hess S. Kinetic theory of spectral line shapes. The transition between Doppler broadening and collisional broadening. Physica 1972;61(1):80–94. doi:10.1016/0031-8914(72)90035-3.
[5] Blackmore R. A modified Boltzmann kinetic equation for line shape functions. J Chem Phys 1987;87(2):791–800. doi:10.1063/1.453286.
[6] Ciuryło R, Bielski A, Drummond JR, Lisak D, May AD, Pine AS, et al. Spectral line shapes. In: Back CA, editor. (AIP, Melville, NY); 2002a. p. 151.
[7] May AD, Liu W-K, McCourt FRW, Ciuryło R, Sanchez-FortStoker J, Shapiro D, et al. The impact theory of spectral line shapes: a paradigm shift. Can J Phys 2013;91(11):879–95. doi:10.1139/cjp-2012-0345.
[8] Hartmann J-M, Tran H, Ngo NH, Landsheere X, Chelin P, Lu Y, et al. *Ab initio* calculations of the spectral shapes of CO_2 isolated lines including non-Voigt effects and comparisons with experiments. Phys Rev A 2013;87:013403. doi:10.1103/PhysRevA.87.013403.
[9] De Vizia MD, Castrillo A, Fasci E, Amodio P, Moretti L, Gianfrani L. Experimental test of the quadratic approximation in the partially correlated speed-dependent hard-collision profile. Phys Rev A 2014;90:022503. doi:10.1103/PhysRevA.90.022503.
[10] Devi VM, Benner DC, Smith MAH, Mantz AW, Sung K, Crawford TJ, et al. Self- and air-broadened line shape parameters in the ν_2+ν_3 band of $^{12}CH_4$: 4500–4630 cm^{-1}. J Quant Spectrosc Radiat Transf 2015;152:149–65. doi:10.1016/j.jqsrt.2014.11.011.
[11] Campargue A, Karlovets EV, Kassi S. The 4-0 band of carbon monoxide by high sensitivity cavity ring down spectroscopy near 8200 cm^{-1}. J Quant Spectrosc Radiat Transf 2015;154:113–19. doi:10.1016/j.jqsrt.2014.12.011.
[12] Wójtewicz S, Masłowski P, Cygan A, Wcisło P, Zaborowski M, Piwiński M, et al. Speed-dependent effects and Dicke narrowing in nitrogen-broadened oxygen. J Quant Spectrosc Radiat Transf 2015;165:68–75. doi:10.1016/j.jqsrt.2015.06.022.
[13] Sironneau VT, Hodges JT. Line shapes, positions and intensities of water transitions near 1.28 µm. J Quant Spectrosc Radiat Transf 2015;152:1–15. doi:10.1016/j.jqsrt.2014.10.020.
[14] Bakr BW, Smith DGA, Patkowski K. Highly accurate potential energy surface for the He-H_2 dimer. J Chem Phys 2013;139(14):144305. doi:10.1063/1.4824299.
[15] Thibault F, Patkowski K, Żuchowski PS, Jóźwiak H, Ciuryło R, Wcisło P. Rovibrational line-shape parameters for H_2 in He and new H_2-He potential energy surface. J Quant Spectrosc Radiat Transf 2017;202:308–20. doi:10.1016/j.jqsrt.2017.08.014.
[16] Wcisło P, Ciuryło R. Influence of the interaction potential shape on the Dicke narrowed spectral line profiles affected by speed-dependent collisional broadening and shifting. J Quant Spectrosc Radiat Transf 2013;120(0):36–43. doi:10.1016/j.jqsrt.2013.02.023.
[17] Wcisło P, Thibault F, Cybulski H, Ciuryło R. Strong competition between velocity-changing and phase- or state-changing collisions in H_2 spectra perturbed by Ar. Phys Rev A 2015;91:052505. doi:10.1103/PhysRevA.91.052505.
[18] Wcisło P, Gordon IE, Cheng C-F, Hu S-M, Ciuryło R. Collision-induced line-shape effects limiting the accuracy in Doppler-limited spectroscopy of H_2. Phys Rev A 2016a;93:022501. doi:10.1103/PhysRevA.93.022501.
[19] Miller CE, Brown LR, Toth RA, Benner DC, Devi VM. Spectroscopic challenges for high accuracy retrievals of atmospheric CO_2 and the orbiting carbon observatory (OCO) experiment. C R Phys 2005;6(8):876–87. doi:10.1016/j.crhy.2005.09.005.
[20] Feuchtgruber H, Lellouch E, Orton G, de Graauw T, Vandenbussche B, Swinyard B, et al. The D/H ratio in the atmospheres of Uranus and Neptune from Herschel-PACS observations. A&A 2013;551:A126. doi:10.1051/0004-6361/201220857.
[21] Miller-Ricci E, Seager S, Sasselov D. The atmospheric signatures of super-Earths: how to distinguish between hydrogen-rich and hydrogen-poor atmospheres. Astrophys J 2008;690(2):1056–67. doi:10.1088/0004-637x/690/2/1056.
[22] Fortney J.J., Robinson T.D., Domagal-Goldman S., Genio A.D.D., Gordon I.E., Gharib-Nezhad E., et al. The need for laboratory measurements and *ab initio* studies to aid understanding of exoplanetary atmospheres. arXiv:1905070642019;URL https://arxiv.org/abs/1905.07064.
[23] Hill C, Gordon IE, Kochanov RV, Barrett L, Wilzewski JS, Rothman LS. HITRANonline: An online interface and the flexible representation of spectroscopic data in the HITRAN database. J Quant Spectrosc Radiat Transf 2016;177:4–14. doi:10.1016/j.jqsrt.2015.12.012.
[24] Gordon I, Rothman L, Hill C, Kochanov R, Tan Y, Bernath P, et al. The HITRAN2016 molecular spectroscopic database. J Quant Spectrosc Radiat Transf 2017;203:3–69. doi:10.1016/j.jqsrt.2017.06.038.
[25] Wcisło P, Gordon I, Tran H, Tan Y, Hu S-M, Campargue A, et al. The implementation of non-Voigt line profiles in the HITRAN database: H_2 case study. J Quant Spectrosc Radiat Transf 2016b;177:75–91. doi:10.1016/j.jqsrt.2016.01.024.
[26] Jóźwiak H, Thibault F, Stolarczyk N, Wcisło P. *Ab initio* line-shape calculations for the S and O branches of H_2 perturbed by He. J Quant Spectrosc Radiat Transf 2018;219:313–22. doi:10.1016/j.jqsrt.2018.08.023.
[27] Pine AS. Asymmetries and correlations in speed-dependent Dicke-narrowed line shapes of argon-broadened HF. J Quant Spectrosc Radiat Transf 1999;62(4):397–423. doi:10.1016/S0022-4073(98)00112-5.
[28] Ngo N, Lisak D, Tran H, Hartmann J-M. An isolated line-shape model to go beyond the Voigt profile in spectroscopic databases and radiative transfer codes. J Quant Spectrosc Radiat Transf 2013;129:89–100. doi:10.1016/j.jqsrt.2013.05.034.
[29] Tennyson J, Bernath PF, Campargue A, Császár AG, Daumont L, Gamache RR, et al. Recommended isolated-line profile for representing high-resolution spectroscopic transitions (IUPAC technical report). Pure Appl Chem 2014;86(12):1931–43. doi:10.1515/pac-2014-0208.
[30] Stolarczyk N, Thibault F, Cybulski H, Jóźwiak H, Kowzan G, Vispoel B, et al. Evaluation of different parameterizations of temperature dependences of the line-shape parameters based on *ab initio* calculations: Case study for the HITRAN database. J Quant Spectrosc Radiat Transf 2020;240:106676. doi:10.1016/j.jqsrt.2019.106676.
[31] Słowiński M, Thibault F, Tan Y, Wang J, Liu A-W, Hu S-M, et al. H_2-He collisions: *ab initio* theory meets cavity-enhanced spectra. Phys Rev A 2020;101:052705. doi:10.1103/PhysRevA.101.052705.

[32] Kochanov R, Gordon I, Rothman L, Wcisło P, Hill C, Wilzewski J. HITRAN Application Programming Interface (HAPI): a comprehensive approach to working with spectroscopic data. J Quant Spectrosc Radiat Transf 2016;177:15–30. doi:10.1016/j.jqsrt.2016.03.005.

[33] Lellouch E, Bézard B, Fouchet T, Feuchtgruber H, Encrenaz T, de Graauw T. The deuterium abundance in Jupiter and Saturn from ISO-SWS observations. A&A 2001;370(2):610–22. doi:10.1051/0004-6361:20010259.

[34] Wcisło P., Thibault F., Stolarczyk N., Jóźwiak H., Słowiński M., Gancewski M., et al. Supplementary material 2020. doi:10.1016/j.jqsrt.2020.107477.

[35] Long D, Havey D, Okumura M, Miller C, Hodges J. O_2 A-band line parameters to support atmospheric remote sensing. J Quant Spectrosc Radiat Transf 2010;111(14):2021–36. doi:10.1016/j.jqsrt.2010.05.011.

[36] Devi VM, Benner DC, Smith M, Mantz A, Sung K, Brown L, et al. Spectral line parameters including temperature dependences of self- and air-broadening in the 2-0 band of CO at 2.3 µm. J Quant Spectrosc Radiat Transf 2012a;113:1013–33. doi:10.1016/j.jqsrt.2012.02.010.

[37] Devi VM, Benner DC, Smith MAH, Mantz AW, Sung K, Brown LR. Spectral line parameters including temperature dependences of air-broadening for the 2-0 bands of $^{13}C^{16}O$ and $^{12}C^{18}O$ at 2.3 µm. J Mol Spectrosc 2012b;276-277:33–48. doi:10.1016/j.jms.2012.05.005.

[38] Li G, Gordon IE, Hajigeorgiou PG, Coxon JA, Rothman LS. Reference spectroscopic data for hydrogen halides, Part II: The line lists. J Quant Spectrosc Radiat Transf 2013;130:284–95. doi:10.1016/j.jqsrt.2013.07.019.

[39] Domysławska J, Wójtewicz S, Masłowski P, Cygan A, Bielska K, Trawiński RS, et al. A new approach to spectral line shapes of the weak oxygen transitions for atmospheric applications. J Quant Spectrosc Radiat Transf 2016;169:111–21. doi:10.1016/j.jqsrt.2015.10.019.

[40] Benner DC, Rinsland CP, Devi VM, Smith MAH, Atkins D. A multispectrum nonlinear least squares fitting technique. J Quant Spectrosc Radiat Transf 1995;53(6):705–21. doi:10.1016/0022-4073(95)00015-D.

[41] Pine A, Ciuryło R. Multispectrum fits of Ar-broadened HF with a generalized asymmetric lineshape: effects of correlation, hardness, speed dependence, and collision duration. J Mol Spectrosc 2001;208(2):180–7. doi:10.1006/jmsp.2001.8375.

[42] Amodio P, Moretti L, Castrillo A, Gianfrani L. Line-narrowing effects in the near-infrared spectrum of water and precision determination of spectroscopic parameters. J Chem Phys 2014;140(4):044310. doi:10.1063/1.4862482.

[43] Ben-Reuven A. Symmetry considerations in pressure-broadening theory. Phys Rev 1966a;141:34–40. doi:10.1103/PhysRev.141.34.

[44] Ben-Reuven A. Impact broadening of microwave spectra. Phys Rev 1966b;145:7–22. doi:10.1103/PhysRev.145.7.

[45] Shafer R, Gordon RG. Quantum scattering theory of rotational relaxation and spectral line shapes in H_2-He gas mixtures. J Chem Phys 1973;58(12):5422–43. doi:10.1063/1.1679162.

[46] Thibault F, Wcisło P, Ciuryło R. A test of H_2-He potential energy surfaces. Eur Phys J D 2016;70:236. doi:10.1140/epjd/e2016-70114-9.

[47] Martínez RZ, Bermejo D, Thibault F, Wcisło P. Testing the *ab initio* quantum-scattering calculations for the D_2-He benchmark system with stimulated Raman spectroscopy. J Raman Spectrosc 2018;49(8):1339–49. doi:10.1002/jrs.5391.

[48] Monchick L, Hunter LW. Diatomic diatomic molecular collision integrals for pressure broadening and Dicke narrowing: a generalization of Hess's theory. J Chem Phys 1986;85(2):713–18. doi:10.1063/1.451277.

[49] Schaefer J, Monchick L. Line shape cross sections of HD immersed in He and H_2 gas. I. Pressure broadening cross sections. J Chem Phys 1987;87(1):171–81. doi:10.1063/1.453612.

[50] Corey GC, McCourt FR. Dicke narrowing and collisional broadening of spectral lines in dilute molecular gases. J Chem Phys 1984;81(5):2318–29. doi:10.1063/1.447930.

[51] Ward J, Cooper J, Smith EW. Correlation effects in the theory of combined Doppler and pressure broadening - I. Classical theory. J Quant Spectrosc Radiat Transf 1974;14(7):555–90. doi:10.1016/0022-4073(74)90036-3.

[52] Lisak D, Hodges JT, Ciuryło R. Comparison of semiclassical line-shape models to rovibrational H_2O spectra measured by frequency-stabilized cavity ring-down spectroscopy. Phys Rev A 2006;73:012507. doi:10.1103/PhysRevA.73.012507.

[53] Wcisło P, Thibault F, Zaborowski M, Wójtewicz S, Cygan A, Kowzan G, et al. Accurate deuterium spectroscopy for fundamental studies. J Quant Spectrosc Radiat Transf 2018;213:41–51. doi:10.1016/j.jqsrt.2018.04.011.

[54] Rohart F, Wlodarczak G, Colmont J-M, Cazzoli G, Dore L, Puzzarini C. Galatry versus speed-dependent Voigt profiles for millimeter lines of O_3 in collision with N_2 and O_2. J Mol Spectrosc 2008;251(1):282–92. doi:10.1016/j.jms.2008.03.005.

[55] Konefał M, Słowiński M, Zaborowski M, Ciuryło R, Lisak D, Wcisło P. Analytical-function correction to the Hartmann Tran profile for more reliable representation of the Dicke-narrowed molecular spectra. J Quant Spectrosc Radiat Transf 2020;242:106784. doi:10.1016/j.jqsrt.2019.106784.

[56] Tran H, Ngo N, Hartmann J-M. Efficient computation of some speed-dependent isolated line profiles. J Quant Spectrosc Radiat Transf 2013;129:199–203. doi:10.1016/j.jqsrt.2013.06.015.

[57] Kowzan G, Wcisło P, Słowiński M, Masłowski P, Viel A, Thibault F. Fully quantum calculations of the line-shape parameters for the Hartmann-Tran profile: A CO-Ar case study. J Quant Spectrosc Radiat Transf 2020;243:106803. doi:10.1016/j.jqsrt.2019.106803.

[58] Private communication with J.-M. Hartmann. 2018.

[59] Wcisło P, Lisak D, Ciuryło R, Pine AS. Multispectrum-fitting of phenomenological collisional line-shape models to a speed-dependent Blackmore profile for spectroscopic analysis and databases. J Phys 2017;810:012061. doi:10.1088/1742-6596/810/1/012061.

[60] Ngo N, Hartmann J-M. A strategy to complete databases with parameters of refined line shapes and its test for CO in He, Ar and Kr. J Quant Spectrosc Radiat Transf 2017;203:334–40. doi:10.1016/j.jqsrt.2017.01.031. HITRAN2016 Special Issue

[61] Słowiński M., et al. In preparation.

[62] Martnez RZ, Bermejo D, Wcisło P, Thibault F. Accurate wavenumber measurements for the $S_0(0)$, $S_0(1)$, and $S_0(2)$ pure rotational Raman lines of D_2. J Raman Spectrosc 2019;50(1):127–9. doi:10.1002/jrs.5499.

[63] Thibault F, Martnez RZ, Bermejo D, Wcisło P. Line-shape parameters for the first rotational lines of HD in He. Mol Astrophys 2020;19:100063. doi:10.1016/j.molap.2020.100063.

[64] Stankiewicz K, Jóźwiak H, Gancewski M, Stolarczyk N, Thibault F, Wcisło P. Ab initio calculations of collisional line–shape parameters and generalized spectroscopic cross-sections for rovibrational dipole lines in HD perturbed by He. J Quant Spectrosc Radiat Transf 2020;254:107194. doi:10.1016/j.jqsrt.2020.107194.

[65] Jóźwiak H., Gancewski M., Stankiewicz K., Wcisło P.. BIGOS computer code, to be published.

[66] Johnson BR. The renormalized Numerov method applied to calculating bound states of the coupled-channel Schrödinger equation. J Chem Phys 1978;69(10):4678–88. doi:10.1063/1.436421.

[67] Rohart F, Nguyen L, Buldyreva J, Colmont J-M, Wlodarczak G. Lineshapes of the 172 and 602 GHz rotational transitions of $HC^{15}N$. J Mol Spectrosc 2007;246(2):213–27. doi:10.1016/j.jms.2007.09.009.

[68] Lisak D, Cygan A, Wcisło P, Ciuryło R. Quadratic speed dependence of collisional broadening and shifting for atmospheric applications. J Quant Spectrosc Radiat Transf 2015;151:43–8. doi:10.1016/j.jqsrt.2014.08.016.

[69] Ciuryło R, Shapiro DA, Drummond JR, May AD. Solving the line-shape problem with speed-dependent broadening and shifting and with Dicke narrowing. II. Application. Phys Rev A 2002b;65:012502. doi:10.1103/PhysRevA.65.012502.

Journal of Quantitative Spectroscopy & Radiative Transfer 276 (2021) 107911

Contents lists available at ScienceDirect

Journal of Quantitative Spectroscopy & Radiative Transfer

journal homepage: www.elsevier.com/locate/jqsrt

Accurate calculations of beyond-Voigt line-shape parameters from first principles for the He-perturbed HD rovibrational lines: A comprehensive dataset in the HITRAN DPL format

Kamil Stankiewicz[a,*], Nikodem Stolarczyk[a], Hubert Jóźwiak[a], Franck Thibault[b], Piotr Wcisło[a]

[a] Institute of Physics, Faculty of Physics, Astronomy and Informatics, Nicolaus Copernicus University, Grudziądzka 5, Toruń, 87–100, Poland
[b] Univ Rennes, CNRS, IPR (Institut de Physique de Rennes)-UMR 6251, F-35000 Rennes, France

ARTICLE INFO

Article history:
Received 12 July 2021
Revised 26 August 2021
Accepted 27 August 2021
Available online 28 August 2021

Keywords:
HD
He
HITRAN
Line–shape parameters
Beyond-Voigt
Quantum scattering

ABSTRACT

We report a comprehensive dataset of beyond-Voigt line-shape parameters (pressure broadening and shift coefficients, their speed-dependences, and the complex Dicke parameters) for all electric dipole and quadrupole transitions within the ground electronic state in He-perturbed HD that are present in the HITRAN database. The parameters are determined from generalized spectroscopic cross-sections which we obtain by solving *ab initio* quantum scattering problem using the close-coupling formulation and the state-of-the-art potential energy surface of the HD-He interaction. We parametrize the temperature dependence of the line-shape parameters with double-power-law representation (DPL), recommended for the HITRAN database. Comparison with the analogous results for the H_2-He system reveals a strong isotopologue dependence.

1. Introduction

Due to its abundance in the Universe, molecular hydrogen is an object of interest in various fields. Because of its simplicity, it is a benchmark system for testing *ab initio* quantum chemistry calculations [1,2] and quantum electrodynamics for molecules [3,4]. Despite its small natural abundance, the HD isotopologue is notable in spectroscopy of gas giants' atmospheres due to the presence of permanent dipole moment, and thus, dipole transitions, the intensities of which are much larger than those of weak quadrupole lines in H_2. HD also possesses a smaller rotational constant than H_2 which entails smaller rotational spacing of the energy levels. Those two facts result in the potential domination of HD molecules in the process of primordial gas cooling under specific physical conditions [5]. The D/H ratios, which are mainly obtained from measurement of abundances of H_2 and HD, are also essential indicators of planetary formation and evolution [6,7]. For precise measurements, a list of accurate values of line-shape parameters is crucial [6,8]. For some observations [6], it turns out that the errors in the analysis can be dominated by the uncertainties of self- and helium-perturbed line-shape parameters.

A mixture of molecular hydrogen and atomic helium is the main constituent of the atmospheres of gas giants in the Solar System. It is also predicted to be a dominant component of atmospheres of some types of exoplanets [9]. Thus, the relevant collisional systems, for which line-shape parameters are sought after, are: H_2 - H_2, H_2-He, HD-H_2, and HD-He. The importance of the beyond-Voigt line-shape parameters was widely discussed in previous studies [10–18]. Populating the entire database of the line-shape parameters for a large number of transitions and different thermodynamical conditions with experimentally determined values is a very challenging task. Not only is it hard because of the wide spectral range of transitions and different measurements' conditions but also due to strong numerical correlations between the line-shape parameters [19]. This problem was addressed by the implementation of a method that allows obtaining accurate line-shape parameters through *ab initio* quantum scattering calculations. The method has been already used for thorough examination of the H_2-He system [1,20,21], which resulted in the first comprehensive dataset of beyond-Voigt line-shape parameters [19] which covers all electric rovibrational transitions within the ground electronic level that are present in the HITRAN

---

[*] Corresponding author.
E-mail addresses: stankiewiczkamil98@gmail.com (K. Stankiewicz), piotr.wcislo@umk.pl (P. Wcisło).

https://doi.org/10.1016/j.jqsrt.2021.107911

database [22] for a wide range of temperatures. The results of those *ab initio* calculations were successfully experimentally verified for several lines [19,23,24]. In the case of the HD-He system, the line-shape parameters for several rotational lines were investigated theoretically and experimentally [25] and calculations for several dozens of dipole rovibrational transitions were conducted [26].

In this work, we utilize the method of obtaining the collisional line-shape parameters through *ab initio* quantum scattering calculations that was presented in Ref. [19], to populate all electric dipole and quadrupole transitions within the ground electronic state that are present in the HITRAN database for He-perturbed HD. Using the state-of-the-art potential energy surface obtained through quantum chemical calculations [1,2] we solve the quantum scattering problem by adopting the close-coupling formulation and obtain the scattering matrices. They are used to calculate the generalized spectroscopic cross-sections (GSXS) which are utilized to derive line-shape parameters that describe pressure broadening, shift, their speed-dependences, and the effect of the velocity-changing collisions. Temperature dependences of the line-shape parameters are expressed using the double-power-law (DPL) representation, which is the recommended parametrization for the HITRAN database [27]. Section 2 provides the details of the calculations. In Section 3, we discuss the dependences of the GSXS and line-shape parameters on the vibrational band, initial rotational level, and the performance of the DPL parametrization. For completeness, we interpolate and extrapolate our large set of *ab initio* calculated line-shape parameters to populate all electric dipole and quadrupole rovibrational transitions within the ground electronic state that are present in the HITRAN database. We also compare our results with the ones presented in Ref. [19] for the H_2-He system. We observe a strong isotopologue dependence which is in contradiction to the results measured for more massive molecules. The GSXS and *ab initio* values of line-shape parameters for calculated lines, as well as DPL coefficients, are provided in the supplementary material [28].

2. Calculations

This section presents the methodology used to obtain the line-shape parameters from *ab initio* calculations for a collisional system consisting of a diatomic molecule and a structureless atom. Section 2.1 describes how to determine the line-shape parameters from the GSXS and Section 2.2 briefly explains the process of obtaining GSXS through quantum scattering calculations.

2.1. Line shape parameters

The pressure broadening and shift of the spectral line may be described by the pressure broadening $\gamma(v)$ and pressure shift $\delta(v)$ coefficients which are functions of the speed, v, of the active molecule (the coefficients also depend on the temperature but for short we do not write it explicitly). They may be obtained from first principles by calculating the generalized spectroscopic cross-section, σ_0^q, (which is described in the next subsection) and averaging it over the velocity distribution of relative motion of the active molecule and the perturber [29–31]:

$$\begin{aligned}\gamma(v)+\mathrm{i}\delta(v)=&\frac{1}{2\pi c}\frac{1}{k_BT}\frac{2}{\sqrt{\pi}\bar{v}_p v}\times\\&\int_0^\infty v_r^2\exp\left(-\frac{v^2+v_r^2}{\bar{v}_p^2}\right)\sinh\left(\frac{2vv_r}{\bar{v}_p^2}\right)\sigma_0^q(v_r)dv_r,\end{aligned}\tag{1}$$

where v_r is the relative speed of colliding partners, $\bar{v}_p$ is the most probable speed of the perturber, k_B is the Boltzmann constant, c is the speed of light, and T denotes temperature.

For most applications, it is inconvenient to store the full speed-dependence of $\gamma(v)$ and $\delta(v)$ and use it in the data analysis. For this reason the new HITRAN DPL format [19,27] adopts their quadratic approximation [32,33]:

$$\gamma(v)+i\delta(v)\approx\gamma_0+i\delta_0+(\gamma_2+i\delta_2)\left(\frac{v^2}{v_m^2}-\frac{3}{2}\right),\tag{2}$$

where v_m denotes the most probable speed of the absorber. γ_0 and δ_0 are the speed-averaged pressure broadening and shift coefficients, which can be calculated directly from [11,27]:

$$\gamma_0+i\delta_0=\frac{1}{2\pi c}\frac{1}{k_BT}\langle v_r\rangle\int_0^\infty xe^{-x}\sigma_0^q(xk_BT)dx,\tag{3}$$

where $x=E_{kin}/k_BT$, E_{kin} is the relative kinetic energy of the collision partners and $\langle v_r\rangle$ is the mean value of their relative speed. Alternatively, γ_0 and δ_0 may be obtained by averaging Eq. (2) over the Maxwell-Boltzmann distribution of the absolute speed at given temperature, T. Parameters γ_2 and δ_2 are obtained by imposing the condition that the slopes of the actual speed-dependence and the quadratic approximation are equal at the most probable absorber speed, v_m:

$$\frac{2}{v_m}(\gamma_2+i\delta_2)=\frac{d}{dv}(\gamma(v)+i\delta(v))|_{v=v_m}.\tag{4}$$

Using this condition together with Eqs. (1) and (2) one can write explicit formula for γ_2 and δ_2 [19]:

$$\begin{aligned}&\gamma_2+i\delta_2=\frac{1}{2\pi c}\frac{1}{k_BT}\frac{\bar{v}_p}{\sqrt{\pi}}e^{-y^2}\times\\&\int_0^\infty\left(2z\cosh(2zy)-\left(\frac{1}{y}+2y\right)\sinh(2zy)\right)\times\\&z^2e^{-z^2}\sigma_0^q(z\bar{v}_p)dz,\end{aligned}\tag{5}$$

where y denotes the $v_m/\bar{v}_p$ ratio and z is equal to $v_r/\bar{v}_p$.

The impact of velocity-changing collisions is quantified by the complex Dicke parameter $\tilde{\nu}_{opt}$, which is also known as the optical frequency of the velocity-changing collisions. It can be calculated as:

$$\begin{aligned}&\tilde{\nu}_{opt}=\tilde{\nu}_{opt}^r+i\tilde{\nu}_{opt}^i=\frac{1}{2\pi c}\frac{1}{k_BT}\langle v_r\rangle M_a\times\\&\int_0^\infty xe^{-x}\left[\frac{2}{3}x\sigma_1^q(xk_BT)-\sigma_0^q(xk_BT)\right]dx,\end{aligned}\tag{6}$$

where $M_a=\frac{m_p}{m_a+m_p}$, m_a and m_p are the masses of the active molecule and the perturber and σ_1^q is the Dicke cross-section.

Altogether, we report six collisional line-shape parameters: γ_0, δ_0, γ_2, δ_2, $\tilde{\nu}_{opt}^r$ $\tilde{\nu}_{opt}^i$, and we provide their temperature dependences using the double-power-law (DPL) [27] format, recommended for the HITRAN database [22]:

$$\begin{aligned}\gamma_0(T)&=g_0(T_{ref}/T)^n+g_0'(T_{ref}/T)^{n'},\\\delta_0(T)&=d_0(T_{ref}/T)^m+d_0'(T_{ref}/T)^{m'},\\\gamma_2(T)&=g_2(T_{ref}/T)^j+g_2'(T_{ref}/T)^{j'},\\\delta_2(T)&=d_2(T_{ref}/T)^k+d_2'(T_{ref}/T)^{k'},\\\tilde{\nu}_{opt}^r(T)&=r(T_{ref}/T)^p+r'(T_{ref}/T)^{p'},\\\tilde{\nu}_{opt}^i(T)&=i(T_{ref}/T)^q+i'(T_{ref}/T)^{q'},\end{aligned}\tag{7}$$

for $T_{ref}=296$ K. The *ab initio* values of the line-shape parameters are calculated at different temperatures ranging from 20 to 1000 K and then projected on the DPL representation. Due to its impotrance from the perspective of the gas giants' atmospheric observations, we prioritized the temperature range between 50 and 200 K by applying weights magnified tenfold in the fitting procedure.

2.2. Generalized spectroscopic cross-sections

In order to obtain the GSXS, one needs to solve the Schrödinger equation for the atom-molecule scattering problem and find the scattering matrices describing the completed collision process. The problem may be addressed through the close-coupling formulation [34,35]. In the case of collision between a diatom molecule and a structureless atom, the potential energy surface (PES), $V(R, r, \theta)$, depends only on three variables – R, which is the distance between the atom and the center of mass of the molecule, r, which is the internal distance between the nuclei in the molecule, and θ, which is the angle between the molecular axis and the axis connecting the atom with the center of mass of the molecule. In our calculations, we use the current state-of-the-art BSP3 PES [1] which is an upgraded version of the Bakr, Smith, Patkowski PES [2]. Because this PES is calculated within the Born-Oppenheimer approximation, it may be used to describe the HD-He interaction by simply shifting the center of mass of the molecule. The dependence on θ is separated by expanding the potential in terms of Legendre polynomials:

$$V(R, r, \theta) = \sum_{\xi=0}^{\xi_{max}} v_\xi(R, r) P_\xi(\cos\theta). \tag{8}$$

In our calculation, we truncate the expansion at $\xi_{\max} = 6$ which gives accurate results due to the small anisotropy of the system [25]. The PES is further expanded in terms of radial molecular wavefunctions $\chi_{v,j}(r)$ of the HD molecule to separate the dependence on r and obtain the radial coupling potential terms:

$$A_{\xi,v,j,v',j'}(R) = \int_0^\infty \chi_{v',j'}(r) v_\xi(R, r) \chi_{v,j}(r) dr, \tag{9}$$

We neglect any vibrational coupling, thus for all non-zero radial terms $v = v'$. Usually, for rovibrational transitions, the centrifugal distortion coming from the difference in the shape of radial molecular wavefunctions for different j is neglected [20] which results in the assumption that $j = j' = 0$. However, it was shown recently [26] that in the case of such a light molecule as HD, the centrifugal distortion cannot be disregarded if one seeks a sub-percent accuracy, especially for transitions that include higher rotational levels.

The quantum scattering calculations are performed using the BIGOS code [36] for kinetic energies (E_{kin}) ranging from 0.1 cm^{-1} to 9000 cm^{-1}. Propagation is carried out between 0.1 and 200 a$_0$ using the renormalized Numerov's algorithm [37] and log-derivative method [38]. Based on calculations for one transition, we determine the value of numerical parameters – propagator's step and the number of closed channels (i.e rovibrational levels in the basis, the energy of which is higher than the total energy of the system) such that they provide sub-percent accuracy for the relevant range of E_{kin}. The determined step of the propagator depends on the energy of the collision, and the number of closed channels is set to 3 (see Section 4 from Ref. [26]). Using boundary conditions imposed on the wavefunction of the system one can obtain the scattering matrix [39] and use it to calculate the GSXS [40,41]:

$$\begin{aligned}\sigma_\lambda^q(v_i, j_i, v_f, j_f; E_{kin}) &= \tfrac{\pi}{k^2} \textstyle\sum_{J_i,J_f,l,l',\bar{l},\bar{l}'}^{\infty} \mathrm{i}^{l-l'-\bar{l}+\bar{l}'} \\ &\times (-1)^{l-l'-\bar{l}+\bar{l}'} [J_i][J_f] \sqrt{[l][l'][\bar{l}][\bar{l}']} \begin{pmatrix} l & \bar{l} & \lambda \\ 0 & 0 & 0 \end{pmatrix} \\ &\times \begin{pmatrix} l' & \bar{l}' & \lambda \\ 0 & 0 & 0 \end{pmatrix} \begin{bmatrix} j_i & j_i & \bar{l} & \bar{l}' \\ j_f & l & j_f & l' \\ q & J_f & J_i & \lambda \end{bmatrix} [\delta_{ll'} \delta_{\bar{l}\bar{l}'} \\ &- \langle v_i j_i l' | \mathbf{S}^{J_i}(E_{T_i}) | v_i j_i l \rangle \langle v_f j_f \bar{l}' | \mathbf{S}^{J_f}(E_{T_f}) | v_f j_f \bar{l} \rangle^*].\end{aligned} \tag{10}$$

In the equation above v_i, j_i, v_f, j_f denote the initial and final states of the optical transition. J_i and J_f are the total angular momenta associated with the initial and final spectroscopic levels, E_{T_i}, E_{T_f} are the total energies of the system in the initial and final spectroscopic states, k is the wavenumber corresponding to the initial kinetic energy, l is the relative angular momentum and E_{kin} is the relative kinetic energy which is the same in both initial and final states of transition. The symbol $[x]$ stands for $(2x + 1)$, the matrix written in square brackets is the Wigner 12-j symbol of the second kind, the matrices in the parenthesis are Wigner 3-j symbols, and q denotes the rank of the radiation-matter interaction tensor. For quadrupole lines $q = 2$ and for dipole lines $q = 1$. The real and imaginary parts of σ_0^q are the pressure broadening and pressure shift cross-sections (PBXS and PSXS, respectively) [42–44] while σ_1^q is the complex Dicke cross-section [40,44,45], the real and imaginary parts of which are denoted by RDXS and IDXS, respectively.

3. Results

The full procedure described in the previous section is conducted for all electric dipole and quadrupole transitions within the ground electronic state for which both the initial and final levels of the HD molecule are described by vibrational levels 0 to 5 and 8, and rotational levels from 0 to 6 and 9 to 11, including hot bands. Such a wide range of vibrational and rotational states allows us to obtain results containing all the most important and the strongest transitions as well as a great number of weaker ones. For each of these transitions, we obtain the GSXS at E_{kin} of HD-He relative motion ranging from 0.1 to 9000 cm^{-1}. The GSXS are used to obtain the line-shape parameters as described in Section 2.1. The temperature dependence of the latter is projected onto the DPL structure [19,27]. The GSXS, the values of line-shape parameters, and the DPL coefficients are provided in the supplementary materials [28]. This work extends the *ab initio* calculations reported in Ref. [26] by the inclusion of the quadrupole transitions, providing speed-dependence parameters, γ_2 and δ_2, performing some additional calculations for transitions involving higher j and v, and expressing the temperature dependence of line-shape parameters with convenient DPL parametrization for the database application. For completeness, to populate all lines within the ground electronic state that are present in the HITRAN database [22] with beyond-Voigt line-shape parameters, we extrapolate our *ab initio* results of the line-shape parameters obtained from calculated GSXS. We also compare our results with calculations for H$_2$-He system [19] and observe a strong isotopologue dependence between them.

3.1. Quantum scattering calculations

In this section, we present the results of our quantum scattering calculations for selected transitions. We also discuss the difference between GSXS for H$_2$-He and HD-He collisional systems on the example of several selected lines.

Fig. 1 shows examples of the GSXS for the cases of the O(2), Q(1), and S(0) lines for different vibrational bands, as a function of the relative kinetic energy of HD-He motion. In the case of dipole lines, a similar presentation was already published and discussed in Ref. [26]. In each panel, the GSXS are compared between vibrational bands from 1-0 to 5-0 and 8-0.

Both the PSXS and IDXS change their signs as the relative kinetic energy increases. The reason for this behavior in the case of the PSXS was presented in Ref. [21] and related to the fact that collisions occurring at different relative kinetic energies probe different regions of the PES. For each rovibrational transition in every branch, the change of the PSXS sign occurs at similar E_{kin} around 10 to 30 cm^{-1}. For the IDXS the change can be observed at E_{kin} around 150 to 300 cm^{-1}. Near the energy at which the PSXS changes its sign, the PBXS reaches its minimum.

It can be seen that the values of the PBXS, RDXS as well as the absolute values of the PSXS and IDXS increase with the vibrational band. For the RDXS, such behavior becomes noticeable

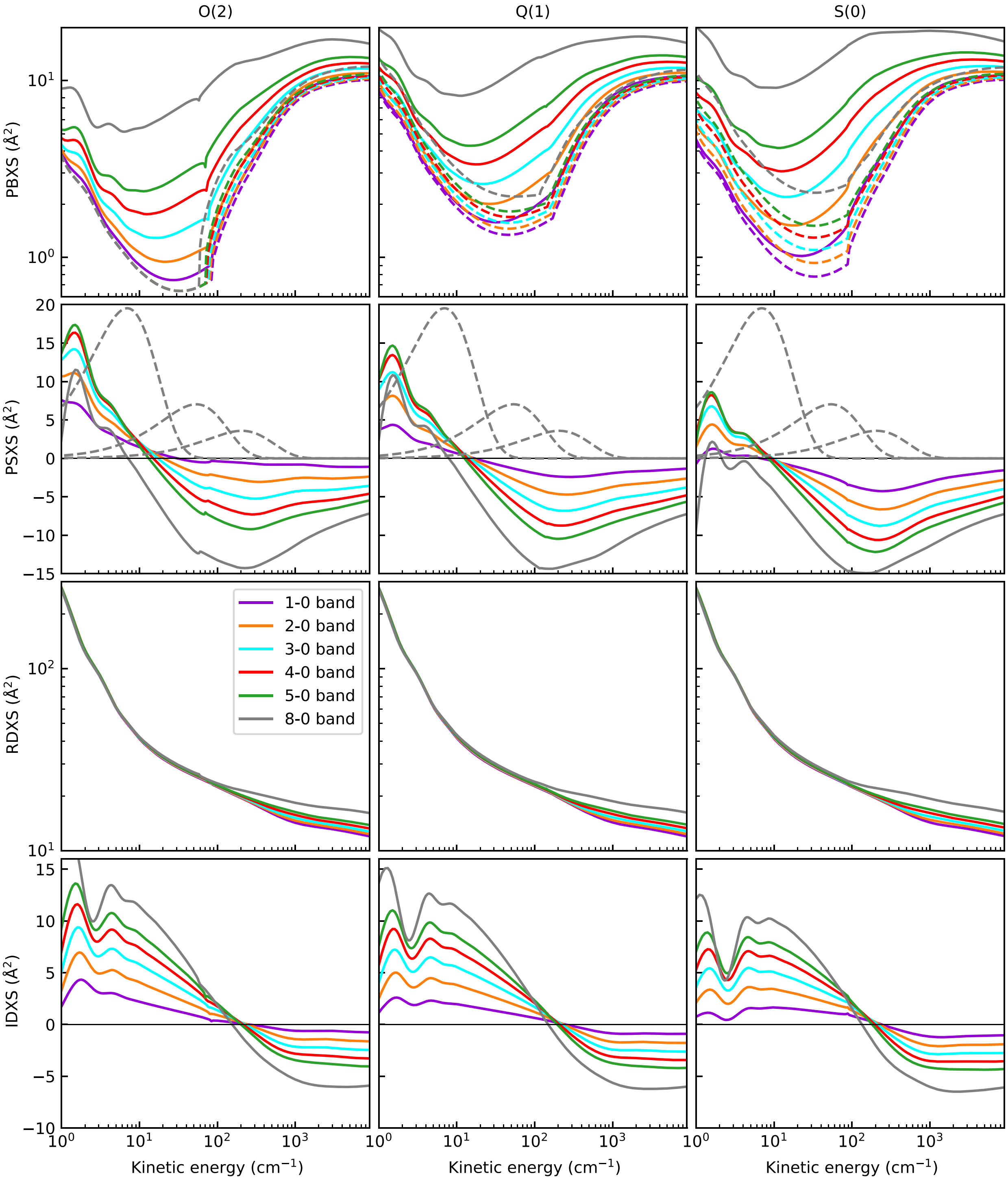

Fig. 1. The PBXS, PSXS, RDXS, and IDXS compared between vibrational bands as a function of the relative motion of HD and He for the O(2), Q(1), and S(0) lines. The inelastic contribution to the PBXS is represented by colored dashed lines in the upper panel. The dashed gray lines in the second row show the Maxwell-Boltzmann distributions at 10 K, 77 K, and 296 K.

at E_{kin} higher than around 200 cm^{-1}. In the case of the PSXS, such behavior is seen at K.E higher than around 10 cm^{-1}. This dependence on the vibrational band results from two phenomena. Firstly, a significant contribution to the PBXS and PSXS for rovibrational transitions comes from rovibrational dephasing. It mainly originates from the difference in the isotropic part of the PES in the initial and final molecular state, which increases with the difference between initial and final vibrational levels. Secondly, the rotational spacing of energy levels decreases with increasing vibrational state, which enlarges the inelastic contribution to the cross-section. It can be easily separated for the PBXS and is marked by colored dashed lines in Fig. 1.

One may notice that for some lines a sharp change of the GSXS can be observed at a certain E_{kin} This is caused by the opening of the first inelastic energy channel in the initial or final molecular state of the optical transition. The opening occurs when the ki-

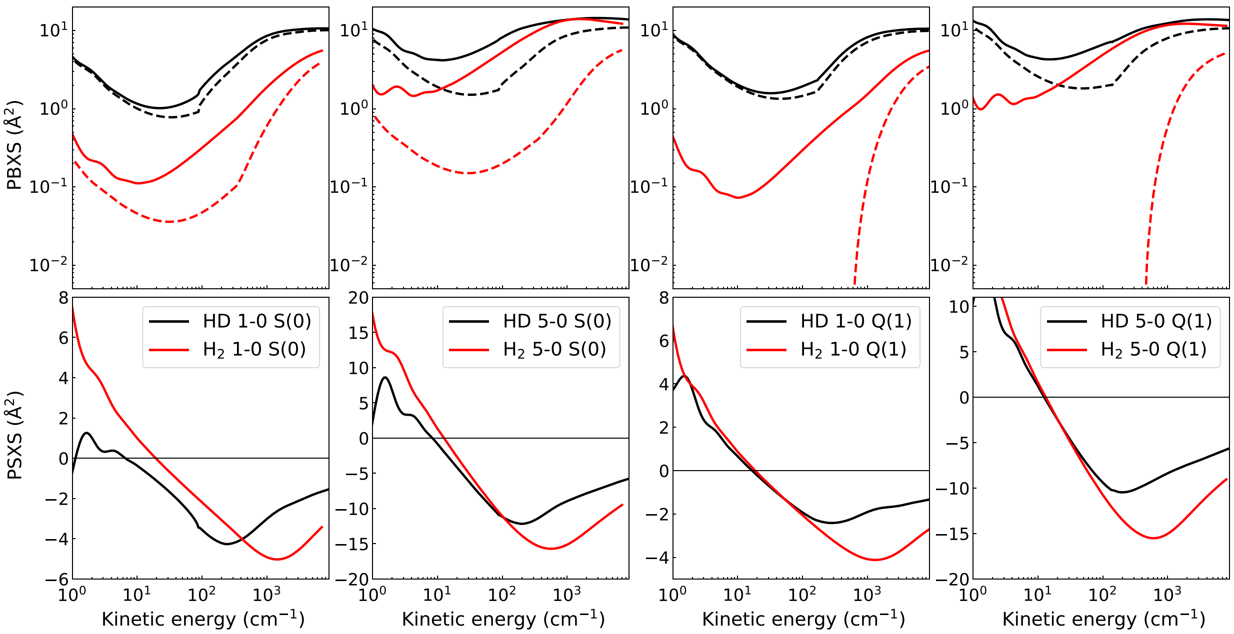

Fig. 2. Comparison of the PBXS and PSXS in HD-He and H_2-He collisional systems for several selected transitions. Starting from the left panels transitions 1-0 S(0), 5-0 S(0), 1-0 Q(1) and 5-0 Q(1) are shown. The dashed lines correspond to the inelastic contribution to the pressure broadening cross-section.

netic energy of the relative motion becomes high enough to induce collisional rotational excitation of the molecule. This may result in a rapid change of the inelastic part of the cross-section. The fact that the rotational constant decreases with the vibrational quantum number explains why the PBXS of O lines split at slightly different E_{kin} (see also Figure 1 and discussion about the $P_v(1)$ and $R_v(0)$ lines in Ref. [26]).

In Fig. 2, a comparison of the PBXS and PSXS between selected quadrupole lines in the HD-He and H_2-He collisional systems are presented. The values of the GSXS for the H_2-He system are taken from Ref. [19]. One can immediately notice that in the case of transitions belonging to the fundamental band, the PBXS for the H_2-He system is significantly smaller than in the case of the HD-He system. The difference comes mainly from the inelastic part of the PBXS, which is a dominant component of the cross-sections for the HD molecule and is significantly greater than the inelastic contribution in the case of H_2. This is further magnified at low K.E in the Q(1) line, where the inelastic contribution is exactly zero for the H_2 molecule. The elastic part generally exhibits a smaller difference between the two systems. The behavior of inelastic contribution is explained as follows. Firstly, the energy spacing between rotational levels is larger in the H_2 than in the HD isotopologue. Secondly, the collisions do not induce transitions between even and odd rotational levels for H_2, since they cannot change the nuclear spin of the molecule. In contrast, the leading anisotropic component of the HD-He PES, the $A_{\xi=1,v,j,v',j'}$ term, allows $\Delta j = |j_f - j_i| = 1$ transitions.

The situation is different for transitions between states for which the difference in vibrational level $\Delta \nu = \nu_f - \nu_i$ is large. In such cases, the dominance of the PBXS cross-section value of HD over H_2 is not that pronounced, because the elastic part of the PBXS starts to play a more important role, as the difference between initial and final molecular wavefunction becomes larger. This can be seen in the panels from the second and fourth columns in Fig. 2. Generally, the elastic part of the PBXS is larger for HD molecule at lower K.E range and smaller at higher E_{kin} This suggests a larger difference between the initial and final states in terms of the repulsive part of the PES of hydrogen-helium interaction as the high-energy collisions probe the repulsive short-range of the PES. For some transitions between states that differ significantly in terms of ν and j, in a certain E_{kin} range, the value of the PBXS in H_2-He system may become larger than in the HD-He system. Finally, the PSXS is similar for the two collisional systems.

3.2. Dataset of beyond-Voigt line-shape parameters

In this section, we describe the final result of our work, i.e., the comprehensive dataset of the beyond-Voigt spectral line-shape parameters of HD perturbed by He. Our dataset covers all the 11 575 rovibrational lines present in the HITRAN database, including electric dipole transitions from the P and R branches, as well as the O, Q, and S electric quadrupole lines. We perform the *ab initio* calculations described in Section 2 to obtain the line-shape parameters for the basic set of 875 transitions at temperatures spanning from 20 to 1000 K. Our calculations are based on the cross-sections which are provided in the supplementary materials to this work [28]. The data for the remaining 10 700 lines (the majority belong to the hot-band lines) comes from interpolation and extrapolation of the data from our basic set. Let us denote a given transition as X(j'') ν' - ν'', where X∈{O, Q, P, R, S} denotes the branch, j'' is the rotational quantum number of the initial state, and ν' and ν'' are the final and initial vibrational states, coupled by the transition. We also denote $\Delta\nu = \nu' - \nu''$. Using this notation, let us describe our interpolation and extrapolation scheme with the following steps (note that after each step the interpolated and extrapolated lines are appended to the basic set).

- if there are at least three lines with the same X, ν' and ν'' in our initial dataset, we use a second-order polynomial to interpolate the missing lines as a function of j'', up to the highest $j'' = j''_{\max}$ from our basic set. For $j'' > j''_{\max}$ we copy the dataset entries of X($j''_{\max}$) ν' - ν'' lines.
- If there are at least three lines with the same X, j'' and ν'', we use a second-order polynomial to interpolate the missing lines in the function of ν', up to the highest $\nu' = \nu'_{\max}$ from our basic

set. For $\nu' > \nu'_{\rm max}$ we copy the dataset entries of X(j'') $\nu'_{\rm max}$ - ν'' lines.
- For each X and j'' we select the lines with the lowest $\Delta\nu = \Delta\nu_{\rm min}$ (i.e., 1-0, 2-1, 3-2... for the O, P and Q branches and 0-0, 1-1, 2-2... for the R and S branches). We extrapolate these subsets with a second-order polynomial in the function of ν'' to obtain entries for the high hot bands with $\Delta\nu = \Delta\nu_{\rm min}$.
- For each X and j'' we approximate the missing hot band entries maintaining constant distances between different subsets with the same $\Delta\nu$, i.e., X(j'') $\nu' - \nu''$ = X(j'') $\Delta\nu$ - 0 - X(j'') $\Delta\nu_{\rm min}$ - 0 + X(j'') ($\nu'' + \Delta\nu_{\rm min}$) - ν'' (for example S(0) 4-2 = S(0) 2-0 - S(0) 0-0 + S(0) 2-2).

The above interpolation and extrapolation scheme is repeated for every considered temperature. We apply the DPL representation defined by Eqs. (7) to represent the temperature dependences in a form adopted in the HITRAN database [27] and recently applied for the H_2-He system [19]. We perform a weighted fitting procedure in the 20 – 1000 K temperature range, prioritizing the range between 50 and 200 K (see the gray-shaded areas in Fig. 3).

Fig. 3 presents examples of the DPL representation applied to the cases of two purely rotational lines, S(0) and R(0) from 0-0 band, and two rovibrational lines, Q(1) 1-0 and R(1) 1-0. The general performance of DPL is satisfying and comparable with the one presented in Ref. [27] on an example of a few collisional systems. As noticed in Refs. [19,27], DPL works the best when the temperature dependence of the line-shape parameters is monotonic, and its performance is worse when sharp extrema are present as can be seen in Fig. 3.

The highest discrepancy can be observed for the δ_2 parameter of the S(0) 0-0 line. However, as shown in Ref. [24] for H_2 isotopologue, the neglection of the speed-dependence effect, which for this molecule has an exceptionally high impact, introduces a change of the line-shape up to a level of a few percent. Thus, in the most important temperature region and its proximity, applying the DPL is expected to cause, at most, sub-percent change of the line-shape due to inaccuracy of δ_2 representation. Good performance of the DPL approximation in the case of the $\widetilde{\nu}^r_{opt}$ may be related to the fact that it can be quite accurately determined from the diffusion coefficient which satisfies the power law temperature dependence [27]. Comparison with analogous results calculated for H_2-He collisional system [19] leads to the observation that both isotopologues H_2 and HD portray similar dependence of the line-shape parameters on temperature.

The dependences of the line-shape parameters on the vibrational band and initial rotational level of the transition are shown in Fig. 4. We present the parameters at two temperatures – 150 K and 296 K. For comparison, in the case of γ_0 and δ_0, we also include the data for the H_2-He collisional system at 296 K [19]. Contrarily to the results obtained for more massive species, such as self- or foreign-gas-perturbed CO, SO_2 and OCS [46–49], the difference between the results for H_2 and HD is pronounced. Therefore we question the "isotopic invariance" paradigm by demonstrating strong isotopologue dependence of the line-shape parameters.

The differences between vibrational bands are clearly visible for γ_0 and δ_0, as both parameters increase with the final vibrational level ν'. This behavior is expected, since γ_0 and δ_0 are proportional to the averaged values of the PBXS and PSXS which, in general, increase with the vibrational band. The difference between the PBXS for the two isotopologues, shown in Fig. 2, is directly manifested in differences between pressure broadening coefficients in Fig. 4. For the bands with lower ν', γ_0 in HD is dominated by the inelastic contribution at 296 K. Hence, γ_0 is much larger for HD than for H_2, for which the inelastic contribution is considerably reduced due to the lack of collision-induced transitions between para- and ortho-H_2 and larger rotational spacing. In the case of the S(0) 0-0 line, γ_0 for HD is more than ten times larger than for the H_2 molecule. As the ν' increases, the elastic contribution that comes mainly from the difference in radial coupling terms of the potential in the initial and final states becomes more important and γ_0 in H_2 becomes even slightly larger than in HD.

The dependences of γ_2 and δ_2 on the vibrational band mirror the dependences of γ_0 and δ_0 – they become larger as the speed-averaged pressure broadening and shift increase. The real and imaginary part of the Dicke coefficient $\widetilde{\nu}_{opt}$, in turn, decrease with the vibrational band. Although the RDXS and the absolute value of IDXS grow with ν', the velocity-changing effect is correlated with coherence damping and dephasing and, as it can be seen in Eq. (6) for the Dicke parameter, σ^q_0 cross-section is included in the equation.

The pressure broadening coefficient decreases with the initial rotational number j'' due to the fact that each subsequent rotational level differs increasingly in energy in accordance to the quadratic relation $E_{j''} = Bj''(j''+1)$. This behavior was also observed before in many collisional systems [50–52]. For purely rotational lines, γ_0 drops to nearly zero as j'' increases because the elastic contribution, emerging from the difference of initial and final molecular wavefunctions, is very low (for pure rotational lines, the vibrational state is the same and only a slight role is played by centrifugal distortion), and because the states with higher j'' are less sensitive to the elastic effects coming from the attractive part of a PES. In the case of H_2 molecule, γ_0 coefficient is very small thus the dependence on j'' is not well pronounced. For rovibrational bands in HD, γ_0 generally also decrease with j'', but as it can be seen in Ref. [19] for H_2 it is not always the case. As an example, for the Q branch of the 2-0 band, γ_0 is not monotonic at the beginning and for higher j'' it has a nearly constant value. Thus, it is another manifestation of the isotopologue dependence. Again, the δ_2 and γ_2 coefficients mirror the dependence of γ_0 and δ_0. Due to the relatively low value of γ_0 for purely rotational lines and nearly transition independent RDXS, the real part of Dicke parameter $\widetilde{\nu}^r_{opt}$ is almost constant with j''. Comparisons of *ab initio* calculations with available experimental data can be found in Refs. [25,26]. There is a need for accurate measurements of the line-shape for rovibrational transitions for further validation.

To estimate the uncertainties of our *ab initio* results, we perform some additional calculations for the R(0) line of the 1-0 band at temperatures 77 K, 195 K, and 296 K, and investigate how the variation of the PES and dynamical numerical parameters of the propagation process (the initial and final points of the propagation, the propagation step and the number of asymptotically closed energy channels) affect the value of the *ab initio* coefficients. Conservative estimations show that the uncertainty of the used PES [1] is not greater than 1 % [21]. Thus, we repeat the calculation using potential radial terms multiplied by 1.01 and for the considered cases the highest obtained deviation is 0.45 %. The convergence of our calculations with the dynamical numerical parameters is obtained as follows. We set the initial and the final points of the propagation, $R_{\rm min}$ and $R_{\rm max}$, the number of propagation steps, and the number of asymptotically closed energy channels such that only a sub-percent deviation of the line-shape parameters is introduced upon halving of $R_{\rm min}$ and $R_{\rm max}$, doubling the number of propagation steps and adding the next asymptotically closed energy level. In total, we estimate the uncertainty of the calculated parameters at 0.6 %. It should be noted that in the case of interpolated and extrapolated parameters for the weaker transitions the deviation may be higher. There is also a second type of uncertainty originating from the DPL approximation (estimated by the root mean square error in the prioritized temperature range). The total combined uncertainty of each parameter is provided in the supplementary materials in the column DPL-err [28].

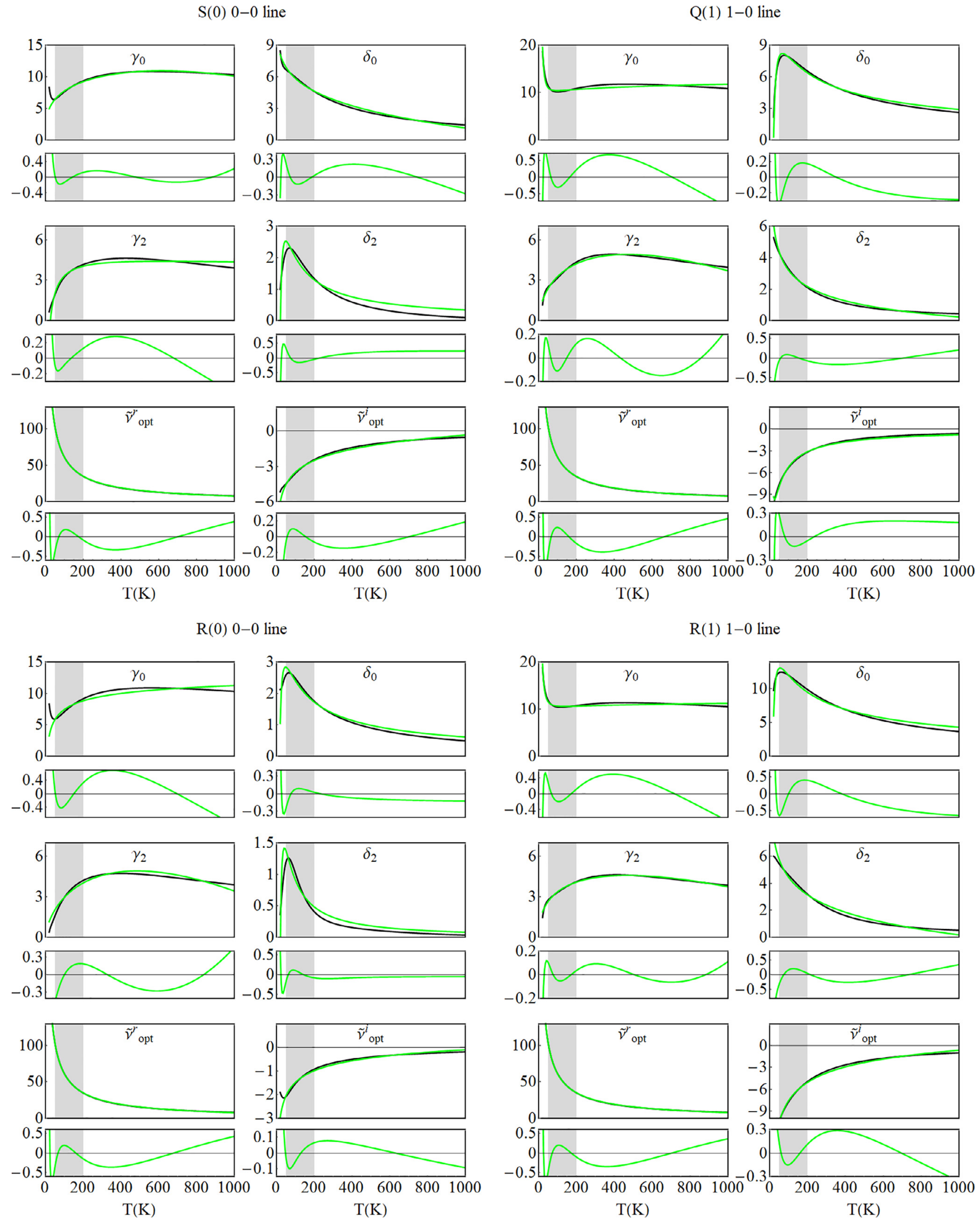

Fig. 3. Temperature dependences of the six collisional line-shape parameters, γ_0, δ_0, γ_2, δ_2, $\tilde{\nu}^{r}_{opt}$ and $\tilde{\nu}^{i}_{opt}$, for the four sample lines of HD perturbed by He. The black and green lines are the *ab initio* values and DPL representations, respectively. Each large graph is accompanied by a small one, presenting the residuals of the DPL fits. The vertical axes for all the panels (including residuals) are in 10^{-3}cm^{-1}atm^{-1}. The gray-shaded areas indicate the temperature range prioritized in the DPL fits. (For interpretation of the references to colour in this figure legend, the reader is referred to the web version of this article.)

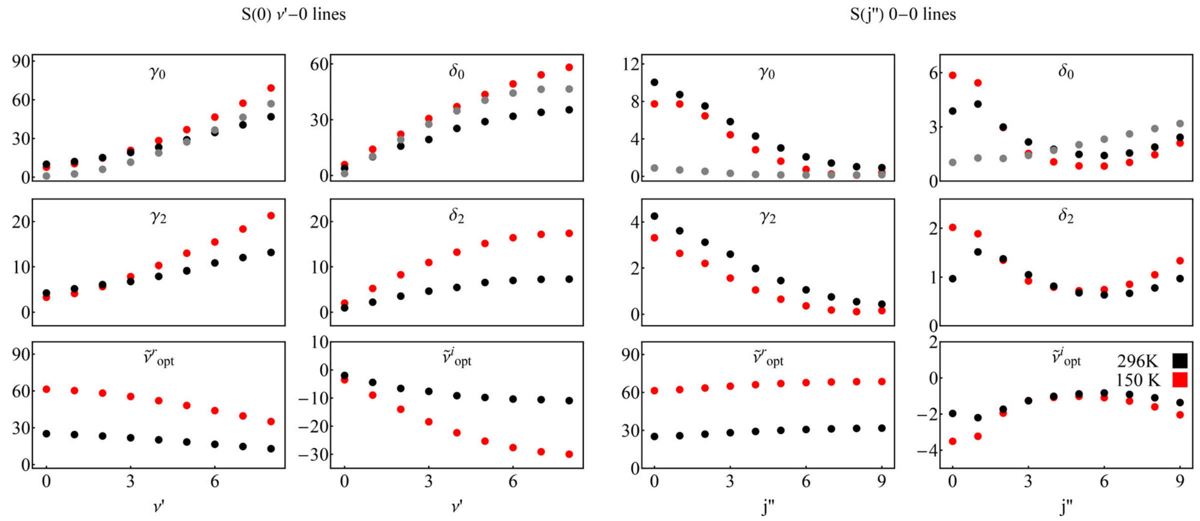

Fig. 4. Examples of the vibrational and rotational dependences of the six line-shape parameters reported in our dataset. Red and black dots correspond to the line-shape parameters for HD-He system at 150 K and 296 K, respectively. For comparison, we also added values of the line-shape parameters for the H_2-He system at $T = 296$ K marked by gray dots. All the parameters are expressed in units of 10^{-3} $\mathrm{cm}^{-1}\mathrm{atm}^{-1}$. The values of the line-shape parameters shown in this plot are not directly taken from *ab initio* calculations, but reconstructed from the DPL relations, Eqs. (7), based on the coefficients from our dataset.

4. Conclusion

Using the methodology presented in Ref. [19] to we performed accurate *ab initio* quantum scattering calculations, obtaining generalized spectroscopic cross-sections and line-shape parameters for electric dipole and quadrupole transitions within the ground electronic state for He-perturbed HD. The line-shape parameters describe the pressure broadening and shift, γ_0, δ_0, and the most important beyond-Voigt effects, the speed-dependences of γ_0, δ_0 through quadratic approximation, γ_2, δ_2, and the velocity-changing collisions through the complex Dicke parameter $\tilde{\nu}_{opt}$. Temperature dependences of the line-shape parameters were expressed by the double-power-law representation recommended for the HITRAN database. Calculations of generalized spectroscopic cross-sections were performed in kinetic energy range from 0.1 to 9000 cm^{-1} and line-shape parameters were obtained at temperatures from 20 to 1000 K which is the relevant range for investigations of gas giants and exoplanets atmospheres. The *ab initio* results cover all transitions including hot bands which involve vibrational levels from 0 to 5 or 8 and rotational levels from 0 to 6 and 9 to 11. Such a wide range was fully sufficient for populating all strongest and most important transitions and a great number of weaker ones. The values for exotic lines were obtained by interpolation and extrapolation of our *ab initio* results. This allowed us to populate all 11 575 rovibrational lines present in the HITRAN database. Comparison with values for H_2-He system led to the observation of strong isotopologue dependence for hydrogen molecule and helium atom system which arises mainly from the limitation of inelastic contribution in the case of H_2. Calculated generalized spectroscopic cross-sections, line-shape parameters, and double-power-law coefficients are provided in the supplementary material [28].

In principle, our methodology can be readily applied to any diatomic molecule in a $^1\Sigma$ electronic state interacting with a structureless atom. Similar calculations could also be done for not too massive linear molecules interacting with an atom, for example, C_2H_2-Ne [53]. For simple diatomic or linear molecules manifesting fine [54] or hyperfine structure [55], the theory (for recoupling the various angular momenta) exists and could be used to produce line-shape parameters for selected lines. Usually, the main problem which one needs to overcome during the calculations for more massive systems is the increased size of the basis caused by the fact that more massive molecules have lower rotational constants, and thus, their rotational levels are less energetically separated. Nevertheless, such calculations could be handled for selected lines of various rovibrational bands by neglecting the rovibrational couplings, i.e. the potential centrifugal distortion. One may also limit the calculations to the transitions that do not involve high vibrational bands.

For two interacting diatomic or linear molecules calculations become more challenging. However, numerous attempts have been already conducted within the above limitations for selected transitions. The examples of these are molecules in dihydrogen baths such as CO-H_2 [56], N_2 - H_2 [57] or C_2H_2 - H_2 [58,59]. Recently, successful attempts were performed for some collisional partners relevant from the perspective of Earth's atmosphere studies – Ar-perturbed CO [60], N_2-perturbed CO [61,62] and N_2-perturbed O_2 [63] (the last work is also an example of application of the method for an active molecule with non-zero spin).

The problem of a large rotational basis may be addressed through the use of various approximations such as the coupled state approximation [61] or its improved version that includes the nearest neighbor Coriolis coupling [64]. The efficiency of these approximations should be more deeply investigated in the future. For some systems, the limitation of the method may be imposed by the absence of sufficiently accurate potential energy surfaces including the vibrational dependence of the active molecule.

Declaration of Competing Interest

The authors declare that they have no known competing financial interests or personal relationships that could have appeared to influence the work reported in this paper.

CRediT authorship contribution statement

Kamil Stankiewicz: Conceptualization, Software, Investigation, Writing – original draft, Writing – review & editing, Visualization. **Nikodem Stolarczyk:** Conceptualization, Software, Investigation, Validation, Writing – original draft, Writing – review & editing, Visualization. **Hubert Jóźwiak:** Conceptualization, Software, Investigation, Validation, Writing – review & editing. **Franck Thibault:** Conceptualization, Methodology, Software, Resources, Writing – review & editing. **Piotr Wcisło:** Conceptualization, Methodology, Writing – review & editing, Supervision, Project administration, Funding acquisition.

Acknowledgment

KS contribution is supported by the National Science Centre in Poland through project no. 2018/30/E/ST2/00864. HJ and PW contributions are supported by the National Science Centre in Poland through project no. 2018/31/B/ST2/00720. NS contribution is supported by the National Science Centre in Poland through project no. 2019/35/B/ST2/01118. The project is supported by the French-Polish PHC Polonium program (project 42769ZK for the French part). The project is co-financed by the Polish National Agency for Academic Exchange under the PHC Polonium program (dec.PPN/X/PS/318/2018). The research was part of the program of the National Laboratory FAMO in Toruń, Poland. Part of the calculations have been carried out using resources provided by Wroclaw Centre for Networking and Supercomputing (http://wcss.pl), grant no. 546.

Supplementary material

Supplementary material associated with this article can be found, in the online version, at doi:10.1016/j.jqsrt.2021.107911.

References

[1] Thibault F, Patkowski K, Zuchowski P, Jóźwiak H, Ciuryło R, Wcisło P. Rovibrational line-shape parameters for H_2 in he and new H_2-He potential energy surface. J Quant Spectrosc Radiat Transf 2017;202:308–20. doi:10.1016/j.jqsrt.2017.08.014.

[2] Bakr B, Smith D, Patkowski K. Highly accurate potential energy surface for the He-H_2 dimer. J Chem Phys 2013;139:144305. doi:10.1063/1.4824299.

[3] Czachorowski P, Puchalski M, Komasa J, Pachucki K. Nonadiabatic relativistic correction in H_2, D_2, and HD. Phys Rev A 2018;98:052506. doi:10.1103/PhysRevA.98.052506.

[4] Komasa J, Puchalski M, Czachorowski P, Lach G, Pachucki K. Rovibrational energy levels of the hydrogen molecule through nonadiabatic perturbation theory. Phys Rev A 2019;100:032519. doi:10.1103/PhysRevA.100.032519.

[5] Nolte J, Stancil P, Lee T, Balakrishnan N, Forrey R. Rovirational quenching rate coefficients of HD in collisions with He. Astrophys J 2012;744:62. doi:10.1088/0004-637x/744/1/62.

[6] Feuchtgruber H, Lellouch E, Orton G, Graauw T, Vandenbussche B, Swinyard B, et al. The D/H ratio in the atmospheres of Uranus and Neptune from Herschel-PACS observations. Astron Astrophys 2013;551:A126. doi:10.1051/0004-6361/201220857.

[7] Sung K, Wishnow E, Manceron L, Drouin B, Nixon C. Progress report on the measurements of pressure-broadening of HD rotational transitions for Jovian atmospheres. Bulletin of the AAS 2020;52.

[8] Lellouch E, Bézard B, Fouchet T, Feuchtgruber H, Encrenaz T, Graauw T. The deuterium abundance in Jupiter and Saturn from ISO-SWS observations. Astron Astrophys 2001;370:610–22. doi:10.1051/0004-6361:20010259.

[9] Miller-Ricci E, Sasselov D, Seager S. The atmospheric signatures of super-Earths: how to distinguish between hydrogen-rich and hydrogen-poor atmospheres. Astrophys J 2008;690:1056–67. doi:10.1088/0004-637X/690/2/1056.

[10] Dicke RH. The effect of collisions upon the Doppler width of spectral lines. Phys Rev 1953;89:472–3. doi:10.1103/PhysRev.89.472.

[11] Berman PR. Speed-dependent collisional width and shift parameters in spectral profiles. J Quant Spectrosc Radiat Transf 1972;12:1331–42. doi:10.1016/0022-4073(72)90189-6.

[12] Hess S. Kinetic theory of spectral line shapes. The transition between Doppler broadening and collisional broadening. Physica 1972;61:80–94. doi:10.1016/0031-8914(72)90035-3.

[13] Ciuryło R, Bielski A, Drummond JR, Lisak D, May AD, Pine AS, et al. High-resolution studies on the influence of velocity-changing collisions on atomic and molecular line shapes. AIP Conf Proc 2002;645:151–60. doi:10.1063/1.1525447.

[14] Tran H, Hartmann J-M, Chaussard F, Gupta M. An isolated line-shape model based on the Keilson-Storer function for velocity changes. II. molecular dynamics simulations and the Q(1) lines for pure H_2. J Chem Phys 2009;131:154303. doi:10.1063/1.3247898.

[15] Hartmann J-M, Tran H, Ngo NH, Landsheere X, Chelin P, Lu Y, et al. *Ab initio* calculations of the spectral shapes of CO_2 isolated lines including non-Voigt effects and comparisons with experiments. Phys Rev A 2013;87:013403. doi:10.1103/PhysRevA.87.013403.

[16] May A, Liu W-K, McCourt F, Ciuryło R, Sanchez-Fortún Stoker J, Shapiro D, et al. The impact theory of spectral line shapes: a paradigm shift. Can J Phys 2013;91:879–95. doi:10.1139/cjp-2012-0345.

[17] Tennyson J, Bernath P, Campargue A, Csaszar A, Daumont L, Gamache R, et al. Recommended isolated-line profile for representing high-resolution spectroscopic transitions (IUPAC Technical Report). Pure Appl Chem 2014;86:1931–43. doi:10.1515/pac-2014-0208.

[18] Fortney JJ, Robinson TD, Domagal-Goldman S, Genio ADD, Gordon IE, Gharib-Nezhad E, et al. The need for laboratory measurements and *ab initio* studies to aid understanding of exoplanetary atmospheres. arXivorg 2019.

[19] Wcisło P, Thibault F, Stolarczyk N, Jóźwiak H, Słowiński M, Gancewski M, et al. The first comprehensive dataset of beyond-Voigt line-shape parameters from *ab initio* quantum scattering calculations for the HITRAN database: He-perturbed H_2 case study. J Quant Spectrosc Radiat Transf 2021;260:107477. doi:10.1016/j.jqsrt.2020.107477.

[20] Thibault F, Wcisło P, Ciuryło R. A test of H_2-He potential energy surfaces. Eur Phys J D 2016;70:236. doi:10.1140/epjd/e2016-70114-9.

[21] Jóźwiak H, Thibault F, Stolarczyk N, Wcisło P. *Ab initio* line-shape calculations for the S and O branches of H_2 perturbed by He. J Quant Spectrosc Radiat Transf 2018;219:313–22. doi:10.1016/j.jqsrt.2018.08.023.

[22] Gordon IE, Rothman LS, Hargreaves RJ, Hashemi R, Karlovets EV, Skinner FM, et al. The HITRAN2020 molecular spectroscopic database. J Quant Spectrosc Radiat Transf (submitted) 2021.

[23] Słowiński M, Thibault F, Tan Y, Wang J, Liu A-W, Hu S-M, Kassi S, Campargue A, Konefał M, Jóźwiak H, Patkowski K, Zuchowski P, Ciuryło R, Lisak D, Wcisło P. H_2-He Collisions: *ab initio* theory meets cavity-enhanced spectra. Phys Rev A 2020:052705. doi:10.1103/PhysRevA.101.052705.

[24] Słowiński M, Jóźwiak H, Gancewski M, Stankiewicz K, Stolarczyk N, Tan Y, et al. Collisional line-shape effects in accurate He-perturbed H_2 spectra. J Quant Spectrosc Radiat Transf (submitted) 2021.

[25] Thibault F, Martínez R, Bermejo D, Wcisło P. Line-shape parameters for the first rotational lines of HD in He. Mol Astrophys 2020:100063. doi:10.1016/j.molap.2020.100063.

[26] Stankiewicz K, Jóźwiak H, Gancewski M, Stolarczyk N, Thibault F, Wcisło P. *Ab initio* calculations of collisional line-shape parameters and generalized spectroscopic cross-sections for rovibrational dipole lines in HD perturbed by He. J Quant Spectrosc Radiat Transf 2020;254:107194. doi:10.1016/j.jqsrt.2020.107194.

[27] Stolarczyk N, Thibault F, Cybulski H, Jóźwiak H, Kowzan G, Vispoel B, et al. Evaluation of different parameterizations of temperature dependences of the line-shape parameters based on *ab initio* calculations: Case study for the HITRAN database. J Quant Spectrosc Radiat Transfr 2020;240:106676. doi:10.1016/j.jqsrt.2019.106676.

[28] Stankiewicz K, Stolarczyk N, Jóźwiak H, Thibault F, Wcisło P. Supplementary material. J Quant Spectrosc Radiat Transf 2021.

[29] Wcisło P, Thibault F, Zaborowski M, Wójtewicz S, Cygan A, Kowzan G, et al. Accurate deuterium spectroscopy for fundamental studies. J Quant Spectrosc Radiat Transf 2018;213:41–51. doi:10.1016/j.jqsrt.2018.04.011.

[30] Pine A. Asymmetries and correlations in speed-dependent Dicke-narrowed line shapes of argon-broadened HF. J Quant Spectrosc Radiat Transf 1999;62:397–423. doi:10.1016/S0022-4073(98)00112-5.

[31] Rautian SG, Sobel'man II. The effect of collisions on the Doppler broadening of spectral lines. Sov Phys Uspekhi 1967;9:701–16. doi:10.1070/PU1967v009n05ABEH003212.

[32] Ciuryło R, Jaworski R, Jurkowski J, Pine AS, Szudy J. Spectral line shapes modeled by a quadratic speed-dependent Galatry profile. Phys Rev A 2001;63:032507. doi:10.1103/PhysRevA.63.032507.

[33] Rohart F, Mäder H, Nicolaisen H. Speed dependence of rotational relaxation induced by foreign gas collisions: studies on CH_3F by millimeter wave coherent transients. J Chem Phys 1994;101:6475–86. doi:10.1063/1.468342.

[34] Arthurs A, Dalgarno A. The theory of scattering by a rigid rotator. Proc R Soc A 1960;256:540–51. doi:10.1098/rspa.1960.0125.

[35] Flower D. Molecular collisions in the interstellar medium. Cambridge University Press; 2007. doi:101017/cbo9780511536229.

[36] Jóźwiak H., Gancewski M., Stankiewicz K., Wcisło P. BIGOS computer code. to be published

[37] Johnson BR. The renormalized Numerov method applied to calculating bound states of the coupled-channel Schrödinger equation. J Chem Phys 1978;69:4678–88. doi:10.1063/1.436421.

[38] Manolopoulos DE. An improved log derivative method for inelastic scattering. J Chem Phys 1986;85:6425–9. doi:10.1063/1.451472.

[39] Johnson B. Multichannel log-derivative method for scattering calculations. J Comput Phys 1973;13:445–9. doi:10.1016/0021-9991(73)90049-1.

[40] Monchick L, Hunter L. Diatomic-diatomic molecular collision integrals for pressure broadening and Dicke narrowing - A generalization of Hess's theory. J Chem Phys 1986;85:713–18. doi:10.1063/1.451277.

[41] Schaefer J, Monchick L. Line broadening of HD immersed in He and H_2 gas. Astron Astrophys 1992;265:859–68.

[42] Shafer R, Gordon RG. Quantum scattering theory of rotational relaxation and spectral line shapes in H_2-He gas mixtures. J Chem Phys 1973;58:5422–43. doi:10.1063/1.1679162.

[43] Ben-Reuven A. Symmetry considerations in pressure-broadening theory. Phys Rev 1966;141:34–40. doi:10.1103/PhysRev.141.34.

[44] Schaefer J, Monchick L. Line shape cross sections of HD immersed in He and H_2 gas. I. Pressure broadening cross sections. J Chem Phys 1987;87:171–81. doi:10.1063/1.453612.

[45] Corey GC, McCourt FR. Dicke narrowing and collisional broadening of spectral lines in dilute molecular gases. J Chem Phys 1984;81:2318–29. doi:10.1063/1.447930.

[46] Mehrotra S, Bestmann G, Dreizler H, Mäder H. A contribution to the investigation of T_2relaxation: rotational transitions of OCS and SO_2. Zeitschrift für Naturforschung A 1984;39:633–6. doi:10.1515/zna-1984-0707.

[47] Cazzoli G, Dore L. Lineshape measurements of rotational lines in the millimeter-wave region by second harmonic detection. J Mol Spectrosc 1990;141:49–58. doi:10.1016/0022-2852(90)90277-W.

[48] Puzzarini C, Dore L, Cazzoli G. A comparison of lineshape models in the analysis of modulated and natural rotational line profiles: application to the pressure broadening of OCS and CO. J Mol Spectrosc 2002;216:428–36. doi:10.1006/jmsp.2002.8663.

[49] Mantz A, Thibault F, Cacheiro J, Fernandez B, Pedersen T, Koch H, et al. Argon broadening of the ^{13}CO R(0) and R(7) transitions in the fundamental band at temperatures between 80 and 297K: comparison between experiment and theory. J Mol Spectrosc 2003;222:131–41. doi:10.1016/S0022-2852(03)00200-5.

[50] Predoi-Cross A, Luo C, Sinclair P, Drummond J, May A. Line broadening and the temperature exponent of the fundamental band in CO-N_2 mixtures. J Mol Spectrosc 1999;198:291–303. doi:10.1006/jmsp.1999.7940.

[51] Hartmann J-M, Boulet C. Line shape parameters for HF in a bath of argon as a test of classical path models. J Chem Phys 2000;113:9000–10. doi:10.1063/1.1319346.

[52] Boulet C, Flaud P-M, Hartmann J-M. Infrared line collisional parameters of HCl in argon, beyond the impact approximation: Measurements and classical path calculations. J Chem Phys 2004;120:11053–61. doi:10.1063/1.1714794.

[53] Thibault F, Cappelletti D, Pirani F, Blanquet G, Bartolomei M. Molecular-beam scattering and pressure broadening cross sections for the acetylene-neon system. Eur Phys J D 2007;44:337–44. doi:10.1140/epjd/e2007-00180-y.

[54] Grimminck DLAG, Spiering FR, Janssen LMC, van der Avoird A, van der Zande WJ, Groenenboom GC. A theoretical and experimental study of pressure broadening of the oxygen A-band by helium. J Chem Phys 2014;140:204314. doi:10.1063/1.4878666.

[55] Ronningen TJ, De Lucia FC. Helium induced pressure broadening and shifting of HCN hyperfine transitions between 1.3 and 20 K. J Chem Phys 2005;122:184319. doi:10.1063/1.1895905.

[56] Faure A, Wiesenfeld L, Drouin B, Tennyson J. Pressure broadening of water and carbon monoxide transitions by molecular hydrogen at high temperatures. J Quant Spectrosc Radiat Transf 2013;116:79–86. doi:10.1016/j.jqsrt.2012.09.015.

[57] Gómez L, Martínez RZ, Bermejo D, Thibault F, Joubert P, Bussery-Honvault B, et al. Q-Branch linewidths of N_2 perturbed by H_2: experiments and quantum calculations from an ab initio potential. J Chem Phys 2007;126:204302. doi:10.1063/1.2731789.

[58] Thibault F, Ivanov SV, Buzykin OG, Gomez L, Dhyne M, Joubert P, et al. Comparison of classical, semiclassical and quantum methods in hydrogen broadening of acetylene lines. J Quant Spectrosc Radiat Transf 2011;112:1429–37. doi:10.1016/j.jqsrt.2011.02.011.

[59] Thibault F, Martínez RZ, Bermejo D, Ivanov SV, Buzykin OG, Ma Q. An experimental and theoretical study of nitrogen-broadened acetylene lines. J Quant Spectrosc Radiat Transf 2014;142:17–24. doi:10.1016/j.jqsrt.2014.03.009.

[60] Serov E, Stolarczyk N, Makarov D, Vilkov I, Golubiatnikov G, Balashov A, et al. CO-Ar collisions: *ab initio* model matches experimental spectra at a sub percent level over a wide pressure range. J Quant Spectrosc Radiat Transf 2021;272:107807. doi:10.1016/j.jqsrt.2021.107807.

[61] Jóźwiak H, Thibault F, Cybulski H, Wcisło P. *Ab initio* investigation of the CO-N_2 quantum scattering: the collisional perturbation of the pure rotational R(0) line in CO. J Chem Phys 2021;154:054314. doi:10.1063/5.0040438.

[62] Paredes-Roibás D, Martínez RZ, Jóźwiak H, Thibault F. Collisional line broadening and mixing in the Raman spectrum of CO perturbed by N_2: experimental measurements and theoretical calculations. J Quant Spectrosc Radiat Transf 2021:107868. doi:10.1016/j.jqsrt.2021.107868.

[63] Gancewski M, Jóźwiak H, Quintas-Sánchez E, Dawes R, Thibault F, Wcisło P. Fully quantum calculations of O_2–N_2 scattering using a new potential energy surface: collisional perturbations of the oxygen 118 GHz fine structure line. J Chem Phys (submitted) 2021.

[64] Yang D, Hu X, Zhang DH, Xie D. An improved coupled-states approximation including the nearest neighbor Coriolis couplings for diatom-diatom inelastic collision. J Chem Phys 2018;148:084101. doi:10.1063/1.5010807.

Astronomy & Astrophysics manuscript no. output
April 26, 2024

Accurate reference spectra of HD in an H_2–He bath for planetary applications

H. Jóźwiak[1], N. Stolarczyk[1], K. Stankiewicz[1], M. Zaborowski[1], D. Lisak[1], S. Wójtewicz[1], P. Jankowski[2], K. Patkowski[3], K. Szalewicz[4], F. Thibault[5], I.E. Gordon[6], P. Wcisło[1]

[1] Institute of Physics, Faculty of Physics, Astronomy and Informatics, Nicolaus Copernicus University in Toruń, Grudziadzka 5, 87-100 Toruń, Poland
[2] Faculty of Chemistry, Nicolaus Copernicus University in Toruń, Gagarina 7, 87-100 Toruń, Poland
[3] Department of Chemistry and Biochemistry, Auburn University, Auburn, Alabama 36849, USA
[4] Department of Physics and Astronomy, University of Delaware, Newark, Delaware 19716, USA
[5] Univ Rennes, IPR (Institut de Physique de Rennes) – UMR 6251, F-35000 Rennes, France
[6] Harvard-Smithsonian Center for Astrophysics, Atomic and Molecular Physics Division, Cambridge 02138, USA

April 26, 2024

ABSTRACT

Context. The hydrogen deuteride (HD) molecule is an important deuterium tracer in astrophysical studies. The atmospheres of gas giants are dominated by molecular hydrogen, and the simultaneous observation of H_2 and HD lines provides reliable information on the D/H ratios on these planets. The reference spectroscopic parameters play a crucial role in such studies. Under the thermodynamic conditions encountered in these atmospheres, spectroscopic studies of HD require not only the knowledge of line intensities and positions but also accurate reference data on pressure-induced line shapes and shifts.
Aims. Our aim is to provide accurate collision-induced line-shape parameters for HD lines that cover any thermodynamic conditions relevant to the atmospheres of giant planets, namely any relevant temperature, pressure, and perturbing gas composition (the H_2–He mixture).
Methods. We performed quantum-scattering calculations on our new, highly accurate ab initio potential energy surface (PES), and we used scattering S matrices obtained in this way to determine the collision-induced line-shape parameters. We used cavity ring-down spectroscopy to validate our theoretical methodology.
Results. We report accurate collision-induced line-shape parameters for the pure rotational R(0), R(1), and R(2) lines, the most relevant HD lines for investigations of the atmospheres of the giant planets. Besides the basic Voigt-profile collisional parameters (i.e., the broadening and shift parameters), we also report their speed dependences and the complex Dicke parameter, which can influence the effective width and height of the HD lines up to almost a factor of 2 for giant planet conditions. The sub-percent-level accuracy reached in this work is a considerable improvement over previously available data. All the reported parameters (and their temperature dependences) are consistent with the HITRAN database format, hence allowing for the use of the HITRAN Application Programming Interface (HAPI) for generating the beyond-Voigt spectra of HD.

Key words. atomic data – molecular data – line: profiles – scattering – planets and satellites: atmospheres

1. Introduction

Hydrogen deuteride (HD), the second most abundant isotopolog of molecular hydrogen, is an important tracer of deuterium in the Universe. The small and constant primordial fraction of deuterium to hydrogen, D/H ($(2.8\pm0.2)\times10^{-5}$; Pettini et al. 2008), is one of the key arguments supporting the Big Bang theory. Measurements of the D/H ratio in the Solar System provide information about planetary formation and evolution. The standard ratio on Earth is considered to be Vienna Standard Mean Ocean Water (VSMOW; D/H = 1.5576×10^{-4}; Araguás-Araguás et al. 1998). Employing it, Donahue et al. (1982) found the D/H ratio in the Venusian atmosphere to be $(1.6\pm0.2)\times10^{-2}$ (i.e., two orders of magnitude higher than VSMOW). This higher ratio is attributed to the evaporation of oceans and the subsequent photodissociation of H_2O in the upper parts of the atmosphere (Donahue & Pollack 1983). A comparison of the D/H ratios on Earth and Mars with those determined for various comets indicates the role of this ratio in the volatile accretion on these two planets (Drake & Righter 2002; Hartogh et al. 2011). The two largest gas giants, Jupiter and Saturn, are incapable of nuclear fusion; thus, planetary models predict that the D/H ratio in their atmospheres should be close to the primordial value for the Solar System (Lellouch et al. 2001) or slightly larger due to the accretion of deuterium-rich icy grains and planetesimals (Guillot 1999). The abundance of deuterium is larger by a factor of 2.5 in the atmospheres of Uranus and Neptune (Feuchtgruber et al. 2013), owing to their ice-rich interiors (Guillot 1999). Additionally, the determination of the D/H ratio in comets and moons provides information about the formation of ices in the early Solar System (Hersant et al. 2001; Gautier & Hersant 2005; Horner et al. 2006).

The D/H ratio in planets, moons, or comets can be derived from either in situ mass spectrometry (Eberhardt et al. 1995; Mahaffy et al. 1998; Niemann et al. 2005; Altwegg et al. 2015) or spectroscopic observations of various molecules and their deuterated isotopologs in the millimeter and infrared range (Bockelée-Morvan et al. 1998; Meier et al. 1998; Crovisier et al. 2004; Fletcher et al. 2009; Pierel et al. 2017; Krasnopolsky

Article published by EDP Sciences, to be cited as https://doi.org/10.1051/0004-6361/202449889

et al. 2013; Blake et al. 2021). Interestingly, as pointed out by Krasnopolsky et al. (2013), the ratios determined from spectra of different molecules can differ substantially. Moreover, even on Earth, the HDO/H_2O ratio in the atmosphere can vary substantially across the globe (Araguás-Araguás et al. 1998). In this context, the observation of isotopologs of molecular hydrogen can be a reliable benchmark for determining D/H ratios. The most accurate values of the D/H ratio in gas giants stem from analyses of the pure rotational R(0), R(1), R(2), and R(3) lines of HD and S(0) and S(1) lines in H_2. Lellouch et al. (2001) determined the D/H ratio in the Jovian atmosphere using the Short Wavelength Spectrometer (SWS) on board the Infrared Space Observatory to be $(2.25 \pm 0.35) \times 10^{-5}$. Pierel et al. (2017) analyzed the far-infrared spectra of Saturn's atmosphere gathered by Cassini's Composite Infrared Spectrometer. Interestingly, the Pierel et al. result suggests that the D/H ratio on Saturn is lower than that of Jupiter, which contradicts predictions based on interior models (Guillot 1999; Owen & Encrenaz 2006) and points to an unknown mechanism of deuterium fractionating in Saturn's atmosphere. The D/H ratio in the atmospheres of Uranus and Neptune was determined from measurements of the pure rotational R(0), R(1), and R(2) lines in HD using the Photoconductor Array Camera and Spectrometer (PACS) on board the *Herschel* space observatory (Feuchtgruber et al. 2013). The analysis revealed similar values for these two giants – $(4.4 \pm 0.4) \times 10^{-5}$ and $(4.1 \pm 0.4) \times 10^{-5}$, respectively – confirming the expected deuterium enrichment with respect to the protosolar value.

Atmospheric models of the Solar System's gas giants, from which the relative abundance of HD with respect to H_2 is retrieved (and consequently, the D/H ratio), require knowledge about the line parameters of HD and H_2. The temperature profiles considered in the models cover seven orders of magnitude of pressure (1 μbar–10 bar; see for instance Pierel et al. 2017). Thus, in addition to line position and intensity, knowledge about collisional effects that perturb the shape of observed lines is crucial for the accurate determination of the relative HD abundance. Furthermore, the incorporation of non-Voigt line-shape effects (such as Dicke narrowing and speed-dependent effects) allows for reducing the systematic errors in atmospheric models, as shown for Jupiter (Smith 1989) and for Uranus and Neptune (Baines et al. 1995). Indeed, although the spectral lines of most molecules observed in planetary atmospheres are not sensitive to non-Voigt effects, considering the resolving power of available telescopes, the lines of molecular hydrogen and its isotopologs are (Smith 1989; Baines et al. 1995).

In this article we report accurate collision-induced line-shape parameters for the rotational transitions R(0), R(1), and R(2) within the ground vibrational state. These HD lines are most frequently used for studies of the atmospheres of the giant planets. The results cover all thermodynamic conditions relevant to the atmospheres of giant planets in the Solar System, that is, all relevant temperatures, pressures, and H_2–He perturbing gas compositions (the HD-H_2 data are provided in this work, while the HD-He data are taken from Stankiewicz et al. 2020, 2021). Besides the basic Voigt-profile collisional parameters (i.e., the broadening and shift parameters), we also report their speed dependences and the complex Dicke parameter, which, as we will show, can influence the effective width and height of the HD lines up to almost a factor of 2 for giant planet conditions. For the R(0) line, the non-Voigt regime coincides with the maximum of the monochromatic contribution function (see Fig. 1 in Feuchtgruber et al. 2013), which has a direct influence on the abundance of HD inferred from observations.

We performed quantum-scattering calculations on our new, highly accurate ab initio 6D potential energy surface (PES), and we used the scattering S matrices obtained in this way to determine the collision-induced line-shape parameters. We used the cavity ring-down spectroscopy to validate our theoretical methodology, demonstrating a sub-percent-level accuracy that considerably surpasses the accuracy of any previous theoretical (Schaefer & Monchick 1992) or experimental study of line-shape parameters of pure rotational lines in HD (Ulivi et al. 1989; Lu et al. 1993; Sung et al. 2022) and offers valuable input for the HITRAN database (Gordon et al. 2022). This work represents significant methodological and computational progress; calculations at this level of theory and accurate experimental validation have already been performed for a molecule-atom system (3D PES; Słowiński et al. 2020; Słowiński et al. 2022), but in this work we extend it to a molecule-molecule system (6D PES). All the reported parameters (and their temperature dependences) are consistent with the HITRAN database format, hence allowing for the use of the HITRAN Application Programming Interface (HAPI; Kochanov et al. 2016) for generating the beyond-Voigt spectra of HD for any H_2–He perturbing gas composition and thermodynamic condition.

2. Ab initio calculations of the line-shape parameters

In recent years, the methodology for accurate ab initio calculations of the line-shape parameters (including the beyond-Voigt parameters) was developed and experimentally tested for He-perturbed H_2 and HD rovibrational lines, starting from accurate ab initio H_2-He PES calculations (Bakr et al. 2013; Thibault et al. 2017), through the state-of-the-art quantum scattering calculations and line-shape parameter determination (Thibault et al. 2017; Jóźwiak et al. 2018), up to accurate experimental validation (Słowiński et al. 2020; Słowiński et al. 2022) and using the results for populating the HITRAN database (Wcisło et al. 2021; Stankiewicz et al. 2021).

In this work we extend the entire methodology to a much more complex system of a diatomic molecule colliding with another diatomic molecule. First, we calculated an accurate 6D H_2-H_2 PES. Second, we performed state-of-the-art quantum-scattering calculations. Third, we calculated the full set of the six line-shape parameters in a wide temperature range. Finally, we report the results in a format consistent with the HITRAN database.

The 6D PES was obtained using the supermolecular approach based on the level of theory similar to that used to calculate the 4D H_2-H_2 surface (Patkowski et al. 2008). The crucial contributions involve: (1) interaction energy calculated at the Hartree-Fock (HF) level, (2) the correlation contribution to the interaction energy calculated using the coupled-cluster method with up to perturbative triple excitations, CCSD(T), with the results extrapolated to the complete basis set limit (Halkier et al. 1999), (3) electron correlation effects beyond CCSD(T) up to full configuration interaction (FCI), and (4) the diagonal Born-Oppenheimer correction (DBOC; Handy et al. 1986). The details regarding the basis sets used in calculations of each contribution and the analytical fit to the interaction energies are given in Appendix A. The PES is expected to be valid for intramolecular distances $r_i \in [0.85, 2.25]\, a_0$.

For the purpose of performing quantum scattering calculations, the 6D PES was expanded over a set of appropriate angular functions and the resulting 3D numerical function in radial coordinates was then expanded in terms of rovibrational wave functions of isolated molecules (see Appendix B for details). The close-coupling equations were solved in the body-fixed frame using a renormalized Numerov's algorithm, for the total number of 3 014 energies ($E_T = E_{\mathrm{kin}} + E_{v_1 j_1} + E_{v_2 j_2}$, where E_{kin} is the relative kinetic energy of the colliding pair, and $E_{v_1 j_1}$ and $E_{v_2 j_2}$ are the rovibrational energies of the two molecules at large separations) in a range from 10^{-3} cm^{-1} to 4000 cm^{-1}. Calculations were performed using the quantum scattering code from the BIGOS package developed in our group (Jóźwiak et al. 2024; Jóźwiak 2024). The scattering S matrix elements were obtained from boundary conditions imposed on the radial scattering function. Convergence of the calculated S matrix elements was ensured by a proper choice of the integration range, propagator step, and the size of the rovibrational basis (see Appendix C for details).

Next, we calculated the generalized spectroscopic cross-sections, σ_λ^q (Monchick & Hunter 1986; Schaefer & Monchick 1992), which describe how collisions perturb the shape of molecular resonance. Contrary to the state-to-state cross-sections, which give the rate coefficients (see, for instance, Wan et al. (2019)), the σ_λ^q cross-sections are complex. For $\lambda = 0$, real and imaginary parts of this cross-section correspond to the pressure broadening and shift cross-section, respectively. For $\lambda = 1$, the complex cross-section describes the collisional perturbation of the translational motion and is crucial for the proper description of the Dicke effect. The index q is the tensor rank of the spectral transition operator and equals 1 for electric dipole lines considered here.

We used the σ_0^1 and σ_1^1 cross-sections to calculate the six line-shape parameters relevant to collision-perturbed HD spectra, the collisional broadening, and the shift,

$$\gamma_0 - i\delta_0 = \frac{1}{2\pi c}\frac{1}{k_B T}\langle v_r\rangle \int_0^\infty x e^{-x} \sigma_0^1(x) \mathrm{d}x, \quad (1)$$

the speed dependences of collisional broadening and shift,

$$\gamma_2 - i\delta_2 = \frac{1}{2\pi c}\frac{1}{k_B T}\frac{\langle v_r\rangle \sqrt{M_a}}{2} e^{-y^2} \times \int_0^\infty \left(2\bar{x}\cosh(2\bar{x}y) - \left(\frac{1}{y} + 2y\right)\sinh(2\bar{x}y)\right) \bar{x}^2 e^{-\bar{x}^2} \sigma_0^1(\bar{x}\bar{v}_p) d\bar{x}, \quad (2)$$

and the real and imaginary parts of the complex Dicke parameter,

$$\tilde{\nu}_{opt}^r - i\tilde{\nu}_{opt}^i = \frac{1}{2\pi c}\frac{\langle v_r\rangle M_a}{k_B T} \int_0^\infty x e^{-x}\left[\frac{2}{3} x \sigma_1^1(x k_B T) - \sigma_0^1(x k_B T)\right] dx, \quad (3)$$

where v_r is the relative (absorber to perturber) speed of the colliding molecules, $\langle v_r\rangle$ is its mean value at temperature T, $\bar{v}_p$ is the most probable speed of the perturbed distribution, $M_a = \frac{m_a}{m_a + m_p}$, $x = \frac{E_{\mathrm{kin}}}{k_B T}$, $\bar{x} = \frac{2 v_r}{\sqrt{\pi M_a}\langle v_r\rangle}$, $y = \sqrt{\frac{m_p}{m_a}}$ and m_a and m_p are the masses of the active and perturbing molecules, respectively (Wcisło et al. (2021)). We estimate the uncertainty of the calculated line-shape parameters in Appendix C. The six line-shape parameters define the modified Hartmann-Tran (mHT) profile (see Appendix D), which encapsulates the relevant beyond-Voigt effects. To make the outcome of this work consistent with the HITRAN database (Gordon et al. 2022), we provide temperature dependences of the calculated line-shape parameters within the double-power-law (DPL) format (Gamache & Vispoel 2018; Stolarczyk et al. 2020):

$$\begin{aligned}
\gamma_0(T) &= g_0(T_{\mathrm{ref}}/T)^n + g_0'(T_{\mathrm{ref}}/T)^{n'},\\
\delta_0(T) &= d_0(T_{\mathrm{ref}}/T)^m + d_0'(T_{\mathrm{ref}}/T)^{m'},\\
\gamma_2(T) &= g_2(T_{\mathrm{ref}}/T)^j + g_2'(T_{\mathrm{ref}}/T)^{j'},\\
\delta_2(T) &= d_2(T_{\mathrm{ref}}/T)^k + d_2'(T_{\mathrm{ref}}/T)^{k'},\\
\tilde{\nu}_{opt}^r(T) &= r(T_{\mathrm{ref}}/T)^p + r'(T_{\mathrm{ref}}/T)^{p'},\\
\tilde{\nu}_{opt}^i(T) &= i(T_{\mathrm{ref}}/T)^q + i'(T_{\mathrm{ref}}/T)^{q'},
\end{aligned} \quad (4)$$

where $T_{\mathrm{ref}} = 296$ K.

3. Results: Line-shape parameters for the R(0), R(1), and R(2) lines in HD perturbed by a mixture of H_2 and He

In Figure 1 we show the main result of this work: all six line-shape parameters for the R(0), R(1), and R(2) 0-0 lines in H_2-perturbed HD calculated as a function of temperature. Figure 1 covers the temperature range relevant for the giant planets, 50 to 200 K (Lellouch et al. 2001; Feuchtgruber et al. 2013; Pierel et al. 2017; for our full temperature range, 20 to 1000 K, see the Supplementary Material). In Figure 1 we also recall the corresponding He-perturbed data calculated with the same methodology at the same accuracy level (Stankiewicz et al. (2021)). The difference between the two perturbers is not negligible, and for many cases the line-shape parameters differ by a factor of 2 or even more.

The data shown in Fig. 1 are given in Table 1 in a numerical form within the HITRAN DPL format (see Eq. (4)). The accuracy of our ab initio line-shape parameters is within 1% of the magnitude of each parameter (see Appendix C for details). The DPL approximation of the temperature dependences introduces additional errors. For $\gamma_0(T)$ and $\tilde{\nu}_{opt}^r(T)$, the DPL error is negligible, for $\delta_0(T)$ the DPL error is at the 1 % level, and for other line-shape parameters it can be even higher, but their impact on the final line profile is much smaller (see Appendix E for details). For applications that require the full accuracy of our ab initio line-shape parameters, we provide the line-shape parameter values explicitly on a dense temperature grid in the Supplementary Material.

The set of parameters in Table 1 contains all the information necessary to simulate the collision-perturbed shapes of the three HD lines at a high level of accuracy at any conditions relevant to the atmospheres of giant planets (pressure, temperature, and He/H_2 relative concentration). In Figure 2 we show an example of simulated spectra based on the data from Table 1. It should be emphasized that at the conditions relevant to giant planets, the shapes of the HD lines may considerably deviate from the simple Voigt profile. In Figure 2 (a) we show the difference between the Voigt profile and a more physical profile, which includes the relevant beyond-Voigt effects such as Dicke narrowing and the dependence on the speed of the broadening and shift (the mHT profile; see Appendix D). For the moderate pressures, the error introduced by the Voigt-profile approximation can reach almost 70%. The orange, yellow, red, and black lines in Fig. 2 (a) are the temperature-pressure profiles for Jupiter (Seiff et al. 1998), Saturn (Lindal et al. 1985), Uranus (Lindal et al. 1987), and Neptune (Lindal et al. 1990), respectively. We illustrate this with

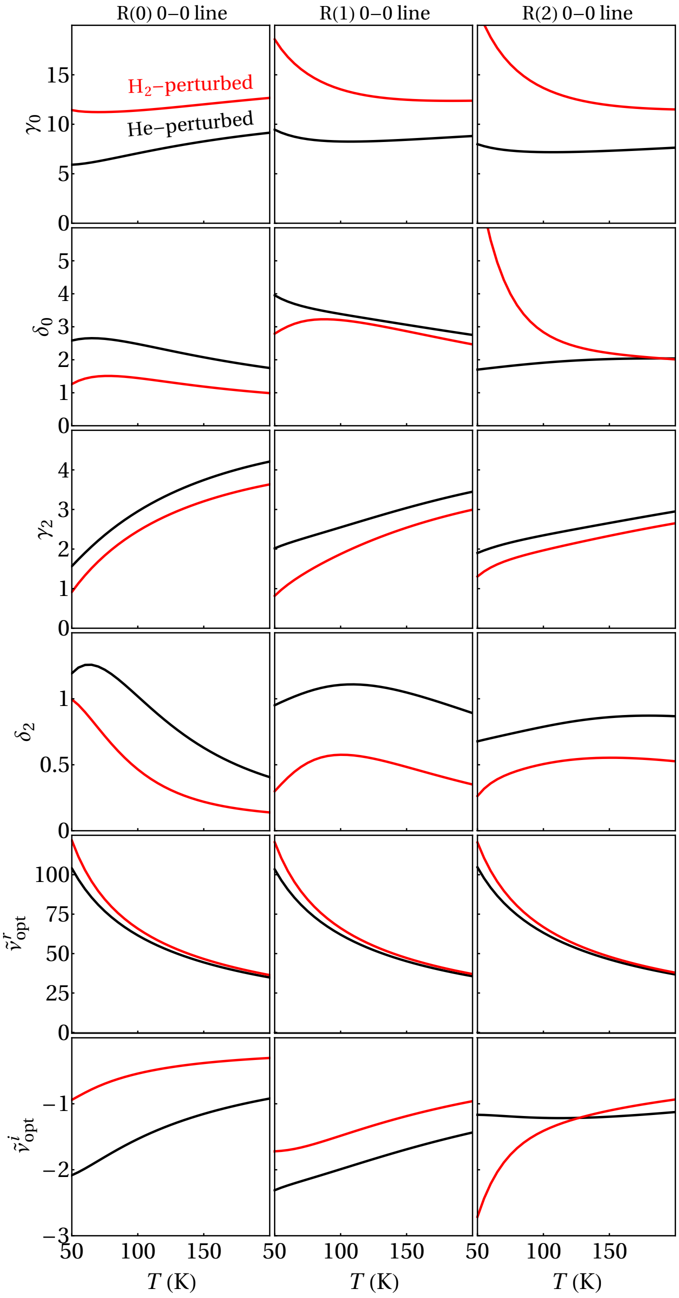

Fig. 1. Ab initio temperature dependences of the collisional line-shape parameters (in units of 10^{-3}cm^{-1}atm^{-1}) of the first three electric dipole lines of HD perturbed by H_2 (red curves) and He (black curves).

spectra simulations for the case of Neptune's atmosphere (panels (b)-(d) corresponds to the black dots in Fig. 2 (a)). Panels (b)-(d) illustrate three different regimes. Panel (b) is the low-pressure regime with a small collisional contribution in which the line shape collapses to Gaussian, and hence the beyond-Voigt effects are small. Panel (d) is the opposite: the shape of a resonance is dominated by the collisional effects, but the simple Lorentzian broadening dominates over other collisional effects and again the beyond-Voigt effects are small. Panel (c) illustrates the nontrivial situation in which the shape of resonance is dominated by the beyond-Voigt effects (see the green horizontal ridges in Fig. 2 (a)). The discrepancies between the beyond-Voigt line-shape model and the Voigt profile are also clearly seen as a difference between the blue lines and blue shadows in panel (c).

In the context of the giant planet studies, it should be noted that the beyond-Voigt regions marked in panel (a) (the green horizontal ridges) coincide well with the maxima of the monochromatic contribution functions for these three HD lines (see Fig. 1 in Feuchtgruber et al. 2013 for the case of the atmospheres of Neptune and Uranus).

Panels (b)-(d) of Fig. 2 also illustrate the influence of atmosphere composition on the collision-induced shapes of the HD lines for the example of Neptune atmosphere. The differences between the He- and H_2-perturbers are negligible in the low-pressure regime (panel (b)) since at these conditions the line shape is mainly determined by thermal Doppler broadening. In moderate- and high-pressure ranges (panels (c) and (d)), the profiles differ at the peak by a factor of 2. Hence, including both perturbing species is important for spectra analyses of the atmospheres of giant planets, especially for the R(0) line, whose contribution function dominates at moderate and high pressures (Feuchtgruber et al. (2013)).

The data reported in this article (see Table 1) account for three factors that are necessary for reaching sub-percent-level accuracy: (1) separate ab initio data for both perturbers (which allows one to simulate perturbation by any H_2–He mixture), (2) accurate representation of temperature dependences, and (3) parametrization of the beyond-Voigt line-shape effects. In general, simulating the beyond-Voigt line-shape profiles is a complex task (see Appendix D). In this work, we used HAPI (Kochanov et al. 2016) to generate the beyond-Voigt spectra shown in Fig. 2 (based on the DPL parameters from Table 1):

```
from hapi import *
db_begin (’hitran_data’)
nu,coef = absorptionCoefficient_mHT(
    SourceTables=’HD’,
    Diluent={’He’:0.2,’H2’:0.8},
    WavenumberRange=[xmin,xmax],
    WavenumberStep=step,
    Environment={’p’:press,’T’:temp},
    HITRAN_units=True)
```

The combination of the data reported in Table 1 and the Python-based HAPI constitutes a powerful tool that allows one to efficiently generate accurate HD spectra (based on advanced beyond-Voigt model, the mHT profile) for arbitrary temperature, pressure, and mixture composition.

At low temperatures, relevant for studies of giant planet atmospheres and the chemistry and dynamics of the interstellar medium and protoplanetary disks, the spin isomer (*para*/*ortho*) concentration ratio of H_2 at thermal equilibrium (eq-H_2) deviates from 1:3 (the ratio of so-called normal H_2, n-H_2). Moreover, various processes, such as diffusion between atmospheric layers in gas giants, might result in the sub-equilibrium distribution of H_2. These nontrivial *para*/*ortho* distributions play a key role in atmospheric models that involve collision-induced absorption (Karman et al. (2019)) and spectral features originating from hydrogen dimers (Fletcher et al. (2018)), as well as in isotope chemistry of the interstellar medium, where *para*/*ortho* ratio controls the deuterium fractionation process (Flower et al. 2006; Nomura et al. 2022). In Figure 3, we show the influence of the spin isomer concentration on the line-shape parameters. Spin isomer concentration has a large impact at low temperatures. All the line-shape parameters reported in this work are calculated for the thermal equilibrium spin isomer concentration.

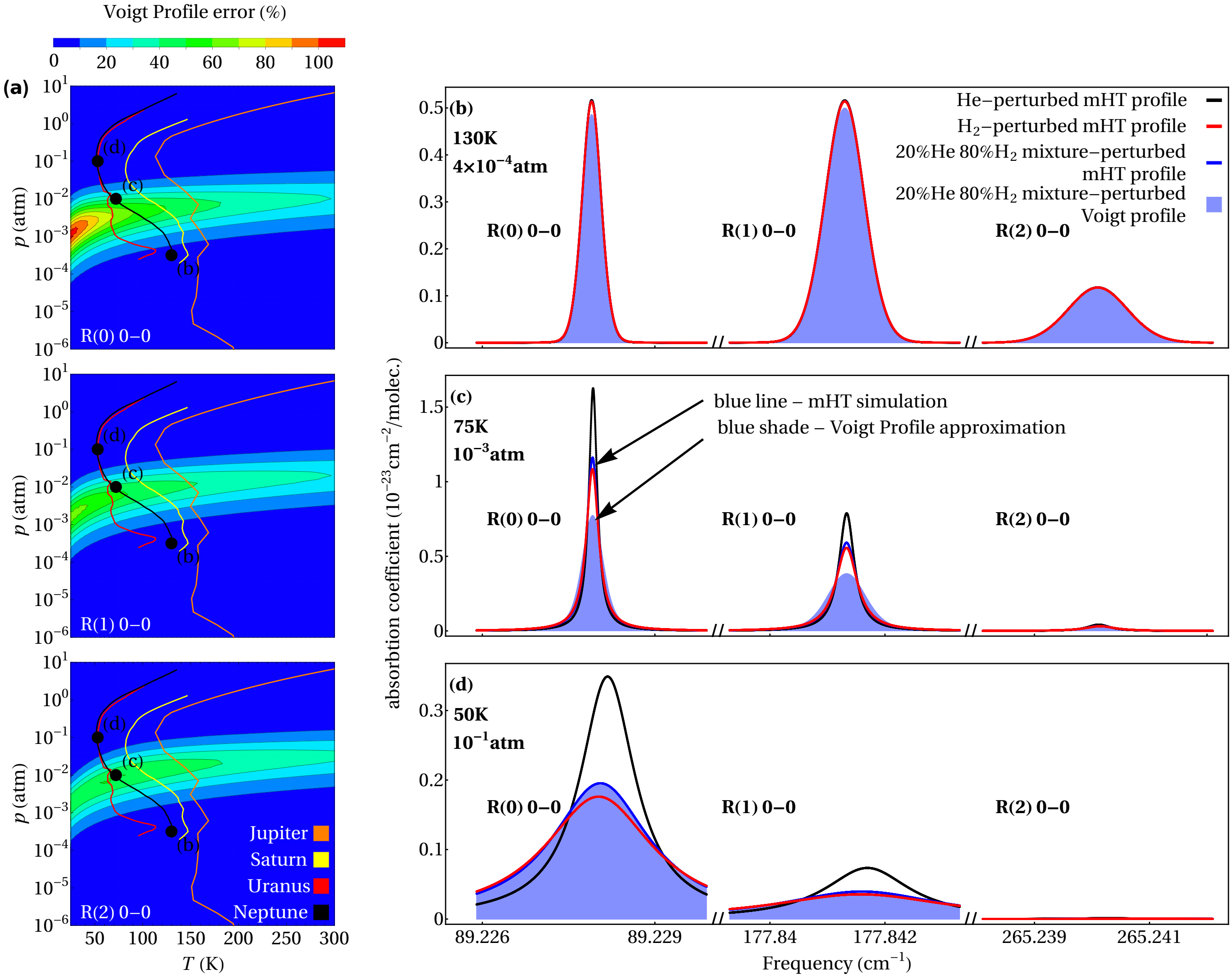

Fig. 2. Impact of the beyond-Voigt effects and bath mixture composition on collision-perturbed spectra of HD at conditions relevant for giant planet atmospheres. Panel (a): Relative error of the Voigt-profile approximation as a function of pressure and temperature, shown as the relative difference between the Voigt and mHT profiles at profile maximum. The panels show, from top to bottom, the R(0), R(1), and R(2) lines. Panels (b), (c), and (d): Simulations of the HD spectra (blue lines) at conditions relevant for the Neptune atmosphere (the perturbing bath is 80% H_2 and 20% He). The spectra are generated with the mHT profile using HAPI based on the DPL temperature parametrization. As a reference, we show the same lines for the cases of pure H_2 and pure He perturbers (see the red and black lines, respectively). The blue shadows show the same simulations as the blue lines but generated with the simple Voigt profile. Panels (b), (c), and (d) correspond to points (b), (c), and (d) shown in the temperature-pressure maps in panel (a) (the three selected points lie on the Neptune temperature-pressure line). The three cases illustrate three different line-shape regimes. The first one, (b), is the low-pressure case in which the lines are broadened mainly by the Doppler effect, and the pressure-induced collisional effects do not dominate the line shapes. The intermediate-pressure case, panel (c), illustrates the extreme non-Voigt regime (the differences between the blue curves and blue shadows reach almost a factor of 2; see also the green ridge in the maps in the bottom panel). The third case, panel (d), illustrates the high-pressure regime at which the HD lines are well described by a simple Voigt profile (the blue shadows almost overlap with the blue lines), but setting a proper composition of the perturber gas components plays an important role.

Table 1. DPL parameterization of the temperature dependences of the line-shape parameters of HD perturbed by He and H_2. Coefficients 1 and 2 are in 10^{-3}cm^{-1}atm^{-1}. Exponents 1 and 2 are dimensionless.

		He-perturbed HD		
		R(0) 0-0 line		
$\gamma_0(T)$	$g_0= 218.905$	$g'_0= -209.398$	$n= 0.0929083$	$n'= 0.105086$
$\delta_0(T)$	$d_0= 76.1358$	$d'_0= -74.6225$	$m= -0.102987$	$m'= -0.116673$
$\gamma_2(T)$	$g_2= 210.682$	$g'_2= -206.11$	$j= -0.862904$	$j'= -0.876244$
$\delta_2(T)$	$d_2= 7.77569$	$d'_2= -7.45369$	$k= 1.43509$	$k'= 1.45106$
$\tilde{\nu}^r_{opt}(T)$	$r= 157.867$	$r'= -132.815$	$p= 0.569778$	$p'= 0.512484$
$\tilde{\nu}^i_{opt}(T)$	$i= -0.0148171$	$i'= -0.732168$	$q= 0.589866$	$q'= 0.589866$
		R(1) 0-0 line		
$\gamma_0(T)$	$g_0= 8.98598$	$g'_0= 0.07062$	$n= -0.116463$	$n'= 1.83834$
$\delta_0(T)$	$d_0= 3.27647$	$d'_0= -0.997538$	$m= 0.171067$	$m'= -0.548127$
$\gamma_2(T)$	$g_2= 5.47783$	$g'_2= -1.63047$	$j= -0.540645$	$j'= -1.19601$
$\delta_2(T)$	$d_2= 64.7968$	$d'_2= -64.0672$	$k= -0.314427$	$k'= -0.325103$
$\tilde{\nu}^r_{opt}(T)$	$r= 39.7564$	$r'= -13.9988$	$p= 0.652375$	$p'= 0.276761$
$\tilde{\nu}^i_{opt}(T)$	$i= -0.0600157$	$i'= -1.04666$	$q= 0.478987$	$q'= 0.478987$
		R(2) 0-0 line		
$\gamma_0(T)$	$g_0= 7.91606$	$g'_0= 0.106818$	$n= -0.158512$	$n'= 1.59926$
$\delta_0(T)$	$d_0= 60.8755$	$d'_0= -59.1362$	$m= -0.560989$	$m'= 0.57118$
$\gamma_2(T)$	$g_2= 3.44668$	$g'_2= -0.0918827$	$j= -0.351514$	$j'= -2.42064$
$\delta_2(T)$	$d_2= 48.9743$	$d'_2= -48.2166$	$k= -0.522538$	$k'= -0.53522$
$\tilde{\nu}^r_{opt}(T)$	$r= 33.4337$	$r'= -6.77194$	$p= 0.682741$	$p'= 0.0477307$
$\tilde{\nu}^i_{opt}(T)$	$i= -0.160883$	$i'= -0.705905$	$q= 0.278356$	$q'= 0.278356$
		H_2-perturbed HD		
		R(0) 0-0 line		
$\gamma_0(T)$	$g_0= 13.1538$	$g'_0= -0.0209275$	$n= -0.102409$	$n'= -4.47666$
$\delta_0(T)$	$d_0= 21.8124$	$d'_0= -21.0255$	$m= 1.06916$	$m'= 1.08444$
$\gamma_2(T)$	$g_2= 215.242$	$g'_2= -211.197$	$j= -1.0114$	$j'= -1.02533$
$\delta_2(T)$	$d_2= 17.5611$	$d'_2= -17.4505$	$k= 0.41528$	$k'= 0.405624$
$\tilde{\nu}^r_{opt}(T)$	$r= 25.0013$	$r'= 0.0005783$	$p= 0.889907$	$p'= 4.16595$
$\tilde{\nu}^i_{opt}(T)$	$i= -0.0049349$	$i'= -0.257607$	$q= 0.64352$	$q'= 0.64352$
		R(1) 0-0 line		
$\gamma_0(T)$	$g_0= 11.5582$	$g'_0= 0.165258$	$n= 0.0781601$	$n'= 1.89474$
$\delta_0(T)$	$d_0= 133.353$	$d'_0= -131.231$	$m= -0.244838$	$m'= -0.257492$
$\gamma_2(T)$	$g_2= 131.359$	$g'_2= -128.602$	$j= 0.484966$	$j'= 0.495567$
$\delta_2(T)$	$d_2= 35.3179$	$d'_2= -35.0081$	$k= -0.330198$	$k'= -0.33988$
$\tilde{\nu}^r_{opt}(T)$	$r= 12.373$	$r'= 12.3606$	$p= 1.02771$	$p'= 0.755534$
$\tilde{\nu}^i_{opt}(T)$	$i= -0.307423$	$i'= -0.307142$	$q= 0.656905$	$q'= 0.656905$
		R(2) 0-0 line		
$\gamma_0(T)$	$g_0= 5.05367$	$g'_0= 5.04862$	$n= 0.767269$	$n'= -0.528791$
$\delta_0(T)$	$d_0= 1.10007$	$d'_0= 0.346535$	$m= 0.0896926$	$m'= 1.57482$
$\gamma_2(T)$	$g_2= 4.9771$	$g'_2= -1.86783$	$j= -0.69627$	$j'= -1.38558$
$\delta_2(T)$	$d_2= 63.3239$	$d'_2= -62.865$	$k= -0.627633$	$k'= -0.634526$
$\tilde{\nu}^r_{opt}(T)$	$r= 26.3022$	$r'= 0.0004301$	$p= 0.856557$	$p'= 4.29539$
$\tilde{\nu}^i_{opt}(T)$	$i= -0.208711$	$i'= -0.208511$	$q= 1.07071$	$q'= 1.07071$

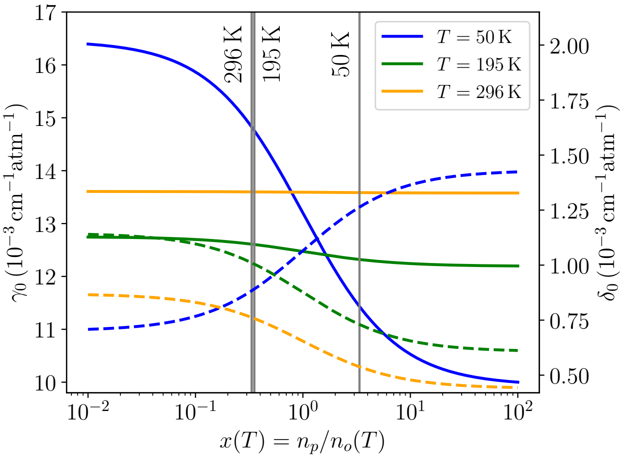

Fig. 3. Dependence of pressure broadening, γ_0 (solid lines), and shift, δ_0 (dashed lines), on the spin isomer concentration ratio ($x = n_p/n_o$) for the H_2-perturbed R(0) line in HD at different temperatures. The vertical gray lines correspond to the value of x for normal H_2, $x = 1/3$, and $x_{eq}(T)$, as determined by the Boltzmann distribution at $T = 50$, 195, and 296 K.

4. Experimental validation

In Figure 4 we show a comparison between our ab initio calculations (black lines) and the experimental data available in the literature. Fourier-transformed scans from the Michelson interferometer were used to obtain the high-pressure spectra reported in the works of Ulivi et al. (1989) and Lu et al. (1993); the spectra were collected in a temperature range from 77 to 296 K. Recently, the same lines were measured at low pressures (< 1 bar) with the Fourier transform spectrometer coupled to the Soleil-synchrotron far-infrared source (Sung et al. (2022)) in a temperature range from 98 to 296 K (see the olive lines in Fig. 4). The discrepancy between these experimental data is by far too large to test our theoretical results at the one percent level.

To validate our ab initio calculations at the estimated accuracy level, we performed accurate measurements using a frequency-stabilized cavity ring-down spectrometer linked to an optical frequency comb, referenced to a primary frequency standard (Cygan et al. (2016, 2019); Zaborowski et al. (2020)). Our 73.5-cm-long ultrahigh finesse ($\mathcal{F} = 637\ 000$) optical cavity operates in the frequency-agile rapid scanning spectroscopy mode (Truong et al. 2013; Cygan et al. 2016, 2019; see Zaborowski et al. 2020 for details regarding the experimental setup). Since our spectrometer operates at 1.6 μm, we chose the S(2) 2-0 line in the H_2-perturbed D_2 (we repeated all the ab initio calculations for this case). From the perspective of theoretical methodology, the H_2-perturbed D_2 and H_2-perturbed HD are equivalent and either can be used for validating the theoretical methodology (for both cases two distinguishable diatomic molecules are considered and the PES is the same except for the almost negligible DBOC term; see Appendix A). We used a sample of 2% D_2 and 98% of H_2 mixture and collected the spectra at four pressures (0.5, 1, 1.5, and 2 atm) and two temperatures (296 and 330 K; see the black dots in Fig. 5). The corresponding theoretical spectra are the red curves. The methodology for simulating the collision-perturbed shapes of molecular lines (based on the line-shape parameters calculated from Eqs. (1)-(3)) is described in our previous works (Wcisło et al. 2018; Słowiński et al. 2020; Słowiński et al. 2022). The two sets of residuals depicted in Fig. 5 show comparisons with two line-shape models, the speed-dependent billiard-ball (SDBB) profile and the mHT profile. The SDBB profile (Shapiro et al. 2002; Ciuryło et al. 2002) is the state-of-the-art approach that gives the most realistic description of the underlying collisional processes. As expected it gives the best agreement with experimental spectra (the mean residuals are 0.65%; see Fig. 5), but it is computationally very expensive (Wcisło et al. (2013)). The mHT profile is slightly less accurate (the mean residuals are 1.23%) but it is highly efficient from a computational perspective and, hence, well suited for practical spectroscopic applications. In conclusion, the ab initio line-shape parameters reported in this work (Fig. 1 and Table 1) lead to profiles that are in excellent agreement with accurate experimental spectra, and the theory-experiment comparison is limited by a choice of a line-shape model used to simulate the experimental spectra.

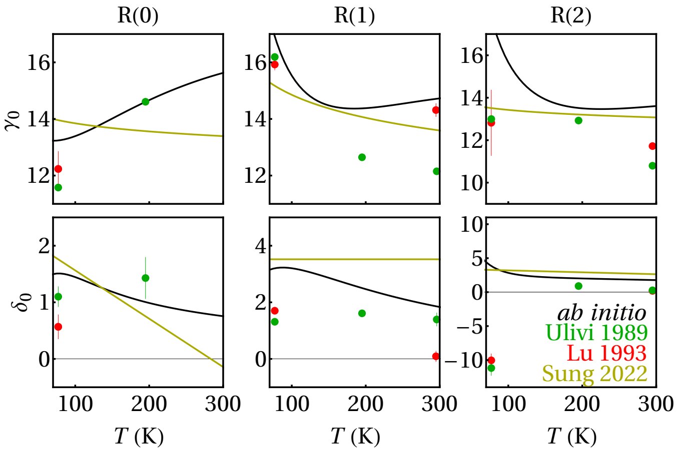

Fig. 4. Comparison of the experimental and theoretical values of the pressure broadening and shift parameters, γ_0 and δ_0 (in units of $10^{-3}\mathrm{cm}^{-1}\mathrm{atm}^{-1}$). Black curves correspond to the ab initio calculations performed in this work, while green and red points report the experimental measurements from Ulivi et al. (1989) and Lu et al. (1993), respectively. The olive curves are the single-power-law (for γ_0) and linear (for δ_0) temperature dependences retrieved from the measurements of Sung et al. (2022).

5. Conclusion

We have computed accurate collision-induced line-shape parameters for the three pure rotational HD lines (R(0), R(1), and R(2)) that are currently employed for the analysis of the giant planets' atmospheres. To this end, we investigated HD–H_2 collisions using coupled channel quantum scattering calculations on a new, highly accurate ab initio PES. Scattering S matrices determined from these calculations allowed us to obtain the collisional width and shift, as well as their speed dependences and the complex Dicke parameter of H_2-perturbed HD lines. By integrating data from our previous work on the HD-He system (Stankiewicz et al. 2020, 2021), we provide comprehensive results that cover a wide range of thermodynamic conditions, including temperature, pressure, and H_2–He concentration, relevant to the atmospheres of giant planets. We validated our theoretical methodology using cavity ring-down spectroscopy, demonstrating a sub-percent-level accuracy that surpasses the accuracy of previous

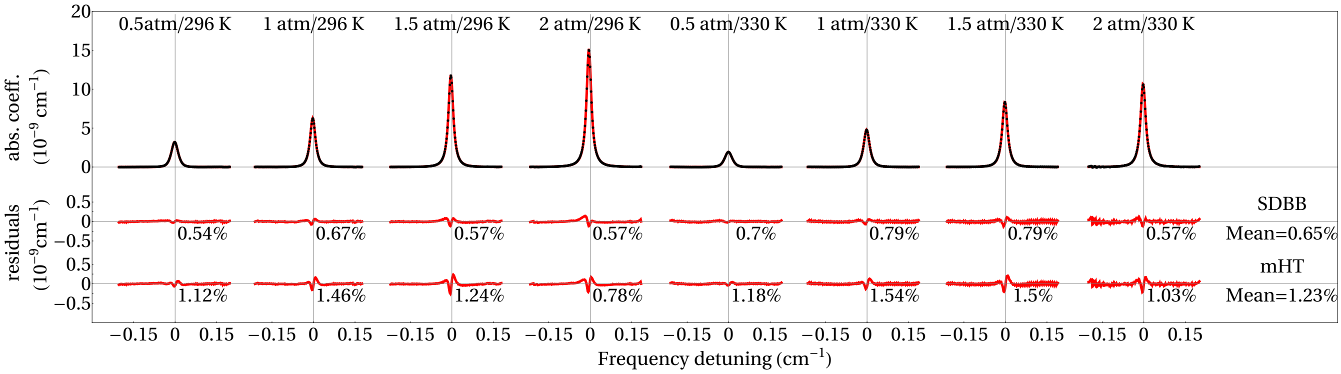

Fig. 5. Direct validation of the ab initio quantum-scattering calculations on the accurate experimental spectra of the S(2) 2-0 line of D_2 perturbed by collisions with H_2 molecules (see the main text for details). The black dots are the experimental spectra, and the red lines are the ab initio profiles. Below each profile, we show the absolute residuals of two models: the SDBB profile and the mHT profile. To quantify how well theory agrees with experiments, we report the relative (with respect to the profile peak value) root mean square errors (rRMSEs) of the experiment-theory differences calculated within the ±FWHM range around the line center (see the percentages below the residuals). The mean rRMSEs are also summarized for each of the models (see the numbers on the right side of the figure).

theoretical and experimental studies of line-shape parameters in HD.

All the reported line-shape parameters and their temperature dependences are consistent with the HITRAN database format. Utilizing HAPI, we demonstrated how our results can be applied to simulate HD spectra under various conditions pertinent to giant planets in the Solar System.

Until now, the analysis of observed collision-perturbed spectra in astrophysical studies has predominantly relied on the simple Voigt profile. We have introduced a methodology and provided a comprehensive dataset that enables the simulation of beyond-Voigt shapes for HD in H_2–He atmospheres. Our work demonstrates that accounting for the speed dependence of collisional width and shift, along with the complex Dicke parameter, is crucial. These factors can alter the effective width and height of HD lines by up to a factor of 2. To quantitatively assess the impact of these results on the D/H ratio on giant planets, radiative transfer modeling is necessary. Given that the beyond-Voigt effects result in a narrower line width (Fig. 2 (c)), the previously inferred HD abundance from astrophysical observations may be underestimated.

Acknowledgements. H.J. and N.S. were supported by the National Science Centre in Poland through Project No. 2019/35/B/ST2/01118. H.J. was supported by the Foundation for Polish Science (FNP). K.S contribution is supported by budgetary funds within the Minister of Education and Science program "Perły Nauki", Project No. PN/01/0196/2022. D.L. was supported by the National Science Centre in Poland through Project No. 2020/39/B/ST2/00719. S.W. was supported by the National Science Centre in Poland through Project No. 2021/42/E/ST2/00152. P. J. was supported by the National Science Centre in Poland through Project No. 2017/25/B/ST4/01300. K.P. was supported by the U.S. National Science Foundation award CHE-1955328. K.Sz. was supported by the US NSF award CHE-2313826. IEG's contribution was supported through NASA grant 80NSSC24K0080. P.W. was supported by the National Science Centre in Poland through Project No. 2022/46/E/ST2/00282. For the purpose of Open Access, the author has applied a CC-BY public copyright licence to any Author Accepted Manuscript (AAM) version arising from this submission. We gratefully acknowledge Polish high-performance computing infrastructure PLGrid (HPC Centers: ACK Cyfronet AGH, CI TASK) for providing computer facilities and support within the computational grant, Grant No. PLG/2023/016409. Calculations have been carried out using resources provided by the Wroclaw Centre for Networking and Supercomputing (http://wcss.pl), Grant No. 546. The research is a part of the program of the National Laboratory FAMO in Toruń, Poland.

References

Altwegg, K., Balsiger, H., Bar-Nun, A., et al. 2015, Science, 347, 1261952
Araguás-Araguás, L., Froehlich, K., & Rozanski, K. 1998, J. Geophys. Res. Atmos, 103, 28721
Babin, V., Leforestier, C., & Paesani, F. 2013, J. Chem. Theory Comput., 9, 5395
Baines, K. H., Mickelson, M. E., Larson, L. E., & Ferguson, D. W. 1995, Icarus, 114, 328
Bakr, B. W., Smith, D. G. A., & Patkowski, K. 2013, J. Chem. Phys., 139, 144305
Blake, J. S. D., Fletcher, L. N., Greathouse, T. K., et al. 2021, A&A, 653, A66
Bockelée-Morvan, D., Gautier, D., Lis, D., et al. 1998, Icarus, 133, 147
Braams, B. J. & Bowman, J. M. 2009, Intern. Rev. Phys. Chem., 28, 577
Ciuryło, R., Shapiro, D. A., Drummond, J. R., & May, A. D. 2002, Phys. Rev. A, 65, 012502
Crovisier, J., Bockelée-Morvan, D., Colom, P., et al. 2004, A& A, 418, 1141
Cygan, A., Wcisło, P., Wójtewicz, S., et al. 2019, Opt. Express, 27, 21810
Cygan, A., Wójtewicz, S., Kowzan, G., et al. 2016, J. Chem. Phys., 144, 214202
Donahue, T. M., Hoffman, J. H., Hodges, R. R., & Watson, A. J. 1982, Science, 216, 630
Donahue, T. M. & Pollack, J. B. 1983, in Venus (University of Arizona Press), 1003–1036
Drake, M. J. & Righter, K. 2002, Nature, 416, 39
Dubernet, M.-L. & Tuckey, P. 1999, Chem. Phys. Lett., 300, 275
Eberhardt, P., Reber, M., Krankowsky, D., & Hodges, R. 1995, A&A, 302, 301
Fernández, B., Koch, H., & Makarewicz, J. 1999, J. Chem. Phys., 110, 8525
Feuchtgruber, H., Lellouch, E., Orton, G., et al. 2013, A&A, 551, A126
Fletcher, L., Orton, G., Teanby, N., Irwin, P., & Bjoraker, G. 2009, Icarus, 199, 351
Fletcher, L. N., Gustafsson, M., & Orton, G. S. 2018, ApJS, 235, 24
Flower, D., Pineau des Forêts, G., & Walmsley, C. 2006, A & A, 449, 621
Gamache, R. R. & Vispoel, B. 2018, J. Quant. Spectrosc. Radiat. Transf., 217, 440
Gancewski, M., Jóźwiak, H., Quintas-Sánchez, E., et al. 2021, J. Chem. Phys., 155, 124307
Gauss, J., A.Tajti, Kállay, M., & Szalay, J. F. S. P. G. 2006, J. Chem. Phys., 125, 144111
Gautier, D. & Hersant, F. 2005, SSR, 116, 25
Gordon, I., Rothman, L., Hargreaves, R., et al. 2022, J. Quant. Spectrosc. Radiat. Transf., 277, 107949
Green, S., Blackmore, R., & Monchick, L. 1989, J. Chem. Phys., 91, 52
Guillot, T. 1999, P&SS, 47, 1183
Halkier, A., Klopper, W., Helgaker, T., Jørgensen, P., & Taylor, P. R. 1999, J. Chem. Phys., 111, 9157
Handy, N. C., Yamaguchi, Y., & Schaefer III, H. F. 1986, J. Chem. Phys., 84, 4481
Hartogh, P., Lis, D. C., Bockelée-Morvan, D., et al. 2011, Nature, 478, 218
Hersant, F., Gautier, D., & Hure, J.-M. 2001, ApJ, 554, 391
Horner, J., Mousis, O., & Hersant, F. 2006, Earth Moon Planets, 100, 43
Jóźwiak, H. 2024, the SCATTERING code adjusted for diatom-atom calculations

Jóźwiak, H., Thibault, F., Cybulski, H., & Wcisło, P. 2021, J. Chem. Phys., 154, 054314

Jóźwiak, H., Thibault, F., Stolarczyk, N., & Wcisło, P. 2018, J. Quant. Spectrosc. Radiat. Transf., 219, 313

Jóźwiak, H., Thibault, F., Viel, A., Wcisło, P., & Lique, F. 2024, accepted for publication in A &A

Karman, T., Gordon, I. E., van der Avoird, A., et al. 2019, Icarus, 328, 160

Kendall, R. A., Dunning, Jr., T. H., & Harrison, R. J. 1992, J. Chem Phys., 96, 6796

Kochanov, R., Gordon, I., Rothman, L., et al. 2016, J. Quant. Spectrosc. Radiat. Transf., 177, 15

Konefał, M., Słowiński, M., Zaborowski, M., et al. 2020, J. Quant. Spectrosc. Radiat. Transf., 242, 106784

Krasnopolsky, V., Belyaev, D., Gordon, I., Li, G., & Rothman, L. 2013, Icarus, 224, 57

Lellouch, E., Bézard, B., Fouchet, T., et al. 2001, A &A, 370, 610

Lindal, G. F., Lyons, J. R., Sweetnam, D. N., et al. 1987, J. Geophys. Res. Space Phys., 92, 14987–15001

Lindal, G. F., Lyons, J. R., Sweetnam, D. N., et al. 1990, Geophysical Research Letters, 17, 1733–1736

Lindal, G. F., Sweetnam, D. N., & Eshleman, V. R. 1985, Astron. J., 90, 1136

Lu, Z., Tabisz, G. C., & Ulivi, L. 1993, Phys. Rev. A, 47, 1159

Mahaffy, P. R., Donahue, T. M., Atreya, S. K., Owen, T. C., & Niemann, H. B. 1998, SSR, 251

Meier, R., Owen, T. C., Matthews, H. E., et al. 1998, Science, 279, 842

Monchick, L. & Hunter, L. W. 1986, J. Chem. Phys., 85, 713

Niemann, H., Atreya, S., Bauer, S., et al. 2005, Nature, 438, 779

Nomura, H., Furuya, K., Cordiner, M., et al. 2022, arXiv preprint arXiv:2203.10863

Owen, T. & Encrenaz, T. 2006, P& SS, 54, 1188

Patkowski, K., Cencek, W., Jankowski, P., et al. 2008, J. Chem. Phys., 129, 094304

Pettini, M., Zych, B. J., Murphy, M. T., Lewis, A., & Steidel, C. C. 2008, MNRAS, 391, 1499

Pierel, J. D. R., Nixon, C. A., Lellouch, E., et al. 2017, ApJ, 154, 178

Schaefer, J. & Monchick, L. 1992, A&A, 265, 859

Schwenke, D. W. 1988, J. Chem. Phys., 89, 2076

Seiff, A., Kirk, D. B., Knight, T. C. D., et al. 1998, J. Geophys. Res. Planets, 103, 22857–22889

Shafer, R. & Gordon, R. G. 1973, J. Chem. Phys., 58, 5422

Shapiro, D. A., Ciuryło, R., Drummond, J. R., & May, A. D. 2002, Phys. Rev. A, 65, 012501

Słowiński, M., Thibault, F., Tan, Y., et al. 2020, Phys. Rev. A, 101, 052705

Słowiński, M., Jóźwiak, H., Gancewski, M., et al. 2022, J. Quant. Spectrosc. Radiat. Transf., 277, 107951

Smith, W. H. 1989, Icarus, 81, 429

Stankiewicz, K., Jóźwiak, H., Gancewski, M., et al. 2020, J. Quant. Spectrosc. Radiat. Transf., 254, 107194

Stankiewicz, K., Stolarczyk, N., Jóźwiak, H., Thibault, F., & Wcisło, P. 2021, J. Quant. Spectrosc. Radiat. Transf., 276, 107911

Stolarczyk, N., Thibault, F., Cybulski, H., et al. 2020, J Quant Spectrosc Radiat Transfr, 240, 106676

Sung, K., Wishnow, E. H., Drouin, B. J., et al. 2022, J. Quant. Spectrosc. Radiat. Transf., 108412

Thibault, F., Patkowski, K., Żuchowski, P. S., et al. 2017, J. Quant. Spectrosc. Radiat. Transf., 202, 308

Thibault, F., Wcisło, P., & Ciuryło, R. 2016, EPJD, 70

Truong, G.-W., Douglass, K. O., Maxwell, S. E., et al. 2013, Nat. Photonics, 7, 532

Ulivi, L., Lu, Z., & Tabisz, G. C. 1989, Phys. Rev. A, 40, 642

Valeev, E. F. & Sherrill, C. D. 2003, J. Chem. Phys., 118, 3921

Wan, Y., Balakrishnan, N., Yang, B. H., Forrey, R. C., & Stancil, P. C. 2019, MNRAS, 488, 381

Wcisło, P., Cygan, A., Lisak, D., & Ciuryło, R. 2013, Phys. Rev. A, 88, 12517

Wcisło, P., Gordon, I., Tran, H., et al. 2016, J. Quant. Spectrosc. Radiat. Transf., 177, 75

Wcisło, P., Thibault, F., Stolarczyk, N., et al. 2021, J. Quant. Spectrosc. Radiat. Transf., 260, 107477

Wcisło, P., Thibault, F., Zaborowski, M., et al. 2018, J. Quant. Spectrosc. Radiat. Transf., 213, 41

Zaborowski, M., Słowiński, M., Stankiewicz, K., et al. 2020, Opt. Lett., 45, 1603

Zadrożny, A., Jóźwiak, H., Quintas-Sánchez, E., Dawes, R., & Wcisło, P. 2022, J. Chem. Phys., 157, 174310

Zuo, J., Croft, J. F. E., Yao, Q., Balakrishnan, N., & Guo, H. 2021, J. Chem. Theory Comput., 17, 6747

Appendix A: Details of the PES calculations

The 6D PES for the H_2-H_2 system was calculated at the following level of theory;

$$E_{\rm int} = E^{\rm HF}_{\rm int}[5] + \delta E^{\rm CCSD(T)}_{\rm int}[Q5] + \delta E^{\rm T(Q)}_{\rm int}[Q] + \delta E^{\rm FCI}_{\rm int}[T] + \delta E^{\rm DBOC}_{\rm int}[T]. \tag{A.1}$$

In all cases, the aug-cc-pVXZ basis sets (Kendall et al. 1992) were employed with the cardinal number X taking values 2 (D), 3 (T), 4 (Q), and 5. The consecutive terms are defined in the following way: $E^{\rm HF}_{\rm int}[5]$ is the interaction energy calculated at the HF level using the aug-cc-pV5Z basis set, $\delta E^{\rm CCSD(T)}_{\rm int}[Q5]$ is the correlation contribution to the interaction energy calculated using the coupled-cluster method with up to perturbative triple excitations, CCSD(T), with the results extrapolated to complete basis set limits using the $1/X^3$ formula (Halkier et al. 1999) from the calculations in the aug-cc-pVQZ and aug-cc-pV5Z basis sets. The next contribution, $\delta E^{\rm T(Q)}_{\rm int}[Q] = E^{\rm CCSDT(Q)}_{\rm int}[Q] - E^{\rm CCSD(T)}_{\rm int}[Q]$, accounts for the electron correlation effects beyond CCSD(T) included in the CC method with up to perturbative quadruple excitations, CCSDT(Q), computed with the aug-cc-pVQZ basis set, whereas $\delta E^{\rm FCI}_{\rm int}[T] = E^{\rm FCI}_{\rm int}[T] - E^{\rm CCSDT(Q)}_{\rm int}[T]$ describes the electron correlation effects beyond CCSDT(Q), calculated with the aug-cc-pVTZ basis set. The DBOC (Handy et al. 1986), $\delta E^{\rm DBOC}_{\rm int}[T]$, was calculated with the masses of ^{1}H with the CCSD densities (Valeev & Sherrill 2003; Gauss et al. 2006) obtained with the aug-cc-pVTZ basis set. The $\delta E^{\rm DBOC}_{\rm int}$ term is the only one that depends on masses. However, it is small compared to other terms and would be even smaller if calculated for HD–H_2 instead of H_2–H_2. Thus, the resulting surface can be applied to the former system with full confidence.

The interaction energies were fitted by an analytic function that consisted of short- and long-range parts, with a smooth switching at R values between 9 and 10 a_0, using the switching function from Babin et al. (2013). The short-range part was taken in the form of a sum of products of exponentials $e^{-\alpha r_{ab}}$, where r_{ab} are atom-atom distances (Fernández et al. 1999; Braams & Bowman 2009). In contrast to most published work that uses the same α for all terms, we used four different optimized values. The form of the long-range part was taken from Patkowski et al. (2008), but the parameters $C^{l_1 l_2 l}_n$ were multiplied by linear combinations of symmetry-invariant polynomials of r_1, r_2, and of magnitudes of their differences. The linear coefficients are determined from the fit to the ab initio energies obtained at the same level of theory as for the short-range part. The PES is expected to be valid for $r_i \in [0.85, 2.25]\, a_0$. Zuo et al. (2021) recently published a 6D PES for the H_2 dimer obtained from the complete active space self-consistent field calculations combined with the multi-reference configuration interaction calculations. According to Zuo et al. (2021), the potential is valid up to $r_i = 3.45\, a_0$, beyond the upper limit of our PES. However, in the region of validity of both PESs, our surface should be more accurate due to the higher level of theory used.

Appendix B: Quantum scattering calculation details

The dependence of the 6D PES on the three Jacobi angles was separated from the radial and intramolecular distances by the expansion of the PES over the bi-spherical harmonics, $I_{l_1 l_2 l}(\theta_1, \theta_2, \phi)$:

$$V(R, r_1, r_2, \theta_1, \theta_2, \phi) = \sum_{l_1, l_2, l} A_{l_1 l_2 l}(R, r_1, r_2) I_{l_1 l_2 l}(\theta_1, \theta_2, \phi), \tag{B.1}$$

where the bi-spherical harmonics are defined as

$$I_{l_1 l_2 l}(\theta_1, \theta_2, \phi = \phi_1 - \phi_2) = \sqrt{\frac{2l+1}{4\pi}} \sum_m (l_1\, m\, l_2 -m \,|\, l_1\, l_2\, l\, 0) Y_{l_1 m}(\theta_1, \phi_1) Y_{l_2 -m}(\theta_2, \phi_2). \tag{B.2}$$

If the i-th ($i = 1, 2$) molecule is homo-nuclear, the l_i index in the expansion in Eq. (B.1) takes only even values. The $A_{l_1 l_2 l}(R, r_1, r_2)$ expansion coefficients were obtained by integrating the product of the PES and the corresponding bi-spherical harmonic, over Jacobi angles (see, for instance, Eq. (3) in Zadrożny et al. (2022) and the discussion therein). We employed a 19-point Gauss-Legendre quadrature to integrate over θ_1 and θ_2 and a 19-point Simpson's rule for the integral over ϕ. The integration resulted in a tabular representation of the $A_{l_1 l_2 l}(R, r_1, r_2)$ expansion coefficients, calculated for R in the range of 2.5 to 200 a_0 with a step of 0.1 a_0, and for intramolecular distances ranging from 0.85 to 2.25 a_0 with a step of 0.1 a_0.

In this work we used terms up to the $I_{448}(\theta_1, \theta_2, \phi)$ bi-spherical harmonic, which corresponds to a total of 19 and 32 terms in the D_2-H_2 and HD-H_2 case, respectively. Such numbers of terms represent an intermediate complexity of the problem – the number of terms in the HD-H_2 case is larger by a factor of 4 in comparison to the HD-He case (Stankiewicz et al. (2020, 2021)), but significantly smaller in comparison to more anisotropic PESs, studied in our previous works (85 for O_2-N_2 (Gancewski et al. (2021)), and 205 for CO-N_2 and CO-O_2 (Jóźwiak et al. (2021); Zadrożny et al. (2022))). The error introduced by the truncation of the PES expansion is discussed in Appendix C.

The dependence of the expansion coefficients on r_1 and r_2 was reduced by averaging $A_{l_1 l_2 l}(R, r_1, r_2)$ over rovibrational wave functions of isolated molecules, $(\chi_{\eta_i}(r_i))$:

$$A_{l_1 l_2 l, \eta_1, \eta_1', \eta_2, \eta_2'}(R) = \int dr_2 \chi_{\eta_2}(r_2) \left(\int dr_1 \chi_{\eta_1}(r_1) A_{l_1 l_2 l}(R, r_1, r_2) \chi_{\eta_1'}(r_1) \right) \chi_{\eta_2'}(r_2), \tag{B.3}$$

where $\eta_i = (v_i, j_i)$ denotes the quantum numbers of a rovibrational state of the i-th molecule. The wave functions of H_2, HD, and D_2 were obtained by solving the nuclear Schrödinger equation for isolated molecules using the potential energy curve of Schwenke

(1988). We used the standard trapezoidal rule to perform the integration in Eq. (B.3), and we obtain $A_{l_1 l_2 l,\eta_1,\eta_1',\eta_2,\eta_2'}(R)$ coupling terms for R within the range 2.5 to 200 a_0, with a step size of 0.1 a_0.

The average in Eq. (B.3) provides a large number of possible coupling terms. In the HD-H_2 case, we considered pure rotational transitions (up to 1000 K); thus, we neglected the terms that couple excited vibrational states ($v'_{\mathrm{HD}} \neq v_{\mathrm{HD}}$, $v'_{\mathrm{H_2}} \neq v_{\mathrm{H_2}}$). In the D_2-H_2 case, we observe that the terms that couple different vibrational levels are three orders of magnitude smaller than terms diagonal in v. Since we performed quantum scattering calculations in the $v_{\mathrm{D_2}} = 0$ and $v_{\mathrm{D_2}} = 2$ states separately (while maintaining $v_{\mathrm{H_2}} = 0$), we neglected radial coupling terms off-diagonal in vibrational quantum numbers. This approximation is additionally justified by the fact that the 2-0 S(2) line in H_2-perturbed deuterium is measured at room temperature, where the population of H_2 in vibrationally excited states is negligible.

The dependence of the coupling terms in Eq. (B.3) on rotational quantum numbers (usually at the level of a few percent) is one of the key factors that affect theoretical predictions of the pressure shift of pure rotational lines in light molecules (Shafer & Gordon 1973; Dubernet & Tuckey 1999; Thibault et al. 2016; Jóźwiak et al. 2018). This is due to the fact that the line shift is sensitive to the difference in the scattering amplitude in the two rotational states that participate in an optical transition. Some authors neglect the j dependence of the radial coupling terms (the centrifugal distortion of the PES) in scattering calculations for rovibrational transitions (Green et al. (1989); Thibault et al. (2017)) and average the expansion coefficients for a given vibrational v over the rovibrational wave function $v, j = 0$. This approximation is invoked either to save computational resources or due to a lack of information about the dependence of the PES on the stretching coordinates but works well for Q(j) lines. We have shown that taking the centrifugal distortion of the PES into account is crucial for achieving a sub-percent agreement with the experimental spectra in He-perturbed vibrational lines in H_2 (Słowiński et al. 2022) and HD (Stankiewicz et al. 2020). Thus, in both the HD-H_2 and D_2-H_2 cases, we included centrifugal distortion of the PES in the scattering calculations. This leads to a large number of coupling terms (22 960 for $v = 0$ state in HD, 16 359 in $v = 0$ of D_2 and 17 157 for $v = 2$), which is an order of magnitude more than in the case of HD-He (1 029). Similar to the HD-He case, this effect is crucial for achieving a sub-percent agreement with the cavity-enhanced spectra.

Appendix C: Convergence of quantum scattering calculations and uncertainty budget for line-shape parameters

Table C.1. Uncertainties associated with each convergence parameter in the quantum scattering calculations. The values with slashes in the "Basis set size" line correspond to the case of collisions with *para*-H_2 and *ortho*-H_2, respectively. See the main text for details.

Parameter	Value	Reference value	Maximum relative uncertainty (%)					
			γ_0	δ_0	γ_2	δ_2	Re(ν_{opt})	Im(ν_{opt})
$R_{\max}$	100 a_0	200 a_0	0.01	1	0.01	1	0.001	0.5
N_{steps}	200/100/50	500	0.4	1	0.5	3	0.1	5
$(l_1^{\max}, l_2^{\max}, l_{12}^{\max})$ in Eq. (B.1)	(4,4,8)	(6,6,12)	0.01	0.1	0.02	1	0.01	0.2
Basis set size ($j_{\mathrm{HD}}^{\max}$, $j_{\mathrm{H_2}}^{\max}$)	see text	(6,6)/(7,7)	0.01	0.2	0.01	0.2	0.01	0.2
Total			0.4	1.4	0.5	3.5	0.1	5

In this appendix we provide a detailed analysis of the convergence of generalized spectroscopic cross-sections with respect to specific parameters and how these parameters influence the uncertainty of the line-shape parameters. They include the range of propagation, the propagator step, the number of terms in the expansion of the PES (B.1), the size of the rotational basis set, and the number of partial waves. The uncertainties were estimated by calculating six line-shape parameters for the R(0) line at temperatures ranging from 20 to 1000 K. These values were then compared with those obtained from the generalized spectroscopic cross-sections calculated with the reference values of each parameter, which are significantly larger than the ones used in the final calculations. The stated uncertainties represent the maximum error observed within this temperature range. We assume that a similar level of accuracy is maintained for all other transitions considered in this paper. The results are summarized in Table C.1.

The range of propagation is defined by the starting and ending points ($R_{\min}$ and $R_{\max}$). The smallest R value that can be reliably calculated using quantum chemistry methods was employed as $R_{\min}$, which in this case (taking into account the coordinate transformation from the H_2-H_2 to HD-H_2 system) was 3 a_0. On the other hand, $R_{\max}$ should be large enough to apply boundary conditions to the scattering equations (i.e., in the range of R where the PES becomes negligible compared to the centrifugal barrier). We tested the sensitivity of our results to $R_{\max}$ by performing calculations with $R_{\max} = 50\ a_0$, 75 a_0, 100 a_0, 150 a_0, and 200 a_0. After assessing the tradeoff between computational cost and accuracy, we chose $R_{\max} = 100\ a_0$ for the final calculations. Table C.1 provides uncertainties for six line-shape parameters impacted by this choice, estimated with respect to the reference calculations with $R_{\max} = 200\ a_0$.

The step size of the propagation directly affects the precision and the computational cost of the quantum scattering calculations. We performed tests with a varying number of steps per half-de Broglie wavelength (N_{steps}), including 10, 20, 30, 50, 100, 200, and 500. Based on these tests, we chose a step size of 50 for $E_{\mathrm{kin}} > 3\ \mathrm{cm}^{-1}$, 100 for $E_{\mathrm{kin}} \in \langle 1.5, 3\rangle\ \mathrm{cm}^{-1}$, and 200 for $E_{\mathrm{kin}} \leq 1.5\ \mathrm{cm}^{-1}$. Uncertainties introduced by the choice of the number of steps, estimated with respect to the reference calculations with 500 steps per half-de Broglie wavelength, are gathered in Table C.1.

We tested the convergence of the results with respect to the number of terms in the PES expansion (Eq. (B.1)), comparing line-shape parameters for the R(0) line obtained from cross-sections calculated using a truncated expansion of the PES (with terms up to the $I_{448}(\theta_1, \theta_2, \phi)$ bi-spherical harmonic) and an expanded set of expansion coefficients describing higher anisotropies of the system (up to the $I_{6612}(\theta_1, \theta_2, \phi)$ term). The results are gathered in Table C.1.

The number of partial waves (or equivalently, blocks with given total angular momentum J) necessary to converge the scattering equations was determined based on a criterion of stability in the calculated cross-sections. We solved the coupled equations for an increasing number of J-blocks until four consecutive J-blocks contributed to the largest elastic and inelastic state-to-state cross-sections by less than 10^{-4} Å^2. The convergence criterion ensured that the estimated error introduced by the number of partial waves was smaller than the smallest uncertainty attributable to the other parameters in our study. This implies that the uncertainty in the number of partial waves did not significantly contribute to the overall uncertainty in our results; thus, we do not consider this factor in Table C.1.

The size of the rotational basis set is a critical factor in quantum scattering calculations, and it was chosen with great care to ensure a consistent level of accuracy across different rotational states. For each calculation, we checked that the basis set included all energetically accessible (open) levels of the colliding pair, as well as a certain number of asymptotically energetically inaccessible (closed) levels. We gradually increased the size of the basis set until the calculated cross-sections did not show appreciable differences, identifying a fully converged basis set. We then determined the smallest basis set that ensured convergence to better than 1% with respect to the fully converged basis. This was done for each initial state of the HD-H_2 system in a way that the estimated error for all transitions (R($j_{\rm HD}$), $j_{\rm HD}$=0, 1, 2), including those involving rotationally excited states, remained within the specified limit.

The tests were conducted separately for collisions with *para*-H_2 (which involves only even rotational quantum numbers) and *ortho*-H_2 (which involves only odd rotational quantum numbers). In the case of *para*-H_2, all rotational levels of HD and H_2 with $j \leq j^{\rm max} = 4$ were consistently included in the calculations. For specific calculations with H_2 initially in the $j_{\rm H_2} = 4$ state, or HD initially in the $j_{\rm HD} = 3$ state, the basis set was expanded to incorporate all rotational levels of HD and H_2 with $j \leq 6$. For *ortho*-H_2, the basis set consistently included all rotational levels of HD and H_2 with $j \leq j^{\rm max} = 5$. We extended the basis set to cover $j^{\rm max}_{\rm HD} = 6$ and $j^{\rm max}_{\rm H_2} = 5$ for cases where HD and H_2 were initially in the $(j_{\rm HD}, j_{\rm H_2})$ = (0,3), (1,3), or (2,1) states. The largest basis set, with $j^{\rm max}_{\rm HD} = j_{\rm H_2} = 7$, was employed in all calculations involving HD and H_2 in $(j_{\rm HD}, j_{\rm H_2})$ = (0,5), (1,5), (2,3), (2,5), (3,1), (3,3), and (3,5) states.

Assuming the uncertainties associated with each parameter as independent, we estimated the maximum total uncertainty of each line-shape parameter using the root-sum-square method. The results are gathered in the last line of Table C.1.

Appendix D: Modified Hartmann-Tran profile

This appendix describes the mHT profile, which we used to simulate the spectra. We considered the mHT profile to be the best compromise between the accurate but computationally demanding SDBB profile and the simple Voigt profile. The mHT profile can be expressed as a quotient of two quadratic speed-dependent Voigt (qSDV) profiles,

$$\tilde{I}_{\rm mHT}(f) = \frac{\tilde{I}^*_{\rm qSDV}(f)}{1 - (\nu^r_{opt} + i\nu^i_{opt})\pi \tilde{I}^*_{\rm qSDV}(f)}, \tag{D.1}$$

which are directly linked to the spectral line-shape parameters from Eqs (1)-(3),

$$\tilde{I}^*_{\rm qSDV}(f) = \frac{1}{\pi}\int d^3\boldsymbol{v} f_m(\boldsymbol{v}) \frac{1}{\Gamma_0 + i\Delta_0 + (\Gamma_2 + i\Delta_2)(v^2/v_m^2 - 3/2) + \nu^r_{opt} + i\nu^i_{opt} - i(f - f_0 - f_D v_z/v_m)}. \tag{D.2}$$

The line-shape profile uses the parameters in the pressure-dependent form:

$$\begin{aligned} &\Gamma_0 = \gamma_0 \cdot p,\ \Delta_0 = \delta_0 \cdot p \\ &\Gamma_2 = \gamma_2 \cdot p,\ \Delta_2 = \delta_2 \cdot p \\ &\nu^r_{opt} = \tilde{\nu}^r_{opt} \cdot p,\ \nu^i_{opt} = \tilde{\nu}^i_{opt} \cdot p. \end{aligned} \tag{D.3}$$

The $f_m(\boldsymbol{v})$ is the Maxwell-Boltzmann distribution of the active molecule velocity, v_m is its most probable speed, and v_z is one of the three Cartesian components of the $\boldsymbol{v}$ vector. The f, f_0, and f_D are the frequency of light, the central frequency of the transition, and the Doppler frequency, respectively.

The hard-collision model of the velocity-changing collisions, which is used in the mHT profile, suffices to describe the velocity-changing line-shape effects (such as the Dicke narrowing) in the majority of the molecular species. However, in the cases with a significant Dicke narrowing, such as molecular hydrogen transitions, the hard-collision model does not reproduce the line shapes at the required accuracy level. To overcome this problem, a simple analytical correction (the β correction function) was introduced (Wcisło et al. 2016; Konefał et al. 2020), which mimics the behavior of the billiard ball model and, hence, considerably improves the accuracy of the mHT profile for hydrogen, at negligible numerical cost. The correction is made by replacing the ν^r_{opt} with $\beta_\alpha(\chi)\nu^r_{opt}$, where α is the perturber-to-absorber mass ratio and $\chi = \nu^r_{opt}/\Gamma_D$ (where Γ_D is the Doppler width; see Konefał et al. (2020) for details). It should be emphasized that the β correction does not require any additional transition-specific parameters (it depends only on the perturber-to-absorber mass ratio α). The β correction was applied every time the mHT profile was used in this work.

Appendix E: DPL representation of the temperature dependences

In this appendix, we discuss the details of the DPL representation of the temperature dependences of the spectral line-shape parameters. The DPL function is used to convert the exact temperature dependence of the line-shape parameters into a simple, analytical expression, suitable for storing in spectroscopic databases (Stolarczyk et al. (2020)). This conversion is done by fitting the DPL function to the actual ab initio temperature dependence data.

Within this work, we calculated the ab initio values at temperatures ranging from 50 to 1000 K. Due to its relevance to the atmospheres of giant planets, we chose to prioritize the 50-200 K temperature range and use the data only from this range to generate the DPL coefficients (Stolarczyk et al. 2020). Projection of the ab initio data on the DPL representation is performed by fitting the DPL function in the selected temperature range. For the most faithful reconstruction of the temperature dependence, we performed several different fitting procedures (i.e., Newton, Quasi-Newton, Levenberg-Marquardt, global optimization, and gradient methods) and selected the one that gives the best result (i.e., the lowest relative root mean square error; see the next paragraph). This selection was done separately for each of the line-shape parameters and molecular transitions. Mathematically, the two terms of the DPL functions are identical. Thus, to avoid swapping them, we followed the convention that the first base coefficients should always be greater than second base coefficients. Furthermore, to reduce the number of significant digits, if the two base coefficients have opposite signs, we required that their absolute values differ at least by 1‰.

Table E.1. Relative root mean square error of the DPL representation. We fitted the DPL function (see Eq. (4)) to the ab initio data at the temperature range of 50-200 K. This table presents the root mean square differences between the actual ab initio data and the DPL representation in this range (see Fig. E.1), divided by the value of the line-shape parameter at 296 K.

parameter	R(0)	R(1)	R(2)
γ_0	0.04%	0.04%	0.03%
δ_0	0.48%	1.04%	0.29%
γ_2	0.29%	0.20%	0.21%
δ_2	2.36%	4.40%	1.20%
$\tilde{\nu}^r_{\text{opt}}$	0.03%	0.03%	0.03%
$\tilde{\nu}^i_{\text{opt}}$	1.51%	1.39%	0.53%

The DPL coefficients listed in Table 1 can be used to retrieve the temperature dependence of the line-shape parameters through Eq. (4). The efficiency of the DPL representation is depicted in Fig. E.1. The red curves show the results of the ab initio calculations, while the black curves (covered by the red ones in some cases) are the values reconstructed from the DPL coefficients from Table 1. The corresponding residuals are presented under each of the plots. Table E.1 quantifies the accuracy of the DPL representation by presenting the values of the relative root mean square error (rRMSE) of the differences between the ab initio data and the DPL fit. The values of the rRMSE are normalized with respect to the value of the corresponding line-shape parameter at 296 K. Even though the rRMSE values for some parameters are on the level of several percent, the overall error of the shape of the line is much smaller because the two parameters that impose the highest impact on the line width, γ_0 and $\tilde{\nu}^r_{\text{opt}}$, are reproduced with high accuracy. A detailed discussion of the propagation of errors from the parameters to the final shape of the line is provided in Słowiński et al. (2022).

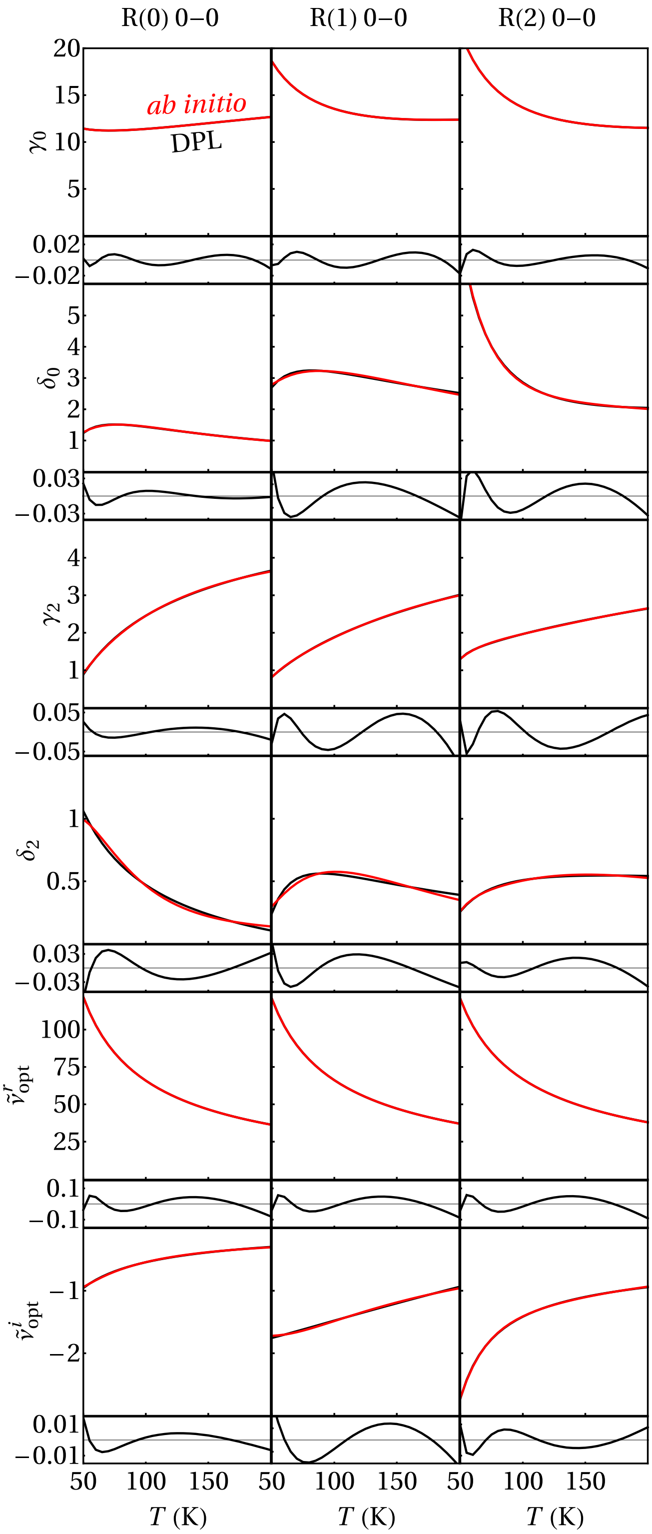

Fig. E.1. Temperature dependences of the six collisional line-shape parameters, γ_0, δ_0, γ_2, δ_2, $\tilde{\nu}^r_{\rm opt}$, and $\tilde{\nu}^i_{\rm opt}$, of the R(0) 0-0, R(1) 0-0, and R(2) 0-0 lines of HD perturbed by H_2. The red and black curves are the ab initio results and DPL approximations, respectively. The small panels show the residuals from the DPL fits. The vertical axes for all the panels (including residuals) are in 10^{-3} cm^{-1} atm^{-1}.

Journal of Quantitative Spectroscopy & Radiative Transfer 277 (2022) 107951

Contents lists available at ScienceDirect

Journal of Quantitative Spectroscopy & Radiative Transfer

journal homepage: www.elsevier.com/locate/jqsrt

Collisional line-shape effects in accurate He-perturbed H_2 spectra

Michał Słowiński[a,*], Hubert Jóźwiak[a], Maciej Gancewski[a], Kamil Stankiewicz[a], Nikodem Stolarczyk[a], Yan Tan[b], Jin Wang[b], An-Wen Liu[b], Shui-Ming Hu[b], Samir Kassi[c], Alain Campargue[c], Konrad Patkowski[d], Piotr S. Żuchowski[a], Roman Ciuryło[a], Franck Thibault[e], Piotr Wcisło[a]

[a] Institute of Physics, Faculty of Physics, Astronomy and Informatics, Nicolaus Copernicus University in Toruń, Grudziadzka 5, Torun 87-100, Poland
[b] Hefei National Laboratory for Physical Sciences at Microscale, iChEM, University of Science and Technology of China, Hefei, 230026 China
[c] University of Grenoble Alpes, CNRS, LIPhy, Grenoble F-38000, France
[d] Department of Chemistry and Biochemistry, Auburn University, Auburn, AL 36849 USA
[e] Univ Rennes, CNRS, IPR (Institut de Physique de Rennes) - UMR 6251, Rennes F-35000, France

ARTICLE INFO

Article history:
Received 26 March 2021
Revised 21 September 2021
Accepted 21 September 2021
Available online 23 September 2021

Keywords:
ab initio quantum-scattering Calculations
Molecular hydrogen
Spectral line shape
Collisional line-shape effects

ABSTRACT

We investigate collisional line-shape effects that are present in highly accurate experimental spectra of the 3-0 S(1) and 2-0 Q(1) molecular hydrogen absorption lines perturbed by helium. We clearly distinguish the influence of six different collisional effects (i.e.: collisional broadening and shift, their speed dependencies and the complex Dicke effect) on the shapes of H_2 lines. We demonstrate that only a very specific combination of these six contributions, determined from our *ab initio* calculations, gives unprecedentedly good agreement with experimental spectra. If any of the six contributions is neglected, then the experiment-theory comparison deteriorates at least several times. We also analyze the influence of the centrifugal distortion on our *ab initio* calculations and we demonstrate that the inclusion of this effect slightly improves the agreement with the experimental spectra.

1. Introduction

Hydrogen molecule, which is the simplest neutral chemically bound system, colliding with a helium atom constitutes a benchmark system well suited for testing and validating [1] the *ab initio* quantum chemical calculations of potential energy surfaces (PESs) [2,3]. The way the collisional effects are manifested in rovibrational spectra is particularly interesting in the case of the H_2 molecule. Due to a large rotational constant [4] and the lack of low-temperature inelastic channels in H_2 scattering [5], the nontrivial beyond-Voigt collisional line-shape effects are atypically strong [6], which makes it a perfect system for testing the collision-induced line-shape effects together with the quantum-scattering calculations associated with them.

Recently, low-temperature experiments with coexpanded supersonic beams allowed to measure rotationally inelastic scattering of the HD molecule colliding with D_2 [7,8] and with He [9]. The influence of collisions of H_2 isotopologues or noble gas atoms with a hydrogen molecule on the shapes of the H_2 lines was studied in a wide temperature range, spanning from 20 to 1200 K [10–17]. In particular, the widths and shifts of the H_2 rovibrational lines affected by the H_2-He collisions were subjected to intense theoretical and experimental studies [3,5,15,18–26]. Recently, the *ab initio* calculations carried out for two rovibrational lines of molecular hydrogen achieved a subpercent agreement with experimental spectra [1].

In this work, we investigate the shapes of two molecular hydrogen absorption lines perturbed by helium. We clearly distinguish the influence of six different collisional effects (i.e.: collisional broadening and shift, speed dependence of the broadening and the shift, and real and imaginary Dicke effect) on the shapes of H_2 lines. We demonstrate that only a specific combination of these six contributions, as resulting from our *ab initio* calculations, gives unprecedentedly good agreement with experimental spectra (0.87% for the 3-0 S(1) line and 0.33% for the 2-0 Q(1) line). Additionally, we extend the previous analysis [1] by introducing into our quantum-scattering calculations the impact of the centrifugal distortion (CD) on the H_2-He interaction. We note that the CD is

---

[*] Corresponding author.
E-mail addresses: mslowinski@umk.pl (M. Słowiński), piotr.wcislo@umk.pl (P. Wcisło).

https://doi.org/10.1016/j.jqsrt.2021.107951

introduced into our quantum-scattering calculations in a twofold manner. First, CD influences the calculations of the structure of the H_2 molecule, i.e. the energies of the rovibrational levels. This effect was already taken into account in all our previous analyses of the He-perturbed hydrogen lines [1,3,5,21–23,26]. In fact, we used the energy levels of H_2 reported in Ref. [27]. Second, CD influences the H_2-He interaction calculated from the PES for a given rovibrational state of H_2. This is because as the H_2 molecule rotates, its rovibrational wave function, $\chi_{\upsilon j}(r_{\mathrm{HH}})$, is slightly stretched. Thus, the full H_2-He PES should be averaged over wave functions which include this stretching (see Section 4 for details). In this paper, while referring to CD, we refer to the second meaning of those stated above. In the previous works it was pointed out that CD can be crucial for purely rotational lines [5]. Here, we demonstrate that while for the 2-0 Q(1) line, CD does not impact the line-shape parameters significantly, it influences the line-shape parameters of the 3-0 S(1) line at the 6% level and, hence, cannot be neglected in the interpretation of highly accurate experimental spectra.

Besides its importance for studying molecular interactions and collisions, accurate determination of the collisional line-shape parameters is important for astrophysical research. Spectroscopic studies of the atmospheres of giant planets need an accurate determination of pressure broadening and shift for electric-quadrupole H_2 lines [28–31]. Higher H_2 overtones are also used to study the atmospheres of giant planets [32,33], where beyond-Voigt line-shape parameters were proven to be necessary to interpret the measured spectra.

2. Line shape description

Our line-shape calculations [1,34–37] are based on the generalized Hess method (GHM) [38–40]. Instead of fitting, we calculate the line-shape parameters, namely the speed-dependent pressure broadening, $\Gamma(\upsilon)$, and shift, $\Delta(\upsilon)$ [41–43], along with the complex Dicke parameter, ν_{opt} [3,44–48], directly from the generalized spectroscopic cross sections

$$\Gamma(\upsilon) + i\Delta(\upsilon) = \left(\frac{n_p}{2\pi c}\right)\frac{2\tilde{\upsilon}_p^2}{\upsilon\sqrt{\pi}}\exp\left(-\upsilon^2/\tilde{\upsilon}_p^2\right) \times \\ \times \int_0^\infty x^2 e^{-x^2}\sinh\left(2\upsilon x/\tilde{\upsilon}_p\right)\sigma_0^q(x\tilde{\upsilon}_p)\mathrm{d}x, \tag{1a}$$

$$\nu_{\mathrm{opt}} = \left(\frac{n_p}{2\pi c}\right)\frac{m_p}{m+m_p}\int_0^\infty \upsilon_r f_m(\upsilon_r) \times \\ \times\left[\frac{2}{3}\frac{\upsilon_r^2}{\bar{\upsilon}_r^2}\sigma_1^q(\upsilon_r) - \sigma_0^q(\upsilon_r)\right]\mathrm{d}\upsilon_r, \tag{1b}$$

where n_p is the number density of the perturber, c is the speed of light, υ_p, υ and υ_r are the speed of the perturber with the most probable value $\tilde{\upsilon}_p$, the speed of the active molecule and their relative speed with mean value $\bar{\upsilon}_r$, respectively, with $x = \upsilon_r/\tilde{\upsilon}_p$. m_p and m are the masses of the perturber and the active molecule, respectively, and $f_m(\upsilon)$ is the Maxwell-Boltzmann speed distribution. The cross sections, $\sigma_\epsilon^q(\upsilon)$, are determined from the S-matrices that are obtained, from the binary impact approximation, from the quantum-scattering calculations [22], which are performed on the state-of-the-art H_2-He PES, i.e. extended Bakr, Smith and Patkowski potential (BSP3) [2,3]. The q superscript denotes the tensorial rank of radiation-matter interaction, which describes the type of a spectroscopic transition. In absorption spectroscopy, $q = 1$ corresponds to electric dipole transitions and $q = 2$ corresponds to the electric quadrupole transitions considered here. In the case of Raman spectroscopy, $q = 0$ describes isotropic Q lines, while $q = 2$ corresponds to anisotropic transitions. ϵ denotes the rank of the velocity tensor. For $\epsilon = 0$, the real and imaginary part of $\sigma_\epsilon^q(\upsilon)$ are referred to as the pressure broadening and pressure shift cross sections, respectively [49–51], which describe the damping and dephasing of the optical coherence. For $\epsilon = 1$ the $\sigma_\epsilon^q(\upsilon)$ provides the complex Dicke cross section [39,40,52], the real part of which describes the flow of the optical coherence between different velocity classes. The imaginary part of $\sigma_{\epsilon=1}^q(\upsilon)$ describes the phase changing of the optical coherence during velocity-changing collisions. We note that the cross sections, $\sigma_\epsilon^q(\upsilon)$, include the contribution from the inelastic scattering of the diatomic molecule and the dephasing part, which involves both the reorienting collisions (induced by the anisotropic part of the PES) and purely phase-changing collisions [5].

The isolated absorption line can be described in terms of the transport-relaxation equation [53]

$$1 = -i(\omega - \omega_0 - \mathbf{k}\cdot\mathbf{v})h(\omega,\mathbf{v}) - \hat{S}^{\mathrm{f}}h(\omega,\mathbf{v}), \tag{2}$$

where ω and ω_0 are the laser frequency and the unperturbed line position, respectively, $\mathbf{k}$ is the wave vector, $\hat{S}^{\mathrm{f}}$ is the collision operator, $f_{\mathrm{m}}(\mathbf{v})$ is the Maxwell velocity distribution of the active molecule velocity, $\mathbf{v}$, and $f_{\mathrm{m}}(\mathbf{v})h(\omega,\mathbf{v})$ is a scalar function proportional to the velocity distribution of the optical coherence. The shape of molecular line is calculated as [53]

$$I(\omega) = \frac{1}{\pi}\Re e\int \mathrm{d}^3\mathbf{v}\; f_{\mathrm{m}}(\mathbf{v})h(\omega,\mathbf{v}). \tag{3}$$

The velocity distribution of the optical coherence arises as an interplay between two competing processes. On one hand, the laser light induces the optical excitation within some velocity classes. On the other, collisions change both the internal state of the molecule and its velocity [54–56]. These effects can be incorporated into the collision operator as a sum of the broadening and shift and a velocity-changing operator

$$\hat{S}^{\mathrm{f}} = -\left(\Gamma_0 + i\Delta_0\right) - \left(\Gamma_{\mathrm{SD}}b_\gamma(\upsilon) + i\Delta_{\mathrm{SD}}b_\delta(\upsilon)\right) + \\ + (\nu_{\mathrm{opt}}^{\mathrm{r}} + i\nu_{\mathrm{opt}}^{\mathrm{i}})\hat{M}_\xi^{\mathrm{f}}, \tag{4}$$

where Γ_0 and Δ_0 are the speed-averaged broadening and shift, Γ_{SD} and Δ_{SD} are the parameters describing the magnitude of the speed-dependence of broadening and shift of the line with b_γ and b_δ describing their shape [35], $\nu_{\mathrm{opt}}^{\mathrm{r}}$ and ν_{opt}^{i} are the real and imaginary part of ν_{opt}, respectively. Finally, $\nu_{\mathrm{opt}}\hat{M}_\xi^{\mathrm{f}}$ is the velocity-changing operator [53,57,58] within a given ξ model of collisions

$$\nu_{\mathrm{opt}}\hat{M}_\xi^{\mathrm{f}}h(\omega,\mathbf{v}) = \int\left[f_\xi(\mathbf{v}\leftarrow\mathbf{v}') - f_\xi(\mathbf{v}'\leftarrow\mathbf{v})\right]h(\omega,\mathbf{v}')\mathrm{d}\mathbf{v}', \tag{5}$$

where f_ξ is the collision kernel. We note here that the complex Dicke parameter, ν_{opt}, involves correlation between the internal and translational degrees of freedom [3,39,40,45]. In the original formulation of the GHM, this operator is a simple hard-collision (HC) operator [44,59] whose collision kernel depends only on the Maxwell velocity distribution [60]

$$f_{\mathrm{HC}}(\mathbf{v}\leftarrow\mathbf{v}') = \nu_{\mathrm{opt}}f_{\mathrm{m}}(\mathbf{v}). \tag{6}$$

In this work, we replace the HC collision kernel with the more physically-justified billiard-ball (BB) model [54,57,58], in which the collision kernel takes into account not only the speed after the collision, υ, but also the speed before the collision, υ', the angle ϕ between aforementioned velocities and the perturber-absorber mass ratio, α. The BB collision kernel can be expressed as

$$f_{\mathrm{BB}}(\mathbf{v}\leftarrow\mathbf{v}') = \\ = \nu_{\mathrm{opt}}\frac{1}{\upsilon_{\mathrm{m}}^2}\frac{3}{32\pi}\frac{(1+\alpha)^{5/2}}{\alpha^2}\frac{1}{\sqrt{\upsilon^2 - 2\upsilon\upsilon'\cos(\phi) + \upsilon'^2}} \times \\ \times\exp\left(-\frac{(1-\alpha)^2}{4\alpha}\frac{\upsilon'^2}{\upsilon_{\mathrm{m}}^2} - \frac{(1+\alpha)(1-\alpha)}{2\alpha}\frac{\upsilon\upsilon'}{\upsilon_{\mathrm{m}}^2}\cos(\phi) + \right.$$

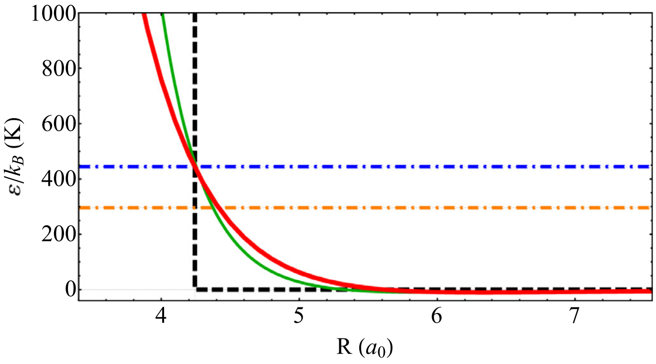

Fig. 1. Isotropic part of the BSP3 PES for colliding H_2-He (red thick solid line) as a function of relative distance, *R*. The hard-sphere potential (black dashed line) was constructed so it intersects the *ab initio* potential curve at the mean collisional energy (ε/k_B=444 K). Green solid line is the Lennard-Jones potential fitted to the isotropic part of the BSP3 PES. Mean collision energy and energy corresponding to the temperature *T* are indicated as the blue (upper) and orange (lower) dot-dashed lines respectively. The mean hard-sphere diameter $d_{H_2-He} = 4.24$ a_0 at 296 K.

$$+ \quad \frac{\alpha v^2 v'^2 \sin^2(\phi)}{v_m^2\left(v^2 - 2vv'\cos(\phi) + v'^2\right)} - \frac{(1+\alpha)^2}{4\alpha}\frac{v^2}{v_m^2}\Bigg), \tag{7}$$

where $v_m = \sqrt{2k_B T/m}$ is the most probable speed of an active molecule of mass *m*, k_B is the Boltzmann constant, and *T* is the temperature. With the BB model of collisions included, we refer to the line shape as the speed-dependent billiard-ball profile (SDBBP).

In this work, we calculate the complex Dicke parameter from the *ab initio* calculations based on the GHM. It is interesting to compare it with the frequency of the velocity-changing collisions (real number), ν_{diff}, calculated from the diffusion [57,61]

$$\nu_{diff} = \frac{v_m^2}{2D}, \tag{8}$$

where *D* is the binary diffusion coefficient. The latter can be simply calculated using a crude hard-sphere model [34,57] or an effective Lennard-Jones (LJ) potential parameters [62]. It can be also determined experimentally [63]. We estimate the mean hard-sphere diameter (σ in Ref. [34]) as the intersection of the true isotropic part of the PES with the mean collisional energy, see black line in Fig. 1. The effective LJ potential was obtained by fitting its parameters to the true isotropic part on the interacting pair in the ground state, see green line in Fig. 1.

Note that while this work focuses on describing the line shape in a physically justified model, we also provide a comprehensive dataset of the line-shape parameters for this system for the quadratic speed-dependent hard-collision profile in a wide temperature range in Ref. [17].

3. Signatures of different collisional line-shape effects in experimental spectra

In this section, we use the experimental spectra reported in Ref. [1]. The He-perturbed 2-0 Q(1) H_2 line was measured in the Grenoble laboratory at temperature 294.2 K and at nine pressures from 0.07 to 1.05 atm and the He-perturbed 3-0 S(1) H_2 line was measured in the Hefei laboratory at temperature 296.6 K and at four pressures from 0.36 to 1.35 atm. The H_2-He mixing ratio is different for both experiments and for the 2-0 Q(1) line has a constant value of 4.9(1)% while for the 3-0 S(1) line spans between 10% and 33%. We perform fully quantum calculations of the line-shape parameters on the newly-developed BIGOS code [64], see Ref. [3,22] for detailed description of the methodology. Comparing to our previous work [1] we perform additional quantum-scattering calculations to check the influence of the CD (which is usually neglected) on the shapes of molecular resonances, see Section 4 for more details. In our spectra analysis, we fit the line position, ω_0, line intensity, *S*, and linear baseline. The fit of the line position was performed by means of multispectrum fitting technique [65], while the line area was fitted separately for every pressure. Line-shape parameters are not fitted, but fixed to calculated *ab initio* values. The results for two chosen pressures are presented in Fig. 2. We have already demonstrated, in Ref. [1], that the consistency between our theoretical line-shape calculations and experimental data reaches subpercent accuracy for the He-perturbed H_2 lines. Here we demonstrate that taking into account more sophisticated line-shape parameters is crucial to achieve this agreement. In a typical case the collisional effects in molecular absorption spectra are dominated by the speed-averaged broadening, Γ_0, and shift, Δ_0, and hence the Voigt Profile (VP) suffices to describe the collision-perturbed shapes of the molecular lines [66,67]. However, the atypical properties of the hydrogen molecule give us an opportunity to experimentally study more subtle line-shape effects that our collision operator, Eq. (4), takes into account. In Sections 3.1–3.3 we demonstrate on the experimental data that none of these collisional effects can be neglected. Indeed, the excellent agreement between theory and experimental spectra, see Fig. 2, is achieved only when the contributions from all six collisional line-shape parameters are taken into account at the same time, see Fig. 3.

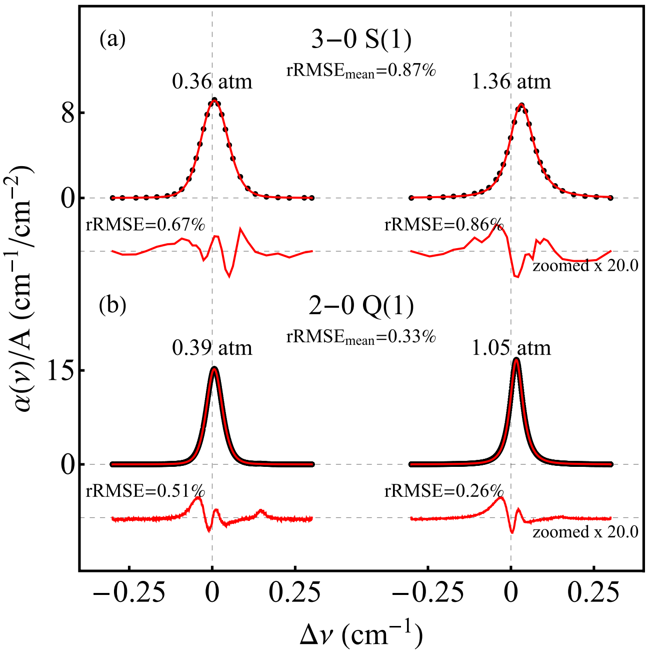

Fig. 2. The raw experimental spectra reported in Ref. [1] (black points) in comparison with the simulated line profiles (red lines). Linear background is subtracted from the spectra. The absorption axis is normalized to the spectral line area, *A*. The red lines under the line profiles show the differences between the experiment and theory enlarged twenty times. Relative root-mean-square error, rRMSE, values in the plots describe the errors relative to the profile amplitude calculated within ±FWHM (Full-Width at Half Maximum) from the line maximum. Vertical gray lines correspond to the theoretical unperturbed line position, ω_0. Deviation of the line maximum from ω_0 highlights that H_2 has atypically large pressure shift.

3.1. Speed-averaged line broadening and shift

The simplest description of the line shape is based on the speed-averaged broadening and shift in conjunction with the Doppler effect. In the absence of any other collisional line-shape effects, this results in the formation of a simple VP. To quantify the impact of these collisional effects on the overall shape of the

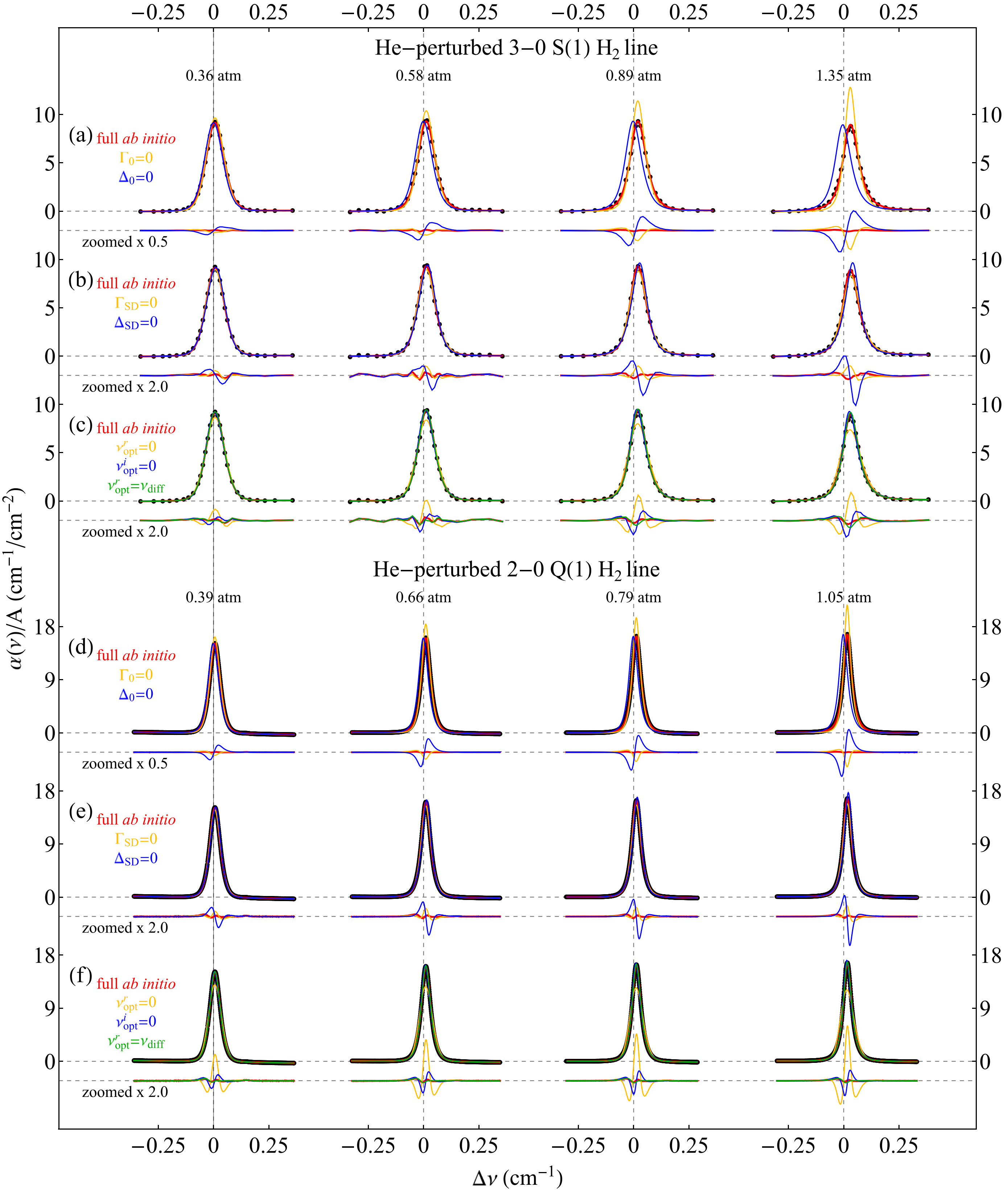

Fig. 3. Influence of different collisional effects on the shapes of the rovibrational transitions in H_2. Black dots are the experimental data reported in Ref. [1] and the red lines are the *ab initio* line shapes. Panels (a-c) and (d-f) correspond to the He-perturbed 3-0 S(1) and 2-0 Q(1) H_2 line, respectively. Panels (a) and (d) present the line shapes in which the speed-averaged line broadening and shift is neglected, i.e. $\Gamma_0 = 0$ (yellow line) and $\Delta_0 = 0$ (blue line). In panels (b) and (e) the speed dependence of the line broadening, $\Gamma_{SD} = 0$ (yellow line) and shift, $\Delta_{SD} = 0$ (blue line) is neglected. In panels (c) and (f) we neglect the complex Dicke parameter; its real, $\nu^{r}_{opt} = 0$ (yellow line), and imaginary, $\nu^{i}_{opt} = 0$ (blue line), parts. These panels also present the effect of replacing ν^{r}_{opt} with ν_{diff} originating from the diffusion model calculated with the hard-sphere approach (green line).

measured H_2 absorption lines, we set the Γ_0 (see yellow lines in Fig. 3a and d) and Δ_0 (see blue lines in Fig. 3a and d) parameters to zero in our *ab initio* profiles and directly superimpose them on the raw experimental data. The resulting large differences show, as expected, that both of these parameters are crucial for a proper description of the spectral profile.

3.2. Speed dependence of the line broadening and shift

For the present molecular system the simple VP is fairly insufficient [43,68,69]. The beyond-Voigt line-shape effects are particularly pronounced for the case of the rovibrational transitions in molecular hydrogen, see Fig. 2e–f in Ref. [1]. The dependence of the collisional width and shift on the speed of the molecules [41] has to be included to increase the agreement with experimental data. To examine its influence, we set the Γ_{SD} (see yellow lines in Fig. 3b and e) and Δ_{SD} (see blue lines in Fig. 3b and e) parameters to zero in our *ab initio* profiles and directly superimpose them on the raw experimental data. The speed dependence of the line width reduces the effective width of the line via the speed class exchanges, while the speed dependence of the shift manifests as inhomogeneous broadening and asymmetry of the line [70,71]. This is clearly confirmed by our experimental data, for $\Gamma_{SD} = 0$ (see aforementioned yellow line) the line-shape profile is broader, i.e., the peak of the line is lower, while for $\Delta_{SD} = 0$ (blue line) the line is narrower, i.e. the line peak is higher, and the residuals are clearly asymmetric.

3.3. Velocity-changing collisions

The influence of the velocity-changing collisions is incredibly pronounced for the H_2 molecule. It is clearly visible while comparing the velocity-changing collisions frequency derived directly from the diffusion coefficient, ν_{diff}, to the speed-averaged width, Γ_0 (for the values refer to the Table 1). Therefore, even if the state/phase- and velocity-changing collisions are correlated, i.e. some fraction of the excited molecules undergoing the change of the velocity are damped, the effective rate of velocity-changing collisions, ν_{opt}, is still much larger than all the other collisional line-shape parameters, see Table 1. We bring this to the fore this in Fig. 3 c and f; the yellow lines show the case when the real part of the complex Dicke parameter, ν^{r}_{opt}, is neglected.

Table 1
Line-shape parameters for the 3-0 S(1) and 2-0 Q(1) H_2 lines, determined with our *ab initio* quantum-scattering calculations that include centrifugal distortion. The calculations are done for $T = 296.6$ K for the 3-0 S(1) line and for $T = 294.2$ K for the 2-0 Q(1) line. As a reference, we calculated also ν_{diff} from Eq. (8) for the hard-sphere and LJ potentials (see Fig. 1). For the hard-sphere potential, $\nu_{diff} = 43.38$ and 43.19 for $T = 296.6$ K and 294.2 K, respectively. For the LJ potential, $\nu_{diff} = 38.67$ and 38.43 for these two temperatures, respectively. For the experimentally determined diffusion coefficient [63], $\nu_{diff} = 40.9$ and 41.15 for $T = 296.6$ K and 294.2 K, respectively. All the parameters are given in 10^{-3} cm^{-1} and are calculated for $n_p = 1$ amg. Abbreviations of the PESs are given in the text.

PES	Γ_0	Δ_0	Γ_{SD}	Δ_{SD}	ν^{r}_{opt}	ν^{i}_{opt}
3-0 S(1) Line						
mMR	6.51	23.38	2.87	8.92	40.99	−13.03
SK	14.59	33.03	7.01	14.25	36.53	−19.28
BSP	12.79	31.52	5.91	12.99	37.32	−18.29
BSP2	12.36	31.15	5.70	12.67	37.57	−17.94
BSP3	12.38	31.14	5.71	12.69	37.56	−17.96
2-0 Q(1) Line						
mMR	3.45	14.28	1.59	5.53	42.63	−7.98
SK	7.04	21.89	3.35	9.25	41.25	−12.62
BSP	5.85	19.58	2.73	8.15	41.59	−11.51
BSP2	5.74	19.36	2.68	7.99	41.66	−11.33
BSP3	5.75	19.36	2.68	8.00	41.65	−11.35

For the considered lines, the real part of the complex Dicke parameter, ν^{r}_{opt}, is close to the one calculated from diffusion coefficient either using a hard-sphere model or LJ potential parameters (see the Appendix B of Ref. [3]), see Eq. (8), Fig. 1 and Table 1. The green lines in Fig. 3 c and f correspond to the case when the *ab initio* calculated ν^{r}_{opt} was replaced with ν_{diff}. Using ν^{r}_{opt} we achieved lower residuals than with this approach, but the differences on the figure scale is almost negligible.

In this analysis we clearly observe in experimental spectra the contribution of the imaginary part of the complex Dicke parameter, ν^{i}_{opt}. It has to be emphasized that here we do not phenomenologically fit the ν^{i}_{opt} parameter to the experimental data (which was done before many times [43,69,72–75]), but we set it to the value determined from our fully *ab initio* calculations and make a direct comparison with the raw experimental spectra, see the red lines in Fig. 3. To see the contribution from the ν^{i}_{opt} parameter we set it to zero and compare with experimental spectra, see the blue lines in Fig. 3 c and f. It can be clearly seen that when the contribution of ν^{i}_{opt} is neglected, then the discrepancy between theory and experiment is a few times larger.

3.4. Other collisional line-shape effects

In this section, we discuss several other collisional line-shape effects which we do not observe in our spectra. We argue that these effects have negligible influence in the cases considered here.

3.4.1. Non-impact (collision duration) effects

To estimate the influence of the collision-duration effect, we use the results obtained for the Ar-perturbed HF lines [76]. The asymmetry parameter, *b*, for this system is at the level of 3×10^{-3}amg^{-1}. At our highest pressure this would correspond to 0.15% rRMSE, which is smaller than the rRMSE of the comparison between experiment and theory reported in this work. This estimation is conservative since the range of the H_2-He interaction is smaller than for HF-Ar and the corresponding collision-duration effects for H_2-He are expected to be smaller as well.

3.4.2. Line mixing

To estimate the influence of the line-mixing effect, we use the results obtained for the selfperturbed HD lines [77]. The line-mixing coefficient, *y*, for HD-HD is at the level of 2×10^{-3}amg^{-1} [77]. At our highest pressure this would correspond to 0.1% rRMSE. Also this estimation is conservative since the separation between the Q lines is much larger for H_2 compared to the HD lines from Ref. [77].

4. Improved accuracy of the *ab initio* calculations

The analysis presented in the previous sections is based on the most recent *ab initio* PES (BSP3) [3]. In Section 3, we demonstrated that the *ab initio* line-shape calculations based on the BSP3 PES agree well with the experimental data. In this section, we use our quantum-scattering and line-shape calculations to validate the PESs available in the literature [2,3,78–80] as well as to quantify the influence of the CD, which is usually neglected in the scattering calculations for rovibrational transitions. The calculations that include CD are performed on the most accurate BSP3 PES using the newly developed BIGOS code [64].

For the purpose of scattering calculations, the PES for the H_2-He system, $V(R, r_{HH}, \theta)$ is expanded over Legendre polynomials [3,5,22]

$$V(R, r_{\mathrm{HH}}, \theta) = \sum_{\lambda=0,2,4,6} V_\lambda(R, r_{\mathrm{HH}}) P_\lambda(\cos\theta), \tag{9}$$

where R is the separation between the helium atom and the center of mass of H_2, r_{HH} is the distance between hydrogen atoms, and θ denotes the angle between R and r_{HH}. Radial coupling terms, which enter the coupled equations, are obtained from the rovibrational average of the $V_\lambda(R, r_{\mathrm{HH}})$ terms over the wave functions of the unperturbed H_2 molecule, $\chi_{vj}(r_{\mathrm{HH}})$,

$$V_{\lambda,vj,v'j'}(R) = \int \mathrm{d}r_{\mathrm{HH}} \chi_{vj}(r_{\mathrm{HH}}) V_\lambda(R, r_{\mathrm{HH}}) \chi_{v'j'}(r_{\mathrm{HH}}), \tag{10}$$

where v and j denote vibrational and rotational quantum numbers, respectively. In this work we neglect the vibrational coupling between molecular states, which means that we use only radial coupling terms with $v' = v$ in the scattering calculations. The non-diagonal vibrational couplings would be too expensive to include. Disregarding the CD, in turn, means that in each vibrational state the coupling terms can be approximated as $V_{\lambda,vj,vj'}(R) \approx V_{\lambda,v0,v0}(R)$.

4.1. H_2-He potential energy surfaces

We consider five different PESs: the PES of Schaefer and Köhler (SK PES) [78], the modified Muchnick-Russek PES (mMR) [79,80], the PES reported by Bakr, Smith and Patkowski (BSP) [2] and its two extensions: BSP2 and BSP3 [3].

The original PES of Schaefer and Köhler was based on the *ab initio* points reported in Ref. [81] with the configuration interaction techniques. The SK PES covered a relatively large range of absorber-perturber distance R, (1.6 – 11 a_0) and was calculated for five intramolecular distances r_{HH} between 0.9 and 2 a_0, with three of them (1.28, 1.449, 1.618 a_0) determined at a higher level of accuracy [78]. The SK PES was originally presented in the form of $V_\lambda(R, r_{\mathrm{HH}})$ values. We made use of the form published in Ref. [80].

The mMR PES was published as a modification of the *ab initio* potential of Muchnick and Russek [79]. The original MR PES covered a narrow range of r_{HH} near 1.4 a_0, but the analytic fit was expected to behave reasonably even up to 4 a_0. The modification of this PES (mMR) [80] was performed to fit to the more accurate *ab initio* values reported in Ref. [82], which were calculated with the complete fourth-order Møller-Plesset approximation.

The BSP PES (and its further extensions) was obtained using the coupled-cluster method with single, double and perturbative triple (CCSD(T)) excitations, taking also into account the contributions from the higher coupled-cluster excitations [2]. This PES was determined for ten values of r_{HH} in the range of $r_{\mathrm{HH}} \in [1.1, 1.75]$ a_0, which turned out to be insufficient for the accurate studies of processes involving vibrationally excited H_2 (see Section 2 of Ref. [5] for details). This problem was solved in the second version of this PES, BSP2, which extended the *ab initio* data points range to $r_{\mathrm{HH}} \in [0.65, 3.75]$ a_0. In the final extension of this potential, BSP3, an improved asymptotic behavior for the large values of R was introduced (for details see Section 2 of Ref. [3]). This PES (denoted as BSP3) was used in Ref. [1].

In Table 1, we report the *ab initio* values of the line-shape parameters for all the considered PESs. There are no fitted line-shape parameters because for the molecular hydrogen they can considerably deviate from the real ones due to a strong numerical correlation. For this reason, we adopt a methodology that is more adequate to study the collisional effects in H_2, i.e., instead of comparing the fitted values of the collisional line-shape parameters with theory, we directly compare the *ab initio* line shapes with experimental spectra and the RMSE of their difference gives us information about the agreement between the theory and experiment.

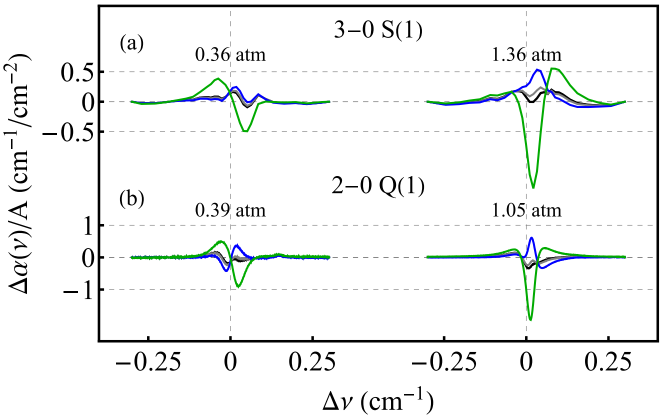

Fig. 4. Differences between experimental data and modelled spectra with central frequency fitted by means of the multispectrum fitting technique and line intensity fixed to the theoretical value [83]. Green, blue, gray and black lines are the residuals for the mMR, SK, BSP and BSP3 potentials, respectively. Vertical gray lines correspond to the unperturbed line position [83].

This way we can also check separately an individual influence of any of the six collisional line-shape parameters, see Fig. 3.

In Fig. 4 we show a comparison between the experiment and theory for different PESs. Contrary to the analysis from Figs. 2 and 3, here the line intensity is not adjusted but settled to the fixed theoretical value [83] (this is why the black residuals from Fig. 4 are slightly larger than the red ones from Figs. 2 and 3) to get a clear comparison and to not artificially compensate inaccurate values of some of the line-shape parameters by the line-fitting procedure.

The smallest residuals are for the most recent BSP3 PES, see the black lines in Fig. 4. The residuals for the BSP2 PES are hardly distinguishable from the ones for BSP3 (hence, we do not show them in Fig. 4). Physically, this means that any inaccuracies of the BSP2 potential at large separations between H_2 and He are minor relative to the sensitivity of the line-shape parameters to the asymptotic behavior of the PES, at this level of accuracy. This is consistent with the expectation that at room-temperature energies the generalized spectroscopic cross sections are hardly sensitive to the long-range part of the PESs (see Appendix C of Ref. [3]). The asymptotic behavior influences the values of the line-shape parameters at the subpercent level, see the BSP2 and BSP3 rows in Table 1.

The residuals for the BSP PES are shown in Fig. 4 as gray lines. The main difference between BSP and BSP3 is that BSP does not cover as large a range of intramolecular separations in H_2, see Fig. 1 in Ref. [5]. For the second overtone, at higher pressures, the residuals for BSP (blue line in the top panel in Fig. 4) are larger than for BSP3 (red line). It is consistent with our expectations but at the present level of accuracy the difference is not yet large enough to unambiguously conclude that we experimentally validate the highly-stretched regions of the PESs.

The residuals for the SK and mMR PESs are shown in Fig. 4 as blue and green lines, respectively. For these two cases, the residuals are much larger (especially for the mMR PES) than for the three versions of the BSP PES. This confirms the preliminary analysis of Ref. [5].

4.2. Centrifugal distortion (CD)

We performed additional scattering calculations on the BSP3 PES to determine the influence of the CD on the accuracy of theoretically modelled spectral line shapes. Figure 5 presents CD of the wave functions of H_2 in the three vibrational states considered in the experiment. The difference between the

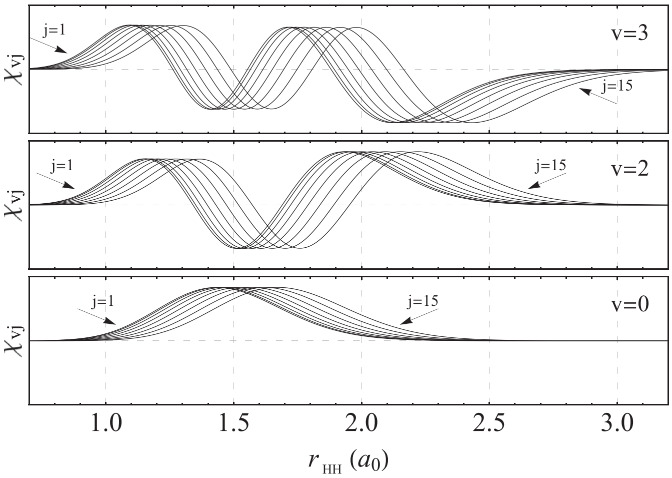

Fig. 5. Rovibrational wave functions of ortho-H$_2$, $\chi_{\upsilon j}(r_{\rm HH})$ ($j=1$ to $j=15$) considered in our scattering calculations. For small j numbers the wave functions are overlapped.

purely vibrational state, $\chi_{\upsilon 0}(r_{\rm HH})$, and the true wave function, $\chi_{\upsilon j}(r_{\rm HH})$, increases with both j and υ. Due to the fact that H$_2$ has a remarkably large rotational constant ($B = 60.853$ cm^{-1} [4]), this effect should be pronounced in the rovibrational spectra of this molecule. The influence of the CD on the pressure broadening and shift coefficients was studied by Green [84] in the He-perturbed Q lines of D$_2$ from the fundamental band and by Shafer and Gordon [49] and Dubernet and Tuckey [85] in the He-perturbed isotropic Raman Q lines of the fundamental band and S purely rotational lines of H$_2$. These studies concluded that CD has a relatively small effect on both the pressure broadening and shift in the fundamental band (about 1–3%), but can significantly modify the pressure shift of the purely rotational lines, which is very sensitive to the difference in the elastic scattering in two rotational states. The majority of recent theoretical investigations [3,5,21–23] took this effect into account for purely rotational lines, but neglected it for rovibrational transitions. It was suggested [5] that in the latter case, CD might be masked due to the large contribution from the vibrational dephasing.

Here, we report values of the six line-shape parameters calculated with and without CD, see Table 2. In Fig. 6 we show the comparison between the experimental spectra and the theoretical line shape calculated with and without including the CD.

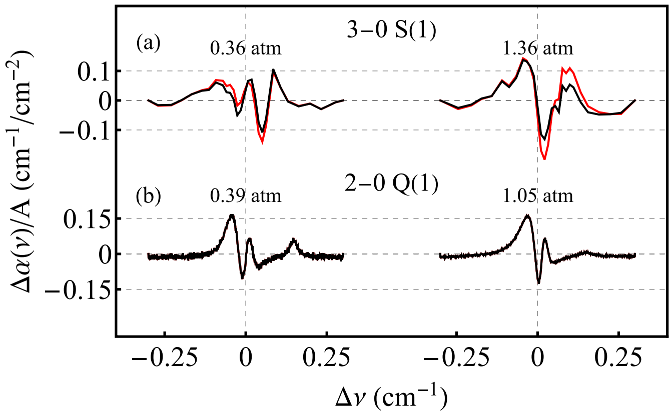

Fig. 6. The influence of centrifugal distortion (CD) on the theory-to-experiment consistency. We present differences between experimental data and modeled spectra with central frequency fitted by means of multispectrum fitting technique and line intensity fitted individually for each pressure. Black and red lines correspond to the cases when the CD was and was not taken into account, respectively. CD has a negligible effect on the Q line, therefore the lines are overlapping. Vertical gray lines correspond to the theoretical unperturbed line position.

For the 3-0 S(1) line, CD modifies the Γ_0 and $\Gamma_{\rm SD}$ by over 5%. The rest of the parameters, in particular, the pressure shift Δ_0, are modified by over 2.5%. CD leads to lower differences between theoretical and experimental spectra, and reduces the mean rRMSE calculated for ±FWHM from 0.99% to 0.89%. In the case of the 2-0 Q(1) line, CD has almost no effect on the calculated line-shape parameters and the spectra calculated with and without it overlap. This result agrees with the observation of Dubernet and Tuckey [85], who reported that the influence of CD on the Q(j) lines is significantly smaller than on the S(j) lines.

The fact that the collisional broadening for the two rovibrational lines which differ only in the final spectroscopic state differs by a factor of two might be surprising. As it turns out, collisional widths of rovibrational lines in H$_2$ (both He- and self-perturbed) exhibit an unusually strong dependence on the vibrational quantum number (see, for example Fig. 6 in Ref. [17] or Fig. 4 in Ref. [6]). This is caused by a large contribution to the line broadening from the vibrational dephasing, which mainly originates from the difference between the isotropic parts of the PES in initial and final vibrational states. As discussed in Refs. [3,5,22], this difference increases for 0-υ transitions with υ. Apart from the dephasing part, there is also a significant difference in the inelastic contribution to the collisional broadening between the Q$_\upsilon$(1) and S$_\upsilon$(1) lines. The former have significantly smaller inelastic contribution to Γ_0, due to the fact that the first inelastic transition from either initial or final spectroscopic state is possible once the first inelastic channel becomes accessible (here, for $E_{\rm kin} \approx 500$cm^{-1}). On the other hand, for the S$_\upsilon$(1) line the inelastic contribution from the scattering in the final spectroscopic state ($\upsilon, J=3$) is non-zero even at very low kinetic energies. Moreover, the inelastic contribution increases with υ because the spacing between the rotational energy levels in a given vibrational state decreases with υ.

4.3. *Propagation of the uncertainties of the line-shape parameters on the residuals*

In the previous section, we demonstrate that an almost-6% change on the line-shape parameters can be introduced with the addition of the CD for the case of the 3-0 S(1) line, see Table 2. At the same time, in Fig. 2 we show that adding the CD improves the mean rRMSE for the 3-0 S(1) line by approximately 0.38% for the highest pressure (from 1.24% in Ref. [1] down to 0.86% in Fig. 2). In this section we explain this apparent inconsistency by analysing how the changes of the line-shape parameters propagate to the magnitude of the residuals. To do it, we directly simulate the line-shape profile for the original and corrected values of the line-shape parameters (the first and middle columns in Table 2, respectively) and we calculate rRMSE of the difference. All of the following discussion is made for the case of the 3-0 S(1) hydrogen line since CD, at this level of accuracy, has insignificant impact on the Q-branch lines [85].

The perturbations of Γ_0 and Δ_0 (by 5.65% and 2.06%, respectively) have the largest impact and change the profile by almost 2% for each of the two parameters in the high-pressure limit, see the top panel in Fig. 7. Curves overlapping with each other are a coincidence. For the case of our experiment, perturbations introduce an approximately 0.2% profile change (rRMSE) for the lowest and approximately 0.8% for the highest pressure. This is over 7 times less than the magnitude of the Γ_0 correction. As a reference for the numerical tests, we derive a simple analytical formula that describes propagation of the Γ_0 and Δ_0 uncertainties on the residuals for the case of the Lorentz Profile (LP), see Appendix A. The analytical values, which are valid in the high-pressure limit in which the profile is close to the LP, are shown in the top panel in

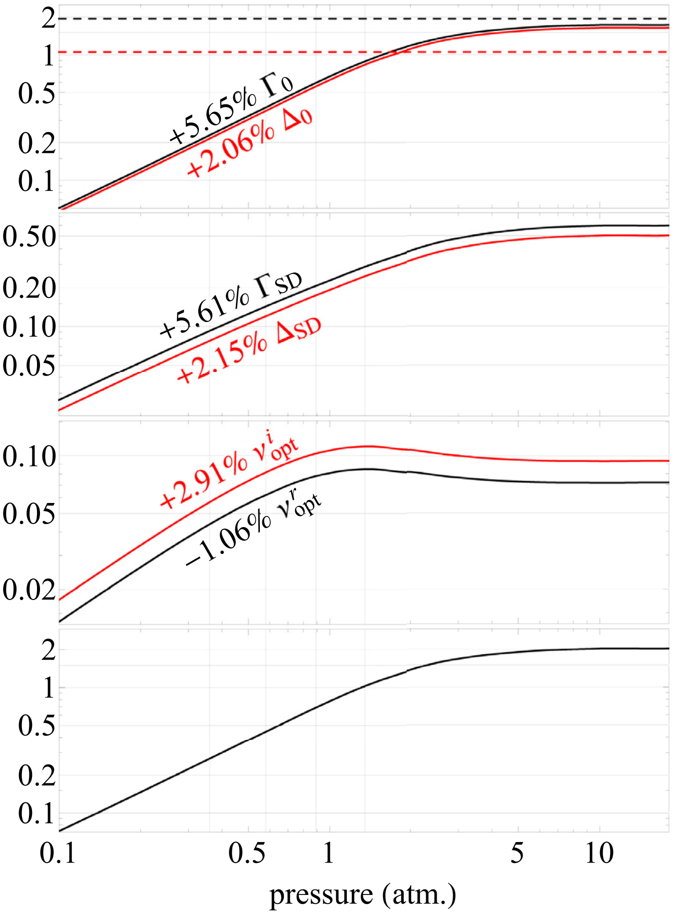

Fig. 7. Propagation of the uncertainties of the line-shape parameters on the residuals for the case of the He-perturbed 3-0 S(1) H_2 line. The vertical axis is rRMSE of the difference between the SDBBP generated for the uncorrected and centrifugal-distortion corrected values of the line-shape parameters (see Table 2). The first three panels show the results for the case when only one line-shape parameter is changed (see the labels in the plots). It is a coincidence that the two lines in the top panel overlap. The bottom panel shows the overall difference when all six line-shape parameters are changed. The dashed lines in the top panel are the analytical reference values (the same color notation as for solid lines), see Appendix A. The gray vertical lines correspond to the experimental pressures covered in this paper.

Table 2
Line-shape parameters for the 3-0 S(1) and 2-0 Q(1) H_2 lines, determined with our *ab initio* quantum-scattering calculations, using the BSP3 PES. Columns show the impact of the centrifugal distortion (CD) included in the calculations, showing both the line-shape parameter values and differences respective to the ones reported in Ref [1]. The calculations are done for $T = 296.6$ K for the 3-0 S(1) line and for $T = 294.2$ K for the 2-0 Q(1) line with the corresponding Doppler frequency equal to $\omega_D = 64.01 \times 10^{-3}$ cm^{-1} and 41.96×10^{-3} cm^{-1}, respectively. All the parameters are given in 10^{-3} cm^{-1} and are calculated for $n_p = 1$ amg.

		Ref. [1]	Ref. [1]+CD	Δ [%]
3-0 S(1) Line	Γ_0	11.72	12.38	5.65
	Δ_0	30.51	31.14	2.06
	Γ_{SD}	5.40	5.71	5.61
	Δ_{SD}	12.42	12.69	2.15
	ν^r_{opt}	37.96	37.56	−1.06
	ν^i_{opt}	−17.45	−17.96	2.91
2-0 Q(1) Line	Γ_0	5.74	5.75	0.17
	Δ_0	19.51	19.36	−0.77
	Γ_{SD}	2.68	2.68	0.00
	Δ_{SD}	8.06	8.00	−0.74
	ν^r_{opt}	41.64	41.65	0.02
	ν^i_{opt}	−11.31	−11.35	0.35

Fig. 7 as the dashed horizontal lines (black for Γ_0 and red for Δ_0). The full numerical values (solid lines in the top panel in Fig. 7) in the high-pressure limit are close to the analytical values. The slight difference is caused by the influence of the speed-dependent effects, the velocity-changing collisions, and the competition between them [70] that are present in our full line-shape model.

The perturbations of Γ_{SD} and Δ_{SD} have an approximately four-times smaller impact on the profile than the speed-averaged ones, with a maximum change of approximately 0.5% in the high-pressure limit and changes approximately 0.07% and 0.3% for lowest and highest experimental pressure, respectively, see the second panel in Fig. 7. The corrections of both ν^r_{opt} and ν^i_{opt} change the rRMSE by approximately 0.1% in the high-pressure limit and by approximately 0.05% and 0.1% for the low and high experimental pressures, respectively, see the third panel in Fig. 7. It is worth mentioning that for the differences introduced by the complex Dicke narrowing changes, the rRMSE curve has a different shape and has a maximum around 1.5 atm instead of an infinite pressure.

Introducing all corrections at once leads to an approximately 2% rRMSE change in the high-pressure limit, see the bottom panel in Fig. 7. For the case of our experiment, the changes are approximately 0.3% and 1% for the lowest and highest experimental pressure, which are impressively low taking into account the almost-6% magnitude of perturbations. The actual difference between residuals (from the theory-experiment comparison) for the cases with and without CD is even smaller than 0.3% and 1% for the lowest and highest experimental pressures. This is caused by the fact that the line intensity and linear baseline were fitted to the experimental data.

4.4. Relation of the present results with the previous works

It is true that the standard phenomenological models, taking into account the speed-dependent broadening and shift and complex Dicke-narrowing, with fitted parameters can provide a better representation of the data. Let us recall some recent works for the H_2 isotopologues. In Ref. [35] for a self-broadened D_2 line, it was shown that the SDBBP is able to fit experimental data within the experimental noise when all the parameters are adjusted. Fitting all the parameters leads to a significant improvement of the quality of the fit, however, some discrepancy between the parameters obtained from the fit and those from *ab initio* calculations was observed. In the case of the pressure broadening parameter it leads to a 14% deviation, while in the case of the parameter characterizing the speed dependence of the collisional width and shift, the deviation can even exceed an order of magnitude. Several D_2 lines from the same band were analyzed in Ref. [86] using the speed-dependent Nelkin-Ghatak profile (SDNGP) with a quadratic speed dependence of collisional broadening and shift. This profile was also able to fit the experimental data within the experimental noise when all the line-shape parameters were fitted. It should be pointed out, however, that the narrowing parameter obtained from the SDNGP fit differs by a factor of about 3 from the SDBBP fit. Also, SDNGP with a quadratic speed dependence of collisional broadening and shifting was applied to the H_2 lines in Ref. [35] and was able to fit experimental data within the experimental noise. The narrowing parameter obtained from this fit differs by a factor of 2 from the expected value and the speed dependence was overestimated (Γ_{SD} was larger than 2/3 Γ_0, which is unphysical). These examples as well as older works in literature considering H_2 lines clearly show that the phenomenological models can fit experimental data well, however, the physical meaning of the parameters is problematic. Therefore, in this work we are focused on a direct comparison of *ab initio* calculations and experimental data rather than on fitting some phenomenological line-shape profiles.

We would like to emphasize that in the present work we performed an advanced analysis of the H_2 spectra that has not been done before. Our analysis provides a deep physical understanding of the collisional effects imprinted in the shapes of the H_2 lines. The key result of the present work is shown in Fig. 3. In contrast to the previous works, here we analyze step-by-step the contribution of each of the six collisional line-shape effects. For instance, the blue line in Fig. 3b shows that the very strong speed dependence of the collisional shift is essential for an accurate description of the spectra. Furthermore, in Fig. 3 we demonstrate the importance of the contribution of the imaginary part of the Dicke parameter. We show that if we set the imaginary part of the Dicke parameter to zero, then the agreement between theory and experiment is a few times worse. In Fig. 3, we also demonstrate that all of these six collisional contributions have to be taken into account to reach this high agreement with experiment. This is a very interesting case in molecular spectroscopy. For most molecular species, the line shape is greatly dominated by one, two, or sometimes three contributions, and others are either completely negligible or have a small impact. Here, we were able to properly interpret all the collisional contributions in the case when all six effects play an important role.

5. Conclusion

In this work, we used the highly accurate experimental spectra of the 3-0 S(1) and 2-0 Q(1) molecular hydrogen absorption lines perturbed by helium to study collisional line-shape effects. We clearly distinguished the influence of six different collisional effects (i.e.: collisional broadening and shift, their speed dependencies, and the complex Dicke effect) on the shapes of the H_2 lines. We showed that only the specific combination of these six contributions, obtained from our *ab initio* calculations, gives unprecedentedly good agreement with experimental spectra. If any one of the six contributions is neglected, then the agreement between the experiment and theory worsens at least several times. We also included the centrifugal distortion in our *ab initio* calculations, which further improved the agreement with the experimental spectra.

Declaration of Competing Interest

The authors declare that they have no known competing financial interests or personal relationships that could have appeared to influence the work reported in this paper.

CRediT authorship contribution statement

Michał Słowiński: Methodology, Software, Validation, Formal analysis, Investigation, Writing – original draft, Writing – review & editing, Visualization. **Hubert Jóźwiak:** Methodology, Software, Validation, Formal analysis, Investigation, Writing – original draft, Writing – review & editing, Visualization. **Maciej Gancewski:** Software, Validation, Investigation. **Kamil Stankiewicz:** Software, Validation, Investigation. **Nikodem Stolarczyk:** Methodology, Validation, Investigation, Writing – original draft, Writing – review & editing, Visualization. **Yan Tan:** Investigation. **Jin Wang:** Investigation. **An-Wen Liu:** Investigation. **Shui-Ming Hu:** Investigation. **Samir Kassi:** Investigation. **Alain Campargue:** Investigation. **Konrad Patkowski:** Software, Investigation, Writing – review & editing. **Piotr S. Żuchowski:** Software, Investigation. **Roman Ciuryło:** Conceptualization, Methodology. **Franck Thibault:** Conceptualization, Methodology, Software, Validation. **Piotr Wcisło:** Conceptualization, Methodology, Validation, Writing – original draft, Writing – review & editing, Project administration.

Acknowledgments

M.S., M.G. and K.S. contributions are supported by the *A next-generation worldwide quantum sensor network with optical atomic clocks* project carried out within the TEAM IV Programme of the Foundation for Polish Science cofinanced by the European Union under the European Regional Development Fund. P.W. and H.J. contributions are supported by the National Science Centre, Poland, Project No. 2018/31/B/ST2/00720. N.S. contribution is supported by the National Science Centre, Poland, Project No. 2019/35/B/ST2/01118. S.-M.H. acknowledges the support from National Natural Science Foundation of China (21688102). S.K. and A.C. acknowledge funding support from the Agence Nationale de la Recherche (Equipex REFIMEVE+ANR-11-EQPX-0039). K.P. is supported by the U.S. National Science Foundation award CHE-1955328. The project is cofinanced by the Polish National Agency for Academic Exchange under the PHC Polonium program (dec. PPN/X/PS/318/2018). The research is part of the program of the National Laboratory FAMO in Toruń, Poland. It is also supported by the COST Action CM1405 MOLIM.

Appendix A

In this Appendix we derive analytical formulas representing the relative root-mean-square error (rRMSE) for the small perturbation of the broadening and shift parameters. By this analysis one can quantify how an error on the line-shape parameters propagates on the final spectral line-shape-profile accuracy. We utilize a simple example of the normalized Lorentz profile

$$L(\omega;\Gamma,\Delta)=\frac{1}{\pi}\frac{\Gamma}{\Gamma^2+(\omega-\Delta)^2}. \tag{A.1}$$

Perturbation of the broadening parameter

We analyze a small change of the broadening parameter $\Gamma\to\Gamma+\epsilon\Gamma$. The relative difference caused by the perturbance of the profile is

$$D_\Gamma(\omega;\epsilon\Gamma)=\frac{L(\omega;\Gamma+\epsilon\Gamma,\Delta)-L(\omega;\Gamma,\Delta)}{L(0;\Gamma,\Delta)}. \tag{A.2}$$

To quantify the error on the final line-shape profile, we utilize rRMSE at ± FWHM of the line center, which can be expressed as

$$rRMSE(\epsilon\Gamma)=\sqrt{\frac{1}{4\Gamma}\int_{-2\Gamma}^{2\Gamma}[D_\Gamma(\omega;\epsilon\Gamma)]^2d\omega}. \tag{A.3}$$

Because $L(0;\Gamma,\Delta)$ is independent on ω, one can calculate typical RMSE and divide it by $L(0;\Gamma,\Delta)$ to determine rRMSE as well.

Since our goal is only to quantify the errors, the actual position of the line is irrelevant and the vertical axis can be adjusted so that $\Delta=0$, which simplifies the further formulas. The integration in Eq. (A.3) can be analytically performed and, since we consider small perturbations of the line-shape parameters, expanded into a series, the linear term of which is

$$rRMSE(\epsilon\Gamma)\approx\frac{\sqrt{\frac{73}{15}+\frac{25\mathrm{atan}2}{2}}}{10}\frac{\epsilon\Gamma}{\Gamma}\approx0.433\frac{\epsilon\Gamma}{\Gamma}. \tag{A.4}$$

The above formula allows to estimate the rRMSE caused by the change $\epsilon\Gamma$ of broadening line-shape parameter, Γ.

Perturbation of the shift parameter

We repeat above discussion for the case of a small change of the shift parameter $\Delta\to\Delta+\epsilon\Delta$. The relative difference caused by the perturbance of the profile is

$$D_\Delta(\omega;\epsilon\Delta)=\frac{L(\omega;\Gamma,\Delta+\epsilon\Delta)-L(\omega;\Gamma,\Delta)}{L(0;\Gamma,\Delta)}. \tag{A.5}$$

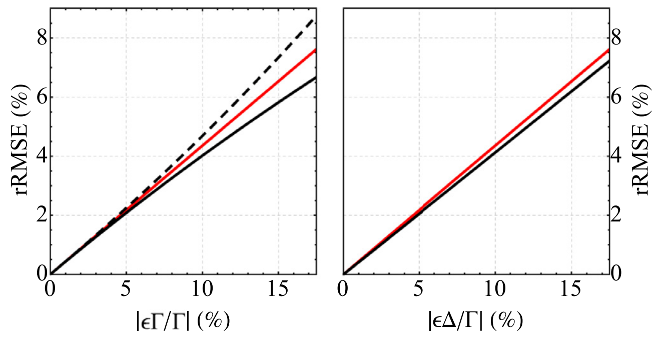

Fig. A1. The numerical validation of the analytical formulas for the relative root mean square errors (see text for more details). The black curves represent the numerical values and the red ones stand for analytical ones. Dashed and plain black curves of left panel corresponds to the negative and positive values of $\epsilon\Gamma/\Gamma$, respectively.

The same reason as mentioned before allows us to exclude Δ parameter and focus only on its distortion, i.e., $\epsilon\Delta$. Again, we quantify the error by calculating rRMSE at ±FWHM, which is

$$rRMSE(\epsilon\Delta) = \sqrt{\frac{1}{4\Gamma}\int_{-2\Gamma}^{2\Gamma}[D_{\Delta}(\omega;\epsilon\Delta)]^2 d\omega}. \tag{A.6}$$

Similarly, rRMSE can be determined by dividing typically calculated RMSE by $L(0;\Gamma,\Delta)$. The integral can be analytically performed, expanded into series and since we consider small perturbations again, approximated by linear term which is

$$rRMSE(\epsilon\Delta) \approx \frac{\sqrt{\frac{77}{15}+\frac{25\mathrm{atan}2}{2}}}{10}\frac{\epsilon\Delta}{\Gamma} \approx 0.436\frac{\epsilon\Delta}{\Gamma}. \tag{A.7}$$

The above formula allows to estimate the rRMSE caused by the change $\epsilon\Delta$ of shift line-shape parameter, Δ.

The direct comparison of the numerical results with Eqs. (A.4) and (A.7) is presented in Fig. A.1.

References

[1] Słowiński M, Thibault F, Tan Y, Wang J, Liu A-W, Hu S-M, Kassi S, Campargue A, Konefał M, Jóźwiak H, Patkowski K, Żuchowski P, Ciuryło R, Lisak D, Wcisło P. H_2-He collisions: *ab initio* theory meets cavity-enhanced spectra. Phys Rev A 2020;101(5):052705. doi:10.1103/physreva.101.052705.

[2] Bakr BW, Smith DGA, Patkowski K. Highly accurate potential energy surface for the He–H_2 dimer. J Chem Phys 2013;139(14):144305. doi:10.1063/1.4824299.

[3] Thibault F, Patkowski K, Żuchowski PS, Jóźwiak H, Ciuryło R, Wcisło P. Rovibrational line-shape parameters for H_2 in He and new H_2-He potential energy surface. J Quant Spectrosc Radiat Transf 2017;202:308–20. doi:10.1016/j.jqsrt.2017.08.014.

[4] Herzberg G, Howe LL. The Lyman bands of molecular hydrogen. Can J Phys 1959;37(5):636–59. doi:10.1139/p59-070.

[5] Thibault F, Wcisło P, Ciuryło R. A test of H_2-He potential energy surfaces. Eur Phys J D 2016;70(11):236. doi:10.1140/epjd/e2016-70114-9.

[6] Wcisło P, Gordon IE, Tran H, Tan Y, Hu S-M, Campargue A, Kassi S, Romanini D, Hill C, Kochanov RV, Rothman LS. The implementation of non-Voigt line profiles in the HITRAN database: H_2 case study. J Quant Spectrosc Radiat Transf 2016;177:75–91. doi:10.1016/j.jqsrt.2016.01.024.

[7] Perreault WE, Mukherjee N, Zare RN. Quantum control of molecular collisions at 1 kelvin. Science 2017;358(6361):356–9. doi:10.1126/science.aao3116.

[8] Perreault WE, Mukherjee N, Zare RN. Cold quantum-controlled rotationally inelastic scattering of HD with H_2 and D_2 reveals collisional partner reorientation. Nat Chem 2018;10(5):561–7. doi:10.1038/s41557-018-0028-5.

[9] Perreault WE, Mukherjee N, Zare RN. HD ($v = 1$, $j = 2$, m) orientation controls HD-He rotationally inelastic scattering near 1 K. J Chem Phys 2019;150(17):174301. doi:10.1063/1.5096531.

[10] Hout KVD, Hermans P, Mazur E, Knaap H. The broadening and shift of the ratational Raman lines for hydrogen isotopes at low temperatures. Physica A 1980;104(3):509–47. doi:10.1016/0378-4371(80)90012-6.

[11] Bragg SL, Smith WH, Brault JW. Line positions and strengths in the H_2 quadrupole spectrum. Astrophys J 1982;263:999. doi:10.1086/160568.

[12] Bischel WK, Dyer MJ. Temperature dependence of the Raman linewidth and line shift for the Q(1) and Q(0) transitions in normal and para–H_2. Phys Rev A 1986;33(5):3113–23. doi:10.1103/physreva.33.3113.

[13] Rahn LA, Rosasco GJ. Measurement of the density shift of the H_2 Q(0–5) transitions from 295 to 1000 K. Phys Rev A 1990;41(7):3698–706. doi:10.1103/physreva.41.3698.

[14] Rahn LA, Farrow RL, Rosasco GJ. Measurement of the self-broadening of the H_2 Q(0–5) Raman transitions from 295 to 1000 K. Phys Rev A 1991;43(11):6075–88. doi:10.1103/physreva.43.6075.

[15] Forsman JW, Bonamy J, Robert D, Berger JP, Saint-Loup R, Berger H. H_2-He vibrational line-shape parameters: measurement and semiclassical calculation. Phys Rev A 1995;52(4):2652–63. doi:10.1103/physreva.52.2652.

[16] Sinclair PM, Berger JP, Michaut X, Saint-Loup R, Chaux R, Berger H, Bonamy J, Robert D. Collisional broadening and shifting parameters of the Raman Q branch of H_2 perturbed by N_2 determined from speed-dependent line profiles at high temperatures. Phys Rev A 1996;54(1):402–9. doi:10.1103/physreva.54.402.

[17] Wcisło P, Thibault F, Stolarczyk N, Jóźwiak H, Słowiński M, Gancewski M, Stankiewicz K, Konefał M, Kassi S, Campargue A, Tan Y, Wang J, Patkowski K, Ciuryło R, Lisak D, Kochanov R, Rothman L, Gordon I. The first comprehensive dataset of beyond-Voigt line-shape parameters from ab initio quantum scattering calculations for the HITRAN database: He-perturbed H_2 case study. J Quant Spectrosc Radiat Transf 2021;260:107477. doi:10.1016/j.jqsrt.2020.107477.

[18] Hermans P, Die AV, Knaap H, Beenakker J. Measurements on the influence of binary collisions on the depolarized Rayleigh and rotational Raman lines for H_2-noble gas systems at low temperatures. Physica A 1985;132(2–3):233–52. doi:10.1016/0378-4371(85)90010-x.

[19] Blackmore R, Green S, Monchick L. Dicke narrowing of the polarized Stokes–Raman Q branch of the v=0→1 transition of D_2 in He. J Chem Phys 1989;91(7):3846–53. doi:10.1063/1.457640.

[20] Michaut X, Saint-Loup R, Berger H, Dubernet ML, Joubert P, Bonamy J. Investigations of pure rotational transitions of H_2 self-perturbed and perturbed by He. I. Measurement, modeling, and quantum calculations. J Chem Phys 1998;109(3):951–61. doi:10.1063/1.476638.

[21] Martínez RZ, Bermejo D, Thibault F, Wcisło P. Testing the ab initio quantum-scattering calculations for the D_2-He benchmark system with stimulated Raman spectroscopy. J Raman Spectrosc 2018;49(8):1339–49. doi:10.1002/jrs.5391.

[22] Jóźwiak H, Thibault F, Stolarczyk N, Wcisło P. Ab initio line-shape calculations for the S and O branches of H_2 perturbed by He. J Quant Spectrosc Radiat Transf 2018;219:313–22. doi:10.1016/j.jqsrt.2018.08.023.

[23] Thibault F, Martínez RZ, Bermejo D, Wcisło P. Line-shape parameters for the first rotational lines of HD in He. Mol Astrophys 2020;19:100063. doi:10.1016/j.molap.2020.100063.

[24] Morita M, Balakrishnan N. Stereodynamics of rotationally inelastic scattering in cold He+HD collisions. J Chem Phys 2020a;153(9):091101. doi:10.1063/5.0022190.

[25] Morita M, Balakrishnan N. Stereodynamics of ultracold rotationally inelastic collisions. J Chem Phys 2020b;153(18):184307. doi:10.1063/5.0030808.

[26] Stankiewicz K, Jóźwiak H, Gancewski M, Stolarczyk N, Thibault F, Wcisło P. Ab initio calculations of collisional line–shape parameters and generalized spectroscopic cross-sections for rovibrational dipole lines in HD perturbed by He. J Quant Spectrosc Radiat Transf 2020;254:107194. doi:10.1016/j.jqsrt.2020.107194.

[27] Komasa J, Piszczatowski K, Łach G, Przybytek M, Jeziorski B, Pachucki K. Quantum electrodynamics effects in rovibrational spectra of molecular hydrogen. J Chem Theory Comput 2011;7(10):3105–15. doi:10.1021/ct200438t.

[28] Feuchtgruber H, Lellouch E, Bézard B, Encrenaz T, de Graauw T, Davis GR. Detection of HD in the atmospheres of Uranus and Neptune: a new determination of the D/H ratio. Astron Astrophys 1999;341:L17–21. https://ui.adsabs.harvard.edu/abs/1999A&A...341L..17F

[29] Lellouch E, Bézard B, Fouchet T, Feuchtgruber H, Encrenaz T, de Graauw T. The deuterium abundance in Jupiter and Saturn from ISO-SWS observations. Astron Astrophys 2001;370(2):610–22. doi:10.1051/0004-6361:20010259.

[30] Lellouch E, Hartogh P, Feuchtgruber H, Vandenbussche B, de Graauw T, Moreno R, Jarchow C, Cavalié T, Orton G, Banaszkiewicz M, Blecka MI, Bockelée-Morvan D, Crovisier J, Encrenaz T, Fulton T, Küppers M, Lara LM, Lis DC, Medvedev AS, Rengel M, Sagawa H, Swinyard B, Szutowicz S, Bensch F, Bergin E, Billebaud F, Biver N, Blake GA, Blommaert JADL, Cernicharo J, Courtin R, Davis GR, Decin L, Encrenaz P, Gonzalez A, Jehin E, Kidger M, Naylor D, Portyankina G, Schieder R, Sidher S, Thomas N, de Val-Borro M, Verdugo E, Waelkens C, Walker H, Aarts H, Comito C, Kawamura JH, Maestrini A, Peacocke T, Teipen R, Tils T, Wildeman K. First results of Herschel-PACS observations of Neptune. Astron Astrophys 2010;518:L152. doi:10.1051/0004-6361/201014600.

[31] Feuchtgruber H, Lellouch E, Orton G, de Graauw T, Vandenbussche B, Swinyard B, Moreno R, Jarchow C, Billebaud F, Cavalié T, Sidher S, Hartogh P. The D/H ratio in the atmospheres of Uranus and Neptune from Herschel-PACS observations. Astron Astrophys 2013;551:A126. doi:10.1051/0004-6361/201220857.

[32] Smith WH. The H_2 4-0 S(0, 1,and 2) quadrupole features in Jupiter. Icarus 1989;81(2):429–40. doi:10.1016/0019-1035(89)90062-6.

[33] Baines KH, Mickelson ME, Larson LE, Ferguson DW. The abundances of methane and ortho/para hydrogen on Uranus and Neptune: implications of new laboratory 4-0 h_2 quadrupole line parameters. Icarus 1995;114(2):328–40. doi:10.1006/icar.1995.1065.

[34] Ciuryło R, Shapiro DA, Drummond JR, May AD. Solving the line-shape problem with speed-dependent broadening and shifting and with Dicke narrowing. II. Application. Phys Rev A 2002a;65(1):012502. doi:10.1103/physreva.65.012502.

[35] Wcisło P, Thibault F, Zaborowski M, Wójtewicz S, Cygan A, Kowzan G, Masłowski P, Komasa J, Puchalski M, Pachucki K, Ciuryło R, Lisak D. Accu-

rate deuterium spectroscopy for fundamental studies. J Quant Spectrosc Radiat Transf 2018;213:41–51. doi:10.1016/j.jqsrt.2018.04.011.

[36] Ciuryło R, Bielski A, Drummond JR, Lisak D, May AD, Pine AS, Shapiro DA, Szudy J, Trawiński RS. High-resolution studies on the influence of velocity-changing collisions on atomic and molecular line shapes. AIP Conf Proc, AIP 2002b. doi:10.1063/1.1525447.

[37] Lisak D, Hodges J, Ciuryło R. Comparison of semiclassical line-shape models to rovibrational H_2O spectra measured by frequency-stabilized cavity ring-down spectroscopy. Phys Rev A 2006;73(1):012507. doi:10.1103/physreva.73.012507.

[38] Hess S. Kinetic theory of spectral line shapes. The transition between doppler broadening and collisional broadening. Physica 1972;61(1):80–94. doi:10.1016/0031-8914(72)90035-3.

[39] Corey GC, McCourt FR. Dicke narrowing and collisional broadening of spectral lines in dilute molecular gases. J Chem Phys 1984;81(5):2318–29. doi:10.1063/1.447930.

[40] Monchick L, Hunter LW. Diatomic–diatomic molecular collision integrals for pressure broadening and Dicke narrowing: a generalization of Hess's theory. J Chem Phys 1986;85(2):713–18. doi:10.1063/1.451277.

[41] Berman PR. Speed-dependent collisional width and shift parameters in spectral profiles. J Quant Spectrosc Radiat Transf 1972;12(9):1331–42. doi:10.1016/0022-4073(72)90189-6.

[42] Pickett HM. Effects of velocity averaging on the shapes of absorption lines. J Chem Phys 1980;73(12):6090–4. doi:10.1063/1.440145.

[43] Pine A. Asymmetries and correlations in speed-dependent Dicke-narrowed line shapes of argon-broadened HF. J Quant Spectrosc Radiat Transf 1999;62(4):397–423. doi:10.1016/s0022-4073(98)00112-5.

[44] Rautian SG, Sobelman II. The effect of collisions on the Doppler broadening of spectral lines. Sov Phys Usp 1967;9(5):701–16. doi:10.1070/pu1967v009n05abeh003212.

[45] Demeio L, Green S, Monchick L. Effects of velocity changing collisions on line shapes of HF in Ar. J Chem Phys 1995;102(23):9160–6. doi:10.1063/1.468864.

[46] Schaefer J, Monchick L. Line broadening of HD immersed in He and H_2 gas. Astron Astrophys 1992;265(2):859–68. doi:10.1063/1.453612.

[47] Stolarczyk N, Thibault F, Cybulski H, Jóźwiak H, Kowzan G, Vispoel B, Gordon I, Rothman L, Gamache R, Wcisło P. Evaluation of different parameterizations of temperature dependences of the line-shape parameters based on ab initio calculations: case study for the HITRAN database. J Quant Spectrosc Radiat Transf 2020;240:106676. doi:10.1016/j.jqsrt.2019.106676.

[48] Kowzan G, Wcisło P, Słowiński M, Masłowski P, Viel A, Thibault F. Fully quantum calculations of the line-shape parameters for the Hartmann-Tran profile: A CO-Ar case study. J Quant Spectrosc Radiat Transf 2020;243:106803. doi:10.1016/j.jqsrt.2019.106803.

[49] Shafer R, Gordon RG. Quantum scattering theory of rotational relaxation and spectral line shapes in H_2–He gas mixtures. J Chem Phys 1973;58(12):5422–43. doi:10.1063/1.1679162.

[50] Ben-Reuven A. Symmetry considerations in pressure-broadening theory. Phys Rev 1966a;141(1):34–40. doi:10.1103/PhysRev.141.34.

[51] Ben-Reuven A. Impact broadening of microwave spectra. Phys Rev 1966b;145(1):7–22. doi:10.1103/PhysRev.145.7.

[52] Schaefer J, Monchick L. Line shape cross sections of HD immersed in HE and H_2 gas. I. Pressure broadening cross sections. J Chem Phys 1987;87(1):171–81. doi:10.1063/1.453612.

[53] Shapiro DA, Ciuryło R, Drummond JR, May AD. Solving the line-shape problem with speed-dependent broadening and shifting and with Dicke narrowing. I. Formalism. Phys Rev A 2002;65(1):012501. doi:10.1103/physreva.65.012501.

[54] Blackmore R. A modified Boltzmann kinetic equation for line shape functions. J Chem Phys 1987;87(2):791–800. doi:10.1063/1.453286.

[55] Smith EW, Cooper J, Chappell W, Dillon T. An impact theory for Doppler and pressure broadening II. Atomic and molecular systems. J Quant Spectrosc Radiat Transf 1971;11(10):1567–76. doi:10.1016/0022-4073(71)90114-2.

[56] Nienhuis G. Effects of the radiator motion in the classical and quantum-mechanical theories of collisional spectral-line broadening. J Quant Spectrosc Radiat Transf 1978;20(3):275–90. doi:10.1016/0022-4073(78)90133-4.

[57] Lindenfeld MJ. Self-structure factor of hard-sphere gases for arbitrary ratio of bath to test particle masses. J Chem Phys 1980;73(11):5817–29. doi:10.1063/1.440066.

[58] Liao PF, Bjorkholm JE, Berman PR. Effects of velocity-changing collisions on two-photon and stepwise-absorption spectroscopic line shapes. Phys Rev A 1980;21(6):1927–38. doi:10.1103/physreva.21.1927.

[59] Nelkin M, Ghatak A. Simple binary collision model for Van Hove's $G_s(r,t)$. Phys Rev 1964;135(1A):A4–9. doi:10.1103/PhysRev.135.A4.

[60] Wcisło P, Tran H, Kassi S, Campargue A, Thibault F, Ciuryło R. Velocity-changing collisions in pure H_2 and H_2-Ar mixture. J Chem Phys 2014;141(7):074301. doi:10.1063/1.4892414.

[61] Chapman S, Cowling TG. The mathematical theory of non-Uniform gases. Cambridge University Press; 1970.

[62] Hirshfelder JO, Curtiss CF, Bird RB. Nonequilibrium phenomena in polyatomic gases. Wiley; 1954.

[63] Taylor WL, Hurly JJ, Meyer BA, Dunlop PJ. Binary diffusion coefficients of helium/hydrogen isotope mixtures. J Chem Phys 1995;103(16):6959–65. doi:10.1063/1.470373.

[64] Jóźwiak H., Gancewski M., Grabowski A., Stankiewicz K., Wcisło P.. BIGOS computer code, to be published.

[65] Benner DC, Rinsland CP, Devi VM, Smith MAH, Atkins D. A multispectrum nonlinear least squares fitting technique. J Quant Spectrosc Radiat Transf 1995;53(6):705–21. doi:10.1016/0022-4073(95)00015-d.

[66] Humlíček J. An efficient method for evaluation of the complex probability function: The Voigt function and its derivatives. J Quant Spectrosc Radiat Transf 1979;21(4):309–13. doi:10.1016/0022-4073(79)90062-1.

[67] Schreier F. Optimized implementations of rational approximations for the Voigt and complex error function. J Quant Spectrosc Radiat Transf 2011;112(6):1010–25. doi:10.1016/j.jqsrt.2010.12.010.

[68] Duggan P, Sinclair P, Berman R, May A, Drummond JR. Testing lineshape models: measurements for v = 1–0 CO broadened by He and Ar. J Mol Spectrosc 1997;186(1):90–8. doi:10.1006/jmsp.1997.7420.

[69] Ngo N, Lisak D, Tran H, Hartmann JM. An isolated line-shape model to go beyond the Voigt profile in spectroscopic databases and radiative transfer codes. J Quant Spectrosc Radiat Transf 2013;129:89–100. doi:10.1016/j.jqsrt.2013.05.034.

[70] Wcisło P, Thibault F, Cybulski H, Ciuryło R. Strong competition between velocity-changing and phase- or state-changing collisions in H_2 spectra perturbed by Ar. Phys Rev A 2015;91(5):052505. doi:10.1103/physreva.91.052505.

[71] Farrow RL, Rahn LA, Sitz GO, Rosasco GJ. Observation of a speed-dependent collisional inhomogeneity in H_2 vibrational line profiles. Phys Rev Lett 1989;63(7):746–9. doi:10.1103/physrevlett.63.746.

[72] Joubert P, Bonamy J, Robert D, Domenech J-L, Bermejo D. A partially correlated strong collision model for velocity- and state-changing collisions. Application to Ar-broadened HF rovibrational line shape. J Quant Spectrosc Radiat Transf 1999;61(4):519–31. doi:10.1016/s0022-4073(98)00038-7.

[73] Ciuryło R, Pine A, Szudy J. A generalized speed-dependent line profile combining soft and hard partially correlated Dicke-narrowing collisions. J Quant Spectrosc Radiat Transf 2001;68(3):257–71. doi:10.1016/s0022-4073(00)00024-8.

[74] Lisak D, Rusciano G, Sasso A. Speed-dependent and correlation effects on the line shape of acetylene. Phys Rev A 2005;72(1):012503. doi:10.1103/physreva.72.012503.

[75] Lisak D, Cygan A, Bermejo D, Domenech J, Hodges J, Tran H. Application of the Hartmann–Tran profile to analysis of H_2O spectra. J Quant Spectrosc Radiat Transf 2015;164:221–30. doi:10.1016/j.jqsrt.2015.06.012.

[76] Marteau P, Boulet C, Robert D. Finite duration of collisions and vibrational dephasing effects on the Ar broadened HF infrared line shapes: asymmetric profiles. J Chem Phys 1984;80(8):3632–9. doi:10.1063/1.447184.

[77] Sheldon G, Sinclair P, Flohic ML, Drummond J, May A. Line mixing and broadening in the Raman Q branch of HD at 304.6 K. J Mol Spectrosc 1998;192(2):406–16. doi:10.1006/jmsp.1998.7696.

[78] Schaefer J, Köhler W. Quantum calculations of rotational and NMR relaxation, depolarized Rayleigh and rotational Raman line shapes for H_2(HD)-He mixtures. Physica A 1985;129(3):469–502. doi:10.1016/0378-4371(85)90181-5.

[79] Muchnick P, Russek A. The HeH_2 energy surface. J Chem Phys 1994;100(6):4336–46. doi:10.1063/1.466316.

[80] Boothroyd AI, Martin PG, Peterson MR. Accurate analytic He–H_2 potential energy surface from a greatly expanded set of ab initio energies. J Chem Phys 2003;119(6):3187–207. doi:10.1063/1.1589734.

[81] Meyer W, Hariharan PC, Kutzelnigg W. Refined ab initio calculation of the potential energy surface of the He–H_2 interaction with special emphasis to the region of the van der Waals minimum. J Chem Phys 1980;73(4):1880–97. doi:10.1063/1.440324.

[82] Tao FM. An accurate ab initio potential energy surface of the He–H_2 interaction. J Chem Phys 1994;100(7):4947–54. doi:10.1063/1.467214.

[83] Campargue A, Kassi S, Pachucki K, Komasa J. The absorption spectrum of H_2: CRDS measurements of the (2-0) band, review of the literature data and accurate ab initio line list up to 35000 cm^{-1}. Phys Chem Chem Phys 2012;14(2):802–15. doi:10.1039/c1cp22912e.

[84] Green S, Blackmore R, Monchick L. Comment on linewidths and shifts in the Stokes–Raman Q branch of D_2 in He. J Chem Phys 1989;91(1):52–5. doi:10.1063/1.457489.

[85] Dubernet M-L, Tuckey P. Raman Q and S line broadening and shifting coefficients: some commonly used assumptions revisited. Chem Phys Lett 1999;300(3–4):275–80. doi:10.1016/s0009-2614(98)01334-7.

[86] Mondelain D, Kassi S, Campargue A. Transition frequencies in the (2-0) band of D2 with MHz accuracy. J Quant Spectrosc Radiat Transf 2020;253:107020. doi:10.1016/j.jqsrt.2020.107020.

Journal of Quantitative Spectroscopy & Radiative Transfer 287 (2022) 108246

Contents lists available at ScienceDirect

Journal of Quantitative Spectroscopy & Radiative Transfer

journal homepage: www.elsevier.com/locate/jqsrt

Inhomogeneous broadening, narrowing and shift of molecular lines under frequent velocity-changing collisions

Nikodem Stolarczyk*, Piotr Wcisło, Roman Ciuryło

Institute of Physics, Faculty of Physics, Astronomy and Informatics, Nicolaus Copernicus University in Toruń, ul Grudziądzka 5, Toruń 87-100, Poland

ARTICLE INFO

Article history:
Received 7 December 2021
Revised 28 April 2022
Accepted 29 April 2022
Available online 2 May 2022

Keywords:
Molecular line shapes
Inhomogeneous broadening and shift
Velocity-changing collisions

ABSTRACT

We demonstrate that speed-dependent hard-collision profiles collapse into a simple Lorentz profile in the regime dominated by the velocity-changing collisions. We present simple analytical formulas for the effective width and shift of the Lorentzian, derived from the speed-dependent collisional broadening and shift. While the effective width increases with speed dependence of collisional shift, it is reduced by speed dependence of collisional width. On the other hand, the effective shift is modified by thermal average of speed dependence of the product of collisional width and shift. We validate these formula numerically applying the quadratic speed dependence of the collisional width and shift.

1. Introduction

Collisional line shapes often deviate significantly from the classical Voigt convolution of a pressure-induced Lorentzian profile and accounting for Doppler effect a Gaussian profile [1]. In such cases, a range of phenomenological [2–4] and *ab initio* [5–9] approaches have been developed to account for Dicke narrowing of the Doppler component caused by velocity-changing collisions [10–12], speed dependence of collisional width and shift [13,14], and correlation between velocity-changing and dephasing or state-changing collisions [15–17].

Particularly sensitive spectra for all these effects are those in molecular hydrogen [18–20]. The proper description of effective spectral line width appeared a challenging problem which finally was solved by realistic modeling [21] including a proper discrimination between velocity and speed changing collisions [22,23]. It was clear that, in the high pressure limit where the Doppler component of line width is suppressed by Dicke narrowing, the width of line caused by collisions depends on interplay between speed-dependence of collisional shift and frequency of the speed-changing collisions. Recently, it was tested numerically [24] that the collisional component of the line width can be described by guessed simple analytical expression for the case when velocity change is given by hard-collision model [11,15] and speed dependence of collisional shift is quadratic [25]. This expression was successfully used for interpretation of experimental data [26], however up to now no derivation of the analytical formulas was provided.

In this work, we analyze the properties of the speed-dependent hard collision profiles [27,28] in the regime of frequent velocity-changing collisions. We present analytical derivation of their collapse into a simple Lorentz profile and relate the effective width and shift of the Lorentzian, with the speed-dependent collisional broadening and shifting and the frequency of the velocity-changing collisions. While the broadening effect of the speed-dependent shift has been quantified phenomenologically [24,26], we provide its analytical derivation. We present the mechanism of line narrowing due to the speed dependence of collisional width. We also find that the thermal average of the speed dependence of both the broadening and shift influence the effective shift. We validate numerically that the effective width and shift converge asymptotically to our analytical formulas as the Dicke parameter becomes dominant.

2. High frequency of the velocity changing-collisions limit

A simple analytical description of molecular spectral lines can be provided within the hard-collision model [11,15,27,28]. Besides the Doppler broadening, the speed-dependent collisional width, $\Gamma(v)$, and shift, $\Delta(v)$, are taken into account [13,14], as well as the velocity changing collisions, having an effective complex optical frequency $\nu_{\mathrm{opt}} = \nu^{r}_{\mathrm{opt}} + i\nu^{i}_{\mathrm{opt}}$ [15,17]. The complex ν_{opt} semi-classically can be seen as result of correlation between velocity-changing and dephasing or state-changing collisions [3,15,29,30]. From quantum point of view it comes from overlap of perturber scattering wave functions in presence of absorbing molecule in states between which optical transition take place [31,32]. It can

---

* Corresponding author.
E-mail address: nikodemstolarczyk319@gmail.com (N. Stolarczyk).

https://doi.org/10.1016/j.jqsrt.2022.108246
0022-4073/

be provided by *ab initio* calculations of collisional line shape parameters [9,16,17].

The profile including speed dependent collisional broadening and shifting as well as velocity changing collisions described by hard collision model is called the speed-dependent Nelkin-Gathak profile (SDNGP) also known as the speed-dependent hard-collision profile (SDHCP) which with complex $\nu_{\rm opt}$ [15,29] was proposed by Pine [28] and can be written in the following form:

$$I(\omega) = {\rm Re}\left\{\frac{J(\omega)}{1-\nu_{\rm opt}\pi J(\omega)}\right\}, \tag{1}$$

where

$$J(\omega) = \frac{1}{\pi}\left\langle\left[\nu_{\rm opt} + \Gamma(v) - i(\omega-\omega_0-\vec{k}\cdot\vec{v}-\Delta(v))\right]^{-1}\right\rangle, \tag{2}$$

ω is the frequency of the absorbed radiation, ω_0 is the frequency of unperturbed molecular transition, $\vec{k}$ is wave vector corresponding to this frequency, and

$$\left\langle\dots\right\rangle = \int d^3\vec{v} f(\vec{v})\dots, \tag{3}$$

denotes averaging over Maxwell-Boltzmann distribution, $f(\vec{v}) = \left(\pi v_m^2\right)^{-3/2} e^{-v^2/v_m^2}$, of the absorber molecule velocity, $\vec{v}$, with $v_m = \sqrt{2k_BT/m}$ being the most probable speed of absorbers having mass m at gas temperature T, k_B is the Boltzmann constant. Here $\nu_{\rm opt}$ is approximated by its thermal average and is speed independent.

Analyzing properties of spectral line shape given by Eq. (1) at conditions where the optical frequency of the velocity changing collisions is dominating, i.e. $|\nu_{\rm opt}| \gg \left|\Gamma(v) - i(\omega-\omega_0-\vec{k}\cdot\vec{v}-\Delta(v))\right|$, we follow and extend the approach from appendix B of Shapiro paper [33]. We rewrite the main term in Eq. (2),

$$\begin{aligned}&\frac{1}{\nu_{\rm opt}+\Gamma(v)-i(\omega-\omega_0-\vec{k}\cdot\vec{v}-\Delta(v))}\\ &\quad= \frac{1}{\nu_{\rm opt}}\frac{1}{1+\frac{\Gamma(v)-i(\omega-\omega_0-\vec{k}\cdot\vec{v}-\Delta(v))}{\nu_{\rm opt}})}\\ &\quad\approx \frac{1}{\nu_{\rm opt}}\left(1-\frac{\Gamma(v)-i(\omega-\omega_0-\vec{k}\cdot\vec{v}-\Delta(v))}{\nu_{\rm opt}}\right.\\ &\quad\left.+\left(\frac{\Gamma(v)-i(\omega-\omega_0-\vec{k}\cdot\vec{v}-\Delta(v))}{\nu_{\rm opt}}\right)^2\right),\end{aligned} \tag{4}$$

using the Taylor expansion in power series, $(1+x)^{-1} \approx 1-x+x^2+\dots$ for $x \ll 1$. Inserting this approximated expression to Eq. (2), the thermal averaging needs to be done. For simplicity of this averaging it is convenient to group the terms present in Eq. (4) in the following way:

$$\begin{aligned}&\Gamma(v) - i\big(\omega-\omega_0-\vec{k}\cdot\vec{v}-\Delta(v)\big)\\ &\quad= (\Gamma_0 - i(\omega-\omega_0-\Delta_0)) + (\Gamma(\vec{v})-\Gamma_0)\\ &\quad+ i(\Delta(\vec{v})-\Delta_0) + i(\vec{k}\cdot\vec{v}),\end{aligned} \tag{5}$$

where

$$\begin{aligned}\Gamma_0 + i\Delta_0 &= \left\langle\Gamma(v)\right\rangle + i\left\langle\Delta(v)\right\rangle\\ &= \frac{4}{\sqrt{\pi}v_m^3}\int_0^\infty dv v^2 e^{-\frac{v^2}{v_m^2}}(\Gamma(v)+i\Delta(v))\end{aligned} \tag{6}$$

are the thermally-averaged collisional width and shift, respectively. Now one can take advantage from the fact that:

$$\left\langle\Gamma(v)-\Gamma_0\right\rangle = 0, \tag{7a}$$

$$\left\langle\Delta(v)-\Delta_0\right\rangle = 0, \tag{7b}$$

$$\left\langle\vec{k}\cdot\vec{v}\right\rangle = 0, \tag{7c}$$

$$\left\langle(\Gamma(v)-\Gamma_0)(\vec{k}\cdot\vec{v})\right\rangle = 0, \tag{7d}$$

$$\left\langle(\Delta(v)-\Delta_0)(\vec{k}\cdot\vec{v})\right\rangle = 0. \tag{7e}$$

The relevant non zero terms are the following:

$$\left\langle(\Gamma(v)-\Gamma_0)^2\right\rangle = \frac{4}{\sqrt{\pi}v_m^3}\int_0^\infty dv v^2 e^{-\frac{v^2}{v_m^2}}(\Gamma(v)-\Gamma_0)^2, \tag{8a}$$

$$\left\langle(\Delta(v)-\Delta_0)^2\right\rangle = \frac{4}{\sqrt{\pi}v_m^3}\int_0^\infty dv v^2 e^{-\frac{v^2}{v_m^2}}(\Delta(v)-\Delta_0)^2, \tag{8b}$$

$$\begin{aligned}&\left\langle(\Gamma(v)-\Gamma_0)(\Delta(v)-\Delta_0)\right\rangle\\ &\quad= \frac{4}{\sqrt{\pi}v_m^3}\int_0^\infty dv v^2 e^{-\frac{v^2}{v_m^2}}(\Gamma(v)-\Gamma_0)(\Delta(v)-\Delta_0),\end{aligned} \tag{8c}$$

$$\left\langle(\vec{k}\cdot\vec{v})^2\right\rangle = k^2\frac{1}{\sqrt{\pi}v_m}\int_{-\infty}^\infty dv_z v_z^2 e^{-\frac{v_z^2}{v_m^2}} = \frac{1}{2}k^2v_m^2 = \frac{1}{2}\omega_D^2, \tag{8d}$$

where $\omega_D = kv_m$ is related to Doppler width of the line [34]. In this way, one can rewrite Eq. (2) in the following form:

$$\begin{aligned}J(\omega) \approx \frac{1}{\pi\nu_{\rm opt}}&\left(1-\frac{1}{\nu_{opt}}(\Gamma_{\rm eff}-i(\omega-\omega_0-\Delta_{\rm eff}))\right.\\ &\left.+\frac{(\Gamma_0-i(\omega-\omega_0-\Delta_0))^2}{\nu_{\rm opt}^2}\right),\end{aligned} \tag{9}$$

where

$$\begin{aligned}\Gamma_{\rm eff}+i\Delta_{\rm eff} = \Gamma_0+i\Delta_0 &- \frac{\left\langle(\Gamma(v)-\Gamma_0)^2\right\rangle}{\nu_{\rm opt}} + \frac{\left\langle(\Delta(v)-\Delta_0)^2\right\rangle}{\nu_{\rm opt}}+\\ &+\frac{\left\langle(\vec{k}\cdot\vec{v})^2\right\rangle}{\nu_{\rm opt}} - 2i\frac{\left\langle(\Gamma(v)-\Gamma_0)(\Delta(v)-\Delta_0)\right\rangle}{\nu_{\rm opt}}.\end{aligned} \tag{10}$$

Finally, inserting Eq. (9) into Eq. (1) and leaving only the dominant term, one gets the spectral line shape in the form of the well-known Lorentz profile,

$$I(\omega) = \frac{1}{\pi}{\rm Re}\left\{\frac{1}{\Gamma_{\rm eff}-i(\omega-\omega_0-\Delta_{\rm eff})}\right\}. \tag{11}$$

The effective collisional width, $\Gamma_{\rm eff}$, and shift, $\Delta_{\rm eff}$, can be split into several components:

$$\Gamma_{\rm eff} = \Gamma_0 + \Gamma_\gamma + \Gamma_\delta + \Gamma_{\gamma\delta} + \Gamma_{\omega_D}, \tag{12a}$$

$$\Delta_{\rm eff} = \Delta_0 + \Delta_\gamma + \Delta_\delta + \Delta_{\gamma\delta} + \Delta_{\omega_D}, \tag{12b}$$

which are given by the following expressions:

$$\Gamma_\gamma = -\frac{\nu_{\rm opt}^r}{|\nu_{\rm opt}|^2}\left\langle(\Gamma(v)-\Gamma_0)^2\right\rangle, \tag{13a}$$

$$\Gamma_\delta = \frac{\nu_{\rm opt}^r}{|\nu_{\rm opt}|^2}\left\langle(\Delta(v)-\Delta_0)^2\right\rangle, \tag{13b}$$

$$\Gamma_{\gamma\delta} = -2\frac{\nu_{\rm opt}^i}{|\nu_{\rm opt}|^2}\left\langle(\Gamma(v)-\Gamma_0)(\Delta(v)-\Delta_0)\right\rangle, \tag{13c}$$

$$\Gamma_{\omega_D} = \frac{\nu_{\rm opt}^r}{|\nu_{\rm opt}|^2}\frac{\omega_D^2}{2}, \tag{13d}$$

$$\Delta_\gamma = \frac{\nu_{\rm opt}^i}{|\nu_{\rm opt}|^2}\left\langle(\Gamma(v)-\Gamma_0)^2\right\rangle, \tag{13e}$$

$$\Delta_\delta = -\frac{\nu^i_{\text{opt}}}{|\nu_{\text{opt}}|^2}\left\langle (\Delta(v)-\Delta_0)^2 \right\rangle, \tag{13f}$$

$$\Delta_{\gamma\delta} = -2\frac{\nu^r_{\text{opt}}}{|\nu_{\text{opt}}|^2}\left\langle (\Gamma(v)-\Gamma_0)(\Delta(v)-\Delta_0) \right\rangle, \tag{13g}$$

$$\Delta_{\omega_D} = -\frac{\nu^i_{\text{opt}}}{|\nu_{\text{opt}}|^2}\frac{\omega_D^2}{2}. \tag{13h}$$

Note that a collapse of the Dicke-narrowed profile into Lorentzian profile is a well-known effect and Eq. (13d), in the case of $\nu_{\text{opt}} = \nu^r_{\text{opt}}$ it can be found in Refs. [15,35].

For simplicity and consistency with original formulation of hard collision model [11] we kept ν_{opt} independent from the absorber speed. Appendix B presents the approach with speed-dependent $\nu_{\text{opt}}(v)$. It should be noted, however, that phenomenological incorporation of the speed dependence to $\nu_{\text{opt}}(v)$ can lead to results which do not agree with *ab initio* calculations as shown in Stolarczyk et al. [36].

3. Physical meaning of the contributions to the effective width and shift of the spectral line

To get an insight into the physical phenomena contributing to the effective Lorentzian width and shift, let us focus on the case when the optical frequency of velocity-changing collisions is real, i.e $\nu_{\text{opt}} = \nu^r_{\text{opt}}$ and $\nu^i_{\text{opt}} = 0$. In such case

$$\Gamma_{\text{eff}} = \Gamma_0 + \Gamma_\gamma + \Gamma_\delta + \Gamma_{\omega_D}, \tag{14a}$$

$$\Delta_{\text{eff}} = \Delta_0 + \Delta_{\gamma\delta}, \tag{14b}$$

and

$$\Gamma_\gamma = -\frac{1}{\nu_{\text{opt}}}\left\langle (\Gamma(v)-\Gamma_0)^2 \right\rangle, \tag{15a}$$

$$\Gamma_\delta = \frac{1}{\nu_{\text{opt}}}\left\langle (\Delta(v)-\Delta_0)^2 \right\rangle, \tag{15b}$$

$$\Gamma_{\omega_D} = \frac{1}{\nu_{\text{opt}}}\frac{\omega_D^2}{2}, \tag{15c}$$

$$\Delta_{\gamma\delta} = -2\frac{1}{\nu_{\text{opt}}}\left\langle (\Gamma(v)-\Gamma_0)(\Delta(v)-\Delta_0) \right\rangle. \tag{15d}$$

It is therefore seen that in Γ_{eff} the thermally averaged collisional width Γ_0 is reduced by Γ_γ, which represents the contribution from the variance of $\Gamma(v)$. On the other hand, the variance of $\Delta(v)$ leads to an increase of Γ_{eff} by Γ_δ. When the Doppler effect, accompanied by diffusive motion of the absorbers leads to the Lorentzian line shape (the so-called diffusive Dicke regime [10,35]), the effective Lorentzian width contains also the Doppler term, Γ_{ω_D}. Analyzing Δ_{eff}, we found that the thermally-averaged collisional shift, Δ_0 is modified by $\Delta_{\gamma\delta}$, which represents the contribution from the covariance of $\Gamma(v)$ and $\Delta(v)$.

The contributions: Γ_γ, Γ_δ, and $\Delta_{\gamma\delta}$ are proportional to the perturbers pressure, similarly to $\Gamma(v)$, $\Delta(v)$, Γ_0, Δ_0, or ν_{opt}. It is in contrast to Γ_{ω_D} which is inverse-proportional to the perturbers pressure and vanishes with increasing pressure. It is a well know result obtained by Dicke [10], see also Wittke and Dicke [35]. In the situation discussed here, all contributions to the effective width and shift are linear with the pressure of the perturbers, except the Γ_{ω_D} and Δ_{ω_D} which will vanish with the increasing pressure of the perturbers. Obviously Δ_{ω_D} will be present only if $\nu^i_{\text{opt}} \neq 0$, the case in more details considered in Appendix A.

To derive Eqs. (13a)–(13h) and Eqs. (15a)–(15d) we assumed that velocity-changing collisions are described by hard-collision model [11]. One of important quantity characterizing velocity-changing collisions is a ratio between frequencies of speed and velocity changing collisions [22,23,37]. For hard-collision model this ratio is equal to 1. It is almost the same like the value which can be obtain for more realistic billiard-ball model [38–40] with perturber mass equal to absorber mass [23,37]. Similar conclusion can be drawn from the classical molecular dynamics simulations (CMDS) [22,37]. Therefore, equations obtained in this paper should be applicable to systems in which perturber mass is comparable to absorber mass. Nevertheless, it should be noted that hard collision model, because of its simplicity, is often used in cases where perturber and absorber masses differ. The problem of collisional line shape collapse to Lorentz profile when perturber and absorber masses differ very significantly is out of the scope of this paper.

4. Quadratic approximation of the speed dependence of collisional width and shift

The experimental spectra are often analyzed approximating the speed dependence of collisional broadening and shift with a quadratic function [25]. Such simplification greatly improves the speed of evaluation of speed dependent hard collision profile known in this case as Hartmann-Tran profile [41]. The quadratic speed-dependent width and shift can be expressed in the following form:

$$\Gamma(v) = \Gamma_0 + \Gamma_2\left(\frac{v^2}{v_m^2} - \frac{3}{2}\right), \tag{16a}$$

$$\Delta(v) = \Delta_0 + \Delta_2\left(\frac{v^2}{v_m^2} - \frac{3}{2}\right), \tag{16b}$$

where Γ_2 and Δ_2 are the parameters describing magnitude of the speed-dependence of the collisional width and shift, respectively. To find the expressions for: $<(\Gamma(v)-\Gamma_0)^2>$, $<(\Delta(v)-\Delta_0)^2>$ and $<(\Gamma(v)-\Gamma_0)(\Delta(v)-\Delta_0)>$, the following integral needs to be calculated:

$$\frac{4}{\sqrt{\pi}}\int_0^\infty dv\frac{v^2}{v_m^3}e^{-\frac{v^2}{v_m^2}}\left(\frac{v^2}{v_m^2} - \frac{3}{2}\right)^2 = \\ = \frac{4}{\sqrt{\pi}}\int_0^\infty dv\frac{v^2}{v_m^3}e^{-\frac{v^2}{v_m^2}}\left(\frac{v^4}{v_m^4} - 3\frac{v^2}{v_m^2} + \frac{9}{4}\right) = \frac{3}{2}. \tag{17}$$

Consequently one gets

$$\left\langle (\Gamma(v)-\Gamma_0)^2 \right\rangle = \frac{3}{2}\Gamma_2^2, \tag{18a}$$

$$\left\langle (\Delta(v)-\Delta_0)^2 \right\rangle = \frac{3}{2}\Delta_2^2, \tag{18b}$$

$$\left\langle (\Gamma(v)-\Gamma_0)(\Delta(v)-\Delta_0) \right\rangle = \frac{3}{2}\Gamma_2\Delta_2. \tag{18c}$$

Finally, for the real ν_{opt}, using Eqs. (15a)–(15d) we find

$$\Gamma_\gamma = -\frac{3}{2}\frac{\Gamma_2^2}{\nu_{\text{opt}}}, \tag{19a}$$

$$\Gamma_\delta = \frac{3}{2}\frac{\Delta_2^2}{\nu_{\text{opt}}}, \tag{19b}$$

$$\Gamma_{\omega_D} = \frac{\omega_D^2}{2\nu_{\text{opt}}}, \tag{19c}$$

$$\Delta_{\gamma\delta} = -3\frac{\Gamma_2\Delta_2}{\nu_{\text{opt}}}. \tag{19d}$$

Therefore we presented a formal proof of Eq. (19b), which was given phenomenologically in [26].

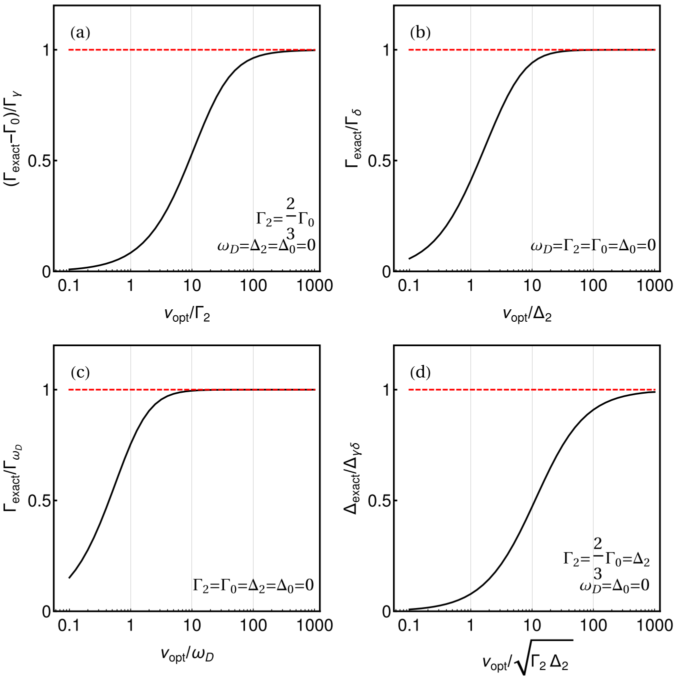

Fig. 1. Numerical verification of approximate formulas for Γ_γ, Γ_δ, Γ_{ω_D} and $\Delta_{\gamma\delta}$, Eqs. (19a)–(19d). In panels (a)–(c) we numerically evaluated the half width at half maximum, Γ_{exact}, of the profile given by Eq. (1), to compare their values with the $\Gamma_\gamma, \Gamma_\delta$ and Γ_{ω_D}, respectively. To test the formula for the effective shift, $\Delta_{\gamma\delta}$, we assumed the same values of the speed dependence parameters, Γ_2 and Δ_2, see panel (d). For the sake of clear presentation, we set the unnecessary parameters either to zero or to their lowest possible values, see the annotations in the figures. It is seen that the black curves converge to red dashed lines, which present the limits imposed by our analytical formulas as the role of the Dicke parameter becomes dominant.

5. Results

In this paper we considered the hard-collision line profile with the Dicke parameter being the dominant term, i.e., in the regime of very frequent velocity-changing collisions. In this regime the line-shape profile is given by Eq. (11) which can be expressed in the following form:

$$\mathrm{I}(\omega)=\frac{1}{\pi}\frac{\Gamma_{\mathrm{eff}}}{\Gamma_{\mathrm{eff}}^2+(\omega-\omega_0-\Delta_{\mathrm{eff}})^2}. \tag{20}$$

The parameters of this profile are described by Eqs. (14a) –(15d).

Applying the quadratic approximation allows one to simplify the contributions to the effective width and shift and relate them to the parameters Γ_2 and Δ_2, see Eqs. (19a)–(19d). Fig. 1 presents numerical test of these formulas. We simulated a series of synthetic hard-collision line-shape profiles, Eq. (1), and determined their half width at half maximum (HWHM) Γ_{exact}. It can be seen that the numerical Γ_{exact} converge to the corresponding approximate values from Eqs. (19a)–(19c), see panels (a)–(c). To test the formula for the effective shift, we simulated the hard-collision profiles with Eq. (1) and numerically evaluated the position of their peak Δ_{exact}. Panel (d) in Fig. 1 presents the efficiency of the approximate formula, Eq. (19d). As the role of the Dicke parameter becomes dominant, the black curves converge to red dashed lines, which present the limits imposed by our analytical formulas.

Moreover, we provide numerical validation of Eqs. (14a)–(14b) and (19a)–(19d) neglecting contribution of ν^i_{opt} for the example case of Q(1) 1-0 transition in H_2 perturbed by He in which ratio $\nu^i_{opt}/\nu^r_{opt}=-0.135$ differs from zero. In conditions not preferable for approximation used in this work, temperature 295 K and pressure of 1 atm, Γ_{eff} and Δ_{eff} reconstruct the exact values calculated for SDNGP with the inaccuracy of 15 % and 3.4 %, respectively, see. Tab. A.1 in Appendix A. As can be expected the approximation is more accurate in higher pressures, matching the exact results within 1.9 % for Γ_{eff} and 0.13 % for Δ_{eff} at 10 atm.

6. Conclusion

We presented that the speed-dependent hard-collision profiles collapse into a simple Lorentz profile in the regime dominated by the velocity-changing collisions. We presented simple analytical formulas for the effective width and shift of a Lorentzian, derived from the speed-dependent collisional broadening and shifting. We observed that, while the effective width increases with speed dependence of collisional shift, it is reduced by the speed dependence of collisional width. On the other hand, the effective shift is modified by thermal average of speed dependence of the product of collisional width and shift. Finally, we provided numerical validation of our formulas, applying the quadratic speed dependence of collisional width and shift.

Author agreement statement

We declare that this manuscript is original, has not been published before and is not currently being considered for publication elsewhere. We confirm that the manuscript has been read and approved by all named authors and that there are no other persons who satisfied the criteria for authorship but are not listed. We further confirm that the order of authors listed in the manuscript has been approved by all of us.

Declaration of Competing Interest

The authors declare that they have no known competing financial interests or personal relationships that could have appeared to influence the work reported in this paper.

Acknowledgements

N.S. was supported by Polish National Science Centre Project No. 2019/35/N/ST2/04145. P.W. was supported by Polish National Science Centre Project No. 2019/35/B/ST2/01118. The research is a part of the program of the National Laboratory FAMO in Toruń, Poland.

Appendix A. The role of the imaginary part of the Dicke narrowing parameter

Discussing the results in the main part of the paper, Secstions 3–5, we focused on the case when the imaginary part of the Dicke parameter could be neglected. However, as we show in Section 2 the presence of $\nu^i_{\mathrm{opt}}\neq 0$ changes the situation. In such case, the variances of $\Gamma(v)$ and $\Delta(v)$ contribute not only to the effective width, Γ_{eff}, but also to effective shift, Δ_{eff}, by Δ_γ and Δ_δ. Similarly, the covariance of $\Gamma(v)$ and $\Delta(v)$ contributes not only to the effective shift, Δ_{eff}, but also to effective width, Γ_{eff}, by $\Gamma_{\gamma\delta}$. Furthermore, the Doppler effect contributes to the effective shift, Δ_{eff}, by Δ_{ω_D}. The sign of all these contributions is related to the sign of ν^i_{opt}. The formulas taking into account both the real and imaginary parts of the Dicke parameter, as well as the quadratic approximation, can be obtained inserting Eqs. (18a)–(18c) into Eqs. (13a)–(13h):

$$\Gamma_\gamma=-\frac{3}{2}\frac{\nu^r_{\mathrm{opt}}}{|\nu_{\mathrm{opt}}|^2}\Gamma_2^2, \tag{A.1a}$$

$$\Gamma_\delta=\frac{3}{2}\frac{\nu^r_{\mathrm{opt}}}{|\nu_{\mathrm{opt}}|^2}\Delta_2^2, \tag{A.1b}$$

Table A1
The comparison of the SDNGP width (HWHM), $\Gamma_{\rm exact}$, and shift, $\Delta_{\rm exact}$, calculated numerically with the effective Lorentzian width (HWHM) $\Gamma_{\rm eff}$ and shift $\Delta_{\rm eff}$ calculated for two cases: $\nu^i_{\rm opt} \neq 0$ from Eqs. (12a)–(12b), (A.1a)–(A.1h) and for $\nu^i_{\rm opt} = 0$ from Eqs. (14a)-(14b), (19a)–(19d). Calculations for Q(1) 1-0 transition in H_2 perturbed by He under pressures 1, 10 and 100 atm, at $T = 295$ K with the SDNGP parameters obtained from the *ab initio* calculations [42]. All quantities in table are listed in units of 10^{-3} cm^{-1}.

	SDNGP parameters		
	1 atm	10 atm	100 atm
Γ_0	2.235	22.346	223.463
Δ_0	9.097	90.971	909.715
Γ_2	1.086	10.856	108.565
Δ_2	3.819	38.192	381.920
$\nu^r_{\rm opt}$	40.415	404.148	4041.480
$\nu^i_{\rm opt}$	-5.470	-54.697	-546.965
ω_D	21.659	21.659	21.659
$\Gamma_{\rm exact}$	7.466	27.388	268.764
$\Delta_{\rm exact}$	8.504	88.005	880.536

Lorentz profile parameters						
	1 atm		10 atm		100 atm	
	$\nu^i_{\rm opt} \neq 0$	$\nu^i_{\rm opt} = 0$	$\nu^i_{\rm opt} \neq 0$	$\nu^i_{\rm opt} = 0$	$\nu^i_{\rm opt} \neq 0$	$\nu^i_{\rm opt} = 0$
Γ_γ	-0.043	-0.044	-0.430	-0.437	-4.296	-4.375
Γ_δ	0.531	0.541	5.316	5.4137	53.163	54.137
$\Gamma_{\gamma\delta}$	0.041		0.409		4.091	
Γ_{ω_D}	5.725	5.830	0572	0.583	0.057	0.058
Δ_γ	-0.006		-0.058		-0.581	
Δ_δ	0.072		0.719		7.195	
$\Delta_{\gamma\delta}$	-0.302	-0.308	-3.022	-3.078	-30.225	-30.778
Δ_{ω_D}	0.774		0.077		0.008	
$\Gamma_{\rm eff}$	8.489	8.562	28.215	27.906	276.479	273.284
$\Delta_{\rm eff}$	9.636	8.789	88.688	87.894	886.112	878.937

$$\Gamma_{\gamma\delta} = -3\frac{\nu^i_{\rm opt}}{|\nu_{\rm opt}|^2}\Gamma_2\Delta_2, \tag{A.1c}$$

$$\Gamma_{\omega_D} = \frac{1}{2}\frac{\nu^r_{\rm opt}}{|\nu_{\rm opt}|^2}\omega_D^2, \tag{A.1d}$$

$$\Delta_\gamma = \frac{3}{2}\frac{\nu^i_{\rm opt}}{|\nu_{\rm opt}|^2}\Gamma_2^2, \tag{A.1e}$$

$$\Delta_\delta = -\frac{3}{2}\frac{\nu^i_{\rm opt}}{|\nu_{\rm opt}|^2}\Delta_2^2, \tag{A.1f}$$

$$\Delta_{\gamma\delta} = -3\frac{\nu^r_{\rm opt}}{|\nu_{\rm opt}|^2}\Gamma_2\Delta_2, \tag{A.1g}$$

$$\Delta_{\omega_D} = -\frac{1}{2}\frac{\nu^i_{\rm opt}}{|\nu_{\rm opt}|^2}\omega_D^2. \tag{A.1h}$$

To provide a quantitative reference, we use an example of Q(1) 1-0 line of H_2 perturbed by He. The *ab initio* values of the SDNGP parameters for this line under normal pressure at $T = 295$ K are taken from Ref. [42]. We use these parameters to calculate individual contributions to the effective Lorenzian width, $\Gamma_{\rm eff}$, and shift, $\Delta_{\rm eff}$, given by Eqs. (A.1a)–(A.1h) for the case where $\nu^i_{\rm opt} \neq 0$ and Eqs. (19a)–(19d) for the case in which we set $\nu^i_{\rm opt} = 0$. Table A.1 gathers those parameters and calculated results for the line under consideration. In this case, neglecting the $\nu^i_{\rm opt}$ has no significant effect on the effective Lorentzian width, $\Gamma_{\rm eff}$. On the other hand, $\nu^i_{\rm opt}$ has noticeable impact on the $\Delta_{\rm eff}$ coming from Doppler contribution Δ_{ω_D}. This contribution, however, vanishes with increasing pressure of perturbers.

It is worth to notice that the *ab-initio*-calculated $-\nu^i_{\rm opt}$ is two times smaller than the Δ_0 [36]. It is in contrast with the fully correlated model given by Rautian and Sobelmann [15]. It can, however, be understood in terms of partial-correlations [15,28–30]. In description given in the appendix of Ref. [3] one can see that the part of collisional shift contributing to the complex narrowing parameter, Eq. (A.19) in Ref. [3], can be significantly smaller than the total collisional shift in Eq. (A.17) in Ref. [3].

Appendix B. The role of the speed-dependence of the Dicke narrowing parameter

Using oversimplified models of the speed-dependence of $\nu_{\rm opt}(v)$ [41] can lead to qualitative deviations from the actual, *ab initio* one [36]. Therefore, we prefer to disregard the speed-dependence instead of using the incorrect one. On the other hand, if available, either the *ab initio* $\nu_{\rm opt}(v)$ or its quadratic approximation should be taken into consideration.

Considering the complex speed-dependent $\nu_{\rm opt}(v)$, the line profile can be written following Pine [28]:

$$I(\omega) = \mathrm{Re}\left\{\frac{J(\omega)}{1 - \pi G(\omega)}\right\}, \tag{B.1}$$

where

$$J(\omega) = \frac{1}{\pi}\left\langle\frac{1}{\nu_{\rm opt}(v) + \Gamma(v) - i(\omega - \omega_0 - \vec{k}\cdot\vec{v} - \Delta(v))}\right\rangle, \tag{B.2}$$

and

$$G(\omega) = \frac{1}{\pi}\left\langle\frac{\nu_{\rm opt}(v)}{\nu_{\rm opt}(v) + \Gamma(v) - i(\omega - \omega_0 - \vec{k}\cdot\vec{v} - \Delta(v))}\right\rangle. \tag{B.3}$$

It is convenient to denote $\nu_{\rm opt}$ as the thermally-averaged $\nu_{\rm opt}(v)$,

$$\left\langle\nu_{\rm opt}(v)\right\rangle = \nu_{\rm opt}, \tag{B.4}$$

In addition, we note that,

$$\left\langle\nu_{\rm opt}(v) - \nu_{\rm opt}\right\rangle = 0 \tag{B.5}$$

and

$$\left\langle(\nu_{\rm opt}(v) - \nu_{\rm opt})(\vec{k}\cdot\vec{v})\right\rangle = 0. \tag{B.6}$$

The subsequent derivations can be performed in a similar way to the ones in Section 2. The terms from Eqs. (B.2) and (B.2) can be rewritten in the following form:

$$\begin{aligned}
&\frac{1}{\nu_{\rm opt}(v) + \Gamma(v) - i(\omega - \omega_0 - \vec{k}\cdot\vec{v} - \Delta(v))} \\
&= \frac{1}{\nu_{\rm opt}}\frac{1}{\left(1 + \frac{\nu_{\rm opt}(v) - \nu_{\rm opt} + \Gamma(v) - i(\omega - \omega_0 - \vec{k}\cdot\vec{v} - \Delta(v)}{\nu_{\rm opt}}\right)} \\
&\approx \frac{1}{\nu_{\rm opt}}\left\{1 - \frac{\nu_{\rm opt}(v) - \nu_{\rm opt} + \Gamma(v) - i(\omega - \omega_0 - \vec{k}\cdot\vec{v} - \Delta(v))}{\nu_{\rm opt}}\right. \\
&\quad\left. + \left(\frac{\nu_{\rm opt}(v) - \nu_{\rm opt} + \Gamma(v) - i\left(\omega - \omega_0 - \vec{k}\cdot\vec{v} - \Delta(v)\right)}{\nu_{\rm opt}}\right)^2\right\}
\end{aligned} \tag{B.7}$$

and

$$\begin{aligned}
&\frac{\nu_{\rm opt}(v)}{\nu_{\rm opt}(v) + \Gamma(v) - i\left(\omega - \omega_0 - \vec{k}\cdot\vec{v} - \Delta(v)\right)} \\
&= \frac{1}{\nu_{\rm opt}}\frac{\nu_{\rm opt}\left(1 + \frac{\nu_{\rm opt}(v) - \nu_{\rm opt}}{\nu_{\rm opt}}\right)}{\left(1 + \frac{\nu_{\rm opt}(v) - \nu_{\rm opt} + \Gamma(v) - i(\omega - \omega_0 - \vec{k}\cdot\vec{v} - \Delta(v)}{\nu_{\rm opt}}\right)}
\end{aligned}$$

$$\approx \left(1+\frac{\nu_{\mathrm{opt}}(v)-\nu_{\mathrm{opt}}}{\nu_{\mathrm{opt}}}\right) \left\{1-\frac{\nu_{\mathrm{opt}}(v)-\nu_{\mathrm{opt}}+\Gamma(v)-i\left(\omega-\omega_0-\vec{k}\cdot\vec{v}-\Delta(v)\right)}{\nu_{\mathrm{opt}}} + \left(\frac{\nu_{\mathrm{opt}}(v)-\nu_{\mathrm{opt}}+\Gamma(v)-i\left(\omega-\omega_0-\vec{k}\cdot\vec{v}-\Delta(v)\right)}{\nu_{\mathrm{opt}}}\right)^2\right\}. \tag{B.8}$$

The second expression can be further reduced to

$$\frac{\nu_{\mathrm{opt}}(v)}{\nu_{\mathrm{opt}}(v)+\Gamma(v)-i\left(\omega-\omega_0-\vec{k}\cdot\vec{v}-\Delta(v)\right)} \approx 1-\frac{\Gamma(v)-i\left(\omega-\omega_0-\vec{k}\cdot\vec{v}-\Delta(v)\right)}{\nu_{\mathrm{opt}}} + \left(\frac{\nu_{\mathrm{opt}}(v)-\nu_{\mathrm{opt}}+\Gamma(v)-i\left(\omega-\omega_0-\vec{k}\cdot\vec{v}-\Delta(v)\right)}{\nu_{\mathrm{opt}}}\right)^2 - \frac{\nu_{\mathrm{opt}}(v)-\nu_{\mathrm{opt}}}{\nu_{\mathrm{opt}}} \left(\frac{\nu_{\mathrm{opt}}(v)-\nu_{\mathrm{opt}}+\Gamma(v)-i\left(\omega-\omega_0-\vec{k}\cdot\vec{v}-\Delta(v)\right)}{\nu_{\mathrm{opt}}}\right). \tag{B.9}$$

Inserting these formulas into Eqs. (B.2) and (B.2), taking the thermal average and leaving leading therms leads to:

$$J(\omega) \approx \frac{1}{\pi\,\nu_{\mathrm{opt}}}, \tag{B.10}$$

and

$$G(\omega) \approx \frac{1}{\pi}\left(1-\frac{1}{\nu_{opt}}\left(\Gamma_{\mathrm{eff}}-i(\omega-\omega_0-\Delta_{\mathrm{eff}})\right)\right). \tag{B.11}$$

With those approximations we reduce the line shape, Eq. (B.1), to Lorentz profile, Eq. (11), with the following effective width and shift:

$$\Gamma_{\mathrm{eff}}+i\Delta_{\mathrm{eff}} = \Gamma_0+i\Delta_0-\frac{\left\langle(\Gamma(v)-\Gamma_0)^2\right\rangle}{\nu_{\mathrm{opt}}}+\frac{\left\langle(\Delta(v)-\Delta_0)^2\right\rangle}{\nu_{\mathrm{opt}}}+ +\frac{\left\langle(\vec{k}\cdot\vec{v})^2\right\rangle}{\nu_{\mathrm{opt}}}-\frac{\left\langle(\nu_{\mathrm{opt}}(v)-\nu_{\mathrm{opt}})(\Gamma(v)-\Gamma_0)\right\rangle}{\nu_{\mathrm{opt}}} -2i\frac{\left\langle(\Gamma(v)-\Gamma_0)(\Delta(v)-\Delta_0)\right\rangle}{\nu_{\mathrm{opt}}} -i\frac{\left\langle(\nu_{\mathrm{opt}}(v)-\nu_{\mathrm{opt}})(\Delta(v)-\Delta_0)\right\rangle}{\nu_{\mathrm{opt}}}. \tag{B.12}$$

In addition to the terms present in Eq. (10), this expression also has terms involving covariances, $<(\nu_{\mathrm{opt}}(v)-\nu_{\mathrm{opt}})(\Gamma(v)-\Gamma_0)>$ and $<(\nu_{\mathrm{opt}}(v)-\nu_{\mathrm{opt}})(\Delta(v)-\Delta_0)>$. However, the variance $<(\nu_{\mathrm{opt}}(v)-\nu_{\mathrm{opt}})^2>$ is absent in Eq. (B.12). When $\nu_{\mathrm{opt}}(v)$ is approximated by quadratic formula

$$\nu_{\mathrm{opt}}(v) = \nu_{\mathrm{opt}}+\nu_{\mathrm{opt},2}\left(\frac{v^2}{v_m^2}-\frac{3}{2}\right) \tag{B.13}$$

the covariances:

$$\left\langle(\nu_{\mathrm{opt}}(v)-\nu_{\mathrm{opt}})(\Gamma(v)-\Gamma_0)\right\rangle = \frac{3}{2}\nu_{\mathrm{opt},2}\Gamma_2, \tag{B.14a}$$

and

$$\left\langle(\nu_{\mathrm{opt}}(v)-\nu_{\mathrm{opt}})(\Delta(v)-\Delta_0)\right\rangle = \frac{3}{2}\nu_{\mathrm{opt},2}\Delta_2. \tag{B.14b}$$

be expressed in terms of parameters $\nu_{\mathrm{opt},2}$, Γ_2, and Δ_2.

References

[1] Hartmann J-M, Boulet C, Robert D. Collisional effects on molecular spectra: laboratory experiments and model, consequences for applications. Amsterdam: Elsevier; 2008.

[2] Lance B, Robert D. An analytical model for collisional effects on spectral line shape from the doppler to the collision regime. J Chem Phys 1999;109:8283. 1998; 111, 789

[3] Ciuryło R, Pine AS, Szudy J. A generalized speed-dependent line profile combining soft and hard partially correlated Dicke-narrowing collisions. J Quant Spectrosc Radiat Transf 2001;68:257–71.

[4] Tran H, Hartmann J-M, Chaussard F, Gupta M. An isolated line-shape model based on the Keilson–Storer function for velocity changes. II. Molecular dynamics simulations and the q(1) lines for pure h$_2$. J Chem Phys 2009;131:154303–9.

[5] Blackmore R. A modified Boltzmann kinetic equation for line shape functions. J Chem Phys 1987;87:791–800.

[6] Ciuryło R, Shapiro DA, Drummond JR, May AD. Solving the line-shape problem with speed-dependent broadening and shifting and with Dicke narrowing. II. Aapplication. Phys Rev A 2002;65:012502–8.

[7] Hartmann J-M, Tran H, Ngo NH, Landsheere X, Chelin P, Lu Y, Liu A-W, Hu S-M, Gianfrani L, Casa G, Castrillo A, Lepère M, Delière Q, Dhyne M, Fissiaux L. *Ab initio* calculations of the spectral shapes of CO$_2$ isolated lines including non-Voigt effects and comparisons with experiments. Phys Rev A 2013;87:013403–11.

[8] Wcisło P, Thibault F, Zaborowski M, Wójtewicz S, Cygan A, Kowzan G, Masłowski P, Komasa J, Puchalski M, Pachucki K, Ciuryło R, Lisak D. Accurate deuterium spectroscopy for fundamental studies. J Quant Spectrosc Radiat Transf 2018;213:41–51.

[9] Słowiński M, Thibault F, Tan Y, Wang J, Liu A-W, Hu S-M, Kassi S, Campargue A, Konefał M, Jóźwiak H, Patkowski K, Żuchowski P, Ciuryło R, Lisak D, Wcisło P. H$_2$-He collisions: *ab initio* theory meets cavity-enhanced spectra. Phys Rev A 2020;65:052705–7.

[10] Dicke R. The effect of collisions upon the Doppler width of spectral lines. Phys Rev 1953;89:472–3.

[11] Nelkin M, Ghatak A. Simple binary collision model for van Hove's $G_s(r,\ t)$. Phys Rev 1964;135:A4–9.

[12] Galatry L. Simultaneous effect of Doppler and foreign gas broadening on spectral lines. Phys Rev 1961;122:1218–23.

[13] Berman PR. Speed-dependent collisional width and shift parameters in spectral profiles. J Quant Spectrosc Radiat Transf 1972;12:1331–42.

[14] Ward J, Cooper J, Smith EW. Correlation effects in the theory of combined Doppler and pressure broadening - I. Classical theory. J Quant Spectrosc Radiat Transf 1974;14:555–90.

[15] Rautian SG, Sobelman II. Usp Fiz Nauk 90, 209 (1966) [Sov Phys Usp 9, 701 (1967)].

[16] Hess S. Kinetic theory of spectral line shapes. The transition between Doppler broadening and collisional broadening. Physica 1972;61:80–94.

[17] Demeio L, Green S, Monchick L. Effects of velocity changing collisions on line shapes of HF in Ar. J Chem Phys 1995;102:9160–6.

[18] Farrow RL, Rahn LA, Sitz GO, Rosasco GJ. Observation of a speed-dependent collisional inhomogeneity in H$_2$ vibrational line profiles. Phys Rev Lett 1989;63:746–9.

[19] Berger JP, Saint-Loup R, Berger H, Bonamy J, Robert D. Measurement of vibrational line profiles in H$_2$–rare-gas mixtures: determination of the speed dependence of the line shift. Phys Rev A 1994;49:3396–406.

[20] Chaussard F, Michaut X, Saint-Loup R, Berger H, Joubert P, Lance B, et al. Collisional effects on spectral line shape from the Doppler to the collisional regime: a rigorous test of a unified model. J Chem Phys 2000;112:158–66.

[21] Wcisło P, Thibault F, Cybulski H, Ciuryło R. Strong competition between velocity-changing and phase- or state-changing collisions in H$_2$ spectra perturbed by Ar. Phys Rev A 2015;91:052505.

[22] Hoang PNM, Joubert P, Robert D. Speed-dependent line-shape models analysis from molecular dynamics simulations: the collision regime. Phys Rev A 2002;65 012507-6.

[23] Ciuryło R, Lisak D, Szudy J. Role of velocity- and speed-changing collisions on speed-dependent line shapes of H$_2$. Phys Rev A 2002;66:032701–3.

[24] Wcisło P, Gordon IE, Tran H, Tan Y, Hu S-M, Campargue A, Kassi S, Romanini D, Hill C, Kochanov RV, Rothman LS. The implementation of non-Voigt line profiles in the HITRAN database: H$_2$ case study. J Quant Spectrosc Radiat Transfer 2016;177:75–91.

[25] Rohart F, Mäder H, Nicolaisen H-W. Speed dependence of rotational relaxation induced by foreign gas collisions: studies on CH$_3$F by millimeter wave coherent transients. J Chem Phys 1994;101:6475–86.

[26] Martínez RZ, Bermejo D, Thibault F, Wcisło P. Testing the ab initio quantum-scattering calculations for the D$_2$–He benchmark system with stimulated raman spectroscopy. J Raman Spectrosc 2018;49:1339–49.

[27] Lance B, Blanquet G, Walrand J, Bouanich J-P. On the speed-Dependent hard collision lineshape models: application to C$_2$H$_2$ perturbed by Xe. J Mol Spectrosc 1997;185:262–71.

[28] Pine AS. Asymmetries and correlations in speed-dependent Dicke-narrowed line shapes of argon-broadened HF. J Quant Spectrosc Radiat Transf 1999;62:397–423.

[29] Pine AS. Line shape asymmetries in Ar-broadened HF(v=1–0) in the Dicke-narrowing regime. J Chem Phys 1994;101(5):3444–52. doi:10.1063/1.467529.

[30] Joubert P, Bonamy J, Robert D, Doménech JL, Bermejo D. A partially corre-

lated strong collision model for velocity-and state-changing collisions application to ar-broadened hf rovibrational line shape. J Quant Spectrosc Radiat Transf 1999;61:519–31. doi:10.1016/S0022-4073(98)00038-7.

[31] Nienhuis G. Effects of the radiator motion in the classical and quantum-mechanical theories of collisional spectral-line broadening. J Quant Spectrosc Radiat Transf 1978;20:275–90.

[32] Berman PR, Mossberg TW, Hartmann SR. Collision kernels and laser spectroscopy. Phys Rev A 1982;25:2550–71.

[33] Shapiro DA, Ciuryło R, Jaworski R, May AD. Modeling the spectral line shapes with speed-dependent broadening and Dicke narrowing. Can J Phys 2001;79:1209–22.

[34] Ciuryło R. Shapes of pressure- and Doppler-broadened spectral lines in the core and near wings. Phys Rev A 1998;58:1029–39.

[35] Wittke JP, Dicke RH. Redetermination of the hyperfine splitting in the ground state of atomic hydrogen. Phys Rev 1956;103:620–31.

[36] Stolarczyk N, Thibault F, Cybulski H, Jóźwiak H, Kowzan G, Vispoel B, Gordon IE, Rothman L, Gamache R, Wcisło P. Evaluation of different parameterizations of temperature dependences of the line-shape parameters based on *ab initio* calculations: case study for the HITRAN database. J Quant Spectrosc Radiat Transf 2020;240 106676-18.

[37] Wcisło P, Tran H, Kassi S, Campargue A, Thibault F, Ciuryło R. Velocity-changing collisions in pure H_2 and H_2-Ar mixture. J Chem Phys 2014;141:074301–14.

[38] Lindenfeld MJ, Shizgal B. Matrix elements of the Boltzmann collision operator for gas mixtures. Chem Phys 1979;41:81–95.

[39] Lindenfeld MJ. Self-structure factor of hard-sphere gases for arbitrary ratio of bath to test particle masses. J Chem Phys 1980;73:5817–29.

[40] Liao PF, Bjorkholm JE, Berman PR. Effects of velocity-changing collisions on two-photon and stepwise-absorption spectroscopic line shapes. Phys Rev 1980;21:1927–38.

[41] Ngo NH, Lisak D, Tran H, Hartmann J-M. An isolated line-shape model to go beyond the Voigt profile in spectroscopic databases and radiative transfer codes. J Quant Spectrosc Radiat Transf 2013;129:89–100. doi:10.1016/j.jqsrt.2013.05.034.

[42] Wcisło P, Thibault F, Stolarczyk N, Jóźwiak H, Słowiński M, Gancewski M, Stankiewicz K, Konefał M, Kassi S, Campargue A, Tan Y, Wang J, Patkowski K, Ciuryło R, Lisak D, Kochanov R, Rothman L, Gordon I. The first comprehensive dataset of beyond-Voigt line-shape parameters from *ab initio* quantum scattering calculations for the HITRAN database: he-perturbed h_2 case study. J Quant Spectrosc Radiat Transf 2021;260:107477.

PHYSICAL REVIEW A **108**, 032810 (2023)

Spectral line shape in the limit of frequent velocity-changing collisions

Nikodem Stolarczyk,* Piotr Wcisło, and Roman Ciuryło
Institute of Physics, Faculty of Physics, Astronomy and Informatics,
Nicolaus Copernicus University in Toruń, ul Grudziądzka 5, 87-100 Toruń, Poland

(Received 23 May 2023; revised 27 July 2023; accepted 11 August 2023; published 11 September 2023)

The speed-dependent spectral line profiles collapse into a simple Lorentz profile in the regime dominated by the velocity-changing collisions. We derive general formulas for the effective width and shift of the Lorentzian for arbitrary speed-dependent collisional broadening and shift and velocity-changing collision operators. For a quadratic speed dependence of collisional broadening and shift, and the billiard ball model of velocity-changing collisions, we provide simple analytical expressions for the effective Lorentzian width and shift. We show that the effective Lorentzian width and shift split into components originating from the well-known Dicke-narrowed Doppler width, speed-averaged collisional broadening and shift, their speed dependencies, and a product term that mixes the contributions of the broadening and shift speed dependencies. We show how the components depend on rates of speed-changing and velocity-changing collisions related to the perturber-absorber mass ratio. We validate analytical formulas numerically on the example of H_2 transition perturbed by He.

DOI: 10.1103/PhysRevA.108.032810

I. INTRODUCTION

The shape of molecular spectral line affected by Doppler broadening and absorber-perturber collisions, in the general case, requires numerical evaluation and cannot be represented by a simple analytical function, unless some simplifications or assumptions are made [1]. The goal of this work is to show that, in the case when the velocity-changing collisions dominate other line shape effects, the spectral line shape collapses to an ordinary Lorentz profile and the expressions for its width and shift can be provided analytically.

The Lorentz profile has been used for over a century to describe collisionally broadened atomic and molecular spectral lines. It is particularly justified at high pressure of perturbers, much lighter than absorbers, in microwave spectral range, where the speed dependence of collisional broadening and shift [2,3], as well as Doppler broadening, can be neglected. Interestingly, also the Gaussian shape of the spectral line can collapse to the Lorentz profile when the velocity-changing collisions reduce the mean-free path of the absorber well below the wavelength of absorbed radiation as predicted by Dicke [4,5] in the 1950s. It was later demonstrated numerically [6] that the weighted sum of Lorentz profiles (WSL) [7,8], under frequent velocity-changing collisions described by the billiard-ball model [9,10] approaches the Lorentz profile and the convergence is faster for lower perturber-absorber mass ratio. It is related to relative contribution of speed change during velocity-changing collisions, which is determined by perturber-absorber mass ratio [11,12]. Recently, studies on line shapes for which width is dominated by the speed-dependent collisional shift led to formulating a simple analytical expression [13,14] (see Eq. (15) in Ref. [13]) for width of Lorentzian profile approximating such line shape when speed-dependent collisional shift is described by a quadratic function [15] and velocity-changing collisions are approximated by the hard-collision model [16,17]. The phenomenological finding from Ref. [13] got justification in a derivation [18] coming from the speed-dependent hard-collision profile [19,20].

In this paper, we generalize the results from Ref. [18]; we derive general formulas for the effective width and shift of a Lorentzian to which a sophisticated line shape model, based on any arbitrary speed-dependent collisional broadening and shift and velocity-changing collision operator, converges in the limit of frequent velocity-changing collisions. For quadratic speed dependencies of collisional width and shift, and the billiard-ball model of velocity-changing collisions, we provide a simple analytical expression for the effective Lorentzian width and shift. We show how their components depend on rates of speed-changing and velocity-changing collisions related to the perturber-absorber mass ratio. We validate the analytical formulas numerically.

II. ALGEBRAIC REPRESENTATION OF A SPECTRAL LINE SHAPE

In general, the shape of an isolated spectral line affected by Doppler broadening and collisions with perturbers can be evaluated [21,22] from a function $h(\omega, \vec{v})$,

$$I(\omega) = \frac{1}{\pi}\mathrm{Re}\,\{(1, h(\omega, \vec{v}))\}, \tag{1}$$

where $(\cdot,\cdot)$ is defined as a product $(a(\vec{v}), b(\vec{v})) = \int d^3\vec{v} f_{m_A}(\vec{v}) a(\vec{v}) b(\vec{v})$ of two functions $a(\vec{v})$, $b(\vec{v})$ of absorber velocity $\vec{v}$, $f_{m_A}(\vec{v}) = (\pi v_{m_A}^2)^{-3/2}\exp(-v^2/v_{m_A}^2)$ is Maxwellian distribution, $v_{m_A} = \sqrt{k_B T/(2m_A)}$ is the most probable speed of the absorber having mass m_A at temperature T,

---

*NikodemStolarczyk319@gmail.com

and k_B is Boltzmann's constant. Function $h(\omega, \vec{v})$ fulfils transport-relaxation kinetic equation [22],

$$1 = -i(\omega - \omega_0 - \vec{k} \cdot \vec{v})h(\omega, \vec{v}) - \hat{S}^f h(\omega, \vec{v}), \tag{2}$$

where ω_0 is unperturbed transition frequency, $\vec{k}$ is a wave vector of radiation, and operator $\hat{S}^f$ describes the effect of collisions with perturbers.

Equations (1) and (2) can be converted into an algebraic form expanding function $h(\omega, \vec{v})$,

$$h(\omega, \vec{v}) = \sum_{s=0}^{\infty} c_s(\omega)\varphi_s(\vec{v}), \tag{3}$$

in a set of orthonormal functions fulfilling condition $(\varphi_s(\vec{v}), \varphi_{s'}(\vec{v})) = \delta_{s,s'}$. We set $\varphi_0(\vec{v}) = 1$. The expansion coefficients $c_s(\omega)$ depend only on frequency for given operator $\hat{S}^f$. In this basis, any operator $\hat{A}$ can be represented by matrix $\mathbf{A}$, having matrix elements $[\mathbf{A}]_{s,s'} = (\varphi_s(\vec{v}), \hat{A}\varphi_{s'}(\vec{v}))$.

The shape of an isolated spectral line can have algebraic representation by a series of Lorentz profiles. Following the approaches from Refs. [10,21,23,24] and notation described in Refs. [6,22,25], the line shape can be written as [6,25,26]:

$$I(\omega) = \frac{1}{\pi}\mathrm{Re}\,\{c_0(\omega)\}, \tag{4}$$

where the coefficient $c_0(\omega)$ can be evaluated by solving a set of complex linear equations,

$$\underline{\mathbf{b}} = \mathbf{L}(\omega)\underline{\mathbf{c}}(\omega), \tag{5}$$

for the coefficients $c_s(\omega)$, where $s = 0, 1, \ldots, s_{\max}$. Here the column $\underline{\mathbf{b}}$ contains unity in the position 0 and zeros in other positions, i.e., $[\underline{\mathbf{b}}]_s = \delta_{0,s}$, and the column $\underline{\mathbf{c}}(\omega)$ consists of the coefficients $c_s(\omega)$, i.e., $[\underline{\mathbf{c}}(\omega)]_s = c_s(\omega)$. The matrix $\mathbf{L}(\omega)$ depends on the frequency ω and has the following form:

$$\mathbf{L}(\omega) = -i(\omega - \omega_0)\mathbf{1} + i\mathbf{K} - \mathbf{S}^f, \tag{6}$$

where ω_0 corresponds to the unperturbed frequency of the transition, $\mathbf{1}$ is the unit matrix, $[\mathbf{1}]_{s,s'} = \delta_{s,s'}$, $\mathbf{K}$ is the matrix that represents the Doppler shift, $\mathbf{S}^f = \mathbf{S}^f_D + \mathbf{S}^f_{VC}$ is the matrix that represents the collision operator split into two components: $\mathbf{S}^f_D$ is the matrix that represents the dephasing and relaxation [27,28] collisional width and shift and $\mathbf{S}^f_{VC}$ is the matrix that represents the velocity-changing collision operator also affected by dephasing and relaxation. The representation used here has a property $[\mathbf{S}^f_{VC}]_{s,0} = [\mathbf{S}^f_{VC}]_{0,s} = 0$ for any s and $[\mathbf{K}]_{0,0} = 0$. Moreover, all matrices discussed in this work are symmetric.

In practice, the coefficient $c_0(\omega)$ is calculated using the diagonalization technique (cf. [24,29,30]). To do it in this way, one needs to find the full set of eigenvectors, $\underline{\mathbf{e}}_j$, and corresponding eigenvalues ε_j, which fulfill the following equation:

$$(i\mathbf{K} - \mathbf{S}^f)\underline{\mathbf{e}}_j = \varepsilon_j\underline{\mathbf{e}}_j, \tag{7}$$

where $j = 0, 1, \ldots, s_{\max}$. Once the eigenvectors and eigenvalues are known, the coefficient $c_0(\omega)$ can be computed from the following expression:

$$c_0(\omega) = \sum_{j=0}^{s_{\max}} \frac{\beta_j[\underline{\mathbf{e}}_j]_0}{\varepsilon_j - i(\omega - \omega_0)}, \tag{8}$$

where the coefficients β_j fulfill the relation $\underline{\mathbf{b}} = \sum_{j=0}^{s_{\max}} \beta_j\underline{\mathbf{e}}_j$. The main advantage of this approach is that the time-consuming diagonalization can be carried out once and this is sufficient to calculate the whole line shape.

III. HIGH FREQUENCY OF THE VELOCITY-CHANGING COLLISIONS LIMIT

Our derivation is carried out in the limit where the velocity-changing collisions dominate over the Doppler broadening and collisional broadening and shift. We assume the absolute values of all matrix elements of $\mathbf{K}$ and $\mathbf{S}^f_D$, as well as detuning, $\omega - \omega_0$, to be much smaller than the absolute value of the effective optical frequency of velocity changing collisions, ν_{opt}. Importantly, ν_{opt} can be complex due to the dephasing associated with optical velocity-changing collisions. All nonzero matrix elements of $\mathbf{S}^f_{VC}$ are directly proportional to ν_{opt}. The recognition of ν_{opt} as a complex quantity was originally put forth by Rautian and Sobelmann [17]. Subsequent support for this notion came from the comparison between measurements [31] and theoretical estimations [32]. The complex form of ν_{opt} has been justified through both semiclassical approaches [17,33–35] and quantum treatments [33,36–41], see also the references cited therein.

For the matrix $\mathbf{S}^f_{VC}$ we can calculate eigenvectors, $\underline{\mathbf{e}}^{VC}_j$, and eigenvalues, ε^{VC}_j, which fulfill the following equation:

$$-\mathbf{S}^f_{VC}\underline{\mathbf{e}}^{VC}_j = \varepsilon^{VC}_j\underline{\mathbf{e}}^{VC}_j. \tag{9}$$

It is easy to see that one of the eigenvectors of the matrix having property $[\mathbf{S}^f_{VC}]_{s,0} = [\mathbf{S}^f_{VC}]_{0,s} = 0$ is vector $\underline{\mathbf{b}}$ and its corresponding eigenvalue is zero. Therefore, we can set $\underline{\mathbf{e}}^{VC}_0 = \underline{\mathbf{b}}$ and $\varepsilon^{VC}_0 = 0$. Consequently, for $j \neq 0$ we have $[\underline{\mathbf{e}}^{VC}_j]_0 = 0$ and $\varepsilon^{VC}_j \sim \nu_{\mathrm{opt}}$.

Now we can rewrite Eq. (7) in the form:

$$\big(-\mathbf{S}^f_{VC} - \mathbf{S}^f_D + i\mathbf{K}\big)\underline{\mathbf{e}}_j = \varepsilon_j\underline{\mathbf{e}}_j, \tag{10}$$

where the matrix, which we want to diagonalize, is split into the dominating part $\mathbf{S}^f_{VC}$ and the perturbation part containing $\mathbf{S}^f_D$ and $\mathbf{K}$. We take advantage of that and approximate eigenvectors $\underline{\mathbf{e}}_j$ by $\underline{\mathbf{e}}^{VC}_j$ and eigenvalues ε_j by ε^{VC}_j and improve them by perturbation corrections. Setting $\underline{\mathbf{e}}_j \approx \underline{\mathbf{e}}^{VC}_j$ we get $\beta_j = \delta_{j,0}$. In this, way Eq. (8) can be approximated with the Lorentz profile:

$$c_0(\omega) \approx \frac{1}{\varepsilon_0 - i(\omega - \omega_0)}, \tag{11}$$

where the eigenvalue ε_0 is approximated by second-order perturbation. The eigenvalues, ε_j, in the second-order perturbation are given by the following expression:

$$\varepsilon_j \approx \varepsilon^{VC}_j + \sum_{s,s'=0}^{s_{\max}} \big[\underline{\mathbf{e}}^{VC}_j\big]_s\big(-\big[\mathbf{S}^f_D\big]_{s,s'} + i[\mathbf{K}]_{s,s'}\big)\big[\underline{\mathbf{e}}^{VC}_j\big]_{s'} + \sum_{\substack{j'=0\\ j'\neq j}}^{s_{\max}} \frac{\Big(\sum_{s,s'=0}^{s_{\max}}\big[\underline{\mathbf{e}}^{VC}_j\big]_s\big(-\big[\mathbf{S}^f_D\big]_{s,s'} + i[\mathbf{K}]_{s,s'}\big)\big[\underline{\mathbf{e}}^{VC}_{j'}\big]_{s'}\Big)^2}{\varepsilon^{VC}_j - \varepsilon^{VC}_{j'}}. \tag{12}$$

This equation for ε_0 simplifies to the following form:

$$\varepsilon_0 \approx -\left[\mathbf{S}_D^f\right]_{0,0} + \sum_{j'=1}^{s_{\max}} \frac{\left\{\sum_{s'=1}^{s_{\max}}\left(-\left[\mathbf{S}_D^f\right]_{0,s'} + i[\mathbf{K}]_{0,s'}\right)\left[\underline{\mathbf{e}}_{j'}^{VC}\right]_{s'}\right\}^2}{-\varepsilon_{j'}^{VC}}, \tag{13}$$

remembering that $\varepsilon_0^{VC} = 0$, $[\underline{\mathbf{e}}_0^{VC}]_s = \delta_{0,s}$ and $[\mathbf{K}]_{0,0} = 0$. In this way, we get a single Lorentz profile,

$$I(\omega) = \frac{1}{\pi}\frac{\Gamma_{\text{eff}}}{\Gamma_{\text{eff}}^2 + (\omega - \omega_0 - \Delta_{\text{eff}})^2}, \tag{14}$$

in the limit of frequent velocity-changing collisions, here

$$\Gamma_{\text{eff}} + i\Delta_{\text{eff}} = \varepsilon_0. \tag{15}$$

It should be noted that we can always use the basis in which matrix $\mathbf{S}_{VC}^f$ is diagonal. In such case $[\underline{\mathbf{e}}_j^{VC}]_s = \delta_{j,s}$, $\varepsilon_j^{VC} = -[\mathbf{S}_{VC}^f]_{j,j}$ and Eq. (13) takes simple form

$$\varepsilon_0 \approx -\left[\mathbf{S}_D^f\right]_{0,0} + \sum_{s=1}^{s_{\max}} \frac{\left(-\left[\mathbf{S}_D^f\right]_{0,s} + i[\mathbf{K}]_{0,s}\right)^2}{\left[\mathbf{S}_{VC}^f\right]_{s,s}}. \tag{16}$$

Furthermore, one can use a basis in which if a matrix element is nonzero, $[\mathbf{S}_D^f]_{0,s} \neq 0$, then the corresponding matrix element is zero, $[\mathbf{K}]_{0,s} = 0$, and, if $[\mathbf{K}]_{0,s} \neq 0$ then $[\mathbf{S}_D^f]_{0,s} = 0$. It is a simple consequence of the symmetry of the corresponding operators. The collisional broadening and shift depend on the absolute value of the absorber velocity, $v = |\vec{v}|$, and are not dependent on velocity direction. On the other hand, the Doppler shift is proportional to the scalar product $\vec{k}\cdot\vec{v}$, which depends on velocity direction. Taking this into account, we can rewrite Eq. (16) in the following form:

$$\varepsilon_0 \approx -\left[\mathbf{S}_D^f\right]_{0,0} - \sum_{s=1}^{s_{\max}} \frac{[\mathbf{K}]_{0,s}^2}{\left[\mathbf{S}_{VC}^f\right]_{s,s}} + \sum_{s=1}^{s_{\max}} \frac{\left[\mathbf{S}_D^f\right]_{0,s}^2}{\left[\mathbf{S}_{VC}^f\right]_{s,s}}. \tag{17}$$

IV. APPLICATION IN CASE OF QUADRATIC SPEED-DEPENDENT COLLISIONAL BROADENING AND SHIFT

To get physical insight into the expressions derived above, we consider matrix representation using Burnett functions [9] described in Appendix A. We assume quadratic speed dependence of collisional broadening and shift [15]. It means that the operator

$$\hat{S}_D^f = -\Gamma(v) - i\Delta(v) \tag{18}$$

is determined by $\Gamma(v)$ and $\Delta(v)$ given in the following form:

$$\Gamma(v) + i\Delta(v) = \Gamma_0 + i\Delta_0 + (\Gamma_2 + i\Delta_2)\left(\frac{v^2}{v_m^2} - \frac{3}{2}\right), \tag{19}$$

where Γ_0 and Δ_0 are the collisional broadening and shift parameters, averaged over absorber velocity, respectively. Quadratic speed dependencies of collisional broadening and shift are described by Γ_2 and Δ_2 parameters, respectively.

Discussing the velocity-changing collisions, we will focus on the case where matrix $\mathbf{S}_{VC}^f$ is diagonal or is approximated by a diagonal matrix. In the Burnett functions basis representation, instead of the index $s = 0, 1, \ldots, s_{\max}$, we prefer to use two other indices, $n = 0, 1, \ldots, n_{\max}$ and $l = 0, 1, \ldots, l_{\max}$. The pair of indices nl can be connected with $s{=}n{+}(n_{\max}{+}1)l$ and $s_{\max} = n_{\max} + (n_{\max}+1)l_{\max}$.

The properties of matrix elements in Burnett functions representation are summarized in Appendix A. The assumptions made above constrain the number of nonzero matrix elements, which contribute to Eq. (17) to only a few,

$$\varepsilon_0 = -\left[\mathbf{S}_D^f\right]_{00,00} - \frac{[\mathbf{K}]_{00,01}^2}{\left[\mathbf{S}_{VC}^f\right]_{01,01}} + \frac{\left[\mathbf{S}_D^f\right]_{00,10}^2}{\left[\mathbf{S}_{VC}^f\right]_{10,10}}. \tag{20}$$

Now we can explicitly express the matrix elements: $[\mathbf{K}]_{00,01} = \omega_D\sqrt{1/2}$, where $\omega_D = kv_{m_A}$, $[\mathbf{S}_D^f]_{00,00} = -(\Gamma_0 + i\Delta_0)$, and $[\mathbf{S}_D^f]_{00,10} = -(\Gamma_2 + i\Delta_2)\sqrt{3/2}$.

A. Hard-collision model

To discuss the velocity-changing collisions we first consider the hard-collision (HC) model [16,17], discussed recently in Ref. [18] in a similar context. The HC model is frequently used due to its simplicity, despite its shortcomings. In many situations, it helps to get some analytical results. The operator $\hat{S}_{HC}^f$ describing hard velocity-changing collisions has the following form:

$$\hat{S}_{HC}^f h(\omega,\vec{v}) = -\nu_{\text{opt}} h(\omega,\vec{v}) + \nu_{\text{opt}}\int d^3\vec{v}' f_{m_A}(\vec{v}')h(\omega,\vec{v}'), \tag{21}$$

where ν_{opt} is the effective optical frequency of velocity-changing collisions, which, in the general case, can be a complex number [17,31,32,36]. It can be shown that in any orthonormal base assuming $\varphi_0(\vec{v}) = 1$, the matrix representation of the $\hat{S}_{HC}^f$ operator is diagonal, $[\mathbf{S}_{HC}^f]_{s,s'} = -\nu_{\text{opt}}\delta_{s,s'}(1 - \delta_{0,s})$. All its diagonal elements are equal to $-\nu_{\text{opt}}$, except $[\mathbf{S}_{HC}^f]_{0,0} = 0$. Therefore, also in the Burnett functions representation, we can write that $[\mathbf{S}_{HC}^f]_{01,01} = [\mathbf{S}_{HC}^f]_{10,10} = -\nu_{\text{opt}}$. Inserting these matrix elements into Eqs. (20) and (15) we got

$$\Gamma_{\text{eff}}^{HC} + i\Delta_{\text{eff}}^{HC} = \Gamma_0 + i\Delta_0 + \frac{\omega_D^2}{2\nu_{\text{opt}}} - \frac{3\Gamma_2^2}{2\nu_{\text{opt}}} + \frac{3\Delta_2^2}{2\nu_{\text{opt}}} - i\frac{3\Gamma_2\Delta_2}{\nu_{\text{opt}}}. \tag{22}$$

The above result has also been obtained in our recent paper with a different method, see Eqs. (19a)–(19d) in Ref. [18], where we have shown that speed-dependent hard-collision profile [20] collapses into a simple Lorentz profile in the limit of frequent velocity-changing collisions.

B. Soft-collision model

In the case when perturbers are much lighter then absorbers, the velocity-changing collisions are described by soft-collision (SC) model [42]. This model was introduced by Galatry [43] into the theory of Dicke-narrowed spectral line shapes. By that time, the Galatry profile (GP) became one of the most frequently used expressions to describe collisionally narrowed spectra. The exact speed-dependent Galatry profile (SDGP) with quadratic speed dependence of collisional width and shift was given in Ref. [44] and should be not confused with its approximated expression provided by Prime *et al.* [45] using approach from Ref. [46]. It was shown in Refs. [9,10] that the velocity-changing soft-collisions operator $\hat{S}^f_{HC}$ is represented with a diagonal matrix operator in the Burnett functions basis. The relevant matrix elements are given by the following expressions: $[\mathbf{S}^f_{SC}]_{00,00} = 0$, $[\mathbf{S}^f_{SC}]_{01,01} = -\nu_{\rm opt}$, $[\mathbf{S}^f_{SC}]_{10,10} = -2\nu_{\rm opt}$, see Refs. [9,10]. In contrast to the HC model, the matrix elements $[\mathbf{S}^f_{SC}]_{01,01}$ and $[\mathbf{S}^f_{SC}]_{10,10}$ are not identical. Inserting these matrix elements into Eqs. (20) and (15) yields:

$$\Gamma^{SC}_{\rm eff} + i\Delta^{SC}_{\rm eff} = \Gamma_0 + i\Delta_0 + \frac{\omega_D^2}{2\nu_{\rm opt}} - \frac{3\Gamma_2^2}{4\nu_{\rm opt}} + \frac{3\Delta_2^2}{4\nu_{\rm opt}} - i\frac{3\Gamma_2\Delta_2}{2\nu_{\rm opt}}. \tag{23}$$

The three last terms of this equation are two times smaller then the ones derived in case of the HC model, Eq. (22) [18].

C. Billiard-ball model

The billiard-ball (BB) model [10] provides a more realistic description of the velocity-changing collisions. This model properly accounts for the perturber-absorber mass ratio, $\alpha = m_p/m_a$. The matrix describing such velocity-changing collisions $[\mathbf{S}^f_{BB}]_{nl,n'l'} = \nu_{\rm opt} f_D M^{E*}_{nl,n'l'}$ is determined by coefficients $M^{E*}_{nl,n'l'}$ [9,10] defined in Appendix A. This matrix is diagonal and the factor $f_D = 1$ in case of $\alpha = 0$, which corresponds to the soft-collision (SC) model. For nonzero α, the matrix $[\mathbf{S}^f_{BB}]_{nl,n'l'}$ is not diagonal and f_D becomes greater than one, reaching $32/(9\pi) \approx 1.132$ for $\alpha = \infty$ [10]. Nevertheless, we can approximate the original matrix by its diagonal simplification with the same diagonal elements $[\mathbf{S}^f_{BB}]_{nl,nl}$. The coefficients $M^{E*}_{01,01} = -1$ and $M^{E*}_{10,10} = -2M_1$, where $M_1 = m_A/(m_A + m_B)$ are of our particular interest since these allow to provide the explicit form of the matrix elements $[\mathbf{S}^f_{BB}]_{01,01} = -\nu_{\rm opt} f_D$ and $[\mathbf{S}^f_{BB}]_{10,10} = -\nu_{\rm opt} f_D 2/(1+\alpha)$. In contrast to the HC model, these matrix elements are not identical. The matrix element $[\mathbf{S}^f_{BB}]_{01,01} \approx \nu_{\vec{v}}$ describes relaxation rate, $\nu_{\vec{v}}$, of the velocity vector, $\vec{v}$. On the other hand, $[\mathbf{S}^f_{BB}]_{10,10} \approx \nu_{v^2}$ describes relaxation rate, ν_{v^2}, of v^2, which is directly related to speed, v. As it was shown in Refs. [12,47], the ratio between the speed, v- or its square, v^2-changing collisions and velocity, $\vec{v}$-changing collisions rate $\nu_{v^2}/\nu_{\vec{v}} = [\mathbf{S}^f_{BB}]_{10,10}/[\mathbf{S}^f_{BB}]_{01,01} = 2/(1+\alpha)$ varies with α. This ratio agrees well with results obtained from the classical molecular dynamics simulations based on realistic molecular interaction potentials [11,47]. Inserting the matrix elements $[\mathbf{S}^f_{BB}]_{01,01}$ and $[\mathbf{S}^f_{BB}]_{10,10}$ into Eqs. (20) and (15) we got

$$\Gamma^{BB}_{\rm eff} + i\Delta^{BB}_{\rm eff} = \Gamma_0 + i\Delta_0 + \frac{\omega_D^2}{2\nu_{\vec{v}}} - \frac{3\Gamma_2^2}{2\nu_{v^2}} + \frac{3\Delta_2^2}{2\nu_{v^2}} - i\frac{3\Gamma_2\Delta_2}{\nu_{v^2}}. \tag{24}$$

We do not need to limit our discussion to the diagonal approximation in this place. We can take into account the full matrix, $[\mathbf{S}^f_{BB}]_{nl,nl}$, and use Eq. (13). However, to derive the exact analytical expressions, we used another method described in Appendix B, where we found that $\nu_{\vec{v}} = \nu_{\rm opt}$, $\nu_{v^2} = \nu_{\rm opt}(2/(1+\alpha))(f_D/f_{v^2})$, and got the following

$$\Gamma^{BB}_{\rm eff} + i\Delta^{BB}_{\rm eff} = \Gamma_0 + i\Delta_0 + \frac{\omega_D^2}{2\nu_{\rm opt}} + \left(-\frac{3\Gamma_2^2}{2\nu_{\rm opt}} + \frac{3\Delta_2^2}{2\nu_{\rm opt}} - i\frac{3\Gamma_2\Delta_2}{\nu_{\rm opt}}\right)\frac{1+\alpha}{2}\frac{f_{v^2}}{f_D}. \tag{25}$$

$\Gamma^{BB}_{\rm eff}$ and $i\Delta^{BB}_{\rm eff}$ are the effective width and shift of the Lorentzian, which the quadratic speed-dependent billiard-ball profile (SDBBP) [6] collapses to, under frequent velocity-changing collisions. This expression is a generalization of Eq. (22) [18] to the arbitrary mass ratio α case. It should be noted that the factor f_{v^2}/f_D (except $\alpha = 0$ and $\alpha = \infty$ for which is equal to one), is slightly greater than unity but not more than 2.36% in the worst case of $\alpha = 2$, see Table I.

Equations (22) and (25) become equivalent when $\alpha = 1$ and corresponding $f_{v^2}/f_D = 1.018756$ is approximated by unity. Some equivalence of the HC model and BB model with $\alpha = 1$ was already discussed in Refs. [6,12,47]. For $\alpha = 0$ and the corresponding $f_{v^2}/f_D = 1$, it means in case of SC [42,43], Eq. (25) provides the effective width and shift of Lorentzian to which quadratic speed-dependent Galatry profile [6,44] collapses under frequent velocity-changing collisions. In this case Eq. (25) is reduced to Eq. (23). It is worth mentioning that comparing the asymptotic behavior of hard- and soft-collision models we can see that the components of the effective width and shift related to suppressed Doppler effect [4] and thermally averaged collisional broadening and shift are the same for both models. In contrast, the components related to the speed dependence of collisional broadening and shift are two times smaller in the case of the soft-collision model. It is a natural consequence of the fact that $\nu^{SC}_{v^2} = 2\nu^{HC}_{v^2}$, when we keep the same $\nu^{SC}_{\vec{v}} = \nu^{HC}_{\vec{v}}$ for both models.

V. COMPONENTS OF EFFECTIVE WIDTH AND SHIFT

In line with our previous paper [18], it is important to note that the Dicke parameter can take on complex values, $\nu_{\rm opt} = \nu^r_{\rm opt} + i\nu^i_{\rm opt}$ [17,31,32,36]. Therefore, we can decompose the effective Lorentzian width and shift of the asymptotic quadratic correlated speed-dependent billiard-ball profile [6,25,27,48] into several contributions:

$$\Gamma_{\rm eff} = \Gamma_0 + \Gamma_\gamma + \Gamma_\delta + \Gamma_{\gamma\delta} + \Gamma_{\omega_D}, \tag{26a}$$

$$\Delta_{\rm eff} = \Delta_0 + \Delta_\gamma + \Delta_\delta + \Delta_{\gamma\delta} + \Delta_{\omega_D}. \tag{26b}$$

Assuming quadratic speed-dependent collisional broadening and shift as well as velocity-changing collisions described by the billiard-ball model, these contributions are

$$\Gamma_\gamma = -\frac{f_{v^2}}{f_D}\frac{1+\alpha}{2}\frac{\nu^r_{\rm opt}}{|\nu_{\rm opt}|^2}\frac{3}{2}\Gamma_2^2, \tag{27a}$$

$$\Gamma_\delta = \frac{f_{v^2}}{f_D}\frac{1+\alpha}{2}\frac{\nu^r_{\rm opt}}{|\nu_{\rm opt}|^2}\frac{3}{2}\Delta_2^2, \tag{27b}$$

$$\Gamma_{\gamma\delta} = -2\frac{f_{v^2}}{f_D}\frac{1+\alpha}{2}\frac{\nu^i_{\rm opt}}{|\nu_{\rm opt}|^2}\frac{3}{2}\Gamma_2\Delta_2, \tag{27c}$$

TABLE I. Coefficients f_D, f_{v^2} and their ratio f_D/f_{v^2} evaluated for different α within billiard ball model.

4α	f_D	f_{v^2}	f_D/f_{v^2}
0	1	1	1
1/100	1.00000331561954	1.00000991995975	0.99999339572530
1/50	1.00001319212471	1.00003935941918	0.99997383373542
1/20	1.00008114950708	1.00023998438455	0.99984120323127
1/10	1.00031613831745	1.00091992503335	0.99939676821212
1/5	1.00119948726834	1.00336387252056	0.99784287105456
1/4	1.00182496341562	1.00501525070746	0.99682563295473
1/3	1.00310178272716	1.00822551613664	0.99491806810334
1/2	1.00636139570140	1.01565719613513	0.99084750202223
2/3	1.01027159637697	1.02349086931942	0.98708413202431
1	1.01895378488101	1.03806540223391	0.98158919725889
3/2	1.03178515946401	1.05522030753985	0.97779122718887
2	1.04294734723661	1.06757150938264	0.97693441429486
3	1.05994565861	1.0835515889	0.9782142996
4	1.0717514674	1.093265697	0.980321134
5	1.08028126	1.09975074	0.982296461
10	1.101660	1.114423	0.9885474
20	1.11523	1.122707	0.99334
50	1.12464	1.1280	0.997
100	1.1280	1.1280	1
∞	$32/9\pi \approx 1.131$	1.131	1

$$\Gamma_{\omega_D} = \frac{\nu^r_{\text{opt}}}{|\nu_{\text{opt}}|^2}\frac{1}{2}\omega_D^2, \tag{27d}$$

$$\Delta_\gamma = \frac{f_{v^2}}{f_D}\frac{1+\alpha}{2}\frac{\nu^i_{\text{opt}}}{|\nu_{\text{opt}}|^2}\frac{3}{2}\Gamma_2^2, \tag{27e}$$

$$\Delta_\delta = -\frac{f_{v^2}}{f_D}\frac{1+\alpha}{2}\frac{\nu^i_{\text{opt}}}{|\nu_{\text{opt}}|^2}\frac{3}{2}\Delta_2^2, \tag{27f}$$

$$\Delta_{\gamma\delta} = -2\frac{f_{v^2}}{f_D}\frac{1+\alpha}{2}\frac{\nu^r_{\text{opt}}}{|\nu_{\text{opt}}|^2}\frac{3}{2}\Gamma_2\Delta_2, \tag{27g}$$

$$\Delta_{\omega_D} = -\frac{\nu^i_{\text{opt}}}{|\nu_{\text{opt}}|^2}\frac{1}{2}\omega_D^2. \tag{27h}$$

For real $\nu_{\text{opt}} = \nu^r_{\text{opt}}$ ($\nu^i_{\text{opt}} = 0$) the components of effective width are: Γ_{ω_D} Γ_0, Γ_γ, Γ_δ. The first two terms represent collisionally suppressed Doppler broadening and velocity-averaged collisional width, respectively. Γ_γ can be seen as a reduction of line width caused by the speed-dependence of collisional broadening. It is qualitatively coherent with findings in the other context of the speed-dependent Voigt profile (SDVP) [2,3], where also the narrowing of the spectral line was triggered by speed dependence of collisional broadening. On the other hand, Γ_δ represents an additional broadening of the line caused by the speed-dependent spread of collisional shift [7,8,49]. The character of these contributions does not depend on the sign of Γ_2 and Δ_2 parameters. The effective shift, in such circumstances, has only two components, Δ_0 and $\Delta_{\gamma\delta}$. The first one represents an ordinary velocity-averaged collisional shift, however, the second term is less obvious and is related to the product of speed dependencies of collisional broadening and shift or their correlation [18].

The other contributions, namely $\Gamma_{\gamma\delta}$, Δ_γ, Δ_δ, and Δ_{ω_D}, only come into play if ν_{opt} has a nonzero imaginary component, i.e., $\nu^i_{\text{opt}} \neq 0$. While we will not delve into a detailed discussion of these contributions, we will touch on the last one, Δ_{ω_D}. This shift arises due to Dicke-suppressed Doppler broadening, and it should decrease inversely with pressure, similar to the well-known Γ_{ω_D} [4]. This is because ν_{opt} is proportional to pressure, while ω_D remains constant at a given temperature. Therefore, in a moderate range of pressures, this term can potentially impact the precise determination of the line position. In fact, as we demonstrate in the following section, under certain conditions, Δ_{ω_D} can contribute up to 2 MHz to the effective line shift, Δ_{eff}.

To describe the relative contribution of each effect ($x = \gamma$, δ, $\gamma\delta$, or ω_D) under specific physical conditions, we introduce dimensionless parameters Γ_x/Γ_0 and Δ_x/Δ_0. It is worth noting that all collisional parameters, including ν_{opt}, Γ_0, Γ_2, Δ_0, and Δ_2, are proportional to gas pressure. Therefore, the dimensionless parameters Γ_x/Γ_0 and Δ_x/Δ_0 for $x = \gamma$, δ, and $\gamma\delta$ are independent of pressure. In fact, as we show in the following section, under certain conditions, Γ_δ can account for approximately 35% of Γ_0, and the absolute value of $\Delta_{\gamma\delta}$ can reach 5% of Δ_0 or 20% of Γ_0. For further details, please refer to the next section.

VI. NUMERICAL VALIDATION

We validated the analytical expressions obtained in the previous section. To achieve this, we compared our results with the numerical half-width at half-maximum (HWHM) Γ_{exact} and the frequency Δ_{exact} corresponding to the position of the maximum of the quadratic speed-dependent billiard-ball profile [6]. Specifically, we focused on validating the formulas for Γ_γ, Γ_δ, Γ_{ω_D}, and $\Delta_{\gamma\delta}$ given by Eqs. (27a), (27b), (27d), and (27g), respectively. To carry out our calculations, we considered four values of $\alpha = 1/3, 1, 3, 10$, assuming real $\nu_{\text{opt}} = \nu^r_{\text{opt}}$, $\nu^i_{\text{opt}} = 0$.

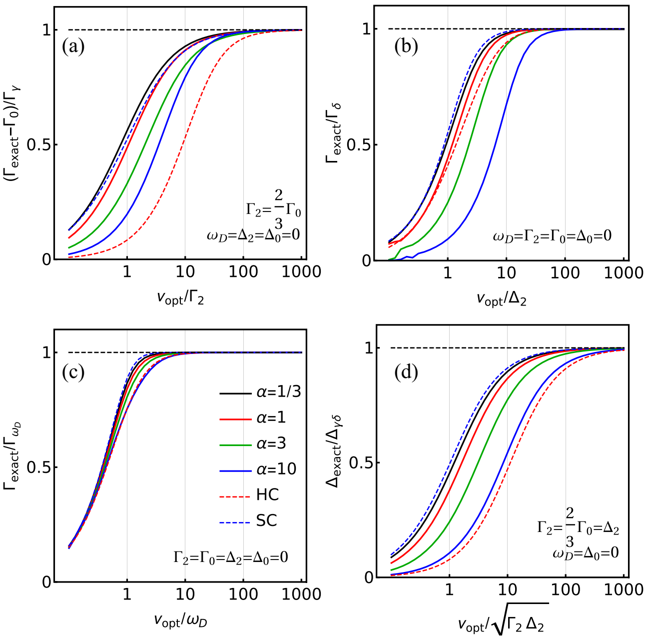

FIG. 1. Numerical verification of asymptotic formulas for Γ_γ, Γ_δ, Γ_{ω_D}, and $\Delta_{\gamma\delta}$. (a)–(c) show ratios of $\Gamma_{exact}/\Gamma_\gamma$, $\Gamma_{exact}/\Gamma_\delta$, $\Gamma_{exact}/\Gamma_{\omega_D}$ as functions of ν_{opt}/Γ_2, ν_{opt}/Δ_2, ν_{opt}/ω_D, respectively, where Γ_{exact} is numerically evaluated half width at half maximum (HWHM) of the quadratic speed-dependent billiard-ball profile. (d) shows the ratio of $\Delta_{exact}/\Delta_{\gamma\delta}$ as a function of $\nu_{opt}/\sqrt{\Gamma_2\Delta_2}$ where Δ_{exact} is numerically evaluated frequency corresponding to a maximum of the quadratic speed-dependent billiard-ball profile. Presented ratios were evaluated for $\alpha = 1/3,\ 1,\ 3,\ 10$ as well as for $\alpha = 0$, it means soft collisions (SC), and hard collisions (HC).

To provide further insight, we also compared our results with those obtained from the soft-collision model, which corresponds to the billiard-ball model with $\alpha = 0$ and the speed-dependent Galatry profile [44] and the hard-collision model [16,17], which we discuss in detail in Ref. [18]. To simplify our analysis, we focused on one effect at a time and set the appropriate values for the line shape parameters: Γ_0, Δ_0, Γ_2, Δ_2, ω_D, ν_{opt} in the quadratic SDBBP.

Our results, shown in Fig. 1, demonstrate that Γ_{exact} converges to Γ_γ, Γ_δ, Γ_{ω_D} as well as Δ_{exact} approaches $\Delta_{\gamma\delta}$ in the limit of high ν_{opt}. However, we observed that the convergence is slower for higher values of α in the case of Γ_γ, Γ_δ, and $\Delta_{\gamma\delta}$. This observation is directly related to the fact that ν_{v^2} decreases with increasing α, while $\nu_{\bar{v}}$ remains constant. On the other hand, the situation is different for Γ_{ω_D}, which is determined by $\nu_{\bar{v}}$ and is not dependent on α. As shown in Fig. 1(c), the variations for α are weak in this case. However, for extremely large values of α, significant discrepancies for different α are observed. This topic has been discussed in detail in Ref. [6].

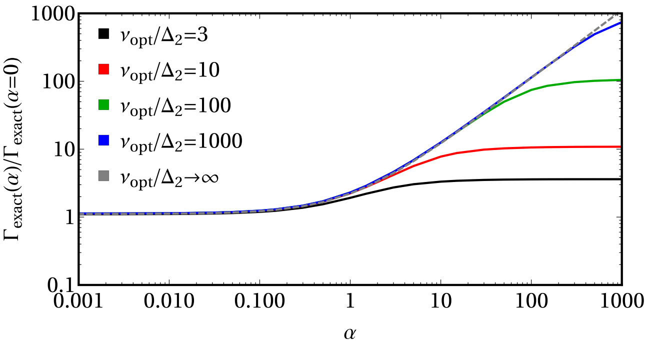

FIG. 2. Ratio of $\Gamma_{exact}(\alpha)/\Gamma_{exact}(\alpha = 0)$ evaluated for several values ν_{opt}/Δ_2 within quadratic speed-dependent billiard-ball profile in which parameters Γ_0, Δ_0, Γ_2, ν^i_{opt}, and ω_D were set to zero and its comparison with ratio $\Gamma_\delta(\alpha)/\Gamma_\delta(\alpha = 0) \approx 1 + \alpha$ obtained for $\nu_{opt}/\Delta_2 \to \infty$.

The discussion of the effective broadening component Γ_δ, which arises from the speed dependence of the collisional shift $\Delta(v)$, is important in this context. As mentioned earlier, an increase in α results in a decrease in ν_{v^2}. Therefore, we anticipate that, with other parameters held constant, an increase in α will result in an increase in Γ_δ. In the frequent velocity-changing collisions regime, where ν_{opt} dominates, an asymptotic analytical relation for quadratic SDBBP [6] can be written as:

$$\frac{\Gamma_\delta(\alpha)}{\Gamma_\delta(\alpha = 0)} = \frac{f_{v^2}}{f_D}(1+\alpha) \approx 1+\alpha. \tag{28}$$

To simplify the calculation, the factor f_{v^2}/f_D in the asymptotic relation can be approximated as unity, introducing an error of less than 2%. We verified the accuracy of this approximation for finite values of ν_{opt}/Δ_2 by simulating quadratic SDBBP for various values of ν_{opt}/Δ_2 and α, while setting all other parameters (Γ_0, Δ_0, Γ_2, ν^i_{opt}, and ω_D) to zero. We then calculated Γ_{exact} for the simulated profiles, and plotted the ratios $\Gamma_{exact}(\alpha)/\Gamma_{exact}(\alpha = 0)$ as a function of α for several values of ν_{opt}/Δ_2 (3, 10, 100, 1000) in Fig. 2. As shown in this figure, for $\nu_{opt}/\Delta_2 = 10$, the simulation results are reproduced by Eq. (28) for small to moderate values of α up to $\alpha = 3$.

As mentioned in Sec. III, our derivation was conducted under the assumption that velocity-changing collisions dominate over both Doppler broadening and collisional broadening and shift, particularly their speed-dependent parts. To satisfy this condition, the interactions between the absorber and perturber molecules at the initial and final molecular states need to be either identical or closely similar [17,33–41]. Physically, this requirement can be met in the case of rovibronic transitions in molecular hydrogen. This can be observed through *ab initio* calculations, as presented in Ref. [50]. Additionally, it has been demonstrated in Refs. [28,51] that such calculations, along with the use of SDBBP [6], can achieve subpercent agreement with experimental data.

It is seen from Fig. 1 that for $\alpha \leqslant 3$ and $\nu_{opt}/\Gamma_2 \geqslant 10$ the error introduced by our approximation of Γ_γ does not exceed 16%. Similarly, for $\nu_{opt}/\Delta_2 \geqslant 10$ our approximation of Γ_δ reproduces the corresponding width with inaccuracy less than 7%. Ultimately, if $\nu_{opt}/\omega_D \geqslant 10$ the error on Γ_{ω_D} is at most 0.3%, which is significantly smaller than in the previous cases. On the other hand, for the pressure shift, if $\nu_{opt}/\sqrt{\Gamma_2\Delta_2} \geqslant 10$ our approximation of $\Delta_{\gamma\delta}$ introduces error, which does not exceed 23%. In conditions where the speed-averaged values Γ_0 and Δ_0 are significantly greater than their speed dependencies, Γ_2 and Δ_2, the combined errors originating from these

TABLE II. Comparison of the Lorentz profile effective parameters for Q(1) 1-0 transition in H_2 perturbed by He ($\alpha = 2$) at 10 atm and 296 K obtained with Eqs. (27a)–(27h) derived from the billiard-ball model (BB) and effective parameters from Ref. [18,50] derived from hard-collision model (HC). The line shape parameters are $\Gamma_0 = 22.346$, $\Delta_0 = 90.971$, $\Gamma_2 = 10.856$, $\Delta_2 = 38.192$, $\nu^r_{\rm opt} = 404.148$, $\nu^i_{\rm opt} = -54.697$, $\omega_D = 21.659$ [50] are given in the units of 10^{-3} cm^{-1}.

Γ_x	$\Gamma^{BB}_x(10^{-3}\ {\rm cm}^{-1})$	Γ^{BB}_x/Γ_0	$\Gamma^{HC}_x(10^{-3}\ {\rm cm}^{-1})$	Γ^{HC}_x/Γ_0
Γ_0	22.346	1.000	22.346	1.000
Γ_γ	−0.645	−0.029	−0.430	−0.019
Γ_δ	7.974	0.357	5.316	0.238
$\Gamma_{\gamma\delta}$	0.613	0.027	0.409	0.018
Γ_{ω_D}	0.572	0.026	0.572	0.026
$\Gamma_{\rm eff}$	30.860	1.381	28.215	1.263
$\Gamma_{\rm exact}$	30.140	1.349	27.388	1.226
Δ_x	$\Delta^{BB}_x(10^{-3}\ {\rm cm}^{-1})$	Δ^{BB}_x/Δ_0	$\Delta^{HC}_x(10^{-3}\ {\rm cm}^{-1})$	Δ^{HC}_x/Δ_0
Δ_0	90.971	1.000	90.971	1.000
Δ_γ	−0.087	0.001	−0.058	−0.0006
Δ_δ	1.079	0.012	0.719	0.008
$\Delta_{\gamma\delta}$	−4.533	−0.050	−3.022	−0.033
Δ_{ω_D}	0.077	0.0008	0.077	0.0008
$\Delta_{\rm eff}$	87.507	0.962	88.688	0.975
$\Delta_{\rm exact}$	86.270	0.948	88.005	0.967

contributions result in a significantly smaller relative error on the entire line profile. Additionally, if the ν_{opt} dominates over the other line shape parameters (i.e., Γ_2, Δ_2, ω_D) by several dozens, our approximation should reproduce the original profile with several percent accuracy.

We compared the collapsed Lorentz profile to the SDBBP [6]. To do this, we examined the Q(1) 1-0 transition in H_2 perturbed by He at a pressure of 10 atm and a temperature of 296 K. We used the same line shape parameters as in Ref. [18], which were obtained from Ref. [50]. The values of the line shape parameters can be found in the caption of Table II. This table lists all contributions Γ_x and Δ_x to the effective Lorentzian width $\Gamma_{\rm eff}$ and shift $\Delta_{\rm eff}$, respectively. These values were calculated using Eqs. (27a)–(27h) under the assumption of a billiard-ball model ($\alpha = 2$) for velocity-changing collisions and the hard-collision model, as described in Ref. [18]. In Table II and Fig. 3, we used the unit of wave numbers $\widetilde{\nu} = 2\pi\omega/c$ instead of circular frequencies ω, which is more common in molecular spectroscopy for line shape parameters.

The ratios $\nu^r_{\rm opt}/\omega_D = 18.7$, $\nu^r_{\rm opt}/\Gamma_2 = 37.2$, and $\nu^r_{\rm opt}/\Delta_2 = 10.6$ demonstrate that our assumption from Sec. III, that the velocity-changing collisions dominate over Doppler broadening and collisional broadening and shift, is valid for the chosen conditions (pressure, temperature, molecular system). It is important to note that the values of Γ_0 and Δ_0 are not relevant in this context, as they only result in a simple convolution with the Lorentz profile determined by these parameters, which are additive in the case of Lorentz profiles. Furthermore, we have verified that the binary collision approximation holds well under these conditions, and the contribution of three-body collisions to collisional width and shift should not exceed the percentage level. For a detailed discussion, see Sec. II B3 in Ref. [1].

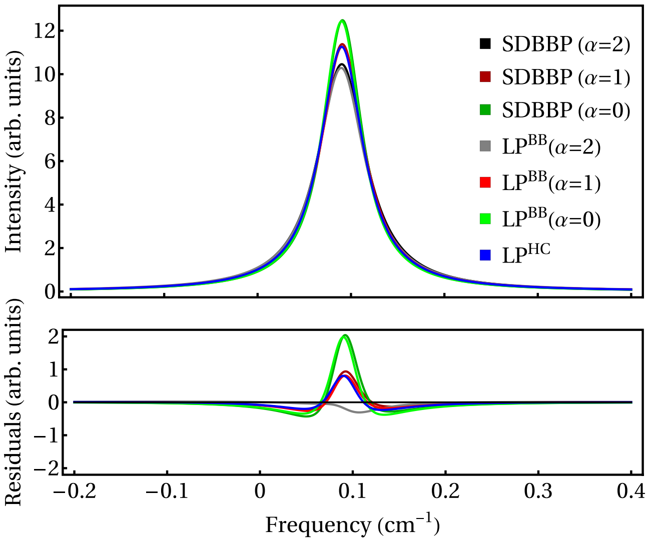

FIG. 3. A comparison of the reference speed-dependent billiard-ball profiles (SDBBP) calculated with $\alpha = 2,\ 1,\ 0$ and parameters listed in the caption of Table II for Q(1) 1-0 transition in H_2 perturbed by He at 10 atm and 296 K [18,50] and Lorentz profiles (LP^{BB}) derived as the collapsed SDBBP calculated with parameters given in this work by Eqs. (26a)–(27h) as well as Lorentz profile (LP^{HC}) derived as the collapsed hard-collision profile from Ref. [18]. The area under each line is normalized to 1. The lower graph presents the residuals against reference SDBBP ($\alpha = 2$) having α corresponding to H_2-He system with the same color notation as in the top panel.

The H_2 spectral line perturbed by He, for which $\alpha = 2$, allows us to observe the importance of the perturber/absorber mass ratio for the collapse of the spectral line shape to a Lorentz profile due to frequent velocity-changing collisions. As shown in Table II, the use of the BB model results in a Lorentz profile that is 9.4% wider than the profile obtained from the HC model [18]. This is mainly due to the fact that Γ_δ, the second most significant contribution to $\Gamma_{\rm eff}$ after Γ_0, is 50% larger in the case of the BB model compared to the HC model. It should be noted that the $\Gamma_{\rm eff}$ and $\Delta_{\rm eff}$ obtained from Eqs. (26a) and (26b), agree with the $\Gamma_{\rm exact}$ and $\Delta_{\rm exact}$ obtained from the original SDBBP within 2.3% and 1.4%, respectively.

Figure 3 compares the SDBBP [6] with $\alpha = 2,\ 1,\ 0$ with Lorentz profiles derived from the BB model (LP^{BB}) and the HC model (LP^{HC}). It shows that LP$^{BB}(\alpha = 2)$ provides a good approximation of SDBBP($\alpha = 2$), with a difference of about 2% at the maximum of the profile. In contrast, LP^{HC} exhibits a much larger deviation. The LP^{HC} follows closely LP$^{BB}(\alpha = 1)$ and SDBBP($\alpha = 1$). The discrepancy between SDBBP($\alpha = 2$) and LP^{HC} is caused by the fact that, in the case of the HC model, the frequency of speed-changing collisions ν_{v^2} does not capture its dependence on α, which is about 2/3 times smaller for the BB model with the same parameter values and $\alpha = 2$. On the other hand the frequency of speed-changing collisions ν_{v^2} for HC model agrees within 2% with those from BB model with $\alpha = 1$. A comparison of SDBBP($\alpha = 2$) with soft-collision profiles LP^{SC} and SDGP [44], which are equivalent to $\mathrm{LP}^{BB}(\alpha = 0)$ and $\mathrm{SDBBP}(\alpha = 0)$, respectively, looks even worse. It is caused by the fact that the BB model with the same parameter values and $\alpha = 2$ has the frequency of speed-changing collisions ν_{v^2} only about $1/3$ of this in SC model (BB model with $\alpha = 0$).

VII. CONCLUSIONS

In summary, we demonstrated that under the limit of frequent velocity-changing collisions, the speed-dependent Dicke-narrowed profile of the spectral line collapses to the Lorentz profile. Our work provides formulas for effective Lorentzian width and shift, which take into account the arbitrary speed dependence of collisional broadening and shift, as well as the velocity-changing collision operator. Specifically, for the asymptotic behavior of the quadratic speed-dependent billiard-ball profile [6], we obtained simple analytical expressions for Lorentzian width and shift. Our results generalize those recently reported in Ref. [18] for the speed-dependent hard-collision profile [20] to the case of arbitrary perturber-absorber mass ratio, α. We verified the applicability of our formulas by comparing them with numerical calculations of quadratic speed-dependent billiard-ball profiles over a wide range of line shape parameters.

Finally, our comparison with the numerical calculation of the H_2 spectral line perturbed by He showed good agreement with the profile derived in this work. This is thanks to properly accounting for the perturber-absorber mass ratio, which was not possible with the hard-collision model. Our results offer a more accurate and general description of spectral line shapes under the limit of frequent velocity-changing collisions, with potential applications in various fields including atmospheric and astrophysical spectroscopy involving rovibrational transitions of molecular hydrogen.

ACKNOWLEDGMENTS

N.S. was supported by Polish National Science Centre Project No. 2019/35/N/ST2/04145. P.W. was supported by Polish National Science Centre Project No. 2019/35/B/ST2/01118. R.C. was supported by Polish National Science Centre Project No. 2021/41/B/ST2/00681. The research is a part of the program of the National Laboratory FAMO in Toruń, Poland. Calculations have been partially carried out using resources provided by the Wroclaw Centre for Networking and Super-computing, Grant No. 546. We gratefully acknowledge Polish high-performance computing infrastructure PLGrid (HPC Centers: ACK Cyfronet AGH, CI TASK) for providing computer facilities and support within computational Grant No. PLG/2023/016279.

APPENDIX A: THE BURNETT FUNCTIONS REPRESENTATION

For evaluation of the speed-dependent Dicke-narrowed spectral line shape from the transport-relaxation equation we use a subset of the Burnett functions having axial symmetry about the wave vector $\vec{k}$ [9]. A detailed discussion of the application of this set of basis functions, as well as matrix representation of the operators present in the transport-relaxation equation, can be found in Ref. [6]. For convenience we recall these results here, using the original formulation.

We assume the basis functions in the following form [10]:

$$\varphi_{nl}(\vec{v}) = N_{nl}\,\left(v/v_{m_A}\right)^l\, L_n^{l+1/2}\!\left(v^2/v_{m_A}^2\right)\, P_l(\vec{e}_k\cdot\vec{e}_v), \tag{A1}$$

where a normalization factor,

$$N_{nl} = \sqrt{\frac{\pi^{1/2}\, n!\,(2l+1)}{2\,\Gamma(n+l+3/2)}}, \tag{A2}$$

$\Gamma(\ldots)$ is the gamma-Euler function. The associated Laguerre polynomials are defined as

$$L_n^{l+1/2}(x^2) = \sum_{m=0}^{n} \frac{(-1)^m\,\Gamma(n+l+3/2)}{m!\,(n-m)!\,\Gamma(m+l+3/2)}\, x^{2m}, \tag{A3}$$

where $x = v/v_{m_A}$ is the reduced speed of the active molecule. The Legendre polynomials are defined as

$$P_l(y) = \frac{1}{2^l}\sum_{k=0}^{[l/2]} \frac{(-1)^k\,(2l-2k)!}{k!\,(l-k)!\,(l-2k)!}\, y^{l-2k}, \tag{A4}$$

where $y = \vec{e}_k\cdot\vec{e}_v$ is the cosine of the angle between the velocity vector $\vec{v} = v\vec{e}_v$ and the wave vector $\vec{k} = k\vec{e}_k$, $\vec{e}_v$ and $\vec{e}_k$ are unit vectors.

The basis functions, $\varphi_{nl}(\vec{v})$, are eigenfunctions of the velocity-changing collision operator in the case of the soft collisions, where perturber-absorber mass ratio $\alpha = 0$. Like in [6], when calculating matrix elements of an operator, $\hat{A}$, we use the following notation $[\mathbf{A}]_{nl,n'l'} = (\varphi_{nl}(\vec{v}), \hat{A}\varphi_{n'l'}(\vec{v})) = \langle nl|\hat{A}|n'l'\rangle$.

The Doppler shift operator, $\vec{k}\cdot\vec{v} = \omega_D\vec{e}_k\cdot\vec{v}/v_{m_A}$, is represented by a matrix, $\mathbf{K}$, the elements of which are [6]

$$[\mathbf{K}]_{nl,n'l'} = \omega_D\langle nl|\vec{e}_k\cdot\vec{v}/v_m|n'l'\rangle, \tag{A5}$$

where $\omega_D = kv_{m_A}$ and

$$\begin{aligned}\langle nl|\vec{e}_k\cdot\vec{v}/v_m|n'l'\rangle &= \left[\sqrt{n+l+3/2}\,\delta_{n,n'} - \sqrt{n}\,\delta_{n,n'+1}\right]\sqrt{\frac{(l+1)^2}{4(l+1)^2-1}}\,\delta_{l,l'-1}\\ &\quad + \left[\sqrt{n+l+1/2}\,\delta_{n,n'} - \sqrt{n+1}\,\delta_{n,n'-1}\right]\sqrt{\frac{l^2}{4l^2-1}}\,\delta_{l,l'+1}.\end{aligned} \tag{A6}$$

The speed-dependent collisional width and shift operator, $\hat{S}_D^f = -\Gamma(v) - i\Delta(v)$, is represented by a matrix, $\mathbf{S}_D^f$, the elements of which are [6,24]

$$\begin{aligned}\left[\mathbf{S}_D^f\right]_{nl,n'l'} &= \frac{4}{\sqrt{\pi}(2l+1)}\,N_{nl}\,N_{n'l}\,\delta_{l,l'}\int_0^\infty dx\, e^{-x^2}x^{2l+2}\\ &\quad\times L_n^{l+1/2}(x^2)\,L_{n'}^{l+1/2}(x^2)\left[\Gamma\!\left(xv_{m_A}\right) + i\Delta\!\left(xv_{m_A}\right)\right].\end{aligned} \tag{A7}$$

In the case of quadratic speed-dependent collisional broadening and shift [15],

$$\Gamma(v) + i\Delta(v) = \Gamma_0 + i\Delta_0 + (\Gamma_2 + i\Delta_2)\left(\frac{v^2}{v_m^2} - \frac{3}{2}\right), \tag{A8}$$

the matrix elements can be written as

$$\begin{aligned}\left[\mathbf{S}^f_D\right]_{nl,n'l'} =& -[\Gamma_0 + i\Delta_0 - (\Gamma_2 + i\Delta_2)3/2]\delta_{n,n'}\delta_{l,l'}\\ &- [\Gamma_2 + i\Delta_2]\langle nl|v^2/v_m^2|n'l'\rangle, \end{aligned}\tag{A9}$$

where

$$\begin{aligned}&\langle nl|v^2/v_m^2|n'l'\rangle\\ &\quad= [(2n+l+3/2)\,\delta_{n,n'} - \sqrt{(n+l+1/2)n}\,\delta_{n,n'+1}\\ &\qquad - \sqrt{(n+l+3/2)(n+1)}\,\delta_{n,n'-1}]\delta_{l,l'}.\end{aligned}\tag{A10}$$

The velocity-changing collisions operator $\hat{S}^f_{BB}$ in the billiard-ball model is represented by a matrix, $\mathbf{S}^f_{BB}$, the elements of which are [9,10]

$$\left[\mathbf{S}^f_{BB}\right]_{nl,n'l'} = \nu^{(0)}\, M^{E*}_{nl,n'l'}, \tag{A11}$$

where $\nu^{(0)} = v_m^2/(2D^{(0)})$ and

$$D^{(0)} = \frac{3}{8}\left(\frac{k_BT}{2\pi\mu}\right)^{1/2}\frac{1}{N\sigma^2} \tag{A12}$$

is the first-order self-diffusion coefficient for rigid spheres, σ is the average of the rigid sphere diameter of the absorber and perturber, N is the number density of perturbers, $\mu = m_Am_P/(m_A+m_P)$ is the reduced mass. The analytical expressions for coefficients $M^{E*}_{nl,n'l'}$ for billiard-ball model were derived by Lindenfeld and Shizgal [9,10]

$$\begin{aligned}M^{E*}_{nl,n'l'} =& -\delta_{l,l'}\,\frac{3\,l!}{8M_2}\sqrt{\frac{n!\,n'!}{\Gamma(n+l+3/2)\Gamma(n'+l+3/2)}}\left\{\sum_{p=0}^{\tilde{n}}\sum_{s=0}^{\tilde{n}-p}\sum_{m=0}^{\tilde{n}-p-s}\sum_{q=0}^{l}\sum_{r=0}^{l-q}\left[\frac{4^p\,(r+s+p+q+1)!}{(p+q+1)!\,r!\,s!}\right]\right.\\ &\times\left.\left[\frac{\Gamma(n+n'-2s-2p-m+l-r-q-1/2)\,B^{(1)}_{p,q}(\infty)}{(n-m-s-p)!\,(n'-m-s-p)!\,(l-r-q)!\,m!}\right]\left[M_1^{l+p-r-q}M_2^{n+n'+q-2m-2s-p}(M_1-M_2)^{m+r+2s}\right]\right\},\end{aligned}\tag{A13}$$

where $M_1 = m_A/(m_A+m_P) = 1 - M_2$, $\tilde{n} = \min(n, n')$ and

$$B^{(1)}_{p,q}(\infty) = \frac{(2p+q+1)!}{2q!\,(2p+1)!} - \frac{2^{q-1}(p+q+1)!}{p!\,q!}. \tag{A14}$$

The exact diffusion coefficient D differs from $D^{(0)}$ and they are related by coefficient $f_D = D/D^{(0)}$ which evaluation is explained in Appendix B. Using these quantities the matrix elements can be written as

$$\left[\mathbf{S}^f_{BB}\right]_{nl,n'l'} = \nu_{\text{diff}}\; f_D\; M^{E*}_{nl,n'l'} \tag{A15}$$

where

$$\nu_{\text{diff}} = \frac{v_m^2}{2D} \tag{A16}$$

is the effective frequency of velocity-changing collisions.

APPENDIX B: NONDIAGONAL CORRECTIONS TO EFFECTIVE LORENTZIAN WIDTH AND SHIFT

Aiming at calculations of spectral line shape with quadratic speed-dependent collisional broadening and shift in the limit dominated by velocity-changing collisions, Eq. (5) can be rewritten in the Burnett functions representation,

$$\begin{aligned}1 =& \left(-i(\omega-\omega_0) - \left[\mathbf{S}^f_D\right]_{00,00}\right)c_{00}(\omega)\\ &+ i[\mathbf{K}]_{00,01}c_{01}(\omega) - \left[\mathbf{S}^f_D\right]_{00,10}c_{10}(\omega),\end{aligned}\tag{B1a}$$

$$0 = i[\mathbf{K}]_{01,00}\delta_{n,0}c_{00}(\omega) - \sum_{n'=0}^{\infty}\left[\mathbf{S}^f_{VC}\right]_{n1,n'1}c_{n'1}(\omega), \tag{B1b}$$

$$0 = -\left[\mathbf{S}^f_D\right]_{10,00}\delta_{n,1}c_{00}(\omega) - \sum_{n'=1}^{\infty}\left[\mathbf{S}^f_{VC}\right]_{n0,n'0}c_{n'0}(\omega). \tag{B1c}$$

We also take advantage of the fact that $c_{00}(\omega)$ is not coupled to other coefficients by matrix $\mathbf{S}^f_{VC}$ and it dominates two other matrices $\mathbf{S}^f_D$ and $\mathbf{K}$. Therefore, in the limit of frequent velocity-changing collisions, we are allowed to use matrix $\mathbf{S}^f_{VC}$ and only those matrix elements of $\mathbf{S}^f_D$ and $\mathbf{K}$, which provide coupling of $c_{00}(\omega)$ to other coefficients in the transport-relaxation equation. With the velocity-changing collision operator in the form from Eq. (A11), we can find $c_{00}(\omega)$ by solving two other sets of linear equations,

$$\delta_{n,0} = -\sum_{n'=0}^{\infty}M^{E*}_{n1,n'1}a_{n'1}, \tag{B2a}$$

$$\delta_{n,1} = -\sum_{n'=1}^{\infty}M^{E*}_{n0,n'0}a_{n'0}. \tag{B2b}$$

Equations (B2a) and (B2b) are equivalent to Eqs. (B1b) and (B1c) when we set

$$c_{n1}(\omega) = -\frac{i[\mathbf{K}]_{01,00}}{\nu^{(0)}}c_{00}(\omega)a_{n1}, \tag{B3a}$$

$$c_{n0}(\omega) = \frac{\left[\mathbf{S}^f_D\right]_{10,00}}{\nu^{(0)}}c_{00}(\omega)a_{n0}. \tag{B3b}$$

Now we can rewrite Eq. (B1a) in the following form:

$$\begin{aligned}1 =& \Bigg(-i(\omega-\omega_0) - \left[\mathbf{S}^f_D\right]_{00,00}\\ &+ \frac{[\mathbf{K}]^2_{01,00}}{\nu^{(0)}}a_{01} - \frac{\left[\mathbf{S}^f_D\right]^2_{10,00}}{\nu^{(0)}}a_{10}.\Bigg)c_{00}(\omega).\end{aligned}\tag{B4}$$

It is convenient to introduce the coefficient $f_D = a_{01}(-M^{E*}_{01,01}) = a_{01}$, were a_{01} can be found by solving Eq. (B2a) [10]. Analogically, we can introduce $f_{v^2} = a_{10}(-M^{E*}_{10,10}) = a_{10}2/(1+\alpha)$, were a_{01} can be found by solving Eq. (B2b).

Table I collects the coefficients f_D and f_{v^2} as well as their ratios for the same set of α. We repeat the calculations of f_D performed by Lindenfeld in 1980 [10] for the billiard-ball model but with higher numerical precision (our results are in good agreement for all but the last digit of the Table 1 of Ref. [10]). With these coefficients we define effective rates $\nu_{\vec{v}} = \nu^{(0)}/f_D$ of change of velocity vector $\vec{v}$ and $\nu_{v^2} = \nu^{(0)}[2/(1+\alpha)]/f_{v^2}$ of change of v^2. From that we can obtain the relation $\nu_{v^2} = \nu_{\vec{v}}[2/(1+\alpha)](f_D/f_{v^2})$ between rates of change of $\vec{v}$ and v^2.

Solving Eq. (B4) yields

$$c_{00}(\omega) = \frac{1}{\Gamma_{\text{eff}} + i\Delta_{\text{eff}} - i(\omega - \omega_0)}, \tag{B5}$$

where the effective Lorentzian width and shift are

$$\Gamma_{\text{eff}} + i\Delta_{\text{eff}} = -[\mathbf{S}_D^f]_{00,00} + \frac{[\mathbf{K}]_{01,00}^2}{\nu_{\vec{v}}} - \frac{[\mathbf{S}_D^f]_{10,00}^2}{\nu_{v^2}}. \tag{B6}$$

This equation can be also written in the following form:

$$\Gamma_{\text{eff}} + i\Delta_{\text{eff}} = \Gamma_0 + i\Delta_0 + \frac{1}{2}\frac{\omega_D}{\nu_{\vec{v}}} - \frac{3}{2}\frac{(\Gamma_2 + i\Delta_2)^2}{\nu_{\vec{v}}}\frac{1+\alpha}{2}\frac{f_{v^2}}{f_D}, \tag{B7}$$

which gives Eq. (25).

To take into account any arbitrary speed dependence of collisional broadening, $\Gamma(v)$, and shift, $\Delta(v)$, we need to include other matrix elements, $[\mathbf{S}_D^f]_{n0,00}$, besides $[\mathbf{S}_D^f]_{10,00}$. In such case, Eqs. (B1a)–(B1b) should be generalized to the following form:

$$1 = \left(-i(\omega-\omega_0) - [\mathbf{S}_D^f]_{00,00}\right)c_{00}(\omega) + i[\mathbf{K}]_{00,01}c_{01}(\omega) - \sum_{n'=1}^{\infty}[\mathbf{S}_D^f]_{00,n'0}c_{n'0}(\omega), \tag{B8a}$$

$$0 = i[\mathbf{K}]_{01,00}\delta_{n,0}c_{00}(\omega) - \sum_{n'=0}^{\infty}[\mathbf{S}_{VC}^f]_{n1,n'1}c_{n'1}(\omega), \tag{B8b}$$

$$0 = -[\mathbf{S}_D^f]_{n0,00}c_{00}(\omega) - \sum_{n'=1}^{\infty}[\mathbf{S}_{VC}^f]_{n0,n'0}c_{n'0}(\omega). \tag{B8c}$$

The coefficient $c_{00}(\omega)$ can be found in analogical way like in Eqs. (B1a)–(B1b). The only difference is that the set of linear equations, Eq. (B2b), is replaced by

$$\frac{[\mathbf{S}_D^f]_{n0,00}}{\sum_{n'=1}^{\infty}[\mathbf{S}_D^f]_{n'0,00}} = -\sum_{n'=1}^{\infty}M_{n0,n'0}^{E*}a_{n'0}, \tag{B9}$$

and scaling Eq. (B3b) is replaced by

$$c_{n0}(\omega) = \frac{\sum_{n'=1}^{\infty}[\mathbf{S}_D^f]_{n'0,00}}{\nu^{(0)}}c_{00}(\omega)a_{n0}. \tag{B10}$$

Now from Eq. (B8a) we get

$$1 = \left(-i(\omega-\omega_0) - [\mathbf{S}_D^f]_{00,00} + \frac{[\mathbf{K}]_{01,00}^2}{\nu^{(0)}}a_{01} - \frac{1}{\nu^{(0)}}\sum_{n=1}^{\infty}[\mathbf{S}_D^f]_{n0,00}\sum_{n'=1}^{\infty}[\mathbf{S}_D^f]_{n'0,00}a_{n'0}\right)c_{00}(\omega), \tag{B11}$$

and, as a consequence, the effective Lorentzian width and shift:

$$\Gamma_{\text{eff}} + i\Delta_{\text{eff}} = -[\mathbf{S}_D^f]_{00,00} + \frac{[\mathbf{K}]_{01,00}^2}{\nu_{\vec{v}}} - \frac{1}{\nu^{(0)}}\sum_{n=1}^{\infty}[\mathbf{S}_D^f]_{n0,00}\sum_{n'=1}^{\infty}[\mathbf{S}_D^f]_{n'0,00}a_{n'0}. \tag{B12}$$

---

[1] J.-M. Hartmann, C. Boulet, and D. Robert, *Collisional Effects on Molecular Spectra: Laboratory Experiments and Model, Consequences for Applications* (Elsevier, Amsterdam, 2008).

[2] P. R. Berman, Speed-dependent collisional width and shift parameters in spectral profiles, J. Quant. Spectrosc. Radiat. Transfer **12**, 1331 (1972).

[3] J. Ward, J. Cooper, and E. W. Smith, Correlation effects in the theory of combined Doppler and pressure broadening – I. Classical theory, J. Quant. Spectrosc. Radiat. Transfer **14**, 555 (1974).

[4] R. H. Dicke, The effect of collisions upon the Doppler width of spectral lines, Phys. Rev. **89**, 472 (1953).

[5] J. P. Wittke and R. H. Dicke, Redetermination of the hyperfine splitting in the ground state of atomic hydrogen, Phys. Rev. **103**, 620 (1956).

[6] R. Ciuryło, D. A. Shapiro, J. R. Drummond, and A. D. May, Solving the line-shape problem with speed-dependent broadening and shifting and with Dicke narrowing. II. Application, Phys. Rev. A **65**, 012502 (2002).

[7] H. M. Pickett, Effects of velocity averaging on the shapes of absorption lines, J. Chem. Phys. **73**, 6090 (1980).

[8] R. L. Farrow, L. A. Rahn, G. O. Sitz, and G. J. Rosasco, Observation of a Speed-Dependent Collisional Inhomogeneity in H_2 Vibrational Line Profiles, Phys. Rev. Lett. **63**, 746 (1989).

[9] M. J. Lindenfeld and B. Shizgal, Matrix elements of the Boltzmann collision operator for gas mixtures, Chem. Phys. **41**, 81 (1979).

[10] M. J. Lindenfeld, Self-structure factor of hard-sphere gases for arbitrary ratio of bath to test particle masses, J. Chem. Phys. **73**, 5817 (1980).

[11] P. N. M. Hoang, P. Joubert, and D. Robert, Speed-dependent line-shape models analysis from molecular dynamics simulations: The collision regime, Phys. Rev. A **65**, 012507 (2001).

[12] R. Ciuryło, D. Lisak, and J. Szudy, Role of velocity- and speed-changing collisions on speed-dependent line shapes of H_2, Phys. Rev. A **66**, 032701 (2002).

[13] P. Wcisło, I. E. Gordon, H. Tran, Y. Tan, S.-M. Hu, A. Campargue, S. Kassi, D. Romanini, C. Hill, R. V. Kochanov, and L. S. Rothman, The implementation of non-Voigt line profiles in the HITRAN database: H_2 case study, J. Quant. Spectrosc. Radiat. Transfer **177**, 75 (2016).

[14] R. Z. Martínez, D. Bermejo, F. Thibault, and P. Wcisło, Testing the ab initio quantum-scattering calculations for the

D_2-He benchmark system with stimulated Raman spectroscopy, J. Raman Spectrosc. **49**, 1339 (2018).

[15] F. Rohart, H. Mäder, and H.-W. Nicolaisen, Speed dependence of rotational relaxation induced by foreign gas collisions: Studies on CH_3F by millimeter wave coherent transients, J. Chem. Phys. **101**, 6475 (1994).

[16] M. Nelkin and A. Ghatak, Simple binary collision model for Van Hove's $G_s(r, t)$, Phys. Rev. **135**, A4 (1964).

[17] S. G. Rautian and I. I. Sobelman, The effect of collisions on the Doppler broadening of spectral lines, Usp. Fiz. Nauk **90**, 209 (1966); The effect of collisions on the Doppler broadening of spectral lines, Sov. Phys. Usp. **9**, 701 (1967).

[18] N. Stolarczyk, P. Wcisło, and R. Ciuryło, Inhomogeneous broadening, narrowing and shift of molecular lines under frequent velocity-changing collisions, J. Quant. Spectrosc. Radiat. Transfer **287**, 108246 (2022).

[19] B. Lance, G. Blanquet, J. Walrand, and J.-P. Bouanich, On the Speed-Dependent Hard Collision Lineshape Models: Application to C_2H_2 Perturbed by Xe, J. Mol. Spectrosc. **185**, 262 (1997).

[20] A. S. Pine, Asymmetries and correlations in speed-dependent Dicke-narrowed line shapes of argon-broadened HF, J. Quant. Spectrosc. Radiat. Transfer **62**, 397 (1999).

[21] R. Blackmore, A modified Boltzmann kinetic equation for line shape functions, J. Chem. Phys. **87**, 791 (1987).

[22] D. A. Shapiro, R. Ciuryło, J. R. Drummond, and A. D. May, Solving the line-shape problem with speed-dependent broadening and shifting and with Dicke narrowing. I. Formalism, Phys. Rev. A **65**, 012501 (2002).

[23] E. V. Podivilov, A. I. Chernykh, and D. A. Shapiro, Ion line narrowing in a dense plasma, Zh. Eksp. Teor. Fiz. **105**, 1214 (1994) [J. Exp. Theo. Phys. **78**, 653 (1994)].

[24] D. Robert and L. Bonamy, Memory effects in speed-changing collisions and their consequences for spectral lineshape: I. Collision regime, Eur. Phys. J. D **2**, 245 (1998).

[25] R. Ciuryło, A. Bielski, J. R. Drummond, D. Lisak, A. D. May, A. S. Pine, D. A. Shapiro, J. Szudy, and R. S. Trawiński, High-resolution studies on the influence of velocity-changing collisions on atomic and molecular line shapes, in *Spectral Line Shapes*, Vol. 12, edited by C. A. Back (American Institute of Physics, New York, 2002), pp. 151–160.

[26] R. Wehr, A. Vitcu, R. Ciuryło, F. Thibault, J. R. Drummond, and A. D. May, Spectral line shape of the P(2) transition in CO-Ar: Uncorrelated *ab initio* calculation, Phys. Rev. A **66**, 062502 (2002).

[27] P. Wcisło, F. Thibault, M. Zaborowski, S. Wójtewicz, A. Cygan, G. Kowzan, P. Masłowski, J. Komasa, M. Puchalski, K. Pachucki, R. Ciuryło, and D. Lisak, Accurate deuterium spectroscopy for fundamental studies, J. Quant. Spectrosc. Radiat. Transfer **213**, 41 (2018).

[28] M. Słowiński, F. Thibault, Y. Tan, J. Wang, A.-W. Liu, S.-M. Hu, S. Kassi, A. Campargue, M. Konefał, H. Jóźwiak, K. Patkowski, P. Żuchowski, R. Ciuryło, D. Lisak, and P. Wcisło, H_2-He collisions: *Ab initio* theory meets cavity-enhanced spectra, Phys. Rev. A **101**, 052705 (2020).

[29] S. Dolbeau, R. Berman, J. R. Drummond, and A. D. May, Dicke narrowing as an example of line mixing, Phys. Rev. A **59**, 3506 (1999).

[30] D. A. Shapiro and A. D. May, Dicke narrowing for rigid spheres of arbitrary mass ratio, Phys. Rev. A **63**, 012701 (2000).

[31] A. S. Pine, Line shape asymmetries in Ar-broadened HF($v = 1$–0) in the Dicke-narrowing regime, J. Chem. Phys. **101**, 3444 (1994).

[32] L. Demeio, S. Green, and L. Monchick, Effects of velocity changing collisions on line shapes of HF in Ar, J. Chem. Phys. **102**, 9160 (1995).

[33] G. Nienhuis, Effects of the radiator motion in the classical and quantum-mechanical theories of collisional spectral-line broadening, J. Quant. Spectrosc. Radiat. Transfer **20**, 275 (1978).

[34] J. P. Loony, Comprehensive theory for the broadening, shifting and narrowing of HF and HCl fundamental band absorption profiles, Ph.D. thesis, The Pennsylvania State University, 1987, https://www.proquest.com/openview/165245d21fbdbdaab98079591dabc53a/1?pq-origsite=gscholar&cbl=18750&diss=y.

[35] R. Ciuryło, A. S. Pine, and J. Szudy, A generalized speed-dependent line profile combining soft and hard partially correlated Dicke-narrowing collisions, J. Quant. Spectrosc. Radiat. Transfer **68**, 257 (2001).

[36] S. Hess, Kinetic theory of spectral line shapes. The transition between Doppler broadening and collisional broadening, Physica **61**, 80 (1972).

[37] V. P. Kochanov, S. G. Rautian, and A. M. Shalagin, Broadening of nonlinear resonances by velocity-changing collisions, Zh. Eksp. Teor. Fiz. **72**, 1358 (1977) [Sov. Phys. JETP **45**, 714 (1977)].

[38] P. R. Berman, T. W. Mossberg, and S. R. Hartmann, Collision kernels and laser spectroscopy, Phys. Rev. A **25**, 2550 (1982).

[39] P. R. Berman, Collisions in atomic vapors, in *Les Houches, Session XXXVIII, 1982 – Tendances actuelles en physique atomique/New trends in atomic physics*, Vol. I, edited by G. Grynberg and R. Stora (Elsevier Science Publisher, Amsterdam, 1984), pp. 451–514.

[40] L. Monchick and L. W. Hunter, Diatomic–diatomic molecular collision integrals for pressure broadening and Dicke narrowing: A generalization of Hess's theory, J. Chem. Phys. **85**, 713 (1986), https://pubs.aip.org/aip/jcp/article-pdf/85/2/713/9724657/713_1_online.pdf.

[41] F. Thibault, K. Patkowski, P. S. Żuchowski, H. Jóźwiak, R. Ciuryło, and P. Wcisło, Rovibrational line-shape parameters for H_2 in He and new H_2-He potential energy surface, J. Quant. Spectrosc. Radiat. Transfer **202**, 308 (2017).

[42] S. Chandrasekhar, Stochastic problems in physics and astronomy, Rev. Mod. Phys. **15**, 1 (1943).

[43] L. Galatry, Simultaneous effect of Doppler and foreign gas broadening on spectral lines, Phys. Rev. **122**, 1218 (1961).

[44] R. Ciuryło, R. Jaworski, J. Jurkowski, A. S. Pine, and J. Szudy, Spectral line shapes modeled by a quadratic speed-dependent Galatry profile, Phys. Rev. A **63**, 032507 (2001).

[45] D. Priem, F. Rohart, J.-M. Colmont, G. Wlodarczak, and J.-P. Bouanich, Lineshape study of the $J = 3 \leftarrow 2$ rotational transition of CO perturbed by N_2 and O_2, J. Mol. Struct. **517–518**, 435 (2000).

[46] R. Ciuryło and R. Szudy, Speed-dependent pressure broadening and shift in the soft collision approximation, J. Quant. Spectrosc. Radiat. Transfer **57**, 411 (1997).

[47] P. Wcisło, H. Tran, S. Kassi, A. Campargue, F. Thibault, and R. Ciuryło, Velocity-changing collisions in pure H_2 and H_2-Ar mixture, J. Chem. Phys. **141**, 074301 (2014).

[48] D. Lisak, J. T. Hodges, and R. Ciuryło, Comparison of semiclassical line-shape models to rovibrational H_2O spectra measured by frequency-stabilized cavity ring-down spectroscopy, Phys. Rev. A **73**, 012507 (2006).

[49] P. Wcisło, F. Thibault, H. Cybulski, and R. Ciuryło, Strong competition between velocity-changing and phase- or state-changing collisions in H_2 spectra perturbed by Ar, Phys. Rev. A **91**, 052505 (2015).

[50] P. Wcisło, F. Thibault, N. Stolarczyk, H. Jóźwiak, M. Słowiński, M. Gancewski, K. Stankiewicz, M. Konefał, S. Kassi, A. Campargue, Y. Tan, J. Wang, K. Patkowski, R. Ciuryło, D. Lisak, R. Kochanov, L. Rothman, and I. Gordon, The first comprehensive dataset of beyond-Voigt line-shape parameters from ab initio quantum scattering calculations for the HITRAN database: He-perturbed H_2 case study, J. Quant. Spectrosc. Radiat. Transfer **260**, 107477 (2021).

[51] M. Słowiński, H. Jóźwiak, M. Gancewski, K. Stankiewicz, N. Stolarczyk, Y. Tan, J. Wang, A.-W. Liu, S.-M. Hu, S. Kassi, A. Campargue, K. Patkowski, P. S. Żuchowski, R. Ciuryło, F. Thibault, and P. Wcisło, Collisional line-shape effects in accurate He-perturbed H_2 spectra, J. Quant. Spectrosc. Radiat. Transfer **277**, 107951 (2022).

Laboratoire Interdisciplinaire de Physique

www-liphy.ujf-grenoble.fr
Unité Mixte de Recherche 5588
CNRS – Université Joseph Fourier
BP 87 – 38402 ST MARTIN D'HERES Cedex FRANCE

Alain CampargueSenior researcher CNRS
tél. +33 4 76 51 43 19
fax. +33 4 76 63 54 95

Grenoble
Wednesday, May 15, 2024

Statement about the contribution of Samir KASSI and Alain CAMPARGUE to two research papers co-authored with Nikodem STOLARCZYK

Our contribution to the two following papers was mainly the recording of the high sensitivity cavity ring down spectra f the 2-0 Q1 line of H2 broadened by helium. These CRDS spectra provided experimental data to analyze collisional line-shape effects described in the two papers.

The first comprehensive dataset of beyond-Voigt line-shape parameters from ab initio quantum scattering calculations for the HITRAN database: He-perturbed H2 case study
Piotr Wcisło, Franck Thibault, N Stolarczyk, H Jóźwiak, M Słowiński, M Gancewski, K Stankiewicz, M Konefał, Samir Kassi, Alain Campargue, Y Tan, J Wang, K Patkowski, R Ciuryło, D Lisak, R Kochanov, Laurence S Rothman, Iouli E Gordon.
https://doi.org/10.1016/j.jqsrt.2020.107477

Collisional line-shape effects in accurate He-perturbed H2 spectra
Michał Słowiński, Hubert Jóźwiak, Maciej Gancewski, Kamil Stankiewicz, Nikodem Stolarczyk, Yan Tan, Jin Wang, An-Wen Liu, Shui-Ming Hu, Samir Kassi, Alain Campargue, Konrad Patkowski, Piotr S Żuchowski, Roman Ciuryło, Franck Thibault, Piotr Wcisło
https://doi.org/10.1016/j.jqsrt.2021.107951

Yours faithfully,

Sami Kassi

Alain Campargue

Prof. dr hab. Daniel Lisak
Uniwersytet Mikołaja Kopernika w Toruniu
Instytut Fizyki, Grudziądzka 5/7, 87-100 Toruń

Toruń, 13.05.2021

Statement about my contribution to the research papers

My contribution to the research published in the paper:

> P. Wcisło, F. Thibault, N. Stolarczyk, H. Jóźwiak, M. Słowiński, M. Gancewski, K. Stankiewicz, M. Konefał, S. Kassi, A. Campargue, Y. Tan, J. Wang, K. Patkowski, R. Ciuryło, D. Lisak, R. Kochanov, L.S. Rothman, I.E. Gordon, *"The first comprehensive dataset of beyond-Voigt line-shape parameters from ab initio quantum scattering calculations for the HITRAN database: He-perturbed* H_2 *case study"*, Journal of Quantitative Spectroscopy & Radiative Transfer **260**, 107477 (2021), https://doi.org/10.1016/j.jqsrt.2020.107477

was related to discussing the results and a way of their presentation with other co-authors, as well as contributing to writing and editing the manuscript.

My contribution to the research published in the paper:

> H. Jóźwiak, N. Stolarczyk, K. Stankiewicz, M. Zaborowski, D. Lisak, S. Wójtewicz, P. Jankowski, K. Patkowski, K. Szalewicz, F. Thibault, I. E. Gordon, P. Wcisło, *"Accurate reference spectra of HD in* H_2*–He bath for planetary applications"*, Astronomy & Astrophysics (2024), https://doi.org/10.1051/0004-6361/202449889

was related to discussing concepts and methodology with other co-authors and contributing to writing and editing the manuscript.

Lisak

Université de Rennes

IPR UMR 6251 CNRS-UR1 Université de Rennes – Campus de Beaulieu 263, avenue du Général Leclerc – Bat 11E 35042 Rennes cedex

15th May 2024

Object : Nikodem STOLARCZYK's doctoral dissertation, Nicolaus Copernicus University in Torun

Dr Franck THIBAULT, Institut de Physique, Université de Rennes, contribution statement

Dear colleagues,

I have coauthored six articles with Nikodem Stolarczyk. I briefly describe my contribution to each of them below.

1. The first comprehensive dataset of beyond-Voigt line-shape parameters from ab initio quantum scattering calculations for the HITRAN database: He-perturbed H_2 case study

Piotr Wcisło, Franck Thibault, N Stolarczyk, H Jóźwiak, M Słowiński, M Gancewski, K Stankiewicz, M Konefał, Samir Kassi, Alain Campargue, Y Tan, J Wang, K Patkowski, R Ciuryło, D Lisak, R Kochanov, Laurence S Rothman, Iouli E Gordon

Journal of Quantitative Spectroscopy & Radiative Transfer 260 (2021) 10747

https://doi.org/10.1016/j.jqsrt.2020.107477

Preparation of the potential energy surface for the scattering calculations. Calculations of generalized spectroscopic cross sections.

Conceptualization, Methodology, Software, Validation, Writing - original draft, Writing - review & editing

2. CO-Ar collisions: ab initio model matches experimental spectra at a sub percent level over a wide pressure range

EA Serov, N Stolarczyk, DS Makarov, IN Vilkov, G Yu Golubiatnikov, AA Balashov, MA Koshelev, P Wcisło, Franck Thibault, M Yu Tretyakov

Journal of Quantitative Spectroscopy & Radiative Transfer 272 (2021) 10780

https://doi.org/10.1016/j.jqsrt.2021.107807

Preparation of the potential energy surface for the scattering calculations. Calculations of generalized spectroscopic cross sections and relaxation matrix elements.

Investigation, Writing - original draft

3. Accurate calculations of beyond-Voigt line-shape parameters from first principles for the He-perturbed HD rovibrational lines: A comprehensive dataset in the HITRAN DPL format

Kamil Stankiewicz, Nikodem Stolarczyk, Hubert Jóźwiak, Franck Thibault, Piotr Wcisło

Journal of Quantitative Spectroscopy & Radiative Transfer 276 (2021) 10791

https://doi.org/10.1016/j.jqsrt.2021.107911

Preparation of the potential energy surface for the scattering calculations. Calculations of generalized spectroscopic cross sections.

Conceptualization, Methodology, Software, Resources, Writing – review & editing.

4. Collisional line-shape effects in accurate He-perturbed H_2 spectra

Michał Słowiński, Hubert Jóźwiak, Maciej Gancewski, Kamil Stankiewicz, Nikodem Stolarczyk, Yan Tan, Jin Wang, An-Wen Liu, Shui-Ming Hu, Samir Kassi, Alain Campargue, Konrad Patkowski, Piotr S Żuchowski, Roman Ciuryło, Franck Thibault, Piotr Wcisło

Journal of Quantitative Spectroscopy & Radiative Transfer 277 (2022) 10795

https://doi.org/10.1016/j.jqsrt.2021.107951

Preparation of the potential energy surface for the scattering calculations. Calculations of generalized spectroscopic cross sections.

Conceptualization, Methodology, Software, Validation

5. High-precision cavity-enhanced spectroscopy for studying the H_2–Ar collisions and interactions

N Stolarczyk, G Kowzan, Franck Thibault, H Cybulski, M Słowiński, Y Tan, J Wang, A-W Liu, S-M Hu, P Wcisło

The Journal of Chemical Physics 158, 094303 (2023)

https://doi.org/10.1063/5.0139229

Preparation of the potential energy surface for the scattering calculations.

Conceptualization (equal); Formal analysis (supporting); Investigation (supporting); Software (supporting); Supervision (supporting); Validation (equal); Writing – review & editing (supporting).

6. Accurate reference spectra of HD in an H_2–He bath for planetary applications

H Józwiak, N Stolarczyk, K Stankiewicz, M Zaborowski, D Lisak, S Wójtewicz, P Jankowski, K Patkowski, K Szalewicz, Franck Thibault, IE Gordon, P Wcisło

Astronomy & Astrophysics, forthcoming article

https://doi.org/10.1051/0004-6361/202449889

Preparation of the potential energy surfaces (HD-He and HD-H_2) for the scattering calculations. Writing codes with Hubert Józwiak to generate the generalized spectroscopic cross sections from S-matrix elements. Review-Editing.

Sincerely yours,

Dr F. Thibault

Email : franck.thibault@univ-rennes.fr

Toruń, 17.05.2024 r.

Dr inż. Grzegorz Kowzan
Instytut Fizyki
Wydział Fizyki, Astronomii i Informatyki Stosowanej
Uniwersytet Mikołaja Kopernika w Toruniu

Statement

In publication

High-precision cavity-enhanced spectroscopy for studying the H2–Ar collisions and interactions
N Stolarczyk, G Kowzan, F Thibault, H Cybulski, M Słowiński, Y Tan, J Wang, A-W Liu, S-M Hu, P Wcisło
The Journal of Chemical Physics 158, 9, 094303 (2023)
https://doi.org/10.1063/5.0139229

my contribution comprised calculations of H_2-Ar scattering. Specifically, I decomposed the potential energy surface in a bases appropriate for different levels of theory, calculated S-matrices using the MOLSCAT software and calculated spectroscopic cross sections. I wrote or edited fragments of the publication describing details of these calculations.

Best regards,
Grzegorz Kowzan

dr Hubert Cybulski, prof. UKW

Uniwersytet Kazimierza Wielkiego, Wydział Fizyki

ul. Powstańców Wielkopolskich 2, 85-090 Bydgoszcz

Bydgoszcz, 14.05.2024

Statement about research contribution

I hereby confirm that my contribution to the research published in the paper:

entitled: 'High-precision cavity-enhanced spectroscopy for studying the H2–Ar collisions and interactions'

by N. Stolarczyk, G. Kowzan, F. Thibault, H. Cybulski, M. Słowiński, Y. Tan, J. Wang, A.-W. Liu, S.-M. Hu, P. Wcisło

published in: The Journal of Chemical Physics, 158, 094303 (2023)

https://doi.org/10.1063/5.0139229

was to calculate the H2–Ar potential energy surface and to participate in writing the final version of the manuscript.

Toruń, 16.05.2024

mgr Hubert Jóźwiak
Szkoła Doktorska Nauk Ścisłych i Przyrodniczych
Academia Scientiarum Thoruniensis
Grudziądzka 5/7
87-100 Toruń

Statement of coauthorship

I hereby declare that my contribution to the four research papers listed below involves:

1. The first comprehensive dataset of beyond-Voigt line-shape parameters from ab initio quantum scattering calculations for the HITRAN database: He-perturbed H_2 case study
   Piotr Wcisło, Franck Thibault, N Stolarczyk, H Jóźwiak, M Słowiński, M Gancewski, K Stankiewicz, M Konefał, Samir Kassi, Alain Campargue, Y Tan, J Wang, K Patkowski, R Ciuryło, D Lisak, R Kochanov, Laurence S Rothman, Iouli E Gordon
   https://doi.org/10.1016/j.jqsrt.2020.107477

   computation of the radial coupling terms of the potential, performing quantum scattering calculations and determination of the generalized spectroscopic cross sections for 321 He-perturbed lines in H_2

2. Accurate calculations of beyond-Voigt line-shape parameters from first principles for the He-perturbed HD rovibrational lines: A comprehensive dataset in the HITRAN DPL format
   Kamil Stankiewicz, Nikodem Stolarczyk, Hubert Jóźwiak, Franck Thibault, Piotr Wcisło
   https://doi.org/10.1016/j.jqsrt.2021.107911

   development of the quantum scattering code, computation of the six line-shape parameters of the modified Hartmann-Tran profile for all He-perturbed HD transitions covered in this work

3. Collisional line-shape effects in accurate He-perturbed H2 spectra
   Michał Słowiński, Hubert Jóźwiak, Maciej Gancewski, Kamil Stankiewicz, Nikodem Stolarczyk, Yan Tan, Jin Wang, An-Wen Liu, Shui-Ming Hu, Samir Kassi, Alain Campargue,

Konrad Patkowski, Piotr S Żuchowski, Roman Ciuryło, Franck Thibault, Piotr Wcisło
https://doi.org/10.1016/j.jqsrt.2021.107951

development of the quantum scattering code, performing quantum scattering calculations that involve the correction originating from the centrifugal distortion of the potential energy surface for the five considered potential energy surfaces, denoted as „SK”, „mMR”, „BSP”, „BSP2” and „BSP3” in the paper, determination of the generalized spectroscopic cross sections

4. Accurate reference spectra of HD in an H2–He bath for planetary applications
   H Józwiak, N Stolarczyk, K Stankiewicz, M Zaborowski, D Lisak, S Wójtewicz, P Jankowski, K Patkowski, K Szalewicz, F Thibault, IE Gordon, P Wcisło
   https://doi.org/10.1051/0004-6361/202449889

   preparation of the potential energy surface for the D_2-H_2 and HD-H_2 scattering calculations, performing quantum scattering calculations in D_2-H_2 and HD-H_2 systems, computation of the generalized optical cross sections and the six line-shape parameters of the modified Hartmann-Tran profile for H_2-perturbed R(0), R(1) and R(2) 0-0 transitions in HD and S(2) 2-0 transition in D_2, writing, editing and submitting the manuscript, preparation of the supplementary material

Hubert Jóźwiak

CENTER FOR ASTROPHYSICS
HARVARD & SMITHSONIAN

05/16/24

Statement about contributions of my group to the research papers.

1. Contribution from myself and my group members Laurence Rothman and Roman Kochanov to the research published in the paper:

Wcisło, P., Thibault, F., Stolarczyk, N., Jóźwiak, H., Słowínski, M., Gancewski, M., Stankiewicz, K., Konefał, M., Kassi, S., Campargue, A., Tan, Y., Wang, J., Patkowski, K., Ciuryło, R., Lisak, D., Kochanov, R., Rothman, L.S., Gordon, I.E., 2021. The first comprehensive dataset of beyond-Voigt line-shape parameters from ab initio quantum scattering calculations for the HITRAN database: He-perturbed H_2 case study. J. Quant. Spectrosc. Radiat. Transf. 260, 107477. https://doi.org/10.1016/j.jqsrt.2020.107477

were related to developing the parametrizations consistent with public spectroscopic databases and related software, as well as discussing the results and a way of their presentation with other co-authors, as well as contributing to writing and editing the manuscript.

2. My contribution to the research published in the paper:

Jóźwiak, H..J., Stolarczyk, N., Stankiewicz, K., Zaborowski, M., Lisak, D., Wójtewicz, S., Jankowski, P., Patkowski, K., Szalewicz, K., Thibault, F., Gordon, I.E., Wcisło, P., 2024. Accurate reference spectra of HD in an H_2-He bath for planetary applications. https://doi.org/10.1051/0004-6361/202449889

was related to formulating the problem in the context of planetary science and discussing concepts and methodology with other co-authors and contributing to writing and editing the manuscript.

Respectfully,

Dr. Iouli E. Gordon
Chair of Atomic and Molecular Physics Division
Director of the HITRAN project
Center for Astrophysics | Harvard&Smithsonian
Atomic and Molecular Physics Division
60 Garden Street
Cambridge MA 02138-1516, USA
e-mail: igordon@cfa.harvard.edu
Tel: (617) 496-2259
www.cfa.harvard.edu/~igordon

DEPARTMENT OF CHEMISTRY
AND BIOCHEMISTRY

AUBURN UNIVERSITY
COLLEGE OF SCIENCES
AND MATHEMATICS

Prof. Konrad Patkowski
Department of Chemistry and Biochemistry
Auburn University
179 Chemistry Building
Auburn, Alabama 36849
United States
`patkowsk@auburn.edu`

May 19, 2024

Dear Sir/Madam:

At the request of Mr. Nikodem Stolarczyk, I declare that my personal contribution to our two joint publications was as follows:

1. M. Słowiński, H. Jóźwiak, M. Gancewski, K. Stankiewicz, N. Stolarczyk, Y. Tan, J. Wang, A.-W. Liu, S.-M. Hu, S. Kassi, A. Campargue, K. Patkowski, P. S. Żuchowski, R. Ciuryło, F. Thibault, and P. Wcisło, *Collisional line-shape effects in accurate He-perturbed* H_2 *spectra*, J. Quant. Spect. Rad. Transf. **2022**, *277*, 107951
   My role in this manuscript was computing and fitting the analytical He–H_2 potential energy surface that was used as input in the calculation of line shape parameters. I also made minor contributions to the writing of the manuscript.
2. H. Jóźwiak, N. Stolarczyk, K. Stankiewicz, M. Zaborowski, D. Lisak, S. Wójtewicz, P. Jankowski, K. Patkowski, K. Szalewicz, F. Thibault, I. E. Gordon, and P.Wcisło, *Accurate reference spectra of HD in an* H_2*–He bath for planetary applications*, Astronomy and Astrophysics **2024**, DOI: 10.1051/0004-6361/202449889
   My role in this manuscript was computing the data points for the HD–H_2 six-dimensional potential energy surface, used in turn by Prof. Piotr Jankowski to generate the analytical form of the potential, subsequently used in the line shape calculations. I also made minor contributions to the writing of the manuscript.

Yours sincerely,

Patkowski

Prof. Konrad Patkowski
S. D. and Karen Worley Professor of Chemistry

Authorship statement

I declare that my contribution to the publications listed below was as follows:

Accurate calculations of beyond-Voigt line-shape parameters from first principles for the He-perturbed HD rovibrational lines: A comprehensive dataset in the HITRAN DPL format,
Kamil Stankiewicz, Nikodem Stolarczyk, Hubert Jóźwiak, Franck Thibault, Piotr Wcisło
https://doi.org/10.1016/j.jqsrt.2021.107911

Contribution: Conceptualization, software preparation and execution of the majority of scattering calculations, visualization of scattering calculation results, data validation, preparation of the majority of the manuscript.

The first comprehensive dataset of beyond-Voigt line-shape parameters from ab initio quantum scattering calculations for the HITRAN database: He-perturbed H2 case study,
Piotr Wcisło, Franck Thibault, N Stolarczyk, H Jóźwiak, M Słowiński, M Gancewski, K Stankiewicz, M Konefał, Samir Kassi, Alain Campargue, Y Tan, J Wang, K Patkowski, R Ciuryło, D Lisak, R Kochanov, Laurence S Rothman, Iouli E Gordon, https://doi.org/10.1016/j.jqsrt.2020.107477

Contribution: Conducting part of the scattering calculations, data validation, collaboration in manuscript preparation.

Collisional line-shape effects in accurate He-perturbed H2 spectra,
Michał Słowiński, Hubert Jóźwiak, Maciej Gancewski, Kamil Stankiewicz, Nikodem Stolarczyk, Yan Tan, Jin Wang, An-Wen Liu, Shui-Ming Hu, Samir Kassi, Alain Campargue, Konrad Patkowski, Piotr S Żuchowski, Roman Ciuryło, Franck Thibault, Piotr Wcisło, https://doi.org/10.1016/j.jqsrt.2021.107951

Contribution: Conducting part of the scattering calculations, data validation.

Accurate reference spectra of HD in an H2–He bath for planetary applications,
H Józwiak, N Stolarczyk, K Stankiewicz, M Zaborowski, D Lisak, S Wójtewicz, P Jankowski, K Patkowski, K Szalewicz, F Thibault, IE Gordon, P Wcisło , https://doi.org/10.1051/0004-6361/202449889

Wkład: Preparation of part of the experimental setup, conducting part of the scattering calculations.

Kamil Stankiewicz
....

Signature

UNIVERSITY OF DELAWARE

DEPARTMENT OF PHYSICS
AND ASTRONOMY

University of Delaware
Newark, Delaware 19716-2570
Ph: 302/831-2661
Fax: 302/831-1637

May 20, 2024

Declaration concerning coauthorship

I declare that my contributions to the paper
"Accurate reference spectra of HD in an H_2–He bath for planetary applications", H Józwiak, N Stolarczyk, K Stankiewicz, M Zaborowski, D Lisak, S Wójtewicz, P Jankowski, K Patkowski, K Szalewicz, F Thibault, IE Gordon, P Wcisło; https://doi.org/10.1051/0004-6361/202449889
are as follows: (*i*) Conceptual development of the methods for calculations of the interaction potential between two H_2 molecules; (*ii*) Analysis of the results of such calculations and of the potential accuracy; (*iii*) Participation in the writing of the manuscript.

Krzysztof Szalewicz

Krzysztof Szalewicz
Profesor of Physics and Chemistry

Statement about my contribution to the research papers

My contribution to the research published in the papers:

> **Title:** The first comprehensive dataset of beyond-Voigt line-shape parameters from *ab initio* quantum scattering calculations for the HITRAN database: He-perturbed H_2 case study
> **Authors:** P. Wcisło, F. Thibault, N. Stolarczyk, H. Jóźwiak, M. Słowiński, M. Gancewski, K. Stankiewicz, M. Konefał, S. Kassi, A. Campargue, Y. Tan, J. Wang, K. Patkowski, R. Ciuryło, D. Lisak, R. Kochanov, L. S. Rothman and I. E. Gordon
> **Journal:** *Journal of Quantitative Spectroscopy and Radiative Transfer* **260**, 107477 (2021); https://doi.org/10.1016/j.jqsrt.2020.107477
>
> **Title:** Collisional line-shape effects in accurate He-perturbed H2 spectra
> **Authors:** Michał Słowiński, Hubert Jóźwiak, Maciej Gancewski, Kamil Stankiewicz, Nikodem Stolarczyk, Yan Tan, Jin Wang, An-Wen Liu, Shui-Ming Hu, Samir Kassi, Alain Campargue, Konrad Patkowski, Piotr S. Żuchowski, Roman Ciuryło, Franck Thibault and Piotr Wcisło
> **Journal:** *Journal of Quantitative Spectroscopy and Radiative Transfer* **277**, 107951 (2022); https://doi.org/10.1016/j.jqsrt.2021.107951

was related to performing quantum scattering calculations, and discussing the concepts and methodology with the other authors.

Maciej Gancewski

Maciej Gancewski

NICOLAUS COPERNICUS
UNIVERSITY
IN TORUŃ
Faculty of Chemistry

RESEARCH
UNIVERSITY
EXCELLENCE INITIATIVE

dr hab. Piotr Jankowski, prof. UMK
Department of Quantum Chemistry
and Atomic Spectroscopy
Faculty of Chemistry
Nicolaus Copernicus University in Toruń
ul. Gagarina 7, 87-100 Toruń

Toruń, 12 May 2024

Statement

Mr. Nikodem Stolarczyk plans to include the following paper in his doctoral dissertation

„Accurate reference spectra of HD in H_2/He bath for planetary applications”,
H. Jóźwiak, N. Stolarczyk, K. Stankiewicz, M. Zaborowski, D. Lisak, S. Wójtewicz,
P. Jankowski, K. Patkowski, K. Szalewicz, F. Thibault, I. E. Gordon, P. Wcisło
(accepted to Astronomy and Astrophysics).

I am a co-author of this publication, and I declare that my contribution to it is as follows:

- I co-authored a new interaction energy surface for the H_2–H_2 dimer used in the paper;
- I participated in writing the manuscript, precisely the part concerning a description of the interaction energy surface.

Sincerely,

Piotr

Piotr Jankowski

NICOLAUS COPERNICUS
UNIVERSITY
IN TORUŃ
Faculty of Physics, Astronomy
and Informatics

Institute of Physics

May 21, 2024

Author contribution statement

1. **High-precision cavity-enhanced spectroscopy for studying the H_2–Ar collisions and interactions**
   N Stolarczyk, G Kowzan, F Thibault, H Cybulski, M Słowiński, Y Tan, J Wang, A-W Liu, S-M Hu, P Wcisło,
   The Journal of Chemical Physics 158, 094303 (2023)
   https://doi.org/10.1063/5.0139229

   My role in this research was: initiator of this research direction, coordination of work and international cooperation, contribution to research in setting the research strategy and supporting the project at technical level, supervising the work of PhD students, participation and supervision over the manuscript preparation.

   I would like to emphasize that Mr Nikdoem Stolarczyk was the main and leading contributor to this work.

2. **CO-Ar collisions: ab initio model matches experimental spectra at a sub percent level over a wide pressure range**
   EA Serov, N Stolarczyk, DS Makarov, IN Vilkov, G Yu Golubiatnikov, AA Balashov, MA Koshelev, P Wcisło, F. Thibault, M Yu Tretyakov,
   Journal of Quantitative Spectroscopy and Radiative Transfer 272, 107807 (2021)
   https://doi.org/10.1016/j.jqsrt.2021.107807

   My contribution was: developing concept for the analysis of experimental data and comparing them with ab initio calculations, support in solving detailed technical problems in the analysis of measurement data and simulations of optical resonances disturbed by collisions, direct supervision of the PhD student, participation in the preparation of the manuscript.

   Additionally, I would like to declare that receiving the author contribution statement from the former collaborators from the Russian Federation was not possible since our entire collaboration was completely frozen since the begging of the full scale Russian war against Ukraine. I declare that the joint contribution of the coauthors: A Serov, DS Makarov, IN Vilkov, G Yu Golubiatnikov, AA Balashov, MA Koshelev, M Yu Tretyakov was related to the construction of the experimental apparatus and performing the laboratory measurements, performing pre-analysis of experimental data as well as writing and editing parts of the manuscript.

   I would like to emphasize that in my opinion the second position of Mr Nikdoem Stolarczyk on the list of coauthors reflects his second-major contribution to the paper.

3. **The first comprehensive dataset of beyond-Voigt line-shape parameters from ab initio quantum scattering calculations for the HITRAN database: He-perturbed H_2 case study**
Piotr Wcisło, Franck Thibault, N Stolarczyk, H Jóźwiak, M Słowiński, M Gancewski, K Stankiewicz, M Konefał, Samir Kassi, Alain Campargue, Y Tan, J Wang, K Patkowski, R Ciuryło, D Lisak, R Kochanov, Laurence S Rothman, Iouli E Gordon
Journal of Quantitative Spectroscopy and Radiative Transfer 260, 107477 (2021)
https://doi.org/10.1016/j.jqsrt.2020.107477

My role in this research was: initiator of this research direction, coordination of work and international cooperation, contribution to research in setting the research strategy and supporting the project at technical level, supervising the work of PhD students, participation and supervision over the manuscript preparation.

Additionally, due to a lack of contact with M. Konefał, as the first author, I declare that the contribution of M Konefał to this work was small and related to supporting the data analysis.

4. **Accurate calculations of beyond-Voigt line-shape parameters from first principles for the He-perturbed HD rovibrational lines: A comprehensive dataset in the HITRAN DPL format**
Kamil Stankiewicz, Nikodem Stolarczyk, Hubert Jóźwiak, Franck Thibault, Piotr Wcisło
Journal of Quantitative Spectroscopy and Radiative Transfer 276, 107911 (2021)
https://doi.org/10.1016/j.jqsrt.2021.107911

My role in this research was: initiator of this research direction, coordination of work and international cooperation, contribution to research in setting the research strategy and supporting the project at technical level, supervising the work of PhD students, participation and supervision over the manuscript preparation.

I would like to emphasize that in my opinion the second position of Mr Nikdoem Stolarczyk on the list of coauthors reflects his second-major contribution to the paper.

5. **Accurate reference spectra of HD in an H_2–He bath for planetary applications**
H Józwiak, N Stolarczyk, K Stankiewicz, M Zaborowski, D Lisak, S Wójtewicz, P Jankowski, K Patkowski, K Szalewicz, F Thibault, IE Gordon, P Wcisło
Astronomy & Astrophysics in press (2024)
https://doi.org/10.1051/0004-6361/202449889

My role in this research was: initiator of this research direction, coordination of work and international cooperation, contribution to research in setting the research strategy and supporting the project at technical level, supervising the work of PhD students, participation and supervision over the manuscript preparation.

I would like to emphasize that in my opinion the second position of Mr Nikdoem Stolarczyk on the list of coauthors reflects his second-major contribution to the paper.

Additionally, due to inability of M. Zaborowski to provide his statement, I as the project leader declare that the contribution of M. Zaborowski was related to construction of the experimental setup and measuring the spectral lines in laboratory.

6. **Collisional line-shape effects in accurate He-perturbed H2 spectra**
   Michał Słowiński, Hubert Jóźwiak, Maciej Gancewski, Kamil Stankiewicz, Nikodem Stolarczyk, Yan Tan, Jin Wang, An-Wen Liu, Shui-Ming Hu, Samir Kassi, Alain Campargue, Konrad Patkowski, Piotr S Żuchowski, Roman Ciuryło, Franck Thibault, Piotr Wcisło
   Journal of Quantitative Spectroscopy and Radiative Transfer 277, 107951 (2022)
   https://doi.org/10.1016/j.jqsrt.2021.107951

   My role in this research was: initiator of this research direction, coordination of work and international cooperation, contribution to research in setting the research strategy and supporting the project at technical level, supervising the work of PhD students, participation and supervision over the manuscript preparation.

7. **Inhomogeneous broadening, narrowing and shift of molecular lines under frequent velocity-changing collisions**
   Nikodem Stolarczyk, Piotr Wcisło, Roman Ciuryło
   Journal of Quantitative Spectroscopy and Radiative Transfer 287, 108246 (2022)
   https://doi.org/10.1016/j.jqsrt.2022.108246

   My role in this research was: initiator of this research direction, validation of theoretical analysis, contribution to the analysis and interpretation of results, participation in the preparation of the manuscript.

   I would like to emphasize that Mr Nikdoem Stolarczyk was the main and leading contributor to this work.

8. **Spectral line shape in the limit of frequent velocity-changing collisions**
   Nikodem Stolarczyk, Piotr Wcisło, Roman Ciuryło
   Physical Review A 108, 032810 (2023)
   https://doi.org/10.1103/PhysRevA.108.032810

   My role in this research was: validation of theoretical analysis, contribution to the analysis and interpretation of results, participation in the preparation of the manuscript.

   I would like to emphasize that Mr Nikdoem Stolarczyk was the main and leading contributor to this work.

Piotr Wcisło

Piotr Wcislo, Physicist
dr. hab., prof. at NCU
Institute of Physics
Nicolaus Copernicus University
Grudziądzka 5, 87-100 Toruń, Poland

UNIWERSYTET
MIKOŁAJA KOPERNIKA
W TORUNIU
Wydział Fizyki, Astronomii
i Informatyki Stosowanej

Instytut Fizyki UMK

Dr hab. Piotr Żuchowski, Prof. UMK
(pzuch@fizyka.umk.pl
piotr.zuchowski@gmail.com
tel +48 784647638
room number 470)

Author statement

In the paper
Collisional line-shape effects in accurate He-perturbed H2 spectra
Michał Słowiński, Hubert Jóźwiak, Maciej Gancewski, Kamil Stankiewicz, Nikodem Stolarczyk, Yan Tan, Jin Wang, An-Wen Liu, Shui-Ming Hu, Samir Kassi, Alain Campargue, Konrad Patkowski, Piotr S Żuchowski, Roman Ciuryło, Franck Thibault, Piotr Wcisło

My contribution involved determining the potential energy surface for significantly stretched atoms, and determining the long-range interaction potential of He-H2

Respectfully

Piotr Żuchowski

Uniwersytet Mikołaja Kopernika w Toruniu
Instytut Fizyki
ul. Grudziądzka 5/7, 87-100 Toruń
tel.: +48 56 611 33 10, fax: +48 56 622 53 97
www.ifiz.umk.pl, ifiz@fizyka.umk.pl

UNIWERSYTET
MIKOŁAJA KOPERNIKA
W TORUNIU
Wydział Fizyki, Astronomii
i Informatyki Stosowanej

Instytut Fizyki UMK

Toruń, 17.05.2024

Authorship statement

I contributed to four papers listed below.

P. Wcisło, F. Thibault, N. Stolarczyk, H. Jóźwiak, M. Słowiński, M. Gancewski, K. Stankiewicz, M. Konefał, S. Kassi, A. Campargue, Y. Tan, J. Wang, K. Patkowski, R. Ciuryło, D. Lisak, R. Kochanov, L. S. Rothman, I. E. Gordon, "The first comprehensive dataset of beyond-Voigt line-shape parameters from *ab initio* quantum scattering calculations for the HITRAN database: He-perturbed H_2 case study", J. Quant. Spectrosc. Radiat. Transfer **260**, 107477-10 (2021).
https://doi.org/10.1016/j.jqsrt.2020.107477

I helped to develop methodology for the efficient line shape description. I helped to interpret obtained results. I contributed to the correction of the final manuscript.

M. Słowiński, H. Jóźwiak, M. Gancewski, K. Stankiewicz, N. Stolarczyk, Y. Tan, J. Wang, A.-W. Liu, S.-M. Hu, S. Kassi, A. Campargue, K. Patkowski, P. S. Żuchowski, R. Ciuryło, F. Thibault, P. Wcisło, "Collisional line-shape effects in accurate He-perturbed H_2 spectra", J. Quant. Spectrosc. Radiat. Transfer **277**, 107951-11 (2022).
https://doi.org/10.1016/j.jqsrt.2021.107951

I helped to develop methodology for the line shape calculations allowing successful confrontation with experimental spectra. I helped to understand influence of different physical effects on the spectral line shape and interpret obtained results. I contributed to the correction of the final manuscript.

N. Stolarczyk, P. Wcisło, R. Ciuryło,
"Inhomogeneous broadening, narrowing and shift of molecular lines under frequent velocity-changing collisions", J. Quant. Spectrosc. Radiat. Transfer **287**, 108246-7 (2022).
https://doi.org/10.1016/j.jqsrt.2022.108246

I helped to develop methodology needed to derive analytical results presented in the paper as well as to understand obtained results. I contributed to preparation of the manuscript. I need to emphasize that the project was led by mgr. Nikodem Stolarczyk and He coordinate all scientific activities related to the project. He developed necessary software, carried out all numerical calculation, prepared all figures and tables, and coordinated work on the manuscript.

N. Stolarczyk, P. Wcisło, R. Ciuryło, "Spectral line shape in the limit of frequent velocity-changing collisions", Phys. Rev. A 108, 032810-12 (2023).
https://doi.org/10.1103/PhysRevA.108.032810

I helped to develop methodology needed to derive analytical results presented in the paper as well as to understand obtained results. I contributed to preparation of the manuscript. I need to emphasize that the project was led by mgr. Nikodem Stolarczyk and He coordinate all scientific activities related to the project. He developed necessary software, carried out all numerical calculation, prepared all figures and tables, and coordinated work on the manuscript.

Prof. dr. hab. Roman Ciuryło

Head of Department of Atomic, Molecular and Optical Physics

Institute of Physics,
Nicolaus Copernicus University,
ul. Grudziądzka 5
87-100 Toruń,
e-mail: rciurylo@fizyka.umk.pl

中国科学技术大学
University of Science and Technology of China, Hefei, Anhui 230026, China

Hefei, China, 17 May 2024

Shui-Ming Hu
Professor, Department of Chemical Physics,
University of Science and Technology of China
+86-551-63606557 smhu@ustc.edu.cn

To whom it may concern,

I acknowledge that Mr. Nikodem Stolarczyk is a coauthor in the paper entitled “Collisional line-shape effects in accurate He-perturbed H2 spectra” published in *Journal of Quantitative Spectroscopy & Radiative Transfer*, 277: 107951 (2022) [https://doi.org/10.1016/j.jqsrt.2021.107951] and “High-precision cavity-enhanced spectroscopy for studying the H2-Ar collisions and interactions” published in *Journal of Chemical Physics*, 158, 094303 (2023) [https://doi.org/10.1063/5.0139229]. Mr. Stolarczyk contributed to the two studies with data analysis, modeling, and manuscript writing. The contribution of my group was the construction of the experimental apparatus and performing the laboratory measurements. We contributed to writing and editing parts of the manuscripts and provided the graphical scheme of the experimental system.

Shui-Ming Hu,
and on behalf of other coauthors from the University of Science and Technology of China

Dr Szymon Wójtewicz
Institute of Physics
Nicolaus Copernicus University in Toruń

Toruń, 15.05.2024

AUTHORSHIP STATEMENT

I declare that in the paper

H. Jóźwiak, N. Stolarczyk, K. Stankiewicz, M. Zaborowski, D. Lisak, S. Wójtewicz, P. Jankowski, K. Patkowski, K. Szalewicz, F. Thibault, I. E. Gordon, P. Wcisło, *Accurate reference spectra of HD in an H_2-He bath for planetary applications*, Astronomy & Astrophysics, https://doi.org/10.1051/0004-6361/202449889

my contribution consisted in preparing the CRDS spectrometer for measurements and in performing measurements of the spectral lines of D_2.

Szymon

THE LIST OF ALL THE ARTICLES CO-AUTHORED BY ME

INCLUDING THOSE NOT SUBMITTED WITHIN THIS DISSERTATION

1. Accurate reference spectra of HD in an H_2–He bath for planetary applications

   H. Jóźwiak, **N. Stolarczyk**, K. Stankiewicz, M. Zaborowski, D. Lisak, S. Wójtewicz, P. Jankowski, K. Patkowski, K. Szalewicz, F. Thibault, I.E. Gordon, P. Wcisło

   Astronomy & Astrophysics in press (2024)

   DOI: 10.1051/0004-6361/202449889

2. Spectral line shape in the limit of frequent velocity-changing collisions

   N. Stolarczyk, P. Wcisło, R. Ciuryło

   Physical Review A 108, 032810 (2023)

   DOI: 10.1103/PhysRevA.108.032810

3. High-precision cavity-enhanced spectroscopy for studying the H_2–Ar collisions and interactions

   N. Stolarczyk, G. Kowzan, F. Thibault, H. Cybulski, M. Słowiński, Y. Tan, J. Wang, A.-W. Liu, S.-M. Hu, P. Wcisło

   The Journal of Chemical Physics 158, 094303 (2023)

   DOI: 10.1063/5.0139229

4. Inhomogeneous broadening, narrowing and shift of molecular lines under frequent velocity-changing collisions

   N. Stolarczyk, P. Wcisło, R. Ciuryło

   Journal of Quantitative Spectroscopy and Radiative Transfer 287, 108246

(2022)

DOI: 10.1016/j.jqsrt.2022.108246

5. Collisional line-shape effects in accurate He-perturbed H_2 spectra

   M. Słowiński, H. Jóźwiak, M. Gancewski, K. Stankiewicz, **N. Stolarczyk**, Y. Tan, J. Wang, A.-W. Liu, S.-M. Hu, S. Kassi, A. Campargue, K. Patkowski, P. S. Żuchowski, R. Ciuryło, F. Thibault, P. Wcisło

   Journal of Quantitative Spectroscopy and Radiative Transfer 277, 107951 (2022)

   DOI: 10.1016/j.jqsrt.2021.107951

6. Accurate calculations of beyond-Voigt line-shape parameters from first principles for the He-perturbed HD rovibrational lines: A comprehensive dataset in the HITRAN DPL format

   K. Stankiewicz, **N. Stolarczyk**, H. Jóźwiak, F. Thibault, P. Wcisło

   Journal of Quantitative Spectroscopy and Radiative Transfer 276, 107911 (2021)

   DOI: 10.1016/j.jqsrt.2021.107911

7. CO-Ar collisions: *ab initio* model matches experimental spectra at a sub percent level over a wide pressure range

   E. A. Serov, **N. Stolarczyk**, D. S. Makarov, I. N. Vilkov, G. Yu. Golubatnikov, A. A. Balashov, M. A. Koshelev, P. Wcisło, F. Thibault, M. Yu. Tretyakov

   Journal of Quantitative Spectroscopy and Radiative Transfer 272, 107807 (2021)

   DOI: 10.1016/j.jqsrt.2021.107807

8. The first comprehensive dataset of beyond-Voigt line-shape parameters from *ab initio* quantum scattering calculations for the HITRAN database: He-perturbed H_2 case study

   P. Wcisło, F. Thibault, **N. Stolarczyk**, H. Jóźwiak, Michał Słowiński, M. Gancewski, K. Stankiewicz, M. Konefał, S. Kassi, A. Campargue, Y. Tan, J. Wang, K. Patkowski, R. Ciuryło, D. Lisak, R. Kochanov, L. S. Rothman,

I. E. Gordon

Journal of Quantitative Spectroscopy and Radiative Transfer 260, 107477 (2021)

DOI: 10.1016/j.jqsrt.2020.107477

9. *Ab initio* calculations of collisional line–shape parameters and generalized spectroscopic cross-sections for rovibrational dipole lines in HD perturbed by He

   K. Stankiewicz, H. Jóźwiak, M. Gancewski, **N. Stolarczyk**, F. Thibault, P. Wcisło

   Journal of Quantitative Spectroscopy and Radiative Transfer 254, 107194 (2020)

   DOI: 10.1016/j.jqsrt.2020.107194

10. Ultrahigh finesse cavity-enhanced spectroscopy for accurate tests of quantum electrodynamics for molecules

    M. Zaborowski, M. Słowiński, K. Stankiewicz, F. Thibault, A. Cygan, H. Jóźwiak, G. Kowzan, P. Masłowski, A. Nishiyama, **N. Stolarczyk**, S. Wójtewicz, R. Ciuryło, D. Lisak, P. Wcisło

    Optics Letters 45 7 (2020)

    DOI: 10.1364/OL.389268

11. Evaluation of different parameterizations of temperature dependences of the line-shape parameters based on ab initio calculations: Case study for the HITRAN database

    N. Stolarczyk, F. Thibault, H. Cybulski, H. Jóźwiak, G. Kowzan, B. Vispoel, I.E. Gordon, L.S. Rothman, R.R. Gamache, P. Wcisło

    Journal of Quantitative Spectroscopy and Radiative Transfer 240, 106676 (2020)

    DOI: 10.1016/j.jqsrt.2019.106676

12. Comb-locked cavity ring-down spectroscopy with variable temperature

    H. Wu, **N. Stolarczyk**, Q.-H. Liu, C.-F. Cheng, T.-P. Hua, Y.R. Sun, S.-M.

Hu

Optics Express 27 26 (2019)

DOI: 10.1364/OE.376572

13. *Ab initio* line-shape calculations for the S and O branches of H_2 perturbed by He

    H. Jóźwiak, F. Thibault, **N. Stolarczyk**, P. Wcisło

    Journal of Quantitative Spectroscopy and Radiative Transfer 219, 313-322 (2018)

    DOI: 10.1016/j.jqsrt.2018.08.023